Heinrich Heine
Universität
Düsseldorf

Synthesis and characterization of covalent triazine frameworks and imine-linked covalent organic frameworks and their application as porous filler materials in mixed-matrix membranes for gas separation

Inaugural-Dissertation

zur Erlangung des Doktorgrades
der Mathematisch-Naturwissenschaftlichen Fakultät
der Heinrich-Heine-Universität Düsseldorf

vorgelegt von

Stefanie Bügel

aus Wuppertal

Düsseldorf, Mai 2022

aus dem Institut für Anorganische Chemie und Strukturchemie I

der Heinrich-Heine-Universität Düsseldorf

Gedruckt mit der Genehmigung der

Mathematisch-Naturwissenschaftlichen Fakultät der

Heinrich-Heine-Universität Düsseldorf

Berichterstatter:

1. Prof. Dr. Christoph Janiak

2. Prof. Dr. Christian Ganter

Tag der mündlichen Prüfung: 15.06.2022

Die vorliegende Arbeit wurde in der Zeit von März 2019 bis Mai 2022 an der Heinrich-Heine Universität Düsseldorf im Institut für Anorganische Chemie und Strukturchemie I im Arbeitskreis von Prof. Dr. Christoph Janiak angefertigt.

Eidesstattliche Erklärung

Ich versichere an Eides statt, dass die Dissertation von mir selbstständig und ohne unzulässige fremde Hilfe unter Beachtung der „Grundsätze zur Sicherung guter wissenschaftlicher Praxis an der Heinrich-Heine-Universität Düsseldorf“ erstellt worden ist. Die aus fremden Quellen direkt oder indirekt übernommenen Gedanken sind als solche kenntlich gemacht. Die Arbeit wurde bisher weder im Inland noch im Ausland in gleicher oder ähnlicher Form einer anderen Prüfungsbehörde vorgelegt. Es wurden keine früheren erfolglosen Promotionsversuche unternommen.

……..... …….....

Ort, Datum Unterschrift

Danksagung

Mein Dank gilt Herrn Prof. Dr. Christoph Janiak für die Möglichkeit, diese Dissertation in seinem Arbeitskreis anfertigen zu können. Im Besonderen möchte ich mich für die große Freiheit bei der Wahl und Bearbeitung der Forschungsinhalte bedanken.

Prof. Dr. Christian Ganter danke ich für Übernahme des Korreferats.

Jutta Bourgeois, Birgit Tommes, Annette Ricken und Marcell Demandt möchte ich für die freundliche Unterstützung bei organisatorischen und technischen Problemen danken.

Glasapparatebauermeister Udo Jung danke ich für die kompetente Hilfe.

Für eine gute Zusammenarbeit danke ich Tom Kunde, Daniel Baier, Tilo Rensch, Nader de Sousa Amadeu, sowie meinen Bachelor- und Masterabsolventen, Quang-Dien Hoang, Mohamed Chamali und Malte Hähnel.

Mein Dank für eine angenehme Atmosphäre und interessante Gespräche gilt zudem allen jetzigen und ehemaligen Mitarbeitern, im Besonderen möchte ich mich bei Yang-Yang Sun, Alexa Schmitz, Anna Goldman, Alex Spieß, Daniel Kommisarek und Moritz Steinert für eine schöne gemeinsame Zeit bedanken.

Meinem Partner, meinen Eltern und meinen guten Freunden danke ich von ganzem Herzen für alle Unterstützung.

Kurzzusammenfassung

Kovalente organische Netzwerke (COFs) und die Unterkategorie der kovalenten triazinbasierten Netzwerke (CTFs) stellen Materialien dar, welche über eine hohe thermische und chemische Stabilität sowie permanente Porosität verfügen können. Die Kombination von verschieden Synthesebausteinen sowie die Möglichkeit der weiteren Funktionalisierung macht diese attraktiv für Anwendungszwecke wie Gasspeicherung und -trennung. Durch den Einsatz von COFs/CTFs als Füllstoffe in Polymermembranen kann die Effizienz der kontinuierlichen Trennung von Gasgemischen durch die resultierenden Mixed-matrix Membranen (MMMs) im Vergleich zu den reinen Polymermembranen gesteigert werden, was die Anwendung von MMMs sowohl aus ökonomischer als auch ökologischer Sicht interessant macht.

Im Rahmen dieser Arbeit wurde durch Friedel-Crafts-Alkylierung CTF-Fluoren synthetisiert und als Füllstoff in den Polymermatrizen Polysulfon (PSF) und Matrimid verwendet. Die hergestellten MMMs zeigten bei der Untersuchung der Trenneffizienz in Bezug auf ein äquimolares CO_2/CH_4 Gasgemisch eine signifikante Verbesserung der Permeabilität. Durch Einbringung von 24 Gewichtsprozent (Gew.-%) des Füllstoffes CTF-Fluoren in eine PSF-Matrix konnten die CO_2- und CH_4-Permeabilitäten von 5,4 und 0,19 Barrer für die reine PSF-Membran auf 12,8 und 0,42 Barrer für die MMM gesteigert werden. Eingebettet in eine Matrimid-Matrix, erhöhte der Füllstoff CTF-Fluoren (24 Gew.-%) die CO_2- und CH_4-Permeabilitäten von 6,8 und 0,16 Barrer für die reine Matrimid-Membran auf 17,8 und 0,40 Barrer für die MMM. Der essenzielle Beitrag der Porosität des Füllstoffs zum Gastransport durch die Membran konnte mittels Berechnung des fraktionellen freien Volumens (FFV) bestätigt werden.

Ein weiteres CTF mit einem höheren Porenvolumen von 0,53 cm^3/g wurde ausgehend von Cyanurchlorid und Biphenyl synthetisiert. Die resultierende Struktur, CTF-Biphenyl wies bei 298 K CO_2- und CH_4-Aufnahmen von 1,87 mmol/g (bei 0,96 bar) und 0,55 mmol/g (bei 0,97 bar) auf. Berechnungen beruhend auf der Theorie der ideal adsorbierten Lösung (IAST) ergaben zudem eine CO_2/CH_4-Selektivität von 10,5 bei 1 bar Druck für ein 50:50 (v:v)-CO_2/CH_4 Gasgemisch. Anschließende CO_2/CH_4-Mischgasmessungen der entsprechenden CTF-Biphenyl/Matrimid MMMs ergaben eine Erhöhung der CO_2 Permeabilität bei gleichbleibender Selektivität. Der Vergleich mit Permeabilitätsmodellen zeigte, dass die 8 Gew.-% MMM einen höheren Anstieg der Permeabilität als erwartet aufwies, begleitet von einem relativ höheren freien Volumen im Vergleich zu den MMMs mit höheren

Füllstoffgehalten. Mit 16 Gew.-% CTF-Biphenyl, welches der optimale Füllstoffgehalt war, wurde die CO_2 Permeabilität auf 15,1 Barrer erhöht. Diese Studie hob den vorteilhaften Beitrag der Porosität zur Membrantrennleistung hervor und zeigte zudem die Grenzen einer weiteren Leistungssteigerung in diesem Membransystem auf.

Zwei bislang literaturunbekannte COFs konnten durch eine Schiff‘sche Basen Reaktion erhalten werden. Durch die Reaktion von 1,3,5-Tris-(4-aminophenyl)triazin mit 4,4'-Biphenyldicarboxaldehyd konnte HHU-COF-1 synthetisiert werden. Das fluorierte Analogon HHU-COF-2 konnte durch Verwendung des Linkers 2,2',3,3',5,5',6,6'-Octafluoro-4,4'-biphenyldicarboxaldehyd erhalten werden. Die erfolgreiche Bildung beider Strukturen wurde durch Festkörper-NMR, Infrarotspektroskopie, Röntgenphotoelektronenspektroskopie und Elementaranalyse bestätigt. Die kristallinen Materialien zeichneten sich durch hohe Brunauer-Emmet-Teller (BET)-Oberflächen von 2352 m^2/g für HHU-COF-1 bzw. 1356 m^2/g für HHU-COF-2 aus. Des Weiteren wurden Synthesen in einem größeren Maßstab durchgeführt und die COFs wurden zur Herstellung von MMMs mit dem Polymer Matrimid verwendet. Die Anwendung von 24 Gew.-% des fluorierten COFs als Füllstoff führte zu einem Anstieg der CO_2 Permeabilität von 6,8 auf 13,0 Barrer bei konstanter Selektivität.

In einer weiteren Arbeit diente das ionothermal dargestellte CTF-1 als dispergierte Phase in einer Matrix des Polymers PSF. Die mit 8, 16 und 24 Gew.-% des CTFs hergestellten MMMs wurden in Einzelgaspermeabilitäts- und Selektivitätsstudien untersucht und für die 24 Gew.-% CTF-1/PSF MMM konnte eine CO_2-Permeabilitätsteigerung von 7,3 auf 12,7 Barrer erreicht werden. Für alle MMMs wurde eine konstante Selektivität bezüglich der Gasgemische O_2/N_2, CO_2/CH_4 und CO_2/N_2 festgestellt und der anschließende Vergleich mit theoretischen Permeabilitätsmodellen wies auf eine gute Kompatibilität des CTFs mit der Matrix hin.

Short Summary

Covalent organic frameworks (COFs) and the subcategory of covalent triazine frameworks (CTFs) represent materials that can possess high thermal and chemical stability as well as permanent porosity. The combination of different building blocks, as well as the possibility of further functionalization, makes them attractive for applications such as gas storage and separation. By applying COFs/CTFs as filler materials in polymer membranes, the efficiency of continuous separation of gas mixtures can be increased by the resulting mixed-matrix membranes (MMMs) compared to the pure polymer membranes, which makes the application of MMMs interesting from both economic and environmental perspectives.

In this work, CTF-fluorene was synthesized via Friedel-Crafts alkylation and applied as a filler in the polymer matrices polysulfone (PSF) and Matrimid. The prepared MMMs showed a significant improvement in permeability when tested for separation efficiency with respect to an equimolar CO_2/CH_4 gas mixture. Incorporation of 24 weight percent (wt%) of the filler material CTF-fluorene into a PSF matrix increased the CO_2 and CH_4 permeability from 5.4 and 0.19 Barrer for the pure PSF membrane to 12.8 and 0.42 Barrer for the MMM. Embedded in a Matrimid matrix, the filler material CTF-fluorene (24 wt%) increased the CO_2 and CH_4 permeability from 6.8 and 0.16 Barrer for the pure Matrimid membrane to 17.8 and 0.40 Barrer for the MMM. The essential contribution of filler porosity for gas transport through the membrane was confirmed by calculations of fractional free volume (FFV).

Another CTF with an even higher pore volume of 0.53 cm^3/g was synthesized starting from cyanuric chloride and biphenyl. The resulting structure, CTF-biphenyl, exhibited CO_2 and CH_4 uptakes of 1.87 mmol/g (at 0.96 bar) and 0.55 mmol/g (at 0.97 bar) at 298 K, respectively. Calculations based on the ideal adsorbed solution theory (IAST) revealed a CO_2/CH_4 selectivity of 10.5 at 1 bar pressure for a 50:50 (v:v) CO_2/CH_4 gas mixture. Subsequent CO_2/CH_4 mixed gas measurements of the corresponding CTF biphenyl/Matrimid MMMs showed an increase in CO_2 permeability while maintaining selectivity. Comparison with permeability models showed that the 8 wt% MMM exhibited a higher increase in permeability than expected, accompanied by a relatively higher free volume compared to the MMMs with higher filler contents. With 16 wt% CTF-biphenyl, which was the optimum filler content, CO_2 permeability was increased to 15.1 Barrer. This study highlighted the beneficial contribution of porosity to membrane separation performance and showed the limitations of further performance enhancement in this membrane system.

Two new COFs were obtained by a Schiff base reaction. HHU-COF-1 was synthesized by the reaction of 1,3,5-tris-(4-aminophenyl)triazine with 4,4'-biphenyldicarboxaldehyde. The fluorinated analog HHU-COF-2 was obtained by applying the linker 2,2',3,3',5,5',6,6'-octafluoro-4,4'-biphenyldicarboxaldehyde. The successful formation of both structures was confirmed by solid-state NMR, infrared spectroscopy, X-ray photoelectron spectroscopy and elemental analysis. The crystalline materials were characterized by high Brunauer-Emmet-Teller (BET) surface areas of 2352 m^2/g for HHU-COF-1 and 1356 m^2/g for HHU-COF-2, respectively. Furthermore, larger scale syntheses were carried out and the COFs were applied to prepare MMMs with the polymer Matrimid. The application of 24 wt% of the fluorinated COF as filler material resulted in an increase in CO_2 permeability from 6.8 to 13.0 Barrer with constant selectivity.

In another work, the ionothermal prepared CTF-1 served as a dispersed phase in a matrix of the polymer PSF. MMMs prepared with 8, 16, and 24 wt% of the CTF were investigated in single gas permeability and selectivity studies, and a CO_2 permeability increase from 7.3 to 12.7 Barrer was achieved for the 24 wt% CTF-1/PSF MMM. Constant selectivity was observed for any MMM with respect to the gas pairs O_2/N_2, CO_2/CH_4 and CO_2/N_2, and subsequent comparison with theoretical permeability models indicated good compatibility of the CTF with the matrix.

List of abbreviations

The list of abbreviations does not include SI units or abbreviations of chemicals which are explained in the text.

BET	Brunauer-Emmett-Teller
CMP	conjugated microporous polymer
CMS	carbon molecular sieve
COF	covalent organic framework
CTF	covalent triazine framework
DFT	density functional theory
EDX	energy dispersive x-ray spectroscopy
EOF	element organic framework
FFV	fractional free volume
FT-IR	Fourier transformed infrared
IAST	ideal adsorbed solution theory
IL	ionic liquid
IUPAC	International Union of Pure and Applied chemistry
MMM	mixed-matrix membrane
MOF	metal-organic framework
NLDFT	non-local density functional theory
NUS	National University of Singapore
PAF	porous aromatic framework
PIM	polymer of intrinsic microporosity
POP	porous organic polymer
PPN	porous polymer network
RT	room temperature
SEM	scanning electron microscopy
SNW	Schiff base network
STP	standard temperature and pressure
T_g	glass transition temperature
wt%	weight percent

Table of contents

1. Introduction

1.1. Gas separation membranes

Membranes are permeable thin layers, that can exhibit selective properties. The main driving forces for the separation of a mixture are concentration, pressure, temperature or the electrochemical gradient.[1] In addition to biological membranes, including cell membranes, artificial membranes can be based on ceramics, glasses, or polymers. Due to the wide range of possible variations of the membrane material and their preparation methods, applications for various separation processes are possible including liquid phase separations such as the desalination of seawater, the rejection of dyes or the separation of gas mixtures.[2,3,4]

Gas separation membranes in particular are receiving increased attention due to their industrial and environmental relevance. Since development of the first industrial application of a hydrogen separation membrane in the 1980s,[5] membranes have been a subject of continuous development in terms of gas separation performance and stability. The broad spectrum of natural or anthropogenic gas mixtures leads to a variety of different separation issues, such as, to name the most currently important ones, the separation of carbon dioxide and methane (CO_2/CH_4), carbon dioxide and nitrogen (CO_2/N_2) or oxygen and nitrogen (O_2/N_2). The main application for CO_2/CH_4 separation is natural gas sweetening or biogas upgrading, where CO_2 (and H_2S) removal is necessary in order to enhance the energy content and lower the corrosive properties.[6] A reduction of CO_2 emissions into the atmosphere can be achieved by the cleaning of flue gas, where CO_2 is separated from a mainly nitrogen containing gas stream. In addition to conventional methods of amine scrubbing with mono- or diethanolamine, the application of membranes offers lower energy requirements.[7] With regard to O_2/N_2 separation, which can be used to separate the two gases from air, membrane-based separation processes are considered to be an emerging alternative to cryogenic distillation and pressure swing adsorption (PSA), since this approach can also benefit from lower costs and less energy consumption.[8,9]

These examples, selected from a much broader range of potential applications, highlight the reasons for the interest in developing new membrane materials and emphasize the importance and benefits of improving membrane performance.

1.1.1. Characteristics for membrane-based gas separation

Gas separation membranes act as selective barriers to an incoming gas mixture, typically referred to as the feed gas stream. The gas stream is divided into the permeate, that passes through the membrane, and the retentate, which is retained by the membrane. Figure 1 schematically shows the functional principle of a gas separation membrane:

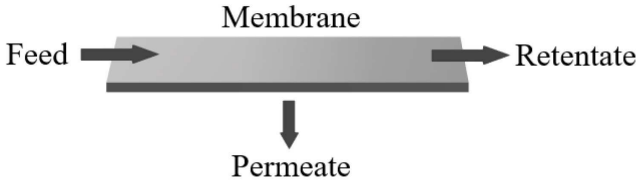

Figure 1: Principle of gas separation with a membrane.

The gas separation performance is mainly characterized by two factors: permeability (P) and selectivity (α or S). Permeability of a gas A (P_A) is defined as a product of the $flux_A$ (quotient of the flow rate and the membrane area) and the membrane thickness (d) divided by the transmembrane pressure (Δp_A) of the gas:[10]

$$P_A = \frac{flux_A \times d}{\Delta p_A} \tag{1}$$

Concerning dense membranes, the permeability of a gas A (P_A) can also be described as the product of the solubility (S_A) and the diffusion coefficient (D_A):

$$P_A = S_A \times D_A \tag{2}$$

The thermodynamic parameter S_A provides information about the sorption, and the kinetic parameter D_A about the mobility of a gas in the membrane.

An established unit for permeability is Barrer, which is defined as volume of a gas that permeates over a certain time (gas flow rate) through a defined membrane area with a certain pressure difference multiplied by the thickness of the material:[11]

$$1\ Barrer = 10^{-10}\ \frac{cm^3(STP)\cdot cm}{cm^2\cdot s\cdot cmHg} \tag{3}$$

If an exact determination of the membrane thickness is not possible, permeance is frequently used. This thickness independent unit is called the gas permeation unit (GPU):

$$1\ GPU = 10^{-6}\ \frac{cm^3(STP)}{cm^2\cdot s\cdot cmHg} \tag{4}$$

In other words, permeability can be described as the thickness-normalized permeance or the thickness- and pressure-normalized flux.

The selectivity is a dimensionless size and is described by the ratio of the permeability (or permeance) of two gases. The ideal selectivity α_{ideal} for the gases A and B is defined as:

$$\alpha_{ideal} = \frac{P_A}{P_B} \tag{5}$$

Selectivity can be determined either as the ideal selectivity or the real selectivity. By application of mixed-gas measurements, competitive adsorption of the gases is considered. The resulting real selectivity α_{real} is determined by following equation,

$$\alpha_{real} = \frac{(x_A/x_B)_{permeate\ side}}{(x_A/x_B)_{feed\ side}} \tag{6}$$

where x_A and x_B are the mole fractions of the gases A and B on the permeate and feed side.

1.1.2. Gas diffusion mechanisms

The mechanism of gas diffusion is highly depended on the membrane material, which can be classified as porous or nonporous. There are five types of mechanisms, which are graphically condensed in Figure 2. For porous membranes the main mechanisms are Knudsen diffusion, surface diffusion, capillary condensation and molecular sieving. Of the five, the main mechanism for gas transport through dense membranes is the solution-diffusion mechanism.

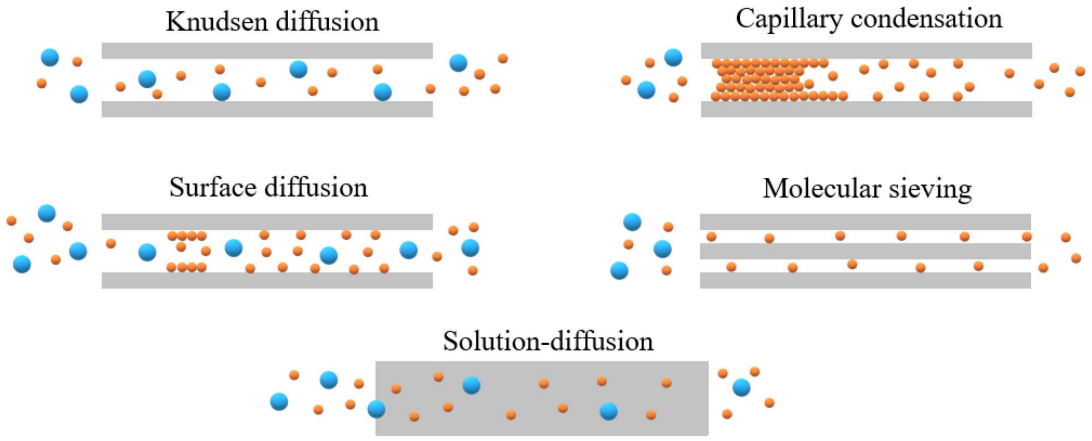

Figure 2: Types of diffusion mechanisms for porous membranes and the solution-diffusion mechanism for dense membranes.

Knudsen diffusion can be defined by the Knudsen number (K_n), which is the ratio of the mean free path of a gas molecule and the pore radius of the membrane. If K_n is larger than 10, mainly

lighter gas molecules pass through the pores. For $1<K_n<10$ the permeation consists of Poiseuille flow and Knudsen diffusion and if K_n is smaller than 1, mainly viscous flow appears, which makes the membrane non-selective.[12] Surface diffusion takes place, when gas molecules get adsorbed on the pore walls and move along the surface. If one gas species of a mixture is more strongly adsorbed, the selectivity can be increased. Capillary condensation appears, if the pores of the membrane are filled with a condensed phase. Depending on the degree of filled pores, the selectivity may also be influenced.[13] Molecular sieving is the separation of molecules determined by the kinetic diameter of the gas molecules. If the pore size of the membrane material becomes smaller than the kinetic diameter of a gas molecule, gases with bigger kinetic diameters are held back. Generally, membranes with pore sizes ranging from 3.0 and 5.2 Å can enhance the selectivity of different gas pairs.[12]

For non-porous (dense) membranes the solution-diffusion model is a well-established mechanism.[14] In contrast to porous membranes, permeability depends on the ability of a gas molecule to dissolve in the membrane material and pass through the membrane by diffusion. When the dissolved amounts of two gases and the diffusion rate differ a selective behavior of the membrane is given.

1.1.3. Membrane classifications

Membranes are principally categorized according to their structure or the material they consist of. An overview of the hierarchical division into structure and material is given in Figure 3.

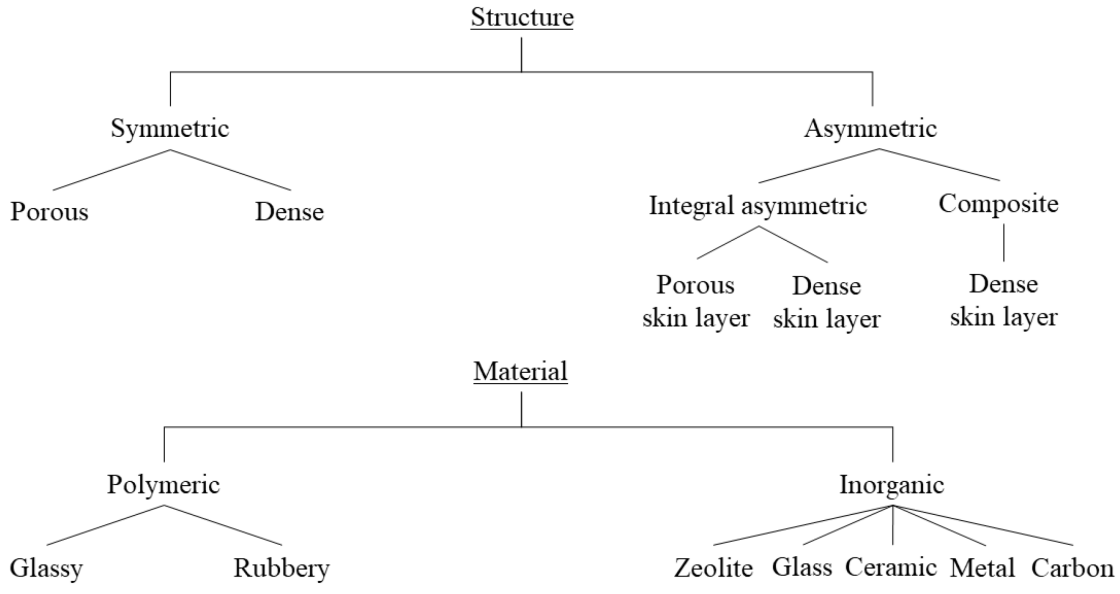

Figure 3: Membrane classifications according to structure and material.

The structures in which membranes can be present are subdivided into symmetrical and asymmetrical (also called anisotropic). Symmetrical membranes can consist of homogeneous porous structures or appear in form of dense membranes. Asymmetric membranes prepared from one material result in integral asymmetric membranes with porous or dense skin layers.[15] Asymmetric composite membranes consist of different materials and are prepared by adjusting a thin selective layer on a porous support in order to achieve an optimal combination of high permeability and good mechanical stability.[16]

Categorization of synthetic membrane materials involves the division into the two major classes: inorganic and polymeric. Inorganic membranes are made from zeolites, silica glass, ceramics, (porous) metals or carbon-based materials such as carbon molecular sieves (CMS), or carbon nanotubes.[17,18] In the category of inorganic membranes there are both porous and dense materials. Compared to porous inorganic membranes, their dense relatives often exhibit higher selectivity and lower permeability. They are mainly used for specialized application like hydrogen separation in the case of palladium-based membranes, or oxygen separation for perovskite-based ($CaTiO_3$ structure type) membranes.[19] Currently, most of the industrially applied membranes are polymeric, which will be discussed more detailed in the next section.

1.1.4. Polymeric membranes

Membranes manufactured from polymeric materials are gaining great industrial attention due to the advantages of low manufacturing and maintenance costs, and simple operating processes.[20] Permeability and selectivity can be tuned by changes in the chemical structure or morphology of the polymer. Further, it is possible to prepare composite membranes with more than one layer. Due to their dense character, gas transport properties can be described by the solution-diffusion model accompanied with Knudsen diffusion. Polymeric membranes can consist of rubbery or glassy polymers, that exhibit significant differences in their gas separation behavior. Polymers in the rubbery state are amorphous materials used above their “softening” temperature, the so-called glass transition temperature (T_g). Early studies in the field of gas separation were already being carried out in the 19th century. Rubbery polymers like “India-rubber” (natural rubber) were used by Thomas Graham to investigate the permeability of different gases.[21] In the middle of the 20th century a variety of synthetic polymers, including rubbery and glassy polymers, could be synthesized and thus became accessible for the preparation of membranes.

Permeability and selectivity of a membrane are dependent on its free volume and chain flexibility. The free volume is the unoccupied space between the polymeric chains and, depending on its amount and distribution, it can enhance the membrane performance. In most cases, rubbery polymers have a higher permeability and glassy polymers exhibit a higher selectivity due to lower free volume and less chain mobility. The decision whether to apply a rubber-like or glass-like polymer must also be made in consideration of the specific gas mixture composition of the feed stream.

For glassy polymers, the determining step for permeability enhancement is diffusion due to the rigid properties of the polymer chains. Consequently, the permeation of smaller molecules such as H_2 or CO_2 is positively affected.[22] The kinetic diameter, which is associated with the mean free path, can be given as a comparative value. Table 1 shows the widely quoted kinetic diameters determined by Hirschfelder, Curtiss, and Bird,[23] and those obtained by quantum mechanical (QM) calculations.[24]

Rubbery polymers show the opposite trend: larger molecules such as ethylene, preferentially permeate. For rubbery membrane systems, solubility dominates and significantly determines the permeability of the respective gas. This makes condensability, which is correlated with the critical temperature (T_c), an important factor, since gases with higher condensability are more soluble in the polymer and can thus lead to higher permeability.

Table 1: Kinetic diameter,[23,25] QM diameter[24] in Å and critical temperature (T_c)[26,27] in K of frequently separated gases.

Gas	Kinetic diameter [Å]	Kinetic diameter, QM [Å]*	Critical temperature, T_c [K]
H_2	2.89	2.88	33.23
CO_2	3.30	3.47	304.20
O_2	3.46	3.34	154.80
N_2	3.64	3.58	126.30
CH_4	3.80	4.05	190.60
Ethylene	3.90	-	281.10
Propane	4.30	-	369.85

* determined by iso-electron density surfaces

Membranes made from glassy polymers, which are used below their T_g (state of non-equilibrium), are generally more effective for separation processes.[28] Nevertheless, long-term stability and industrially specified pressures should be considered as well as the avoidance of

CO_2-induced plasticization, that increases the chain flexibility of the polymer, resulting in lowered selectivity.[29]

Some of the most frequently used polymers for gas separation are depicted in Figure 4. Polysulfone (PSF), poly(methylmethacrylate) (PMMA), poly(vinylalcohol) (PVA), poly(etheretherketone) (PEEK), PIM-1 (polymer of intrinsic microporosity), polybenzimidazole (PBI), as well as the polyimides BTDA/DAPI (Matrimid), 6FDA/ODA, 6FDA/DAM and BPADA/mPDA (Ultem) are all glassy polymers. In addition to commercial names, polymers can be named after their monomer molecules. In the case of Matrimid, the polymer is named BTDA/DAPI, derived from the monomers benzophenone tetracarboxylic dianhydride (BTDA) and a methylated diaminophenylindane species (DAPI). Poly(amide-b-ethylene oxide) (Pebax 1657) and polydimethylsiloxane (PDMS) belong to the category of rubbery polymers with glass transition temperatures of –40 °C[30] and –150 °C,[31] respectively.

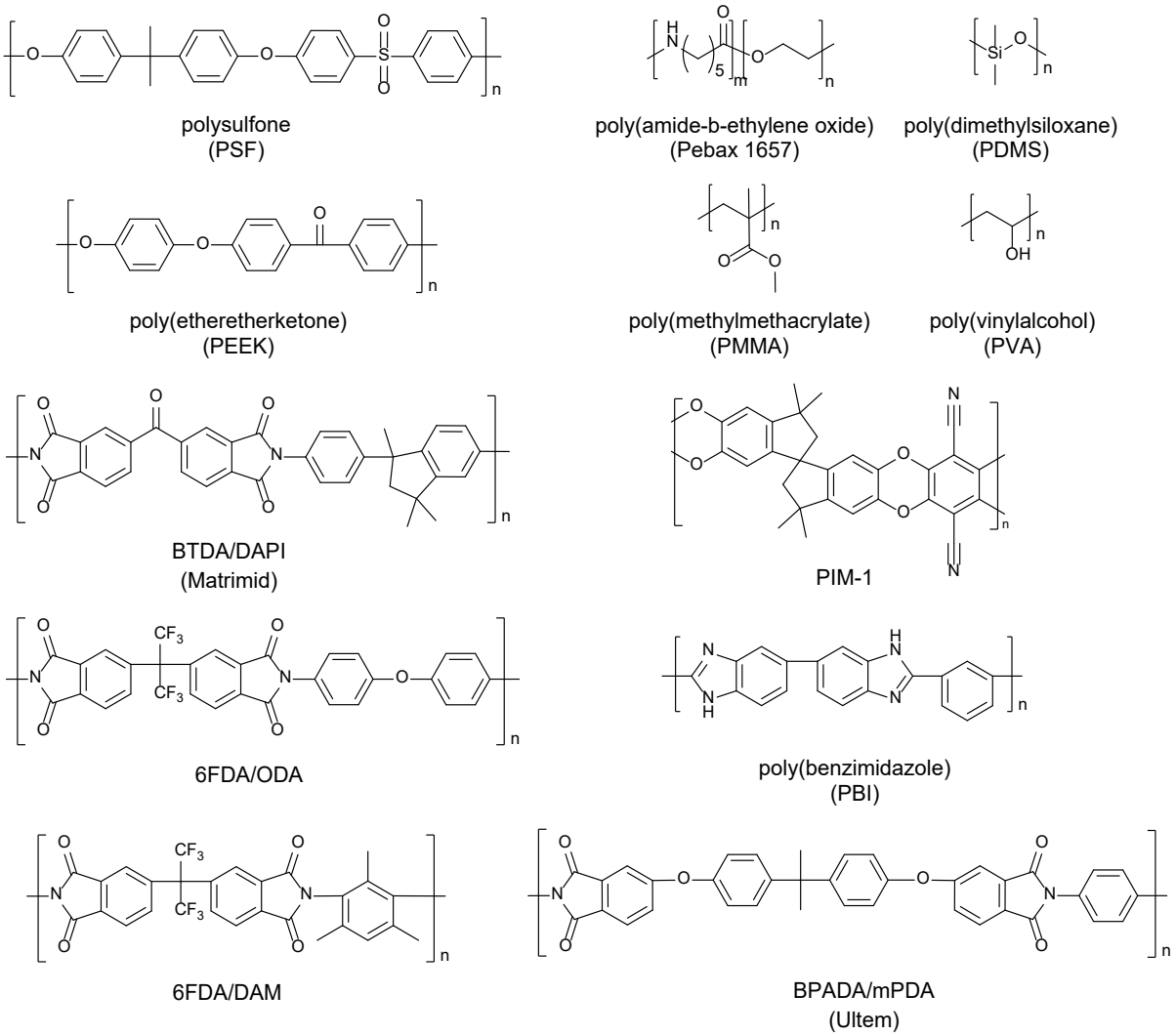

Figure 4: Selection of polymers frequently applied for membrane preparation.

1.1.5. Mixed-matrix membranes

Mixed-matrix membranes (MMMs) consist of a continuous polymer phase (matrix) and a dispersed particle phase (filler material). The first research on MMMs was conducted by Paul *et al*. in 1973, using silicone rubber as a matrix in which crystalline aluminosilicate particles were dispersed.[32] Since then, a variety of different zeolites[33] and mainly other porous materials have been applied as filler materials. CMSs,[34] activated carbons,[35] metal-organic frameworks (MOFs)[36] and porous organic polymers (POPs)/ covalent organic frameworks (COFs)[37] were used to improve membrane performance in order to overcome the Robeson upper-bound limit (Figure 5)[38,39] that describes the permeability-selectivity trade-off relationship. Depending on the gas pair, the upper limit can vary in slope and position, however, the aim is to increase the performance of the membrane, in the best case, both in permeability and selectivity.

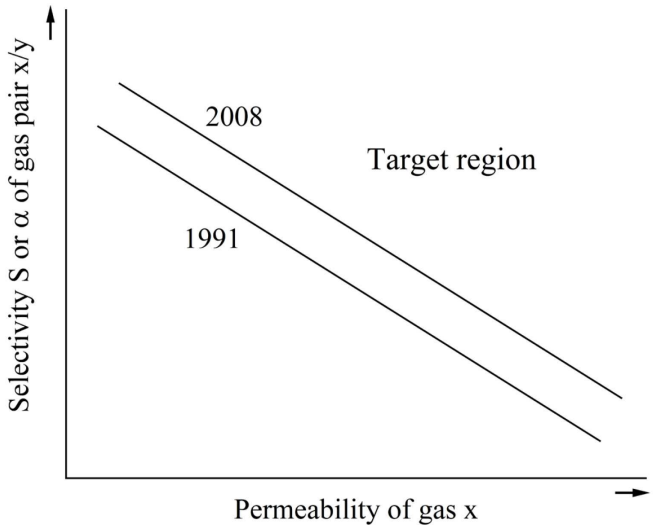

Figure 5: Selectivity of a gas pair (x/y) with x as the gas with the higher permeability against the permeability of gas x. The 1991 and 2008 Robeson upper bounds are shown schematically.

There are three common preparation methods for MMMs.[40] In the case of solution blending,[41,42] the filler material is dispersed in the polymer solution by stirring. The MMM is casted and the solvent is removed. For this method, controlling the evaporation time of the solvent is crucial, since otherwise the risk of sedimentation or aggregation of the filler particles can occur. Another method is in-situ polymerization.[43] This procedure involves mixing the filler particles with the organic monomers in a first step, followed by the polymerization of the monomers.[44] Since aggregation of filler particles can also occur with the in-situ polymerization method, the sol-gel process should be mentioned as an alternative since this preparation method generally leads to more homogeneous membranes. In this process, the precursors of the filler

particles are mixed either with organic monomers or the polymer in a solution to subsequently form nanoparticles in the polymer matrix.[45]

Regarding all of the preparation methods mentioned above, it is desirable to obtain MMMs with an ideal filler/polymer compatibility. The performance of a MMM strongly depends on the morphology of the filler-polymer interface. In general, there are three types of undesirable effects that can affect membrane performance (Figure 6).[46]

For example, if the adhesion between filler material and polymer is not sufficient, interfacial voids can form.[47] In this case, the gas molecules preferentially penetrate through the voids. This also applies to a gas which is normally less able to permeate through the membrane. Consequently, if the void volume is too large, the selectivity of the gas pair will be reduced.

Another case is the formation of rigidified polymer areas near the filler particle.[48] Due to the adsorption of the polymer on the surface of the filler particle, the chain mobility of the polymer is reduced, which in most cases can lead to a decrease in permeability, but to a higher selectivity.[49]

Pore blockage can reduce the permeability enhancing properties of the filler material to some extent or even eliminate these properties entirely. In most cases, the selectivity is the same as for the pure polymer, but the permeability decreases compared to the application of filler materials with open pores. The extent of this effect correlates with the degree of blockage and therefore on the pore size of the filler material and the extent to which the polymer diffuses into the pores.[50]

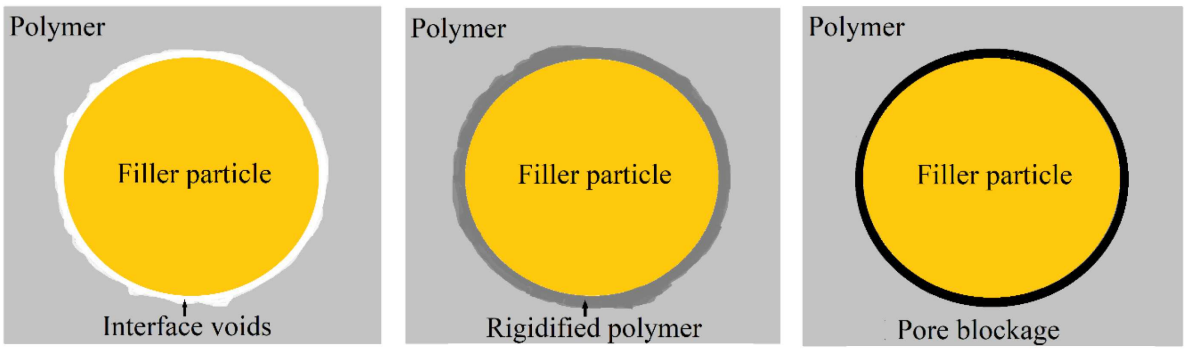

Figure 6: Schematic representation of possible arrangements of the filler particles and the polymer. Based on illustration in [46].

It is possible to predict the permeability of MMMs through the application of theoretical models. The theoretical changes in permeability due to the incorporation of a filler material can be predicted by a variety of models. The most common one is the Maxwell model, which was

originally applied for modelling the electrical conductivity of composite materials.[51] If one assumes, that all filler particles are ideally distributed in the MMM and manifest as uniformly of a spherical shape, the model can be applied for volume fractions of the dispersed phase (ϕ_d) up to 0.2,[52]

$$P_{eff} = P_c \left[\frac{P_d+2P_c-2\phi_d(P_c-P_d)}{P_d+2P_c+\phi_d(P_c-P_d)}\right] \quad (7)$$

where P_{eff} stands for the effective permeability of the MMM, P_d for the permeability of the dispersed phase and P_c for the permeability of the continuous phase, the neat polymer membrane. For the case $P_d >> P_c$ equation 7 can be simplified to:

$$\frac{P_{eff}}{P_c} = \frac{1+2\phi_d}{1-\phi_d} \quad (8)$$

If volume fractions of the filler material increase, filler-filler-interactions can occur, that can have influence on the gas transport characteristics. For the case $\phi_d > 0.2$, the Bruggeman model can be applied, which was originally developed for the prediction of dielectric constants in composites.[53] The simplified form is expressed by the following equation:

$$\frac{P_{eff}}{P_c} = \frac{1}{(1-\phi_d)^3} \quad (9)$$

Both models assume an ideal morphology. Therefore, the filler material should have a good compatibility with the polymer. If repulsive interactions occur interfacial voids are formed, which lead to free volume (void volume). As a consequence, permeability increases, but selectivity decreases up to the formation of completely non-selective membranes. If, on the other hand, pore openings of the filler particles are partially filled with polymer chains, the pore openings are blocked, resulting in a loss of permeability. Insufficient compatibility of the components can also result in stiffening of polymer chains around the filler particles, causing a reduction in diffusion and consequently a reduction in permeability. The filler materials most commonly used to date are inorganic or inorganic-organic in nature. However, it has been shown that organic filler materials and polymers in particular have the advantage of a good compatibility.[54] In the following chapter, porous materials are presented with the main focus on POPs.

1.2. Porous materials

Porous materials possess an external and an internal surface area. The latter includes the surface of the pore walls of the material and the corresponding void volume, which is defined as the pore.[55] According to the International Union of Pure and Applied Chemistry (IUPAC), pores are divided into different classes based on their diameter. Nanopores are present, if the pore diameters are smaller than 100 nm. Those can be further classified according to their diameter into micropores (<2 nm), mesopores (2-50 nm) and macropores (>50 nm).[56]

The group of porous materials includes organic materials such as POPs, and inorganic materials such as zeolites, or hybrid materials such as MOFs.[57] The porous materials studied in the present work belong to the class of POPs. These can be defined as 2D- or 3D-linked polymers, which consist of light-weight elements such as boron, carbon, nitrogen and oxygen.[58] The classification of POPs into different categories results in an overlapping, that is due to their classification according to different characteristics of the polymers. The naming convention can be based on the material properties such as the type of pores that occur, the structure of the polymer, or the type of linker/knot applied. Conjugated microporous polymers (CMPs),[59] COFs,[60] covalent triazine frameworks (CTFs),[61] element organic frameworks (EOFs),[62] porous aromatic frameworks (PAFs),[63] PIMs,[64] porous polymer networks (PPNs)[65] and Schiff base networks (SNWs)[66] all represent common subcategories of POPs. Adjusting the pore size or introducing functional groups provides a basis for various potential applications, such as gas separation and storage,[67,68] removal of contaminants,[69,70] and catalysis,[58] and also enables the application as sensors[71] and electrode materials.[72]

1.2.1. Covalent triazine frameworks

The network character and thus porosity of CTFs results from the linkage of triazine units, more precisely 1,3,5-triazine, with different linker molecules. In 2008, CTF-1 was synthesized via an ionothermal trimerization reaction.[61] Ionothermal reactions are generally catalyzed by the Lewis acid catalyst $ZnCl_2$, which also serves as a solvent and porogen. In the case of CTF-1, the triazine units are formed in situ by the conversion of the cyano-functionalized linker benzene-1,4-dicarbonitrile (Figure 7). Temperatures of 300 to 700 °C during the reaction yield highly porous products, but an associated partial carbonization can lead to the well-known problem of too low nitrogen contents compared to the theoretically calculated values.[73]

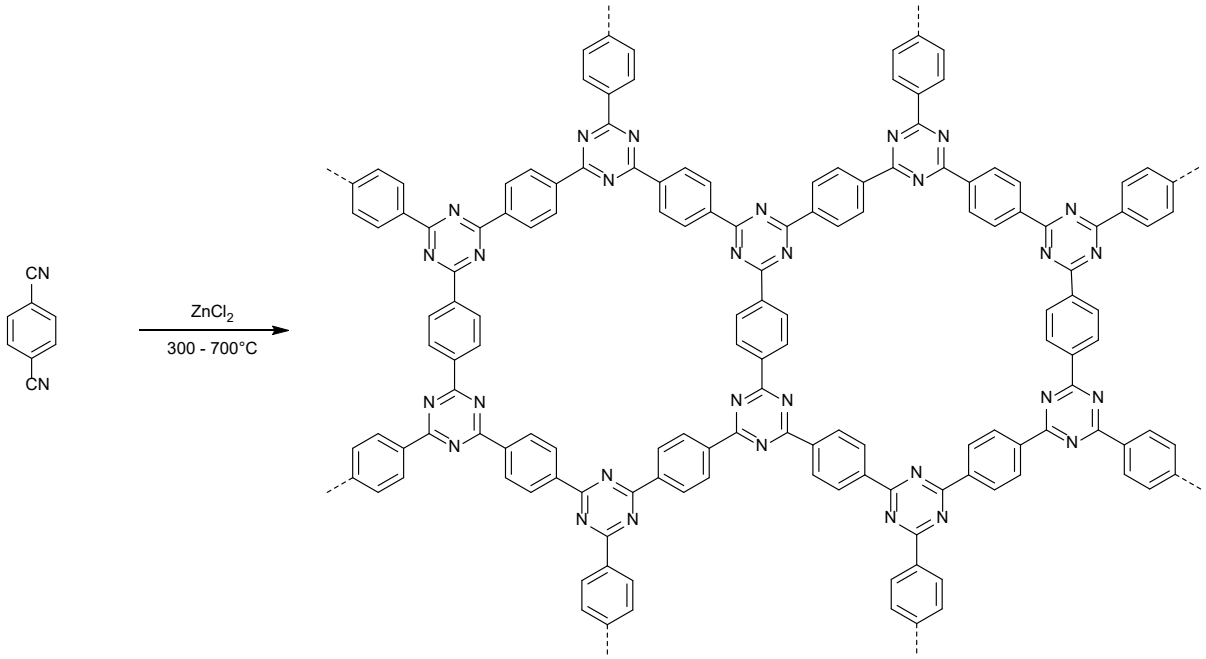

Figure 7: Schematic representation of the ionothermal synthesis of CTF-1.

The formation of triazine rings by the trimerization reaction from nitrile compounds can also be catalyzed by strong Brønsted acids. This method was first mentioned in 1966 by Anderson and Holovka, who synthesized thermally resistant polymers from aromatic dinitriles by a trimerization reaction with chlorosulfonic acid.[74] At this point, it is clear that the syntheses of those polymers, which are now known as CTFs, were carried out decades earlier. The synthesis of CTF-1 in 2008 marked the beginning of intensive research in this field.[61] From that point on, the potential of these compounds in a wide variety of applications was more comprehensively recognized and more thoroughly investigated. In 2012, Ren *et al.* applied the Brønsted acid catalyzed synthesis method and obtained highly porous CTFs from different aromatic linkers. The use of trifluoromethanesulfonic acid made it possible to carry out the synthesis under room temperature and microwave-assisted conditions. The application of 4,4′,4″,4‴-methanetetrayltetrabenzonitrile as an educt led to a CTF with a high Brunauer-Emmet-Teller (BET) surface area of 1152 m^2/g with a CO_2 uptake of 75.39 cm^3/g at 273 K and 1 bar.[75]

The application of different linear, trigonal-planar, and tetrahedral reactant molecules allows two- and three-dimensional CTFs to be obtained by the trimerization reactions described above. The difference in the length of the monomers can affect, for example, the porosity and flexibility of the resulting CTF structure. Through variation of these functionalities, the chemical and physical properties of the resulting structure can be adjusted, allowing optimization with respect

to potential applications. Figure 8 depicts examples of linker molecules used for the ionothermal and/or Brønsted acid catalyzed method.

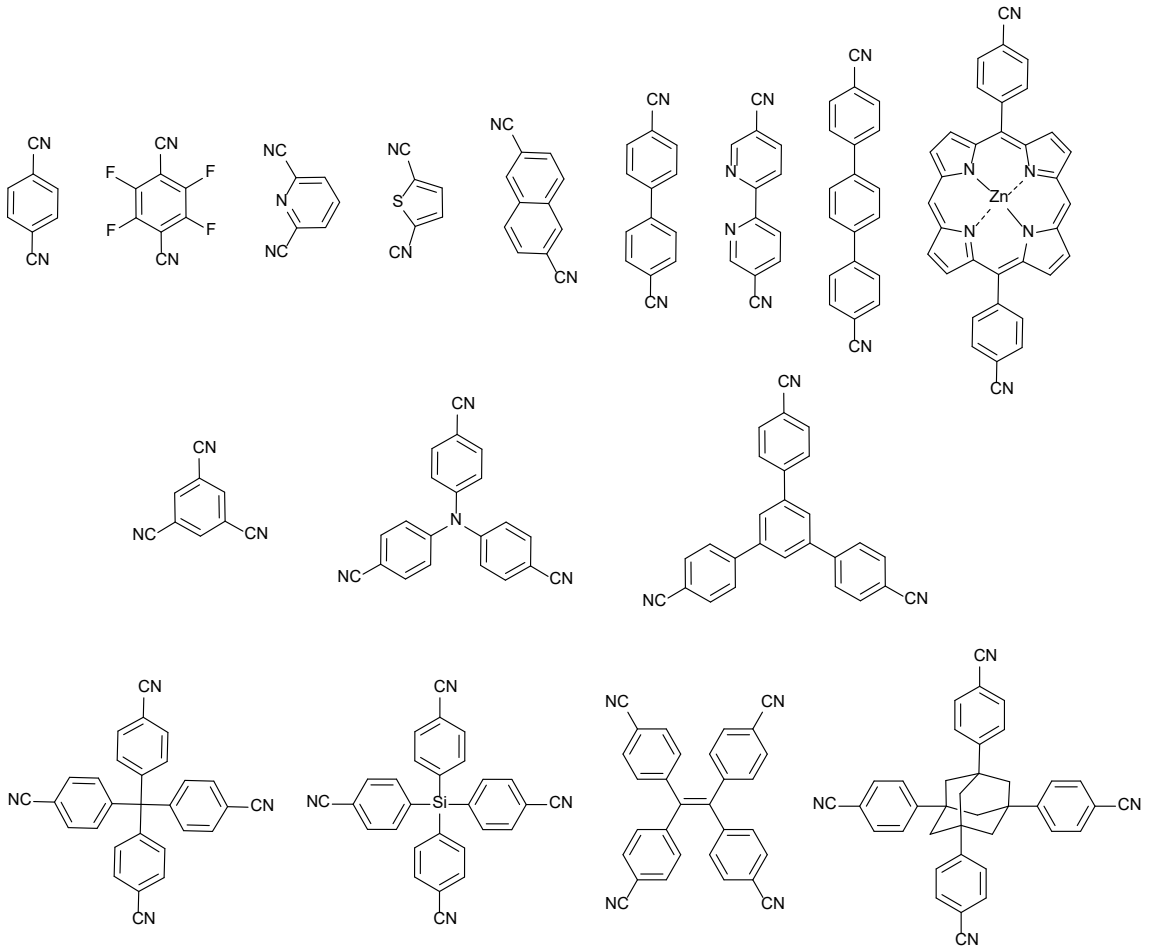

Figure 8: A selection of linear, trigonal-planar and tetrahedral reactant molecules for the ionothermal synthesis of CTFs.

Another possibility for CTF synthesis is the reaction starting from cyanuric chloride, where the triazine moiety is already present. By means of a Friedel-Crafts alkylation with a Lewis acid as catalyst, a C-C bond with non-functionalized linker molecules can be established. In 2012, three structures were synthesized from cyanuric chloride and the linkers benzene, biphenyl and terphenyl, respectively. A 24 h reaction in dichloromethane under reflux was carried out to yield three frameworks with BET surface areas ranging from 558 to 1266 m^2/g and CO_2 uptakes from 38 to 51 cm^3/g at 298 K and 1 bar.[76] Since then, a variety of different linker molecules (Figure 9) have been applied, including trans-stilbene,[82] 1,1,2,2-tetraphenylethylene,[77] fluorene,[78] dibenzofuran,[79] carbazole,[80] spirofluorene,[81] 1,3,5-triphenylbenzene,[82] tetraphenylsilane,[77] triptycene[78] and porphyrin[83].

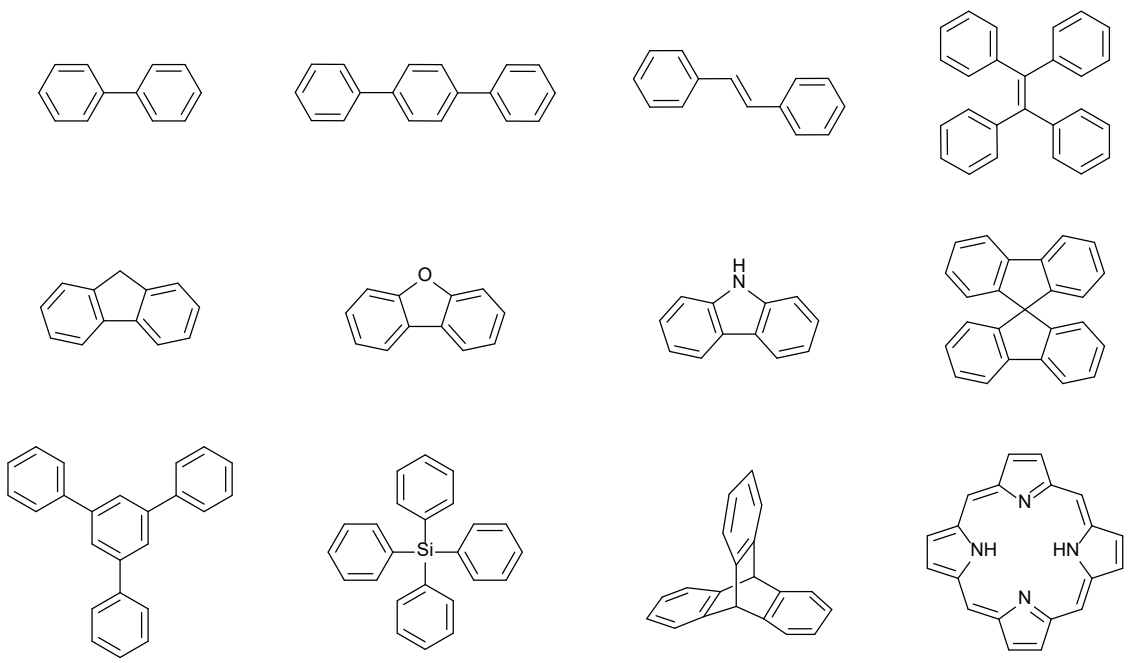

Figure 9: A selection of reactant molecules for the Friedel-Crafts synthesis of CTFs.

The advantage of the Friedel-Crafts synthesis approach is the low cost of cyanuric chloride and most linkers due to their availability as large-scale products. The ease of upscaling FC-synthesized CTFs compared to other synthetic routes, such as ionothermal synthesis, makes this route attractive for CTF applications. A solvent-free method is the mechanochemical Friedel-Crafts synthesis. The reactants, the Lewis acid catalyst and an optional bulking material are ground in either a planetary or vibrating mill. Using this method, the Borchardt group synthesized CTFs from different aromatic monomers. The CTF derived from the model substance carbazole, namely CTF-CBZ, was obtained in an 98% yield after a reaction time of 1 h and exhibited a BET surface area of 570 m^2/g.[84] Compared with the wet-chemical Friedel-Crafts reaction, the BET surface areas of the CTFs obtained by the mechanochemical reaction are generally lower, but it is possible to achieve a higher nitrogen content.

In 2017, another synthesis strategy for CTF materials was reported. A polycondensation reaction of aldehydes and amidines, which did not require temperatures higher than 120 °C and worked in absence of strong acids, was carried out to obtain the so-called CTF-HUSTs. For CTF-HUST-1, which corresponds to the structure of CTF-1, 1,4-phthalaldehyde and terephthalamidine dihydrochloride were applied as educts, with cesium carbonate (Cs_2CO_3) as base and dimethylsulfoxide (DMSO) as solvent. In addition to a narrow pore size distribution at about 12 Å, a BET surface area of 663 m^2/g was determined for CTF-HUST-1.[85] Based on this approach, variation of the synthesis made it possible to obtain CTFs with higher crystallinity with the required aldehydes formed in situ by oxidation of alcohol functionalized

monomers. Controlled oxidation of the resulting alcohol functionalities slowed down the nucleation and consequently enabled the formation of crystalline products. CTF-HUST-C1, which is corresponding to CTF-HUST-1, was synthesized from 1,4-benzenedimethanol instead of 1,4-phthalaldehyde. The analytical results confirmed a good crystallinity and the expected pore size of 12 Å. With a value of 599 m^2/g, the BET surface area was only slightly lower than that of CTF-HUST-1.[86]

A further synthetic method was described by Yu *et al.*, who applied phosphorus pentoxide (P_2O_5) as a catalyst for direct synthesis of a CTF from aromatic amides. P_2O_5 enabled the dehydration reaction from the amide components to the corresponding nitriles.[87] For the structure of the CTF-1 analogue pCTF-1, terephthalamide and P_2O_5 were flame-sealed in a glass ampoule and annealed at 400 °C. The resulting pCTF-1 was isolated in 84% yield and exhibited a high thermal stability up to 600 °C in TGA measurements under N_2 conditions. Gas sorption studies revealed a BET surface area of 2034 m^2/g and an CO_2 uptake of 111 cm^3/g at 273 K and 1 bar.[88]

The porous characteristics of CTFs open up a variety of potential applications. In particular, the high thermal and chemical stability resulting from strong covalent C=N-bonds makes them favorable materials for various applications, such as gas storage and separation, pollutant removal and heterogeneous catalysis.[89] A current field of application is the separation of CO_2 from gas mixtures as well as carbon capture and storage (CCS). The micropore volume and high intrinsic nitrogen content of CTFs are advantageous for these applications. In particular, nitrogen-rich materials such as CTFs are a preferred choice due to quadrupole-dipole interactions between CO_2 and nitrogen atoms.[90] A strongly CO_2-philic CTF with an especially high CO_2 uptake of 7.65 mmol/g (171 cm^3/g) at 273 K and 1 bar was synthesized from triazole-functionalized perfluorinated aromatic trinitrile units (Tz-PFCN) via the ionothermal method. The high reaction temperature of 600 °C led to an in situ defluorination process and the thus the formation of high microporosity in the resulting structure Tz-df-CTF600.[91] CTF-FUM-350 synthesized from the short linker fumaronitrile, and HAT-CTF-450/600 synthesized from a nitrogen-doped methoxy-functionalized hexaazatriphenylene, exhibited high selectivity in gas separation. CTF-FUM-350 showed a CO_2/CH_4 selectivity of 20, calculated from the ratio of the initial slopes of the respective adsorption isotherms at 298 K.[92] The CO_2/N_2 selectivity of HAT-CTF-450/600 was calculated from the ratio of the initial slopes of CO_2 and N_2 adsorption isotherms to be 160 at 273 K. From the isotherms measured at 297 K, CO_2/N_2 selectivity values of 126 and 110 were determined by the initial slope method and ideal adsorbed solution theory

(IAST) calculations, respectively.[93] These examples demonstrate the potential of CTFs for the removal and separation of components from gas mixtures. An effective way for these separations is a continuous separation process, which can be realized by applying membrane materials. The incorporation of CTFs or COFs as filler materials in polymer membranes thus makes a continuous and more efficient separation of gases possible.

1.2.2. Imine-linked covalent organic frameworks

COFs are characterized by permanent porosity, crystallinity, and high thermal stability due to the covalent bonds. The basis for imine-linked COFs was laid with the synthesis of the first COF in 2005. Diboronic acid was applied in a one-step condensation reaction to form the structure of COF-1 (Figure 10). The two-dimensional structure exhibits a BET surface area of 711 m^2/g, accompanied by a pore volume of 0.32 cm^3/g. The covalent bonds between boron, carbon and oxygen lead to a high thermal stability up to a temperature of 500 °C.[60]

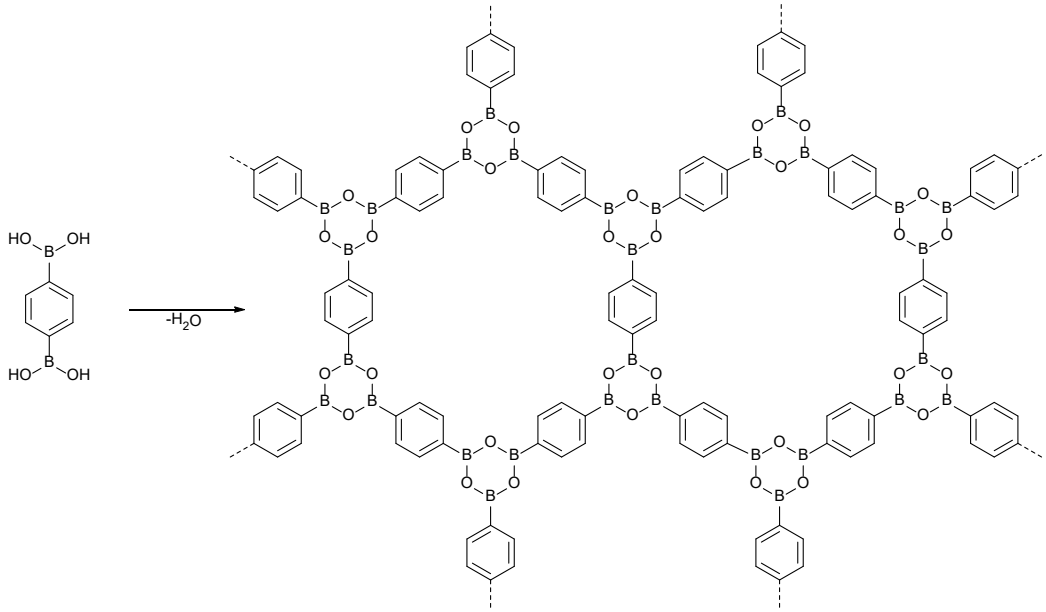

Figure 10: Schematic representation of the synthesis of COF-1 starting from diboronic acid.

In addition to this approach, resulting in a structure synthesized from only one educt molecule, various combinations of monomers can be applied. The choice of monomers thus determines the symmetry of the final structure, leading to triangular, tetragonal or hexagonal lattices. In addition to two-dimensional COFs, three-dimensional structures can be obtained by incorporating, for example, building blocks with a tetragonal geometry.

Besides the boroxine linkage mentioned above, other linkages, such as boronate-ester,[60] hydrazone,[94] azine,[95], imide[96] and imine linkages[97] are applied to design new COF materials.

In particular, imine-linked COFs have attracted attention in recent years due to their high nitrogen content, which makes them promising CO_2 adsorbents. The imine linkage is obtained by a Schiff base reaction, a condensation reaction between an aldehyde and an amine.

In 2009 Yaghi and coworkers synthesized COF-300 from terephthalaldehyde and tetra-(4-anilyl)-methane (Figure 11). A suspension of the two educts in a 10:2 (v:v) mixture of 1,4-dioxane and acetic acid (3 mol/L) was heated in an ampoule at 120 ºC for 72 h. Due to the linear and tetrahedral linker, a three-dimensional COF was obtained. The crystalline structure exhibited a high thermal stability up to 490 °C and a BET surface area of 1360 m^2/g.[97] Nine years later, three-dimensional imine-linked COFs, including COF-300, were successfully obtained as a single crystal. By using an excess of aniline, which acts as a competitive modulator, the reversible imine formation could be slowed down. In this way it was possible for the first time to produce sufficiently large single crystals, allowing them to be more precisely characterized by means of single-crystal x-ray diffraction.[98]

Another imine-linked COF, COF-LZU1, was synthesized from 1,3,5-triformylbenzene and 1,4-diaminobenzene in an analogous synthesis procedure with 1,4-dioxane as solvent and acetic acid as catalyst (Figure 11). The resulting network with hexagonal pores and a layered-sheet arrangement was stable up to 310 °C. From N_2-soption measurements a BET surface area of 410 m^2/g was calculated and the pore size distribution based on nonlocal density functional theory (NLDFT) revealed a narrow distribution at around 1.2 nm pore width. In addition, post-treatment with palladium acetate was carried out, which yielded Pd/COF-LZU1. The resulting compound was utilized for Suzuki-Miyaura coupling reactions and revealed high catalytic activity along with high stability.[99]

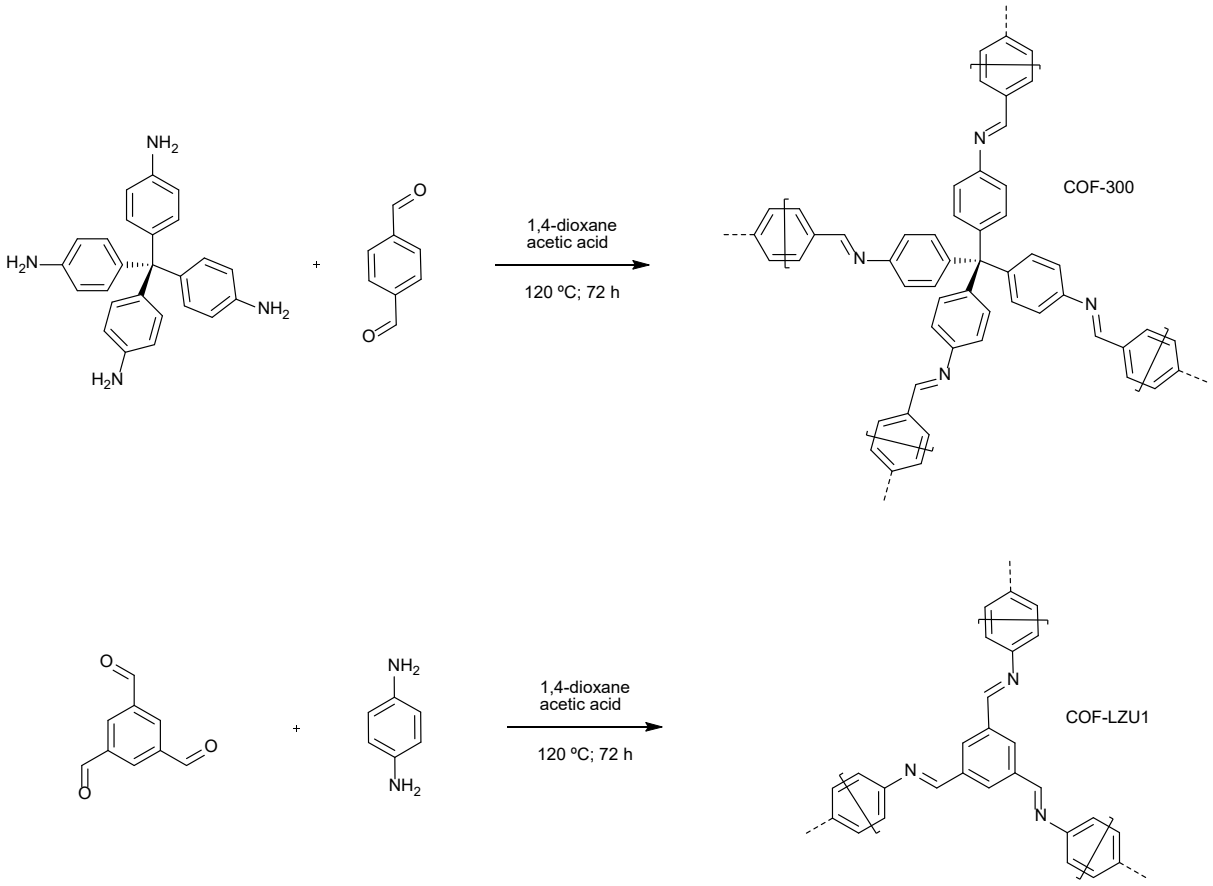

Figure 11: Schematic representation of the synthesis of COF-300[97] and COF-LZU1.[99]

Gomes *et al.* found a way to synthesize an imine-linked COF, named TRITER-1 (Figure 12), under reflux conditions. 1,3,5-tris-(4-aminophenyl)triazine (TAPT) and terephthalaldehyde were reacted in a 12 h reflux synthesis in dimethylformamide (DMF). The resulting structure exhibited a BET surface area of 716 m^2/g and an average pore width of 1.7 nm due to the larger amine compound compared to COF-LZU1. The high porosity and elevated nitrogen content due to the triazine ring and the imine functionality of TRITER-1 led to an CO_2 uptake of 58.9 wt% (13.38 mmol/g) at 273 K under 5 bar pressure.[100]

Two fluorinated COFs were synthesized by changing the terephthalaldehyde linker to 2,3,5,6-tetrafluoroterephthalaldehyde (TFTA). The use of TAPT and 1,3,5-tris(4-aminophenyl)benzene (TAPB) as knots yielded the two COFs SCF-FCOF-1 (Figure 12) and SCF-FCOF-2. A three-day synthesis was carried out in an ampoule with the solvents mesitylene and 1,4-dioxane (1:1; v:v) and no catalyst was necessary. SCF-FCOF-1 and SCF-FCOF-2 exhibited very high BET surface areas of 2056 and 1245 m^2/g with large pore volumes of 1.69 and 0.64 cm^3/g, respectively. Both structures showed a main pore size of 3.5 nm and were stable up to over 400 °C. The crystalline materials were further tested for selective sorption of cationic

dyes. SCF-FCOF-1 exhibited high uptake capacities for the dyes malachite green, crystal violet, and rhodamine B with values of 2701 mg/g, 1106 mg/g, and 1044 mg/g, respectively.[101]

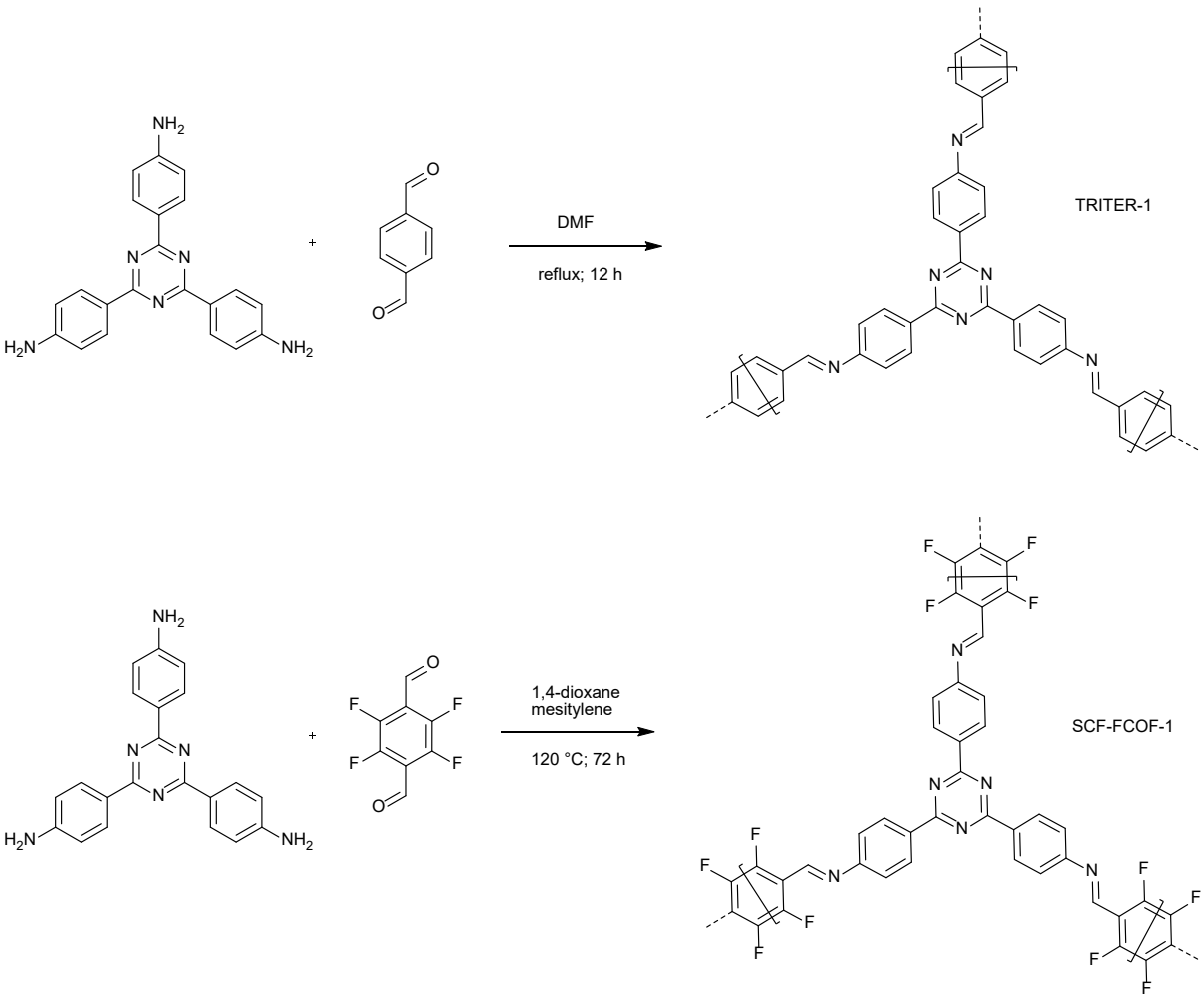

Figure 12: Schematic representation of the synthesis of TRITER-1[100] and SCF-FCOF-1.[101]

As in the case of CTFs, the high thermal stability and permanent porosity of these materials make them suitable for the application as filler materials in MMMs, which will be described in the following chapter.

1.3. COFs/CTFs as filler materials in MMMs for gas separation

MMMs are prepared by dispersion of a filler material in a polymer matrix. The COF or CTF material, which represents the filler material or dispersed phase, has influence on the behavior of a permeating species. The additional passage created by incorporating porous materials can lead to a higher permeability of one permeate component and thus to a higher selectivity if one component permeates preferentially. A variety of COFs and CTFs have been applied as filler materials in MMMs for different applications like dehydration of ethanol,[102] removal of dyes,

protein retention[103] or the separation of the gas mixtures e.g. CO_2/N_2,[104] CO_2/H_2, CO_2/N_2.[105] The focus of this work is on gas separation, more specifically the separation of CO_2 and CH_4. For this reason, a selection of COFs/CTFs for CO_2/CH_4 separation is described. The performance of the MMMs in comparison to the pristine polymer membranes is given in Table 2.

Shan *et al.* used an azine-linked COF, ACOF-1, as dispersed phase and Matrimid as the continuous phase. The MMMs were applied for CO_2/CH_4 separation with an equimolar mixture of the respective gases. The application of 16 wt% ACOF-1 in the MMM resulted in an increase in CO_2 permeability from 6.8 Barrer for the pure polymer to 15.3 Barrer.[106]

COF-300 was chosen as the three-dimensional filler material to form MMMs with the polymers 6FDA-DAM and Pebax 1657. In both cases, a good interfacial compatibility of filler material and matrix was observed. The MMMs prepared from 10 wt% COF-300 and the glassy polymer 6FDA-DAM achieved an increase in CO_2 permeability from 767 Barrer for the pure polymer membrane to 2842 Barrer. The corresponding MMM made from the rubbery polymer Pebax achieved an increase in CO_2 permeability from 73 to 107 Barrer.[107]

A melamine-based COF, named SNW-1, was incorporated into membrane matrices made of the polymers PIM-1, PSF and 6FDA-ODA. In all cases, permeability and selectivity were improved. PIM-1 is a polymer exhibiting superior permeability, but a relatively low selectivity compared to other commercially available polymers. Single gas CO_2/CH_4 separation studies were carried out, and the application of 10 wt% of SNW-1 improved the performance of the MMM by almost 106 % for CO_2 permeability and 27 % for CO_2/CH_4 selectivity. However, the filler content is restricted to low wt%, and at higher filler contents (15 and 20 wt%) the performance of the MMMs decreased.[108] Similar observations could be made for SNW-1/PSF MMMs: the 12 wt% MMM showed the best performance in contrast to the one with 15 wt%, which showed a decrease in selectivity to values lower than that of the pure PSF membrane.[109] In another case, SNW-1 nanoparticles were added to a polyamic acid precursor solution, that was then thermally imidized to the polyimide 6FDA-ODA. The resulting MMMs showed maximum performance at a filler content of 5 wt%. When the SNW-1 content was increased to 7.5 wt%, separation performance of the MMM decreased. Field emission scanning electron microscopy (FESEM) images revealed aggregation of particles, that can promote the formation of interfacial voids and thus decrease the performance of the membrane.[110] These examples demonstrate the different behavior of the filler material in different polymers and underline the importance of a good compatibility between filler material and polymer.

The two COFs, NUS-2 and NUS-3, were also synthesized by aldehyde-amine condensation and transferred to the more stable isomorphs by keto-enol tautomerization. NUS-2 was synthesized from triformylphloroglucinol (TFP) and hydrazine hydrate. For NUS-3, hydrazine hydrate was replaced by 2,5-diethoxy-terephthalohydrazide (DETH). Both materials were used as filler materials in Ultem matrices, and the best membrane performance was achieved with 20 wt% of the COFs. CO_2 permeability and CO_2/CH_4 selectivity were increased from 2.1 Barrer and 19 to 4.4 Barrer and 34 for NUS-2 and 15 Barrer and 30 for NUS-3, respectively. Due to the larger linker molecule DETH, an average pore size of 21 Å was determined for NUS-3.The larger pores resulted in a higher CO_2 permeability as well as a reduced CO_2/CH_4 selectivity compared to NUS-2, which exhibited an average pore size of 9 Å.[111] From this example, the influence of the pore size of the filler material can be observed and, as already described in chapter 1.1.5, the trade-off relationship between permeability and selectivity becomes clear.

Biswal *et al.* presented two membrane systems TpPa-1@PBI-BuI and TpBD@PBI-BuI (5-t-butylisophthalic acid). High pressure CO_2/CH_4 separation at an upstream pressure of 20 atm resulted in CO_2 permeability and CO_2/CH_4 selectivity of 2.3 Barrer and 57.5 for the pure membrane, respectively. Incorporation of 50 wt% TpPa-1 and TpBD increased the permeability to 13.1 and 14.8 Barrer, respectively, but decreased selectivity to 40.3 and 48.7. In this case, it is also evident that although a high increase in CO_2 permeability was possible, the membrane performance may be degraded by a decreasing selectivity.[112]

From 2019 onwards, CTFs have also been applied as filler materials for the preparation of MMMs. Accordingly, there are only a few examples, especially in the field of CO_2/CH_4 separation. By incorporating the covalent triazine-piperazine polymer CTPP into a matrix of the polymer Pebax 1657, the CO_2-philicity of the membrane system could be increased. As a result, with a very low filler content of only 0.025 wt%, the CO_2 permeability was enhanced from 53 Barrer for the pure polymer membrane to 73 Barrer, accompanied by an increase in CO_2/CH_4 selectivity from 17 to 25.[113] A similar improvement in membrane performance was achieved by incorporating 2 wt% FCTF-1 into a PIM-1 matrix. In this case, CO_2 permeability was increased from 5800 to 7300 Barrer and CO_2/CH_4 selectivity from 11.5 to 16.6.[114]

The above examples demonstrate a promising way to optimize gas separation processes by applying organic filler materials such as COFs/CTFs. By combining these materials with polymer matrices, good compatibility can be achieved and it is possible to additionally benefit from the high thermal and chemical stability as well as the permanent porosity of the filler materials.

Table 2: CO_2 permeability and CO_2/CH_4 selectivity for COFs/CTFs as porous filler materials in different polymer matrices. A selection of the MMMs with the best membrane performance of the respective works is presented.

Filler material	Filler content [wt%]	Matrix	P CO_2 [Barrer]	S/α CO_2/CH_4	Ref.
-	-	Matrimid	6.8 ± 0.1[a]	30.5 ± 0.6[a]	106
ACOF-1	16	Matrimid	15.3 ± 0.7[a]	32.4 ± 1.8[a]	
-	-	6FDA-DAM	767 ± 24[b]	22.3 ± 2.1[b]	107
COF-300	10	6FDA-DAM	2842 ± 76[b]	24.6 ± 1.7[b]	
-	-	Pebax 1657	73 ± 4[b]	18.7 ± 1.2[b]	
COF-300	10	Pebax 1657	107 ± 6[b]	25.5 ± 1.3[b]	
-	-	PIM-1	3672[c]	10.6[c] (9.6)[*]	108
SNW-1	10	PIM-1	7553[c]	13.5[c] (12.9)[*]	
-	-	PSF	n.a.	n.a.	109
SNW-1	12	PSF	25.04[d]	27[d] (34)[**]	
-	-	6FDA-ODA	6.02[e]	8.99[e]	110
SNW-1	5	6FDA-ODA	12.43[e]	13.37[e]	
-	-	Ultem	2.08 ± 0.05[f]	18.9[f]	111
NUS-2	20	Ultem	4.41 ± 0.04[f]	33.9[f]	
NUS-3	20	Ultem	15.00 ± 0.10[f]	30.0[f]	
-	-	PBI-BuI	2.3[g]	57.5[g]	112
TpPa-1	50	PBI-BuI	13.1[g]	40.3[g]	
TpBD	50	PBI-BuI	14.8[g]	48.7[g]	
CTPP	-	Pebax 1657	53[h]	17[h]	113
	0.025	Pebax 1657	73[h]	25[h]	
FCTF-1	-	PIM-1	5800[i]	11.5[i]	114
	2	PIM-1	7300[i]	16.6[i]	

[a]Mixed gas, equimolar; 308 K; feed pressure 4 bar; [b]Mixed gas, equimolar; 25 °C; transmembrane pressure 1 bar; [c]Single gas; 30 °C; feed pressure 2 bar; [d]Single gas; 298 K; pressure drop 3.5 bar; [e]Single gas; 25 °C; upstream pressure 4 atm; [f]Single gas; 35 °C; gauge pressure 3.5 bar; [g]Single gas; 35 °C; upstream pressure 20 atm; [h]Single gas; 20 °C; feed pressure 2225 to 3000 Torr; [i]Single gas; 35 °C; feed pressure 1 atm; [*]Mixed gas CO_2/CH_4 30/70 vol%; 30 °C; feed pressure 2 bar; [**]Mixed gas CO_2/CH_4 volume ratio 1:1; 298 K; pressure drop 3.5 bar; Abbreviations: Ref. = reference; n.a. = not available

2. Aim of this thesis

CTFs and imine-linked COFs are porous materials favorable for gas storage and separation. The aim of this work is to synthesize these materials in order to apply the respective materials as filler materials in MMMs for gas separation.

To achieve this, the CTFs should be synthesized via Friedel-Crafts alkylation from cyanuric chloride and the linkers fluorene and biphenyl. New imine-linked COF materials should be synthesized via a Schiff base reaction. For this purpose, 1,3,5-tris-(4-aminophenyl)triazine should be applied as a knot compound and 4,4'-biphenyldicarboxaldehyde and the fluorinated analog 2,2',3,3',5,5',6,6'-octafluoro-4,4'-biphenyldicarboxaldehyd as linkers.

All materials should then be characterized by appropriate analytical methods. In terms of the planned applications, additional CO_2 and CH_4 sorption experiments should be performed to get an overview of each material's potential separation performance. For this purpose, the maximum uptake of the gases must be determined and the IAST selectivity can then be calculated.

Both CTFs and imine-linked COFs should be applied as filler materials in PSF and/or Matrimid matrices. After successful incorporation, the resulting MMMs can then be investigated regarding CO_2/CH_4 mixed-gas separation. The gas separation performance of the MMMs, including those prepared from CTF-1, should be further investigated by application of theoretical permeability models and calculation of the FFV.

3. Cumulative part

This chapter contains the results of this dissertation, which have been published in international journals. The listing is sorted by contribution to publication and appears in chronological order. Each publication stands separately and has its own bibliography. The content of each publication and the author's contribution to the work are summarized on the page preceding.

3.1. Covalent triazine framework CTF-fluorene as porous filler material in mixed matrix membranes for CO_2/CH_4 separation

Stefanie Bügel, Alex Spieß, Christoph Janiak

Microporous Mesoporous Mater. **2021**, *316*, 110941.

DOI: 10.1016/j.micromeso.2021.110941; [115]

The porous and highly stable filler material CTF-fluorene was applied as dispersed phase in MMMs. Its incorporation into PSF and Matrimid matrices led to a significant improvement in CO_2 and CH_4 permeability while maintaining selectivity. Compared with a CO_2 permeability of 5.4 Barrer for the pure PSF membrane, the permeability was increased to 12.8 Barrer with the 24 wt% CTF-fluorene/PSF MMM. With 24 wt% CTF fluorene embedded as a dispersed phase in a Matrimid matrix, an even higher increase in CO_2 permeability was achieved from 6.8 Barrer for the pure Matrimid membrane to 17.8 Barrer. Comparisons with theoretical permeability models were carried out, and FFV calculations confirmed the important role of free volume in improving the permeability of a MMM.

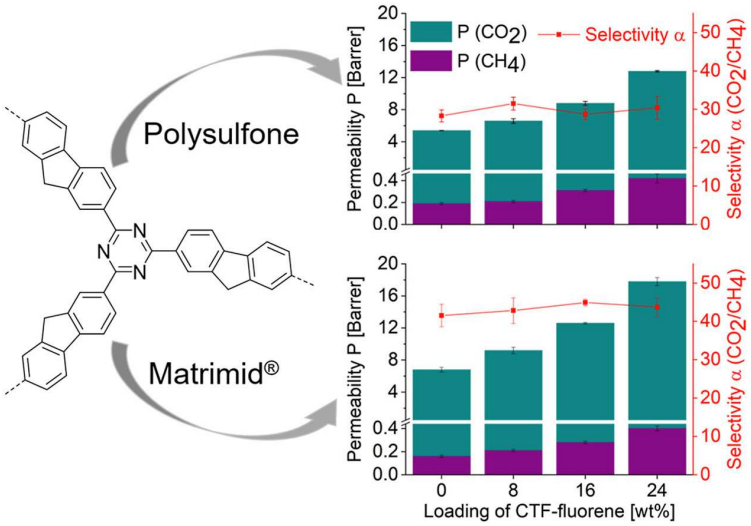

Author's contribution to the work:

- Idea and concept
- Experimental and analytical work
- Data interpretation
- Manuscript writing with corrections by C. Janiak
- A. Spieß: recorded SEM images

The work presented in this chapter has been published as:

Covalent triazine framework CTF-fluorene as porous filler material in mixed matrix membranes for CO_2/CH_4 separation

Stefanie Bügel, Alex Spieß, Christoph Janiak*
Institut für Anorganische Chemie und Strukturchemie, Heinrich-Heine-Universität Düsseldorf, D-40204 Düsseldorf, Germany

*Corresponding author: Christoph Janiak
E-mail address: janiak@hhu.de (C. Janiak)

Abstract

The porous and highly stable filler material CTF-fluorene was incorporated with 8, 16 and 24 wt% into the polymer matrices polysulfone (PSF) and Matrimid®. The resulting mixed matrix membranes (MMMs) were investigated by binary mixture CO_2/CH_4 mixed gas measurements. With increasing filler content in the MMMs, CO_2 and CH_4 permeabilities were enhanced with no loss of CO_2/CH_4 selectivity. All membrane systems were compared to theoretical permeability models and the best agreement could be found applying the Maxwell model. Further, calculations of the fractional free volume (FFV) confirm the contribution of filler porosity to improve the membrane permeability.

Keywords: *mixed matrix membrane (MMM), covalent triazine framework (CTF), polysulfone (PSF), Matrimid®, CO_2/CH_4 separation, permeability models, fractional free volume (FFV)*

1. Introduction

The separation of CO_2 from gas mixtures is an environmentally and economically important aspect. Especially, CO_2/CH_4 separation techniques are industrially relevant for the processing and purification of natural gas ("natural gas sweetening"). Raw natural gas mainly contains CH_4 [1], but it has to be purified from CO_2, hydrocarbons or hydrogen sulfide (H_2S) before utilization [2]. The removal of the acidic gas CO_2 minimizes corrosion in storage and transportation systems and enhances the energy content of natural gas [3]. The fact, that CO_2 can be present in a range from 0.06 up to 42.66 mol% [1] in the raw natural gas, underlines the necessity of CO_2/CH_4 separation.

In contrast to conventional CO_2 separation processes including absorption by monoethanolamine (MEA), pressure swing adsorption (PSA) or cryogenic distillation, polymeric membranes offer the advantages of low maintenance and capital costs as well as simple operation processes [4]. Organic polymer membranes are generally classified as non-porous and can consist of glassy or rubbery polymers, which form a dense film. To enhance the separation performance of the neat polymer membranes fillers can be incorporated in the membrane, resulting in a mixed matrix membrane (MMM). Possible fillers in MMMs are zeolites [5], silicas [6], zeolitic imidazolate frameworks (ZIFs) [7], MOFs [8-12], carbon materials like CMS [13] and POPs [14].

A subclass of POPs are covalent triazine frameworks (CTFs). The first CTF, namely CTF-1, was synthesized under ionothermal conditions (in molten $ZnCl_2$) via polymerization of dicyanobenzene resulting in a chemical and thermal highly stable microporous triazine network [15]. Not only due to their chemical stability, are CTFs favorable as a filler material in CO_2/CH_4 separation MMMs, but the nitrogen rich structure promotes the affinity of CO_2 due to dipole-quadrupole interactions between the nitrogen of the framework and the CO_2 molecules [16,17]. Therefore, a good CO_2 permeability can be expected.

In the last years molecular dynamics simulations and density functional theory calculations with dispersion corrections (DFT-D2) on CTFs as pure membrane material showed promising results in the potential field of desalination and He separation [18,19] A way to synthesize pure CTF membranes was presented by Zhu et al. in 2012. By means of a trimerization reaction of 4,4-biphenyldicarbonitrile in CF_3SO_3H the triazine-framework-based membrane TFM-1 could be produced. The TFM-1 membrane achieved a CO_2 permeability of 518 ± 25 Barrer with a CO_2/N_2 selectivity of 29 ± 2 [20]. Triazine based networks were also employed as selective layers on supporting materials. An organic triazine-piperazine based membrane (CTP membrane) was synthesized by Das et al.. The porous CTP layer was adjusted on the surface of a polyacrylonitrile (PAN) support and dye and salt rejection performances were examined [21]. Further, few-layered 2D-CTF-1 nanosheets on an anodic aluminum oxide substrate were used for dye retention [22]. A different system with CTF-1 nanosheets adjusted on a porous graphene oxide support was applied to form ultrathin membranes resulting in an efficient separation of H_2 from CO_2 [23].

Triazine based networks have also been utilized as filler material in polymer membranes. A biphenyl-based CTF was incorporated into polydimethylsiloxane (PDMS) matrices for n-BuOH recovery from mixtures with water. With the resulting MMM a separation factor of 50 at 40°C was achieved [24]. Up till now, there are only a few examples for triazine based filler

materials for CO_2/CH_4 separation. Thankamony et al. developed a MMM with the covalent triazine piperazine polymer CTPP as a filler in a poly ether-*block*-amide (PEBAX 1657) matrix. With 0.025 wt% of CTPP the permeability for CO_2 compared to the pure polymer increased from 53 to 73 Barrer with a CO_2/CH_4 selectivity increase from 17 to 25 [25]. FCTF-1, a fluorinated CTF, was used as filler material in a PIM-1 membrane resulting in a rise in CO_2/CH_4 selectivity from 11.5 to 14.8 accompanied with an increase in CO_2 permeability from 5800 Barrer to 9400 Barrer for the 5 wt% FCTF-1 membrane [26]. Previous synthesized PSF MMMs with the filler CTF-1 showed a CO_2 permeability of 9.8 Barrer and a CO_2/CH_4 selectivity of 20 for a filler content of 24 wt% CTF-1 [27].

In this work CTF-fluorene is used as a filler material for polysulfone and Matrimid® MMMs and was synthesized via a more economic and less time consuming Friedel-Crafts alkylation in comparison to the ionothermal CTF synthesis. Further, CTF-fluorene shows less loss of nitrogen content compared to other CTFs, such as CTF-triptycene [28]. CTF-fluorene can easily be handled in a scaled-up synthesis, which is essential to keep all membranes comparable by enabling membrane preparation with the filler material from one batch. As matrices the polymers PSF and Matrimid® are chosen. The patent literature underlines that polysulfones are one of the most commonly used polymers for gas separation, especially due to plasticization resistance as well as chemical and thermal durability [29]. The thermoplastic polyimide Matrimid® was chosen as a matrix due to its high thermal stability as well as its high CO_2/CH_4 selectivity [30].

2. Experimental section

2.1. Materials

All chemicals were purchased from commercial sources. *CTF synthesis*: Anhydrous aluminum chloride ($AlCl_3$; 98.5%) was received from Arcos Organics and sublimed in order to remove impurities. Cyanuric chloride (99%) was obtained from Sigma-Aldrich, dichloromethane (DCM; 99.99%) from Fisher Scientific and fluorene (> 98%) from Alfa Aesar. *Solvents for purification*: Acetone (≥ 99.8%) was obtained from Fisher Chemicals, methanol (MeOH; ≥ 99.8%) and tetrahydrofuran (THF; ≥ 99.9%) from Sigma-Aldrich. *Polymers* (Fig. 1): PSF (Ultrason S 6010) was purchased from BASF and Matrimid® 5218 (BTDA/DAPI) was provided by Huntsman Advanced Materials. *Gases*: CO_2 (grade 4.5), CH_4 (grade 4.5) and He (grade 5.0) were received from Air Liquide.

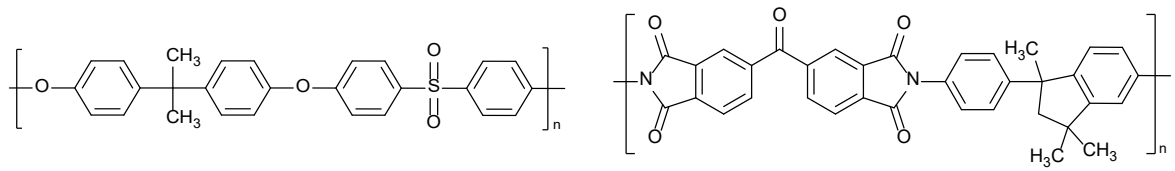

Fig. 1. Structures of PSF (left) and Matrimid® (right).

2.2. Synthesis of CTF-fluorene

CTF-fluorene was synthesized by Friedel-Crafts-alkylation (Fig. 2) in analogy to the literature [28]. To ensure that all membranes could be prepared with the filler material out of the same batch, a 10-fold scaled-up synthesis was carried out. Cyanuric chloride (1.84 g, 10 mmol), fluorene (2.49 g, 15 mmol) and anhydrous $AlCl_3$ (6.00 g, 45 mmol) were refluxed in 500 mL of dichloromethane (DCM) for 16 h. The solid product was separated from the solvent by filtration and washed with water followed by a Soxhlet extraction with methanol to remove unreacted monomers. Further washing steps were carried out with THF and acetone. The product was dried at 120°C for 24 h (yield: 3.00 g; 92.5%).

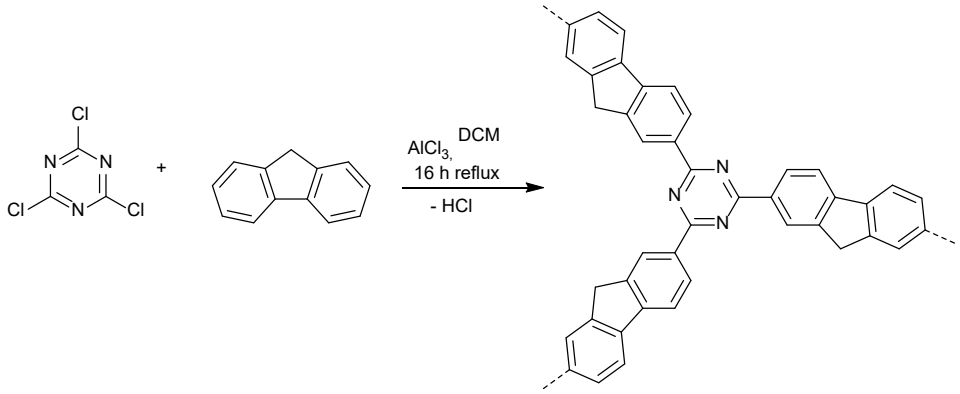

Fig. 2. Idealized reaction scheme of the synthesis of CTF-fluorene.

2.3. Preparation of CTF-fluorene/PSF and CTF-fluorene/Matrimid® MMMs

All MMMs were prepared by solution casting. The filler loadings varied between 0 and 24 wt% and were calculated according to equation (1) :

$$Filler\ loading\ [wt\%] = \frac{m_{filler}}{m_{polymer} + m_{filler}} \times 100\ \% \qquad (1)$$

The membranes were prepared as follows [31]: 400 mg of the pre-dried (80 °C; 5 d) polymer were dissolved in 3.5 mL of DCM. CTF-fluorene was milled with a mixer mill (Retsch, MM301) for 15 min with a frequency of 30 Hz to obtain a fine powder. For example, for the 8 wt% MMM, 35 mg of CTF-fluorene were dispersed in 4.5 mL of DCM. The polymer and the CTF in DCM were both stirred for 24 h. Afterwards, the CTF dispersion was ultrasonicated (Microtip 630-0419, VCX 750 Sonics) three times for 15 min with an amplitude of 20%.

Between the ultra-sonification steps the dispersion was stirred for 30 min. In order to achieve an equal filler/matrix mass ratio, 0.33 mL of the polymer solution were added to the CTF dispersion. After stirring for another 24 h, the same ultra-sonification procedure was carried out again and the remaining polymer solution was added. A final stirring step of 1 h was carried out and the mixture was casted into a metal ring on a flat glass surface. An inverted funnel covered with a paper tissue was placed above the membrane to slow the evaporation of DCM. Once the solvent was evaporated, the membrane was cut out with a scalpel and removed from the glass surface. PSF membranes were further dried at 120 °C and Matrimid® membranes at 150 °C in a vacuum oven (20 mbar) over night. The 16 and 24 wt% membranes were prepared accordingly. By enhancing the filler content to 32 wt%, the MMMs became brittle and susceptible to cracking.

2.4. Instrumentation and characterization methods

Elemental analysis was carried out on a vario MICRO cube (elementar). Attenuated total reflection infrared spectroscopy (ATR-IR) spectra ranging from 4000 cm^{-1} to 500 cm^{-1} were obtained on a Bruker Tensor 37. A Jeol JSM-6510LV with a LaB_6 cathode (20 keV) was used to record scanning electron microscopy (SEM) images. Cross-section images of the membranes were recorded after freeze-fracturing of the liquid nitrogen cooled membrane and coating with gold by a JFC 1200 (Jeol) coater. Thermogravimetric analysis (TGA) was carried out on a TG 209 F3 Tarsus (Netzsch) under synthetic air in a range from 25 °C to 1000 °C with a heating rate of 5 K/min. Differential scanning calorimetry (DSC) curves were measured with a DSC 3 (Mettler-Toledo) under a nitrogen flow of 30 mL/min and a heating rate of 10 K/min. The glass transition temperature (T_g) was determined as the midpoint temperature of the transition sections of the second heating and cooling cycle. Sorption measurements for CTF-fluorene were performed with activated samples, degassed under vacuum at 120 °C for 8 h. An Autosorb-6 (Quantachrome) was used to carry out nitrogen sorption measurements. The Brunauer-Emmett-Teller (BET) surface area was calculated from the nitrogen adsorption isotherm in the range of 0.05 to 0.3 p/p_0 with a correlation coefficient of r = 0.99999. The total pore volume was obtained from the nitrogen sorption isotherm at $p/p_0 = 0.97$. CO_2 and CH_4 sorption isotherms of CTF-fluorene were fitted with the Langmuir (LAI) isotherm model by applying equation (2):

$$q_{eq} = q_{max} \times \frac{K \times p}{1 + K \times p} \qquad (2)$$

For CTF-fluorene (skeletal) density determination a He-pycnometer AccuPyc 1330 (Micromeritics) was used. Due to the fact, that He does not fill the pores of the porous CTF

structure at room temperature, the total pore volume obtained from N_2-sorption was included in the calculation:

$$\rho_{CTF} = \frac{V_{He} + V_{pores}}{m_{CTF}} \quad (3)$$

CO_2/CH_4 mixed gas separation measurements with the membranes were carried out with an OSMO inspector (provided by Convergence Industry B.V.) connected to a gas chromatograph. The schematic set-up is shown in Fig. 3. The Agilent 490 Micro GC (Agilent Technologies) was equipped with a fused silica column PoraPLOT Q and a thermal conductivity detector. The membranes were placed in a permeation module and fixed with a Viton O-ring with an inner diameter of 3.6 cm (area: 11.3 cm^2). The CO_2/CH_4 feed gas volume ratio was 1:1 and helium was used as sweep gas. All measurements were performed with a transmembrane pressure of 3 bar at 25 °C and were carried out every 30 min until equilibrium state was reached. Each membrane was synthesized and measured twice.

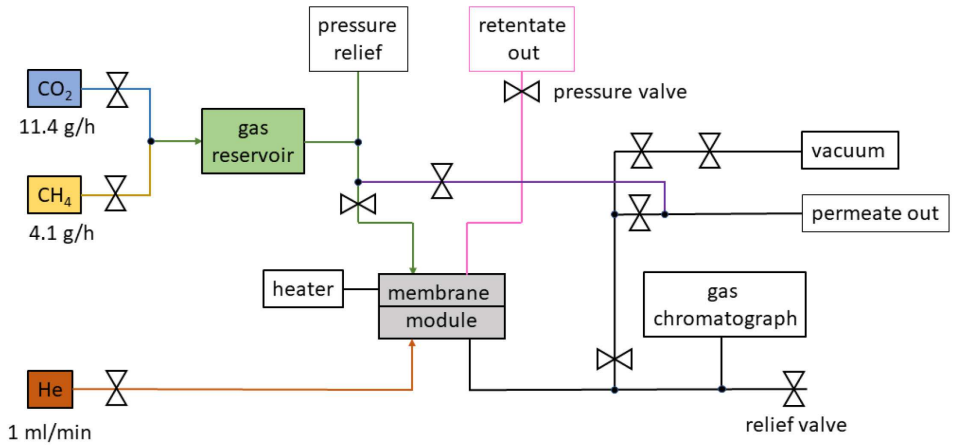

Fig. 3. Schematic set-up for CO_2/CH_4 mixed gas separation measurements.

The permeability P is given in Barrer (1 Barrer = 10^{-10} cm^3(STP) cm cm^{-2} s^{-1} $cmHg^{-1}$) and was calculated according to equation (4):

$$P = \frac{x_A \times Q_{He} \times d}{x_{He} \times A \times (p_2 \times x_A^f - p_1 \times x_A)} \quad (4)$$

x_A: molar fraction of the gas A
Q_{He}: volumetric flow rate of the sweep gas helium [cm^3/s]
d: thickness of the membrane, measured at 10 different points
x_{He}: molar fraction of the sweep gas (permeate)
A: area of the membrane [cm^2]
p_2: feed pressure [cmHg]
x_A^f: molar fraction of the gas A in the feed
p_1: permeate pressure [cmHg]

The selectivity of two gases (A, B) was calculated from the molar fractions (x) on each side, according to equation (5):

$$\alpha_{A,B} = \frac{(x_A/x_B)_{permeate\ side}}{(x_A/x_B)_{feed\ side}} \quad (5)$$

3. Results and discussion

3.1. Characterization of CTF-fluorene

The formation of CTF-fluorene was confirmed by elemental analysis (Table S1) and IR (Figure S1). Elemental analysis showed a good accordance with the literature [28], with the typical lower nitrogen content that was detected than calculated for the idealized structure. We have previously suggested that a partial formation of polymer chains takes place in which the triazine unit is connected only to two bridging fluorene molecules and a terminal fluorene molecule [28]. In earlier work we had also shown that CTFs are hygroscopic due to their micro- to mesoporous nature with a water uptake of up to ~20 wt% at P/P_0 = 0.5-0.6 or 50-60% air humidity when stored under ambient air. Thus, the lower than expected nitrogen but also carbon wt% can be explained by the presence of water and residues of aluminum species from the catalyst. Both, in CTFs synthesized via Friedel-Crafts synthesis and ionothermal synthesis, catalyst residues cannot be removed completely [28,32].

IR spectroscopy revealed bands at 1514 cm^{-1} (s) and 1357 cm^{-1} (m), which are due to aromatic C–N stretching modes of the triazine ring. The absence of the C–Cl stretching band at 846 cm^{-1} confirmed a complete conversion of the educt cyanuric chloride. The TGA curve agrees with the one in the literature [28] (Figure S2) and verifies the thermal stability of over 300 °C. The SEM image (Figure S3) depicts the expected rounded shape of the particles. Nitrogen sorption isotherms of the CTF at 77 K (Figure S4) showed a steep uptake at low relative pressures (p/p_0) followed by a flat slope up to $p/p_0 = 1$, resulting in a Type I(b) isotherm with hysteresis [33]. The calculated BET surface area of 762 m^2/g is in good accordance to the literature (773 m^2/g) [28] and the total pore volume is 0.38 cm^3/g (literature [28]: 0.39 cm^3/g). CO_2 and CH_4 sorption measurements at 298 K (Figure S5) exhibited maximal gas uptakes of 1.44 and 0.44 mmol/g at a pressure of 721 mmHg (literature: 2.14 mmol/g at 293 ± 1 K and 0.66 mmol/g at 273.15 K [28]). Ideal adsorbed solution theory (IAST) calculations based on the Langmuir (LAI) isotherm model fitted CO_2 and CH_4 sorption isotherms yield a CO_2/CH_4 (50:50; v:v) selectivity of 7.6 at 1 bar pressure (Figure S6), which makes CTF-fluorene a potentially good filler in MMMs for CO_2/CH_4 separation.

3.2. Characterization of MMMs

All MMMs were prepared with filler contents of 8, 16 and 24 wt%. Cross-section SEM images (Fig. 4) show the absence of defects and confirm the good contact between the polymer and filler particles. In the 24 wt% CTF-fluorene/Matrimid® MMM agglomeration of the filler particles becomes evident. This can be explained by the high filler content, which makes agglomeration of filler particles more likely. At this loading also, formation of free volume inside the membranes becomes visible, which, however did not lower the selectivity of the membrane (see below). The increase of the CTF-fluorene content from 8 to 24 wt% resulted in a corresponding increase of the membrane thickness (Table S3).

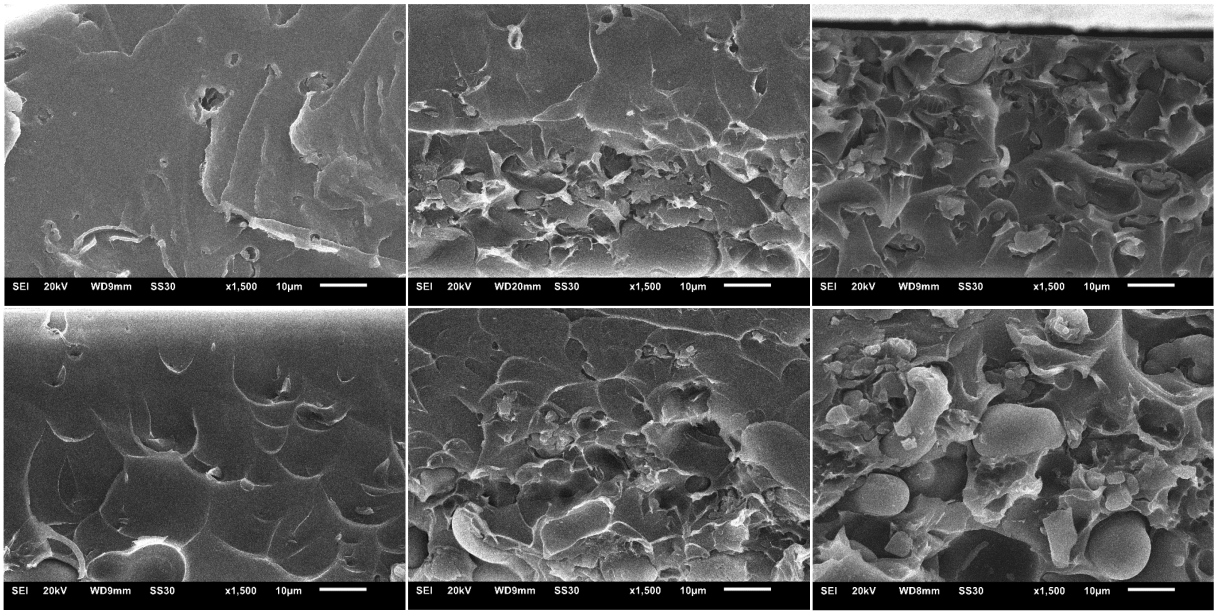

Fig. 4. Cross-section SEM images of CTF-fluorene/PSF MMMs (top) with 8 wt% (left), 16 wt% (middle) and 24 wt% (right) filler and CTF-fluorene/Matrimid® MMMs (bottom) with 8 wt% (left), 16 wt% (middle) and 24 wt% (right) filler.

The thermal stability of the MMMs was verified by TGA measurements of the 24 wt% MMMs. The TGA curves (Figure S8) of the MMMs and the associated pure polymer show no significant differences in the shape of the curve or the decomposition temperature. The incorporation of the filler material CTF-fluorene did not lower the decomposition temperature compared to the pure polymer membranes, which proves a good thermal stability of the MMMs.

In order to get information about the intersegmental mobility, that is the polymer chain stiffness or chain flexibility, the glass transition temperatures (T_g) of the pure polymer membranes and the 24 wt% MMMs were measured with DSC (Table 1). Generally, an increase in T_g can be attributed to reduced chain flexibility due to the presence of filler particles and may also indicate a strong interfacial interaction between polymer and the filler [34]. A decrease in T_g, therefore signals an increase in chain flexibility, may be attributed to an increase in free volume and can

enhance the permeability. The incorporation of CTF-fluorene had no impact on the T_g of the PSF or Matrimid® membranes. Consequently, no change in intersegmental mobility could be observed by DSC measurements.

Table 1

Glass temperatures (T_g) of the pure PSF and Matrimid® membranes and the corresponding 24 wt% membranes.

Membrane	Pure PSF	24 wt% CTF-fluorene/PSF	Pure Matrimid®	24 wt% CTF-fluorene/Matrimid®
T_g [°C]	187 ± 1	187 ± 1	317 ± 0	318 ± 1

3.3. Gas permeability and selectivity

In contrast to molecular sieving through a porous membrane, the permeation of gases through a dense polymeric membrane follows a solution-diffusion mechanism [35]. This mechanism is driven by dissimilarity in physical and chemical interactions of the gas species with the polymer membrane as well as different thermodynamic activities on the feed and permeate side of a membrane, which cause a concentration gradient leading to diffusion towards decreasing activity [36]. The permeability *P* can be described as a product of the diffusion coefficient *D* and the solubility coefficient *S*:

$$P = D \times S \tag{6}$$

The ideal selectivity of a membrane can be calculated by division of the permeabilities measured by single gas experiments. For two different gases A and B equation (7) is applied:

$$\alpha_{ideal,A,B} = \frac{D_A}{D_B} \times \frac{S_A}{S_B} = \frac{P_A}{P_B} \tag{7}$$

For the real selectivity interactions between the gases, e.g. competitive adsorption, binary mixed-gas measurements have to be used [37]. Subsequently, for gas mixtures the ratio of the mole fractions *x* of both gases on the permeate side is then divided by the ratio of the mole fractions of each gas on the feed side to yield the selectivity.

$$\alpha_{A,B} = \frac{(x_A/x_B)_{permeate\ side}}{(x_A/x_B)_{feed\ side}} \tag{8}$$

The CO_2 and CH_4 permeability values as well as the mixed-gas selectivities (α CO_2/CH_4) of the pure membranes, CTF-fluorene/PSF and CTF-fluorene/Matrimid® MMMs are provided in Table 2. Errors are given as standard deviation (1σ). Both, CTF-fluorene/PSF and CTF-fluorene/Matrimid® MMMs exhibited the expected increase in permeability compared to the pure polymer membranes. The CO_2 and CH_4 permeabilities of 5.4 and 0.19 Barrer for the pure PSF membrane improved to 12.8 and 0.42 Barrer for the MMM with 24 wt% of the filler CTF-

fluorene embedded in the PSF matrix. A more than 2.6 times increase of the permeability values was achieved for the CTF-fluorene/Matrimid® MMMs. The CO_2 and CH_4 permeabilities increased from 6.8 and 0.16 Barrer for the pure Matrimid® membrane to 17.8 and 0.40 Barrer for the 24 wt% CTF-fluorene/Matrimid® MMM. The selectivity remained essentially unchanged within experimental error for all MMMs. All permeability and selectivity values are depicted in Fig. 5. Errors for permeability are given as standard deviation (1σ) from two measurements and for the selectivity were derived through error propagation by adding the relative errors which were then computed to the absolute errors.

Table 2

Gas permeabilities (*P*) and mixed-gas selectivity factors (α) of the pure and CTF-polymer membranes.[a]

Matrix	CTF-fluorene content [wt%]	P CO_2 [Barrer]	P CH_4 [Barrer]	α CO_2/CH_4
PSF	0	5.4 ± 0.0	0.19 ± 0.01	28 ± 2
	8	6.6 ± 0.3	0.21 ± 0.01	32 ± 2
	16	8.8 ± 0.3	0.31 ± 0.01	29 ± 0
	24	12.8 ± 0.1	0.42 ± 0.04	30 ± 3
Matrimid®	0	6.8 ± 0.3	0.16 ± 0.01	42 ± 1
	8	9.2 ± 0.4	0.21 ± 0.01	43 ± 1
	16	12.6 ± 0.1	0.28 ± 0.01	45 ± 1
	24	17.8 ± 0.3	0.40 ± 0.02	44 ± 2

[a] The permeability *P* is calculated with the thickness of the membrane (given in Table S3); see equation (4) and in Section 2.3, Supp. Info.

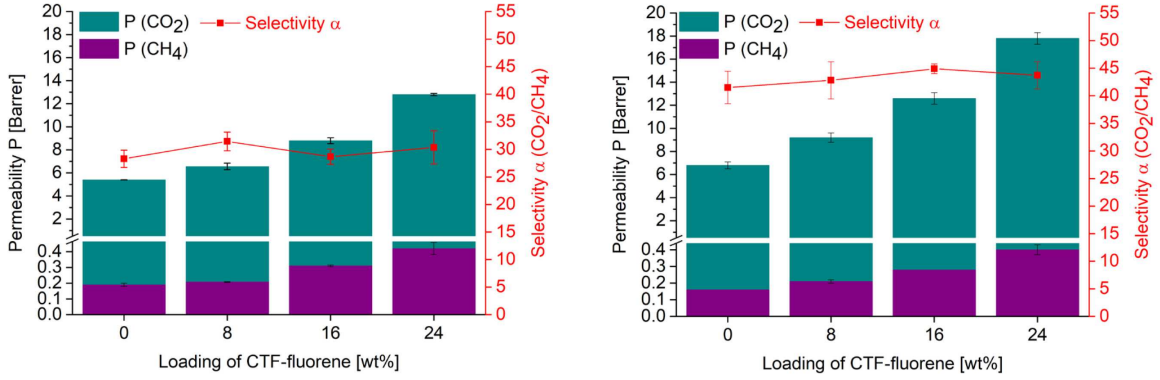

Figure 5. CO_2 and CH_4 permeabilities for 0 wt%, 8 wt%, 16 wt%, 24 wt% and CO_2/CH_4 selectivity for CTF-fluorene/PSF (left) and CTF-fluorene/Matrimid® (right) MMMs.

By adding a porous filler material, here CTF-fluorene, a free volume is generated leading to an increase in diffusion and consequently in permeability. Depending on the pore size distribution of the filler an additional sieving effect may appear which would result in a change in selectivity. The difference of the kinetic diameters of CO_2 and CH_4 (0.33 nm and 0.38 nm) [38] may cause a preferential sieving effect of CO_2 over CH_4. In case of CTF-fluorene as a filler with pore sizes mainly distributed around 5 Å [28] (Figure S4), an impact of a sieving effect can, however, be excluded. This is supported by the unchanged selectivity.

3.4. Permeability models and fractional free volume (FFV) calculations

For the following calculations, the density values for PSF (1.23 g/cm^3) [39] and Matrimid® (1.20 g/cm^3) [40] as well as the FFV values for PSF (0.156) [41] and Matrimid® (0.167) [42] were applied as given from the literature. The density of CTF-fluorene (0.89 g/cm^3) was used as determined.

3.4.1. Permeability models

The permeability of MMMs up to $\phi_d = 0.2$ (ϕ_d: volume fraction of dispersed phase) can be predicted by the Maxwell model [43]. The model assumes spherical filler particles, which are ideally distributed in the continuous polymer phase [43]. The Maxwell equation can be expressed by equation (9), where P_d describes the permeability of the dispersed phase, P_c the permeability of the pure polymer membrane and P_{eff} the permeability of the MMM:

$$P_{eff} = P_c \left[\frac{P_d+2P_c-2\phi_d(P_c-P_d)}{P_d+2P_c+\phi_d(P_c-P_d)}\right] \quad (9)$$

In equation (10) the "reduced permeation polarizability" β is defined, which describes the permeability differences between the continuous phase (with P_c) and the dispersed phase (with P_d) [44]:

$$\beta = \frac{P_d-P_c}{P_d+2P_c} \quad (10)$$

Further, equation (9) can be simplified to equation (11):

$$P_{eff} = P_c \left[\frac{1+2\beta\times\phi_d}{1-\beta\times\phi_d}\right] \quad (11)$$

For $\beta \approx 1$ ($P_d >> P_c$) the dispersed phase is much more permeable than the continuous phase. The resulting equation (12) refers to the Maxwell model for a porous dispersed phase:

$$\frac{P_{eff}}{P_c} = \frac{1+2\phi_d}{1-\phi_d} \quad (12)$$

The limiting case of a non-porous dispersed phase ($P_d << P_c$) can be described by $\beta \approx -0.5$ [44]. To approximate the experimental permeabilities between the two limiting cases of a porous

dispersed phase and non-porous dispersed phase, we assume $P_d = 8P_c$. Leading to $\beta = 0.7$ and thus to equation (13):

$$\frac{P_{eff}}{P_c} = \frac{1+1.4\phi_d}{1-0.7\phi_d} \quad (13)$$

A possibility to predict membrane permeability in the case of $\phi_d > 0.2$ is given by the Bruggeman model [45]. For a porous filler material with $P_d >> P_c$ equation (14) can be applied:

$$\frac{P_{eff}}{P_c} = \frac{1}{(1-\phi_d)^3} \quad (14)$$

The Böttcher-Landauer model was applied for the case of $P_d >> P_c$ using equation (15) [46]:

$$\frac{P_{eff}}{P_c} = \frac{1}{(1-3\phi_d)} \quad (15)$$

The plots of the experimentally determined P_{eff}/P_c versus ϕ_d for CTF-fluorene/PSF, CTF-fluorene/Matrimid® MMMs and of the theoretical predictions based on the equations of the Maxwell, Bruggeman and Böttcher-Landauer model for porous fillers are summarized in Fig. 6.

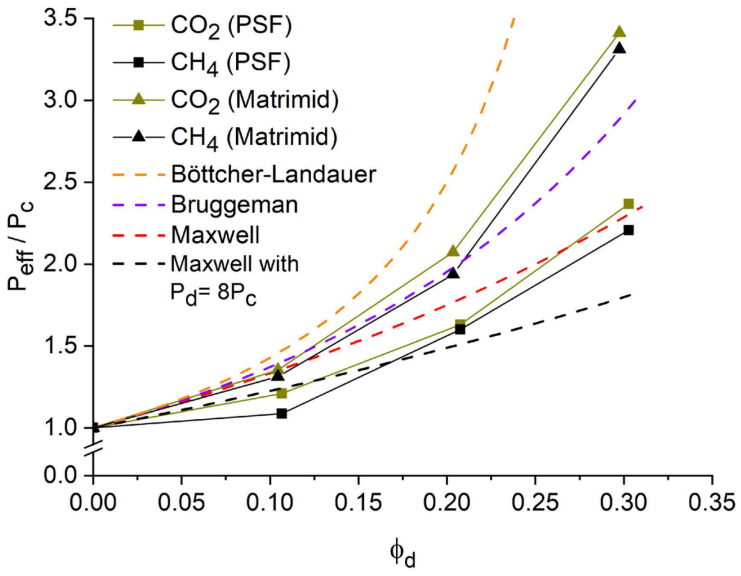

Fig. 6. P_{eff}/P_c versus ϕ_d for 0 wt%, 8 wt%, 16 wt% and 24 wt% CTF-fluorene/PSF and CTF-fluorene/Matrimid® MMMs in comparison to the Maxwell, Maxwell with $P_d = 8P_c$, Bruggeman and Böttcher-Landauer model for porous fillers. The amount of 8 wt%, 16 wt% and 24 wt% of filler correspond to filler volume fractions ϕ_d of ~0.1, 0.2 and 0.3, respectively (exact filler volume fractions ϕ_d depend on the polymer density).

The ratio P_{eff}/P_c for the gases CO_2 and CH_4 increased with enhancement of the filler content for all MMMs. Considering the rather constant CO_2/CH_4 selectivity for both membrane systems, P_{eff}/P_c is generally higher for CO_2 than for CH_4 for the same polymer.

The experimental curves for the CTF-fluorene/PSF MMMs are located between the Maxwell model with $P_d = 8P_c$ and the Maxwell model with $P_d >> P_c$. We also assumed different relations

between P_d and P_c to approximate the experimental P_{eff}/P_c (Figure S9). Lower permeabilities than predicted can be explained by the penetration of polymer chains into the pores of CTF-fluorene resulting in a lowered free volume [47]. Further, deviations from the above-mentioned ideal assumptions of the Maxwell model can result in a change in permeability. Apparently, the Maxwell model acts as a good first approximation for the investigated membrane systems, but does not consider the entirety of component interactions.

The experimental values for the CTF-fluorene/Matrimid® MMMs are in accordance with the Bruggeman model. Only with a filler content of 24 wt% of CTF-fluorene in the Matrimid® matrix, the elevation in permeability is even higher than predicted, which may be attributed to more complex interfacial effects.

3.4.2. Fractional free volume (FFV)

The FFV is a dimensionless number, which is obtained by multiplication of density and pore volume. In order to calculate the total FFV of a MMM, equation (16) is used, where ϕ_c describes the volume fraction of the continuous phase:

$$FFV = FFV_{polymer} * \phi_c + FFV_{filler} * \phi_d \qquad (16)$$

In general, the permeability of a membrane correlates with the total FFV. If the FFV determines the permeability of a membrane a linear correlation of lg permeability P against 1/FFV is expected.

The graphs lg*P* against 1/FFV are shown in Fig. 7. Concerning both membrane systems, the permeability of the membranes does not correlate exactly linear with the inverse FFV. As already described in the context of the permeability models, the membranes with higher filler volumes even exhibit a steeper rise in permeability relatively compared to lower filler contents. This aspect can also be seen in the corresponding FFV plot. The great impact of free volume leading to higher permeabilities is obvious, but with higher filler contents not only filler-polymer interactions of CTF-fluorene and the polymers PSF and Matrimid® are given. Filler-filler interactions, which are also not catchable with this calculation, start to appear. Further, the important aspect of the solubility of a gas in a membrane is additionally responsible for a rise in permeability.

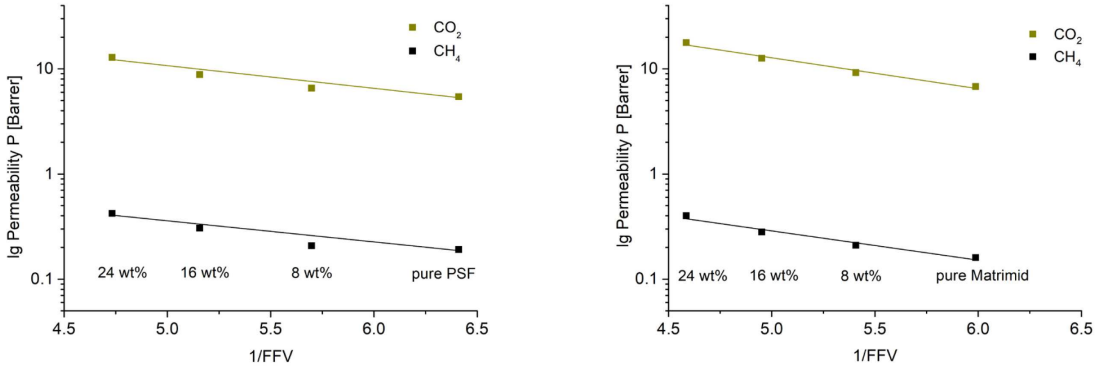

Fig. 7. Logarithm of permeability *P* versus 1/FFV for 0 wt%, 8 wt%, 16 wt%, 24 wt% for CTF-fluorene/PSF (left) and CTF-fluorene/Matrimid® (right) MMMs.

Generally, in the case of glassy polymers, the filler particles can increase the permeability by disturbing the chain packing of the polymer. If additional void volume is generated, e.g. by incompatibility of filler and matrix, the permeability will increase, but the membrane will lose its selectivity. Due to the constant selectivity of both MMM systems as well as the constancy of the measured T_g values of the pure polymer and 24 wt% membranes (Table 1), the formation of exceptional high void volume can be excluded.

For a comparison of CO_2 and CH_4 permeability and selectivity values different CTFs as filler materials are considered. Table 3 lists the MMMs with the best performance considering the trade-off relationship between permeability and selectivity. The 24 wt% CTF-fluorene/PSF MMM showed an elevation in CO_2 permeability by 137% in comparison to the 24 wt% CTF-1/PSF MMM with an elevation by 74% [27]. In both cases CO_2/CH_4 selectivity remains unchanged. For the CTF-fluorene/Matrimid® MMMs, an 162% increase in CO_2 permeability was achieved, accompanied by a constancy of the CO_2/CH_4 selectivity values. The incorporation of the covalent triazine piperazine polymer CTPP in a PEBAX 1657 matrix led to an increase in CO_2 permeability by 38% and an increase in CO_2/CH_4 selectivity by 28 [25]. With the fluorinated framework FCTF-1 as filler material in PIM-1, CO_2 permeability was elevated by 62% and CO_2/CH_4 selectivity by 3 [26]. Although CTF-fluorene as filler material does not show an increase in CO_2/CH_4 selectivity compared to the CTFs CTPP [25] and FCTF-1 [26], the CO_2 permeability can be increased up to 162%, which makes CTF-fluorene an attractive candidate for CO_2/CH_4 gas separation.

Table 3

Comparison of CO_2 permeability and CO_2/CH_4 selectivity for CTFs as filler materials in different polymers.

Filler	Filler content [wt%]	Matrix	*P* CO_2 [Barrer]	α CO_2/CH_4	Ref.
-	-	PSF	5.4 ± 0.0	28 ± 2	This work
CTF-fluorene	24	PSF	12.8 ± 0.1	30 ± 3	
-	-	Matrimid®	6.8 ± 0.3	42 ± 1	This work
CTF-fluorene	24	Matrimid®	17.8 ± 0.3	44 ± 2	
-	-	PSF	7.3 ± 0.2[a]	21 ± 3[a]	27
CTF-1	24	PSF	12.7 ± 0.8[a]	22 ± 3[a]	
-	-	PEBAX 1657	53[b]	51[b]	25
CTPP	0.025	PEBAX 1657	73[b]	79[b]	
-	-	PIM-1	5800[c]	11.5[c]	26
FCTF-1	5	PIM-1	9400[c]	14.8[c]	

a) Single gas; 298 K; feed pressure 3 bar
b) Single gas; 293 K; feed pressure 4 bar
c) Single gas; 303 K; feed pressure 1 atm

4. Conclusion

In summary, two MMM systems have been successfully prepared with the filler material CTF-fluorene. The synthesized CTF showed excellent thermal and chemical stability. Through incorporation into PSF and Matrimid® matrices a significant improvement in CO_2 and CH_4 permeability was achieved while maintaining constant selectivity. In contrast to CO_2 and CH_4 permeabilities of 5.4 and 0.19 Barrer for the pure PSF membrane, the 24 wt% CTF-fluorene/PSF MMM achieved permeabilities of 12.8 and 0.42 Barrer. With 24 wt% CTF-fluorene, embedded as filler in a Matrimid® matrix, an even higher elevation in permeability was achieved. From 6.8 and 0.16 Barrer for CO_2 and CH_4 for the pure Matrimid® membrane up to 17.8 and 0.40 Barrer with the filler CTF-fluorene. The comparison to theoretical permeability models showed the best accordance for the Maxwell model. The important role of free volume in order to enhance the permeability in a MMM was confirmed by FFV calculations. For future projects, the incorporation of organic, porous and highly stable CTFs as fillers in a Matrimid® matrix is a promising subject and provides the opportunity to enhance CO_2 and CH_4 permeability whilst maintaining the Matrimid®-attributed high selectivity.

Author Contribution Statement

SB performed the experiments, collected and interpreted the data and wrote and revised the manuscript. AS made SEM images. CJ outlined the idea together with SB, provided feedback to the work, refined the manuscript.

Declaration of competing interest

The authors declare that they have no known competing financial interests or personal relationships that could have appeared to influence the work reported in this paper.

Acknowledgements

We thank Mrs. Stephanie Scheelen and Prof. Dr. Laura Hartmann at the Institut für Organische und Makromolekulare Chemie, Heinrich-Heine-Universität Düsseldorf for DSC measurements. We acknowledge Mr. Philipp Brandt for CO_2 and CH_4 sorption and Dr. Alexa Schmitz for TGA measurements. Dr. Julian Quodbach, Institut für Pharmazeutische Technologie und Biopharmazie, Heinrich-Heine-Universität Düsseldorf, is thanked for and He-Pycnometry measurements.

Appendix A. Supplementary data

Supplementary data to this article can be found online at https://doi.org/10.1016/j.micromeso.2021.110941.

References

[1] Y. Cheng, Z. Wang, D. Zhao, Ind. Eng. Chem. Res. 57 (2018) 4139−4169. https://doi.org/10.1021/acs.iecr.7b04796

[2] Y. Lin, C. Kong, Q. Zhang, L. Chen, Adv. Energy Mater. 7 (2017) 1601296. https://doi.org/10.1002/aenm.201601296

[3] Y. Zhang, J. Sunarso, S. Liu, R. Wang, Int. J. Greenhouse Gas Control 12 (2013) 84−107. https://doi.org/10.1016/j.ijggc.2012.10.009

[4] W. Mazyan, A. Ahmadi, H. Ahmed, M. Hoorfar, J. Nat. Gas Sci. Eng. 30 (2016) 487−514. https://doi.org/10.1016/j.jngse.2016.02.010

[5] D. Bastani, N. Esmaeili, M. Asadollahi, J. Ind. Eng. Chem. 19 (2013) 375−393. https://doi.org/10.1016/j.jiec.2012.09.019

[6] S. Kim, E. Marand, J. Ida, V.V. Guliants, Chem. Mater. 18 (2006) 1149−1155. https://doi.org/10.1021/cm052305o

[7] M.J.C. Ordoñez, K.J. Balkus Jr., J.P. Ferraris, I.H. Musselman, J. Membr. Sci. 361 (2010) 28−37. https://doi.org/10.1016/j.memsci.2010.06.017

[8] B. Zornoza, C. Tellez, J. Coronas, J. Gascon, F. Kapteijn, Microporous Mesoporous Mater. 166 (2013) 67−78. https://doi.org/10.1016/j.micromeso.2012.03.012

[9] J. Dechnik, C.J. Sumby, C. Janiak, Cryst. Growth Des. 17 (2017) 4467−4488. https://doi.org/10.1021/acs.cgd.7b00595

[10] J. Dechnik, J. Gascon, C.J. Doonan, C. Janiak, C.J. Sumby, Angew. Chem. Int. Ed. 56 (2017) 9292−9310. https://doi.org/10.1002/anie.201701109

[11] H.B. Tanh Jeazet, C. Janiak, in: L.R. MacGillivray, C. Lukehart (Eds.), Metal Organic Framework Materials, John Wiley & Sons, Ltd, Chichester, UK, 2014, pp. 403−418.

[12] H.B. Tanh Jeazet, C. Staudt, C. Janiak, Dalton Trans. 41 (2012) 14003−14027. https://doi.org/10.1039/C2DT31550E

[13] D.Q. Vu, W.J. Koros, S.J. Miller, J. Membr. Sci. 211 (2003) 311−334.https://doi.org/10.1016/S0376-7388(02)00429-5

[14] C. Wang, F. Guo, H. Li, J. Xu, J. Hu, H. Liu, J. Membr. Sci. 564 (2018) 115−122. https://doi.org/10.1016/j.memsci.2018.07.018

[15] P. Kuhn, M. Antonietti, A. Thomas, Angew. Chem. Int. Ed. 47 (2008) 3450−3453. https://doi.org/10.1002/anie.200705710

[16] M. Sevilla, P. Valle-Vigón, A.B. Fuertes, Adv. Funct. Mater. 21 (2011) 2781−2787. https://doi.org/10.1002/adfm.201100291

[17] Z. Li, X. Feng, Y. Zou, Y. Zhang, H. Xia, X. Liu, Y. Mu, Chem. Commun. 50 (2014) 13825−13828. https://doi.org/10.1039/C4CC05665E

[18] L.-C. Lin, J. Choi, J.C. Grossman, Chem. Commun. 51 (2015) 14921−14924. https://doi.org/10.1039/C5CC05969K

[19] Y. Wang, J. Li, Q. Yang, C. Zhong, ACS Appl. Mater. Interfaces 8 (2016) 8694−8701. https://doi.org/10.1021/acsami.6b00657

[20] X. Zhu, C. Tian, S.M. Mahurin, S.-H. Chai, C. Wang, S. Brown, G.M. Veith, H. Luo, H. Liu, S. Dai, J. Am. Chem. Soc. 134 (2012) 10478−10484. https://doi.org/10.1021/ja304879c

[21] S.K. Das, P. Manchanda, K.-V. Peinemann, Sep. Purif. Technol. 213 (2019) 348−358. https://doi.org/10.1016/j.seppur.2018.12.046

[22] G. Li, W. Wang, Q. Fang, F. Liu, J. Membr. Sci. 595 (2019) 117525. https://doi.org/10.1016/j.memsci.2019.117525

[23] Y. Ying, D. Liu, J. Ma, M. Tong, W. Zhang, H. Huang, Q. Yang, C. Zhong, J. Mater. Chem. A 4 (2016) 13444−13449. https://doi.org/10.1039/C6TA04579K

[24] J. Y. Lee, H. Park, J.S. Lee, S. Yoon, J.-H. Lee, J. Membr. Sci. 598 (2020) 117654. https://doi.org/10.1016/j.memsci.2019.117654

[25] R.L. Thankamony, X. Li, S.K. Das, M.M. Ostwal, Z. Lai, J. Membr. Sci. 591 (2019) 117348. https://doi.org/10.1016/j.memsci.2019.117348

[26] H. Jiang, J. Zhang, T. Huang, J. Xue, Y. Ren, Z. Guo, H. Wang, L. Yang, Y. Yin, Z. Jiang, M.D. Guiver, Ind. Eng. Chem. Res. 59 (2020) 5296−5306. https://doi.org/10.1021/acs.iecr.9b04632

[27] S. Dey, S. Bügel, S. Sorribas, A. Nuhnen, A. Bhunia, J. Coronas, C. Janiak, Front. Chem. 7 (2019) 693. https://doi.org/10.3389/fchem.2019.00693

[28] S. Dey, A. Bhunia, D. Esquivel, C. Janiak, J. Mater. Chem. A 4 (2016) 6259−6263. https://doi.org/10.1039/C6TA00638H

[29] C.A. Scholes, S.E. Kentish, G.W. Stevens, Recent Pat. Chem. Eng. 1 (2008) 52−66. https://doi.org/10.2174/2211334710801010052

[30] M. Loloei, A. Moghadassi, M. Omidkhah, A.E. Amooghin, Greenhouse Gas Sci. Technol. 5 (2015) 530−544. https://doi.org/10.1002/ghg.1496

[31] A. Nuhnen, D. Dietrich, S. Millan, C. Janiak, ACS Appl. Mater. Interfaces 10 (2018) 33589−33600. https://doi.org/10.1021/acsami.8b12938

[32] S. Dey, A. Bhunia, H. Breitzke, P.B. Groszewicz, G. Buntkowsky, C. Janiak, J. Mater. Chem. A 5 (2017) 3609−3620. https://doi.org/10.1039/C6TA07076K

[33] M. Thommes, K. Kaneko, A.V. Neimark, J.P. Olivier, F. Rodriguez-Reinoso, J. Rouquerol, K.S.W. Sing, Pure Appl. Chem. 87 (2015) 1051−1069. https://doi.org/10.1515/pac-2014-1117

[34] T.-S. Chung, S.S. Chan, R. Wang, Z. Lu, C. He, J. Membr. Sci. 211 (2003) 91−99. https://doi.org/10.1016/S0376-7388(02)00385-X

[35] P. Pandey, R.S. Chauhan, Prog. Polym. Sci. 26 (2001) 853−893. https://doi.org/10.1016/S0079-6700(01)00009-0

[36] J.G. Wijmans, R.W. Baker, J. Membr. Sci. 107 (1995) 1−21. https://doi.org/10.1016/0376-7388(95)00102-I

[37] G. Dong, H. Li, V.Chen, J. Membr. Sci. 369 (2011) 206−220. https://doi.org/10.1016/j.memsci.2010.11.064

[38] T.A. Barbari, W.J. Koros, D.R. Paul, J. Polym. Sci. B Polym. Phys. 26 (1988) 709−727. https://doi.org/10.1002/polb.1988.090260401

[39] BASF Engineering Plastics, Wyandotte, USA, Product Information, Ultrason® S 6010 Polysulfone (PSU). http://iwww.plasticsportal.com/products/datasheet.html?type=iso&param=Ultrason+S+2010, 2020 (accessed 27 October 2020)

[40] Y. Huang, X. Wang, D.R. Paul, J. Membr. Sci. 277 (2006) 219−229. https://doi.org/10.1016/j.memsci.2005.10.032

[41] S. Thran, G. Kroll, F. Faubel, J. Polym. Sci. B 37 (1999) 3344−3358. https://doi.org/10.1002/(SICI)1099-0488(19991201)37:23<3344::AID-POLB10>3.0.CO;2-A

[42] S. Kanehashi, G.Q. Chen, C.A. Scholes, B. Ozcelik, C. Hua, L. Ciddor, P.D. Southon, D.M. D'Alessandro, S.E. Kentish, J. Membr. Sci. 482 (2015) 49−55. https://doi.org/10.1016/j.memsci.2015.01.046

[43] R.H.B. Bouma, A. Checchetti, G. Chidichimo, E. Drioli, J. Membr. Sci. 128 (1997) 141−149. https://doi.org/10.1016/S0376-7388(96)00303-1

[44] S. Basu, A. Cano-Odena, I.F.J Vankelecom, J. Membr. Sci. 362 (2010) 478–487. https://doi.org/10.1016/j.memsci.2010.07.005

[45] D.A.G. Bruggeman, Ann. Phys. 24 (1935) 636−679. https://doi.org/10.1002/andp.19354160705

[46] Z. Hashin, A. Shtrikman, J. Appl. Phys. 33 (1962) 3125−3131. https://doi.org/10.1063/1.1728579

[47] Y. Li, T.-S. Chung, C. Cao, S. Kulprathipanja, J. Membr. Sci. 260 (2005) 45−55. https://doi.org/10.1016/j.memsci.2005.03.019

Supporting Information

Covalent triazine framework CTF-fluorene as porous filler material in mixed matrix membranes for CO_2/CH_4 separation

Stefanie Bügel, Alex Spieß, Christoph Janiak*

Institut für Anorganische Chemie und Strukturchemie, Heinrich-Heine-Universität Düsseldorf, D-40204 Düsseldorf, Germany

*Corresponding author: Christoph Janiak

E-mail address: janiak@hhu.de (C. Janiak)

Table of Contents

1. Characterization of CTF-fluorene

1.1. Elemental analysis

The elemental analysis of CTF-fluorene is listed in Table S1. The formation of the product is highly reproduceable under chosen reaction conditions, still the content of nitrogen is less than the calculated values, which is a well-known aspect in literature [1,2].

The remaining mass fraction can be explained by oxygen content and residues of aluminum species from the catalyst. Both, in CTFs synthesized via Friedel-Crafts synthesis and ionothermal synthesis, catalyst residues cannot be removed completely.

The low nitrogen content can be traced to the partial formation of polymer chains in which the triazine unit is connected to two bridging and a terminal fluorene molecule [2].

In order to improve the nitrogen content variations of the synthesis conditions have been carried out. The ratio of the educts has been modified in order to obtain CTF-fluorene with a higher nitrogen content. Thereby, a relation between higher nitrogen content and less porosity was observed. The higher the excess of cyanuric chloride, the less porosity was obtained. CTF-fluorene_2, which was synthesized with an excess of cyanuric chloride is given exemplarily in Table S1. The latter CTF exhibited a nitrogen content of 9.9 wt%, but with a BET surface area of 20 m^2/g the material showed no porous properties.

The CTF-fluorene material used in this work showed the highest nitrogen content together with a high porosity.

Table S1

Elemental analysis of CTF-fluorene.

Compound	C [wt%]	H [wt%]	N [wt%]	C/H [wt%/wt%]	calc. H [wt%] [c]	ΔH = found H - calc. H [wt%]
Ideal	83.32	3.73	12.95	22.3	--	
CTF-fluorene (filler material)	76.39	4.15	6.50		3.34	0.81
CTF-fluorene [a]	78.85	3.44	6.65	22.9	--	
CTF-fluorene_2 [b]	72.48	4.02	9.85		3.17	0.85
CTF-fluorene, literature value [2]	74.8	4.8	5.8			

[a] dried (180 °C; vacuum $7x10^{-3}$ bar, 8 h); filled in zinc capsule under argon atmosphere before combustion.

[b] 3 mmol of cyanuric chloride, 1.5 mmol of fluorene, 6 mmol $AlCl_3$, fluorene in DCM was added slowly, dropwise to reaction mixture.

[c] calculated wt% H based on the C/H ratio of 22.9 of the dried and argon covered CTF-fluorene sample in line 3, obtained by dividing the wt% C of the sample by 22.9.

In previous work we had shown that CTFs are hygroscopic, with a water uptake of up to ~20 wt% at P/P_0 = 0.5-0.6 or 50-60% air humidity when stored under ambient air, as it is the case, for example, before a normal elemental analysis sample preparation [2,3]. Proof to this water uptake is also provided here by comparison to a CTF-fluorene CHN analysis, where the CTF was dried at 180 °C under a vacuum of $7x10^{-3}$ bar for 8 h and filled into a zinc capsule under argon atmosphere before CHN combustion analysis. We consider the C/H wt% ratio of this samples which is not far from the ideal ratio and apply this ratio to calculate the wt% H for the other samples based on their different wt% C. We then assume the difference between the found and calc wt% H of 0.81 wt% to be due to adsorbed water. The ideal repeat unit of CTF-fluorene is the triazine ring C_3N_3 and 3/2 of the fluorene groups (minus 2H atoms on each group).

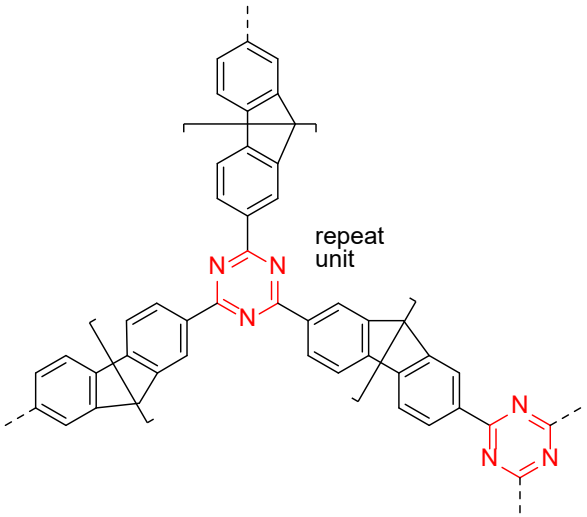

repeat unit: C_3N_3 + 3/2(FL–2H)

C_3N_3+3/2($C_{13}H_8$) = $C_{22.5}H_{12}N_3$; formula weight = 324.365 g/mol: C 83.32, H 3.73, N 12.95%.

With 2.5 H_2O per repeat unit (12 wt% of water) or $C_{22.5}H_{17}N_3O_{2.5}$, M = 369.4 g/mol: C 73.2, H 4.6, N 11.4, O 10.8%.

From Karl-Fischer titration a water content of 12.3-12.7 wt% had been reported for two CTF-fluorene samples which had been stored under ambient air, following their synthesis and drying procedure [2]. We note that the above estimate and inclusion of the water content improves the match between the calculated and found CHN values.

1.2. Infrared spectroscopy (IR)

The IR spectrum (Figure S1) supports the formation of CTF-fluorene. The bands at 1706 cm^{-1} (w) and 1608 cm^{-1} (w) can be assigned to C=C bond stretching vibrations. The bands at 1514 cm^{-1} (s) and 1357 cm^{-1} (m) are due to aromatic C–N stretching modes of the triazine ring [4,5]. The band at 1243 cm^{-1} (m) can also be assigned to C–N bond stretching vibrations of the triazine unit [6]. The absence of the C–Cl stretching band from cyanuric chloride at 846 cm^{-1} (vs) indicates the complete conversion of the educt cyanuric chloride [2].

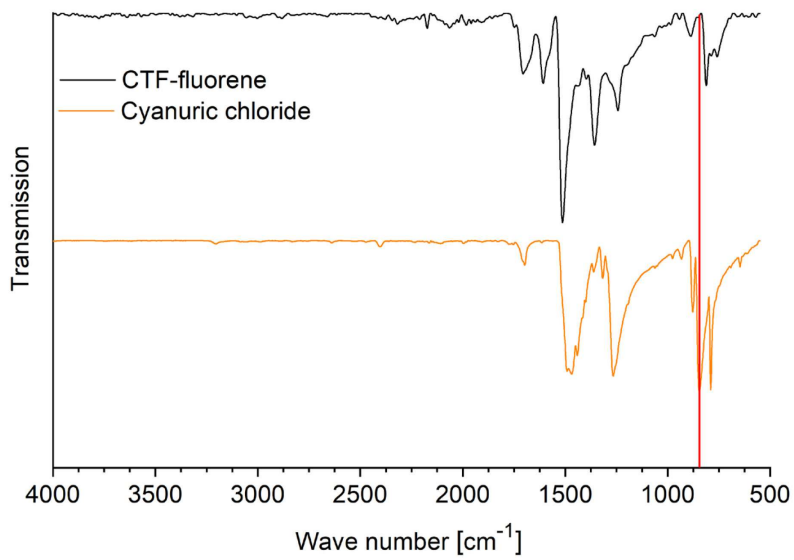

Figure S1. IR spectrum of CTF-Fluorene and cyanuric chloride. The red line at 846 cm^{-1} (vs) shows the C–Cl stretching band from cyanuric chloride.

1.3. Thermogravimetric analysis (TGA)

The thermal stability of CTF-fluorene is determined by a TGA measurement under synthetic air (Figure S2). The TGA curve reveals a weight loss of 2.6 % up to 100 °C, which can be attributed to the evaporation of water. CTF-fluorene is thermally stable up to 311 °C. At a temperature of 632 °C a residual mass of 0.95 % is determined. The comparison of the TGA curve in the literature [2] shows a good accordance and the thermal stability of over 300 °C could be verified.

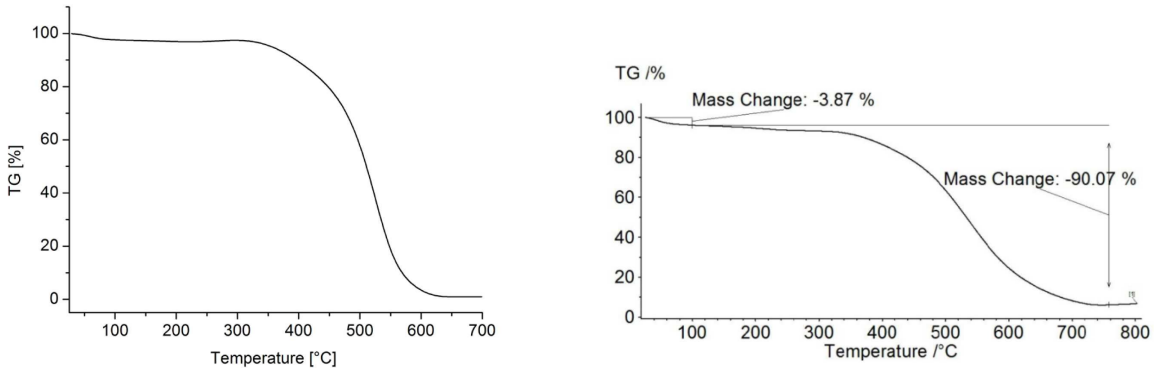

Figure S2. Thermogravimetric analysis of CTF-fluorene (left) and CTF-FL from the literature (right). Reproduced from Ref. [2] with permission from The Royal Society of Chemistry 2020.

1.4. Scanning electron microscopy (SEM)

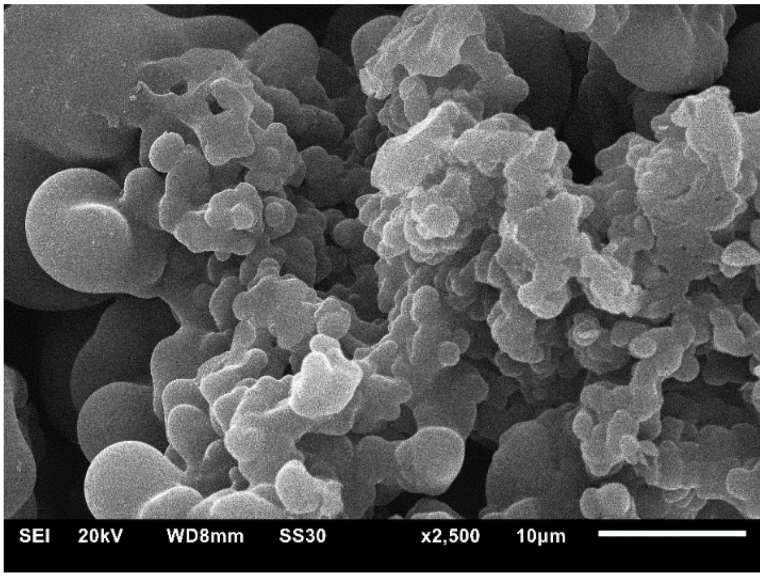

Figure S3. SEM image of CTF-fluorene.

1.5. Sorption measurements

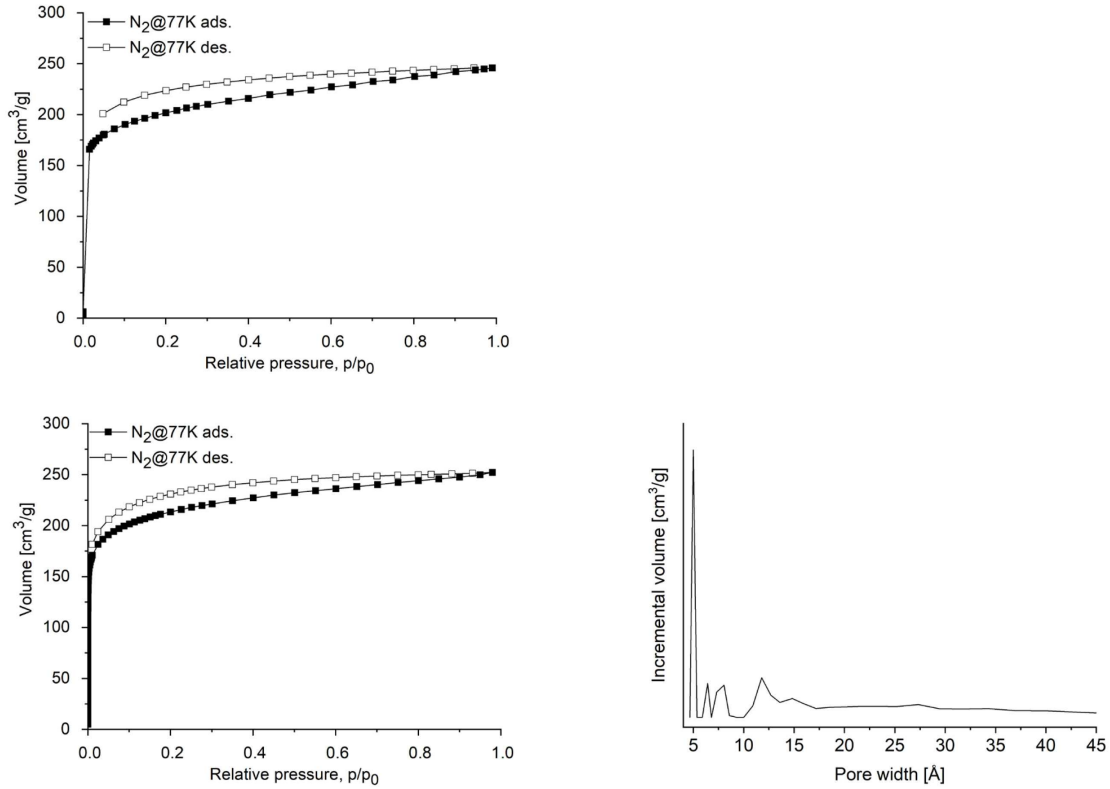

Figure S4. Nitrogen sorption isotherm of CTF-fluorene at 77 K, measured using an Autosorb-6 (Quantachrome) (top). Nitrogen sorption isotherm of CTF-fluorene at 77 K, measured using an ASAP 2020 (Micromeritics) and pore size distribution (bottom) generated from the data used in reference [2].

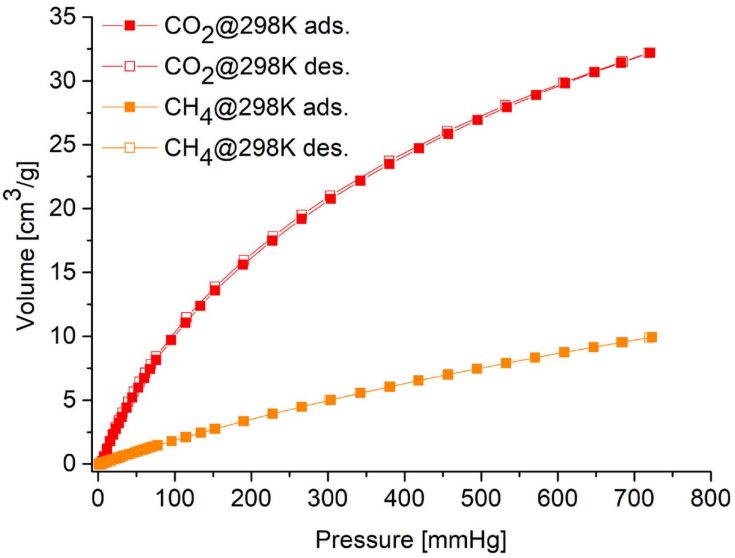

Figure S5. CO_2 and CH_4 sorption isotherms of CTF-fluorene at 298 K (volume given at standard temperature and pressure (STP)).

1.6. Ideal adsorbed solution theory (IAST)

The CO_2 and CH_4 isotherms of CTF-fluorene at 298 K (Figure S5) were fitted with the Langmuir (LAI) isotherm model. The parameters for the LAI fitting are shown in Table S2.

Table S2

Parameters for LAI fitting.

Gas	Temperature [K]	Model	R^2	Affinity constant K [1/bar]	Maximal loading q_{max} [mmol/g]
CO_2	298	LAI	0.9992	1.841	2.208
CH_4	298	LAI	0.9999	0.393	1.591

The selectivity of CTF-fluorene for a binary (50:50; v:v) mixture of the gases CO_2/CH_4 was calculated by applying the ideal adsorbed solution theory (IAST) and is depicted in Figure S as a function of the pressure.

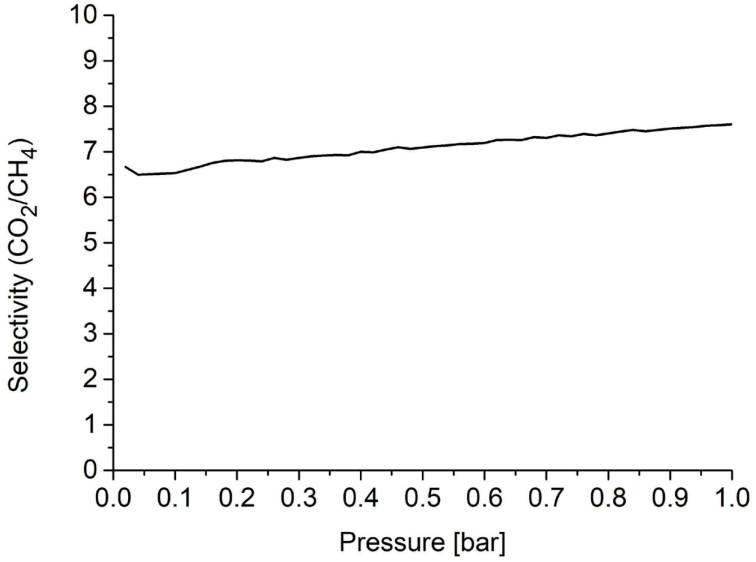

Figure S6. IAST selectivity of CTF-fluorene for a binary (50:50; v:v) mixture of the gases CO_2/CH_4 at 298 K.

2. Characterization of the CTF-fluorene/polymer membranes

2.1. SEM images of pure polymer membranes

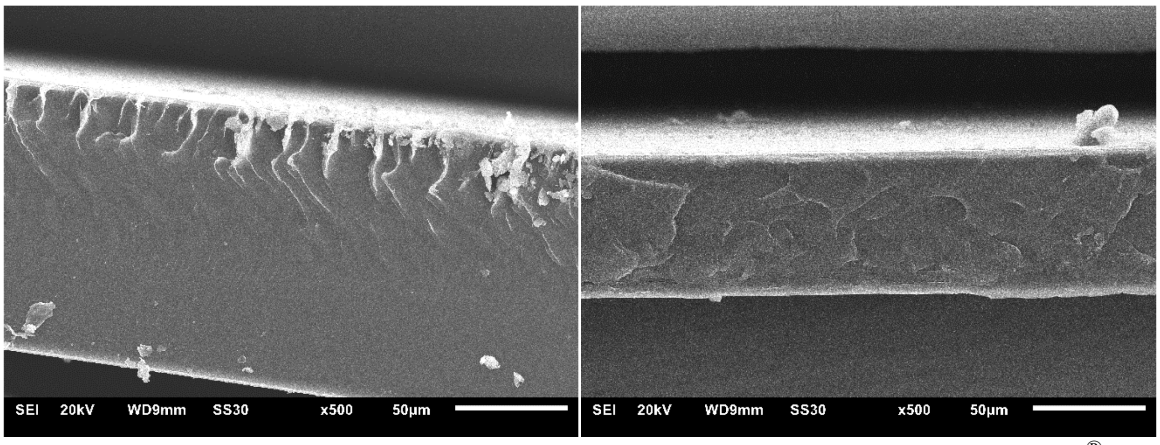

Figure S7. Cross-section SEM images of pure PSF (left) and pure Matrimid® (right) membranes.

2.2. TGA

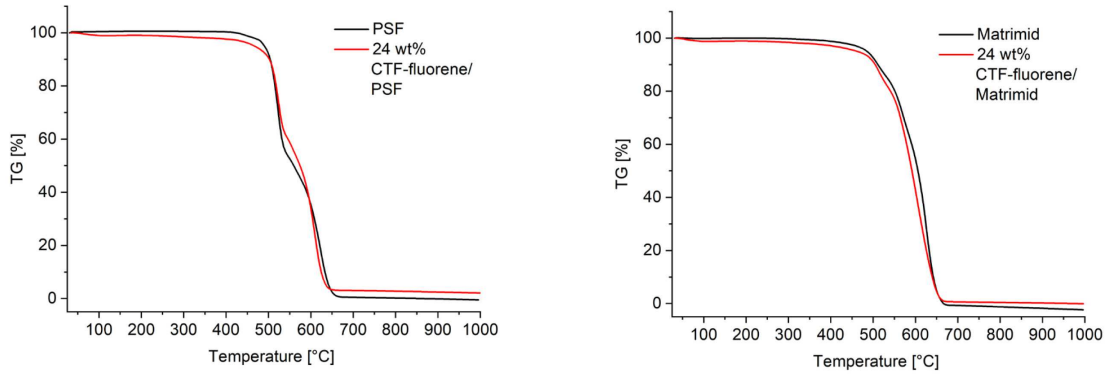

Figure S8. TGA of the 24 wt% CTF-fluorene/PSF MMM in comparison to the pure PSF membrane (left) and of the 24 wt% CTF-fluorene/Matrimid® MMM in comparison to the pure Matrimid® membrane (right). Measurements were conducted under synthetic air with a heating rate of 5 K/min.

2.3. Membrane thickness

While the wt% of the CTF in the membrane is increased, the amount of the polymer stays the same (400 mg polymer for each membrane), which leads to the increased thickness. To produce membranes with a constant thickness regardless of filler content, the amount of polymer and filler would need to be adjusted accordingly. In our opinion, it is more important to prepare all membranes with the constant amount of polymer than adapt the thickness, because the thickness

of every membrane is considered by calculating the permeability *P* in the unit Barrer and not with the gas permeance = *P*/*d* in the gas permeation unit (GPU), so the thickness (*d*) is already considered in the unit.

The thickness *d* of all membranes is listed in Table S3. For the permeability values in Barrer the following equation was used:

$$P = \frac{x_A \times Q_{He} \times d}{x_{He} \times A \times (p_2 \times x_A^f - p_1 \times x_A)}$$

x_A: molar fraction of the gas A

Q_{He}: volumetric flow rate of the sweep gas helium [cm^3/s]

d: thickness of the membrane, measured at 10 different points

x_{He}: molar fraction of the sweep gas (permeate)

A: area of the membrane [cm^2]

p_2: feed pressure [cmHg]

x_A^f: molar fraction of the gas A in the feed

p_1: permeate pressure [cmHg]

The thickness, with the individual membrane values listed in Table S3, were put into the equation for the variable *d*.

Table S3

Thickness of CTF-fluorene/PSF and CTF-fluorene/Matrimid® MMMs.

Matrix	CTF-fluorene content [wt%]	Thickness [a] [µm]		Matrix	CTF-fluorene content [wt%]	Thickness [a] [µm]	
PSF	0	50	56	Matrimid®	0	57	61
	8	60	75		8	61	61
	16	66	68		16	69	72
	24	58	81		24	99	87

[a] The two values correspond to two membranes as each membrane was prepared twice and each had its permeability determined to ensure reproducibility.

2.4. Permeability models

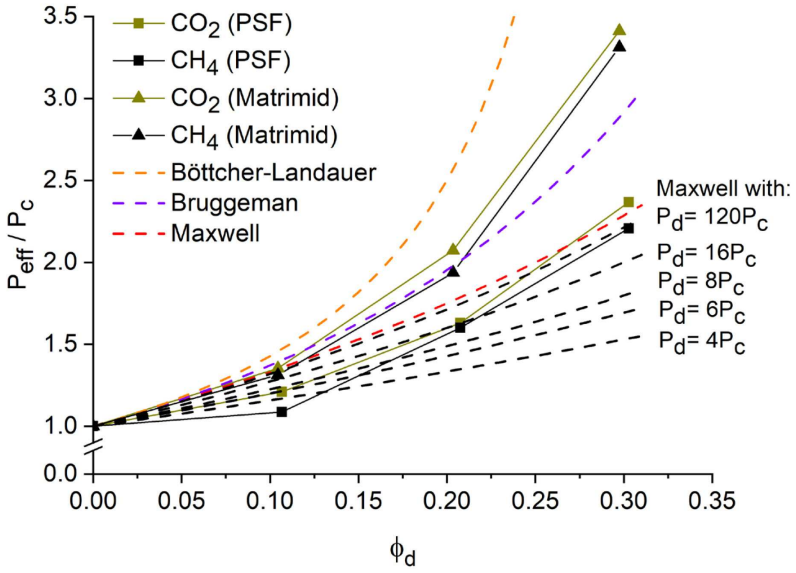

Figure S9. P_{eff}/P_c versus ϕ_d for 0 wt%, 8 wt%, 16 wt% and 24 wt% CTF-fluorene/PSF and CTF-fluorene/Matrimid® MMMs in comparison to the Maxwell, Maxwell with $P_d = xP_c$, Bruggeman and Böttcher-Landauer model for porous fillers.

3. References

[1] P. Puthiaraj, S.-S. Kim, W.-S. Ahn, Chem. Eng. J. 283 (2016) 184–192. https://doi.org/10.1016/j.cej.2015.07.069

[2] S. Dey, A. Bhunia, D. Esquivel, C. Janiak, J. Mater. Chem. A 4 (2016) 6259−6263. https://doi.org/10.1039/C6TA00638H

[3] S. Dey, A. Bhunia, H. Breitzke, P.B. Groszewicz, G. Buntkowsky, C. Janiak, J. Mater. Chem. A 5 (2017) 3609−3620. https://doi.org/10.1039/C6TA07076K

[4] M. J. Bojdys, J. Jeromenok, A. Thomas, M. Antonietti, Adv. Mater. 22 (2010) 2202–2205. https://doi.org/10.1002/adma.200903436

[5] S. Hug, M.B. Mesch, H. Oh, N. Popp, M. Hirscher, J. Senkerd, B.V. Lotsch, J. Mater. Chem. A 2 (2014) 5928–5936. https://doi.org/10.1039/C3TA15417C

[6] M. Prabhaharan, A.R. Prabakaran, S. Srinivasan, S. Gunasekaran, Spectrochim. Acta A 127 (2014) 454–462. https://doi.org/10.1016/j.saa.2014.02.040

3.2. Biphenyl-based covalent triazine framework/Matrimid® mixed-matrix membranes for CO_2/CH_4 separation

Stefanie Bügel, Quang-Dien Hoang, Alex Spieß, Yangyang Sun, Shanghua Xing, Christoph Janiak

Membranes **2021**, *11*, 795.

DOI: 10.3390/membranes11100795; [116]

CO_2/CH_4 separation is an environmentally relevant and timely topic due its value in processes such as biogas upgrading and natural gas sweetening. The application of membranes can solve this separation issue. In the recent years, separation performance could be enhanced by the application of MMMs, in which filler materials are introduced into polymer matrices. In this work, CTF-biphenyl was synthesized via Friedel-Crafts alkylation from cyanuric chloride and biphenyl to be applied as porous filler in Matrimid matrices. MMMs containing 8, 16, and 24 wt% of CTF-biphenyl were applied for binary CO_2/CH_4 mixed-gas separation measurements. It was observed that 16 wt% CTF-biphenyl was the optimum filler content in terms of membrane performance and filler consumption. With this loading of the CTF, CO_2 permeability was increased to 15.1 Barrer, more than doubling that of the pure polymer membrane, while maintaining the high CO_2/CH_4 selectivity of Matrimid.

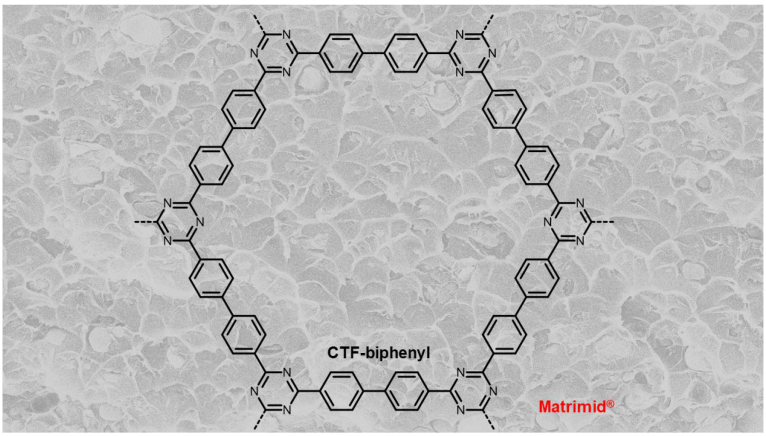

Author's contribution to the work:

- Idea, concept and data interpretation
- CTF synthesis and MMM preparation with Q.-D. Hoang
- Manuscript writing with corrections by C. Janiak
- A. Spieß: recorded SEM images; Y. Sun: carried out TGA measurements; S. Xing: carried out CO_2- and CH_4-sorption measurements

The work presented in this chapter has been published as:

Biphenyl-based covalent triazine framework/Matrimid® mixed-matrix membranes for CO_2/CH_4 separation

Stefanie Bügel[1], Quang-Dien Hoang[1], Alex Spieß[1], Yangyang Sun[1], Shanghua Xing[1,2], Christoph Janiak*[1,2]

[1] Institut für Anorganische Chemie und Strukturchemie, Heinrich-Heine-Universität Düsseldorf, D-40204 Düsseldorf, Germany

[2] Hoffmann Institute of Advanced Materials, Shenzhen Polytechnic, 7098 Liuxian Blvd, Nanshan District, Shenzhen 518055, China

*Corresponding author: Christoph Janiak

Abstract: Processes, such as biogas upgrading and natural gas sweetening, make CO_2/CH_4 separation an environmentally relevant and current topic. One way to overcome this separation issue is the application of membranes. An increase in separation efficiency can be achieved by applying mixed-matrix membranes, in which filler materials are introduced into polymer matrices. In this work, we report the covalent triazine framework CTF-biphenyl as filler material in a matrix of the glassy polyimide Matrimid®. MMMs with 8, 16, and 24 wt% of the filler material are applied for CO_2/CH_4 mixed-gas separation measurements. With a CTF-biphenyl loading of only 16 wt%, the CO_2 permeability is more than doubled compared to the pure polymer membrane, while maintaining the high CO_2/CH_4 selectivity of Matrimid®.

Keywords: *mixed-matrix membrane (MMM); covalent triazine framework (CTF); Matrimid®; CO_2/CH_4 separation*

1. Introduction

Since the first large-scale application of a hydrogen-separating membrane in the 1980s [1], a strong development in membrane technology for various separation tasks has been noticeable. One of these tasks is the separation of CO_2 and CH_4 (for "biogas upgrading" and "natural gas sweetening"), for which the use of polymeric membranes is an appropriate option, since they offer an energy- and cost-efficient separation [2,3]. In order to further increase the CO_2 permeability and CO_2/CH_4 selectivity of gas separation membranes, additional filler

components are used as a dispersed phase embedded in a polymer matrix to form mixed-matrix membranes (MMMs) [4]. In addition to frequently utilized filler materials, such as MOFs [5–10], including ZIFs [11–13] or zeolites [14,15], purely organic porous materials, such as covalent organic frameworks (COFs) or covalent triazine frameworks (CTFs), are also promising materials [16,17]. Especially, in a completely organic MMM, a good compatibility of filler and matrix is more likely than in MMMs with inorganic fillers so that the formation of the unselective void volume may be decreased [18]. Shan et al. synthesized the microporous azine-linked COF material ACOF-1 and incorporated it into a Matrimid® matrix. The gas separation performance was tested with an equimolar CO_2/CH_4 mixture at 308 K, and the 16 wt% MMM showed a rise in CO_2 permeability of 8.5 Barrer without loss of CO_2/CH_4 selectivity [19]. The fluorinated CTF FCTF-1 was applied as filler material in a PIM-1 membrane. The CO_2 permeability increased from 5800 Barrer for the pure membrane to 9400 Barrer for the 5 wt% FCTF-1 membrane and the CO_2/CH_4 selectivity was improved from 11.5 to 14.8 [20]. Previous studies showed that the incorporation of CTF-1 in a PSF matrix exhibited an elevation in CO_2 permeability from 7.3 Barrer for the pristine membrane to 12.7 Barrer for a filler content of 24 wt% CTF-1 whilst maintaining the CO_2/CH_4 selectivity [21].

This ability of organic filler materials to enhance the performance of MMMs was taken as a reason to prepare novel CTF-biphenyl/Matrimid® MMMs. The glassy polymer Matrimid® was chosen as a matrix due to its high CO_2/CH_4 selectivity, thermal stability [22], and the previously proven good compatibility with CTF materials [23]. Further, studies on the effect of the ionic liquid (IL) 1-butyl-3-methylimidazolium bis(trifluoromethanesulfonyl)imide, [BMIm][NTf_2] on membrane performance were investigated due to the high solubility of CO_2 in ILs [24–26] and the positive effects of ILs on membrane performance, which were reported previously [27–30]. CO_2 and CH_4 mixed-gas permeabilities and selectivities were measured for all membrane systems.

2. Materials and Methods

2.1. Materials

For the CTF-biphenyl synthesis, anhydrous aluminum chloride ($AlCl_3$; 98.5%) was received from Arcos Organics, cyanuric chloride (99%) was obtained from Sigma-Aldrich, and biphenyl (99%) from Alfa Aesar. Biphenyl was recrystallized from ethanol before usage. For the synthesis of the IL, [BMIm][NTf_2] 1-chlorobutane (99%) was purchased from Merck, 1-methylimidazole (99%) and lithium bis(trifluoromethanesulfonyl)imide (Li[NTf_2]; 99%) were obtained from Fluorochem, activated charcoal (extra pure) from Merck, and acidic aluminum

oxide (150 m^2/g; Brockmann grade 1) from Alfa Aesar. The solvents acetone (≥99.8%), dichloromethane (DCM; 99.99%), and ethyl acetate (≥99%) were received from Fisher Scientific; and methanol (MeOH; ≥99.8%) and tetrahydrofuran (THF; ≥99.9%) from Sigma-Aldrich. The polymer Matrimid® 5218 (BTDA/DAPI) was provided by Huntsman Advanced Materials. The gases CO_2 (grade 4.5), CH_4 (grade 4.5), and He (grade 5.0) were received from Air Liquide.

2.2. Synthesis of CTF-Biphenyl

CTF-biphenyl was synthesized by Friedel-Crafts alkylation (Scheme 1) due to the possible upscaling, which is not applicable for ionothermal synthesis [31]. The CTF was prepared in analogy to the literature [32]. Biphenyl (2.313 g, 15 mmol), cyanuric chloride (1.844 g, 10 mmol), and anhydrous $AlCl_3$ (6.000 g, 45 mmol) were refluxed in 500 mL of DCM for 16 h. After filtration, the product was washed 15 min for each step with water (3 × 50 mL) and methanol (3 × 50 mL). Further washing steps were carried out with THF (3 × 50 mL) and acetone (3 × 50 mL). The product was dried at 120 °C for 24 h and was milled with a shaker mill (Retsch, MM301) with a frequency of 30 Hz for 15 min to obtain a fine powder (yield: 2.87 g; 94%).

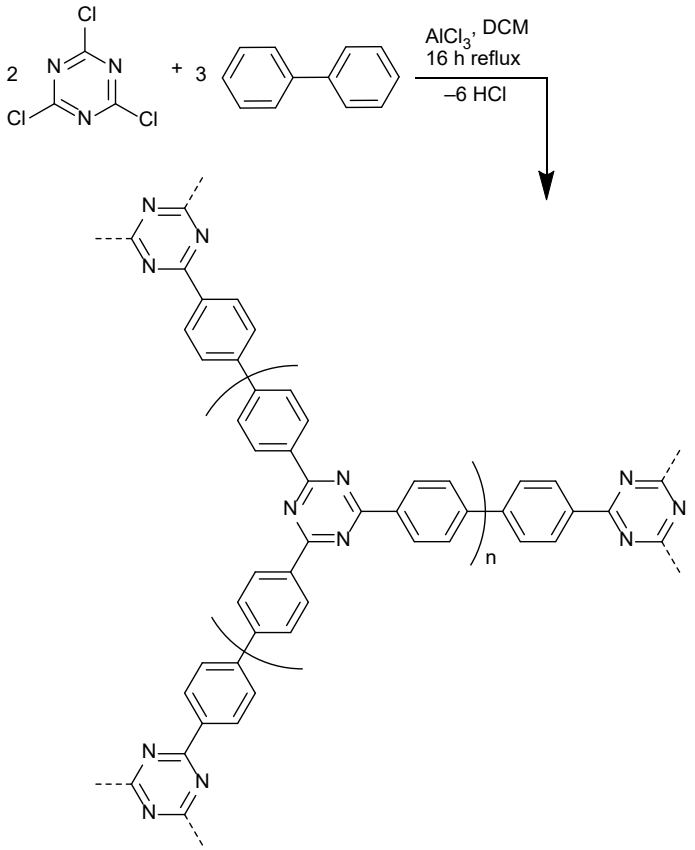

Scheme 1. Synthesis of CTF-biphenyl (idealized structure with repeat unit in parenthesis).

2.3. Membrane Preparation

All membranes were prepared by solution casting. The filler loadings of CTF-biphenyl refer to the combined mass of the polymer and filler according to Equation (1):

$$Filler\ loading\ [wt\%] = \frac{m_{filler}}{m_{polymer} + m_{filler}} \times 100\ \% \quad (1)$$

Matrimid® was dried for 5 days at 80 °C before usage. For the pure Matrimid® membranes, 400 mg of the polymer were dissolved in 5 mL of DCM and stirred for 24 h before casting. The CTF/Matrimid® MMMs were prepared as follows [33]: Matrimid® (400 mg) was dissolved in 3.5 mL of DCM and stirred for 24 h. Meanwhile, CTF-biphenyl (35 mg for 8 wt%, 76 mg for 16 wt%, and 126.5 mg for 24 wt%) was dispersed in 4.5 mL of DCM and stirred for 24 h. The CTF-biphenyl dispersion was ultrasonicated (VCX 750 Sonics; Microtip 630-0419) with an amplitude of 20% three times for 15 min each. After each 15 min ultrasonication procedure, the dispersion was stirred for 30 min. Then, part of the polymer solution (0.33 mL for 8 wt%, 0.72 mL for 16 wt% and 1.20 mL for 24 wt%) was added to the CTF-biphenyl dispersion followed by another 24 h of stirring. After the same three 15 min ultra-sonification steps were repeated, the remaining polymer solution was added and stirred for 1 h. For all membranes, the solution casting and drying was carried out under the same conditions: The mixtures were cast into metal rings placed on a flat glass surface. In order to achieve a controlled evaporation of DCM, an inverted funnel, covered with a paper tissue, was placed above the metal ring. When the DCM was evaporated, the membrane was cut out with a scalpel and dried in a vacuum oven (150 °C, 20 mbar) overnight. For the preparation of the IL-containing membranes, see Section 3 in the Supplementary Materials. All membranes were measured after drying in the vacuum oven and no further treatment with alcohol was performed. In the literature, such an alcohol treatment is sometimes performed to increase the permeability for a certain time period [34].

2.4. Instrumentation and Characterization Methods

Attenuated total reflection infrared spectroscopy (ATR-IR, Platinum ATR-QL, diamond) in the range from 4000 cm^{-1} to 500 cm^{-1} was measured on a Tensor 37 (Bruker). A vario MICRO cube (elementar) was used to perform elemental analysis (C, H, N, S). Scanning electron microscopy (SEM) images were obtained by a JSM-6510LV (Jeol) with a LaB_6 cathode (20 keV) after coating of the sample with gold by a JFC 1200 (Jeol) coater. All membranes were broken through freeze-fracturing after cooling in liquid nitrogen to obtain cross-section images. A TG 209 F3 Tarsus (Netzsch) was used for thermogravimetric analysis (TGA). Measurements were carried out under synthetic air in a range from 25 °C to at least 700 °C with a heating rate

of 5 K/min. The water content of the IL was quantified with coulometric Karl-Fischer titration (KFT) using an AQUA 40.00 (Analytik Jena/ECH) with a headspace module at 170 °C. ^{1}H and ^{13}C-NMR spectra were recorded with an Avance III spectrometer (Bruker) operating at 300 and 75 MHz, respectively. Density determination was carried out with an AccuPyc 1330 helium pycnometer (Micromeritics). A determination was performed in triplicate with 5 measured values each. For the density determination (Equation (2)), the total pore volume from the N_2 sorption was considered due to the fact that helium does not fill the pores of the CTF at room temperature:

$$\rho_{CTF} = \frac{V_{He} + V_{pores}}{m_{CTF}} \quad (2)$$

Nitrogen sorption measurements were performed on an Autosorb-6 (Quantachrome). Brunauer–Emmett–Teller (BET) surface areas were calculated from the adsorption isotherms by applying multipoint analysis in the range of 0.05 to 0.3 p/p_0 with a correlation coefficient of minimum r = 0.999994. CO_2 and CH_4 sorption measurements were performed with a sorption analyzer Autosorb-iQ MP (Quantachrome) and the resulting isotherms were fitted with the Toth model (3Psim software version 1.1.0.7.) by applying Equation (3), where q refers to the loading in mmol/g, K stands for the affinity constant with the unit 1/bar and t refers to the heterogeneity exponent:

$$q_{eq} = q_{max} \times \frac{K \times p}{(1+(K \times p)^t)^{\frac{1}{t}}} \quad (3)$$

All samples were activated before sorption measurements by degassing in vacuum at 120 °C for 8 h. CO_2/CH_4 mixed-gas separation was carried out on an OSMO inspector (provided by Convergence Industry B.V.) connected to an Agilent 490 Micro GC (Agilent Technologies) with a fused silica column PoraPLOT Q. A schematic drawing of the experimental setup has been presented in a previous publication [23]. To ensure that all membranes have an area of 11.3 cm^2 while measuring, the membranes were placed in a permeation module and fixed with a Viton O-ring with an inner diameter of 3.6 cm. The mixed-gas separation experiments were carried out with a transmembrane pressure of 3 bar at 25 °C and were checked every 30 min with GC measurements until an equilibrium state was reached (after about 5–8 h). Once the membranes were equilibrated, the characteristic permeability was calculated from at least the last three recorded measurements. The feed gas consisted of CO_2/CH_4 in a volume ratio of 1:1 and helium was used as sweep gas. Each membrane was prepared and measured twice. The

permeability P in Barrer ($1\ \text{Barrer} = 10^{-10}\text{cm}^3(STP) \times \text{cm} \times \text{cm}^{-2} \times s^{-1} \times cmHg^{-1}$) [35] was calculated according to the following Equation (4):

$$P = \frac{x_A \times Q_{He} \times d}{x_{He} \times A \times (p_2 \times x_A^f - p_1 \times x_A)} \quad (4)$$

where x_A, Q_{He}, and d are the molar fraction of the gas A, the volumetric flow rate of the sweep gas helium, and the thickness of the membrane, measured at 10 different points with a micrometer screw, respectively. x_{He}, A, p_2, x_A^f, and p_1 are the molar fraction of the sweep gas (permeate), the area of the membrane, the feed pressure, the molar fraction of the gas A in the feed, and the permeate pressure, respectively. The mixed-gas selectivity (Equation (5)) of two gases (A and B) was calculated from their molar fractions (x) on the permeate side divided by their molar fractions on the feed side:

$$\alpha_{A,B} = \frac{(x_A/x_B)_{permeate\ side}}{(x_A/x_B)_{feed\ side}} \quad (5)$$

3. Results and Discussion

3.1. Characterization of CTF-Biphenyl

The successful formation of CTF-biphenyl was confirmed by ATR-IR (Figure S1). The bands at 1704 cm^{-1} (w) and 1606 cm^{-1} (w) can be assigned to C=C bond stretching vibrations and the bands at 1511 cm^{-1} (s), 1377 cm^{-1} (w), and 1254 cm^{-1} (m) are due to C–N bond stretching vibrations of the triazine unit [36]. Elemental analysis (Table S1) showed a lower nitrogen content than calculated for the idealized structure, which is a common phenomenon concerning CTFs synthesized by Friedel–Crafts alkylation or by other methods like trifluoromethanesulfonic acid-catalyzed reactions or ionothermal synthesis [32,36,37]. Due to the hygroscopic nature of CTFs with a water uptake of up to ~20 wt% at 50–60% air humidity [32,38], the nitrogen and carbon wt% is already lowered due to adsorbed water during probe handling. For a comparison with other CTF structural analogs to CTF biphenyl, see Section 1 in the Supplementary Materials. TGA measurements (Figure S2) confirmed a thermal stability up to 320 °C under synthetic air and SEM images of CTF-biphenyl (Figure S3) showed particles with a mainly spherical shape. N_2-sorption (Figure S4a) of CTF-biphenyl revealed a transition from Type I to Type II isotherm for the adsorption from low to high relative pressure. The pronounced uptake at low p/p_0 is associated with the filling of micropores. Desorption featured an H4 loop, which is often found with aggregates of micro-mesoporous carbons [39]. The isotherm and hysteresis type are in accordance with the observations from Lim et al., who synthesized the same CTF-biphenyl via Friedel–Crafts alkylation [40]. The CTF synthesized in

this study exhibited a higher BET surface area of 940 m^2/g with a total pore volume of 0.53 cm^3/g (literature 646 m^2/g and 0.31 cm^3/g [40]). The pore size distribution was obtained by applying quenched solid density functional theory (QSDFT), which is favorable for disordered micro/mesoporous carbon materials [41]. The slit pore, equilibrium model (N_2 at 77 K on carbon) was utilized and revealed pore diameters mainly at 9 and 13 Å, with smaller volume contributions up to 40–50 Å (Figure S4b). Further, CO_2 and CH_4 sorption of CTF-biphenyl (Figure S5) at 298 K resulted in CO_2 and CH_4 uptakes of 1.87 mmol/g (at 0.96 bar) and 0.55 mmol/g (at 0.97 bar). The CO_2 and CH_4 sorption isotherm fit with the Toth model (Table S3) allowed ideal adsorbed solution theory (IAST) calculations to be carried out, yielding a CO_2/CH_4 selectivity of 10.5 at 1 bar pressure for a 50:50 (v:v) gas mixture (Figure S6).

3.2. Characterization of CTF-Biphenyl/Matrimid® MMMs and Their Gas Separation Studies

All CTF-based MMMs were analyzed by cross-section SEM images to confirm the incorporation of the filler materials as well as to insure the absence of defects in the MMMs. Figure 1 shows the cross-section SEM images of the CTF/Matrimid® MMMs. The absence of heavy atoms in the CTF and no distinct particle shape yielded a low contrast between the filler and polymer. Unfortunately, the SEM images did not prove very expressive concerning filler–polymer interface compatibility or aggregation. Only for the MMM with 8 wt% can relatively more interfacial voids be observed as compared to the MMMs with higher filler contents. All of the CTF-based MMMs have no major defects that would cause a loss of selectivity in the permeation experiments.

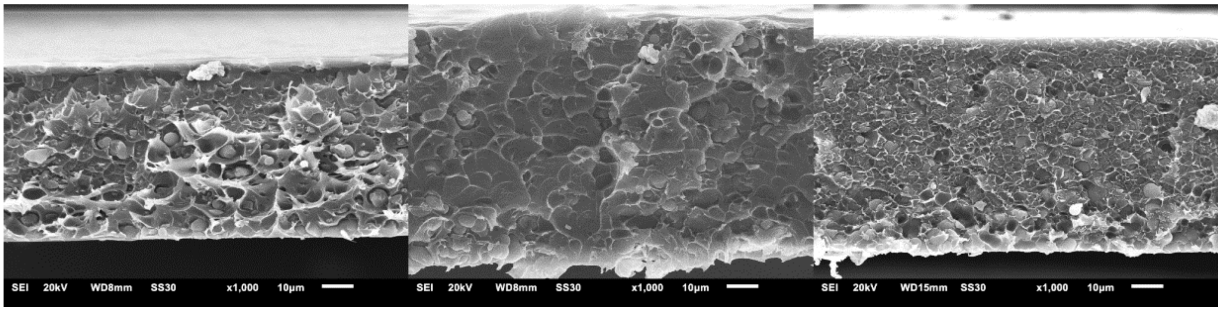

Figure 1. Cross-section SEM images of 8 wt% (**left**), 16 wt% (**middle**), and 24 wt% (**right**) CTF/Matrimid® MMMs. The cross-sections were formed by breaking the membrane through freeze-fracturing after cooling in liquid nitrogen.

The neat polymer membrane and the MMMs were further applied for CO_2/CH_4 mixed-gas separation experiments. For the CTF/Matrimid® MMMs, CO_2 permeability increased from 6.8 Barrer for the neat Matrimid® membrane to 12.0 Barrer for 8 wt% of CTF-biphenyl. For a filler content of 16 wt% CTF-biphenyl, the CO_2 permeability was raised further to 15.1 Barrer. With

elevation of the filler content to 24 wt%, the permeability stayed essentially constant within the experimental error, reaching a value of 15.4 Barrer (Table 1 and Figure 2). The CH_4 permeability of all membranes was below 0.35 Barrer. A constant permeability for 16 and 24 wt% was also observed for CH_4. Consequently, the CO_2/CH_4 mixed-gas selectivities remained constant within the experimental error for all amounts of CTF-biphenyl applied. The higher the filler content, the lower the proportional increase in CO_2 permeability. In conclusion, the 16 wt% MMM showed the optimal membrane performance considering its high absolute permeability value, constant selectivity, and the medium consumption of the filler material.

Table 1. Gas permeabilities (*P*) and mixed-gas selectivity factors (α) of the pure Matrimid® membrane and CTF/Matrimid® MMMs [1].

CTF-Biphenyl [wt%]	P CO_2 [Barrer]	P CH_4 [Barrer]	α CO_2/CH_4
0 (neat Matrimid®)	6.8 ± 0.3	0.16 ± 0.01	42 ± 1
8	12.0 ± 0.2	0.27 ± 0.01	43 ± 1
16	15.1 ± 0.2	0.34 ± 0.01	44 ± 1
24	15.4 ± 0.5	0.35 ± 0.01	44 ± 1

[1] The errors for the permeability (*P*) and for the selectivity (α) were taken from the range of two measurements.

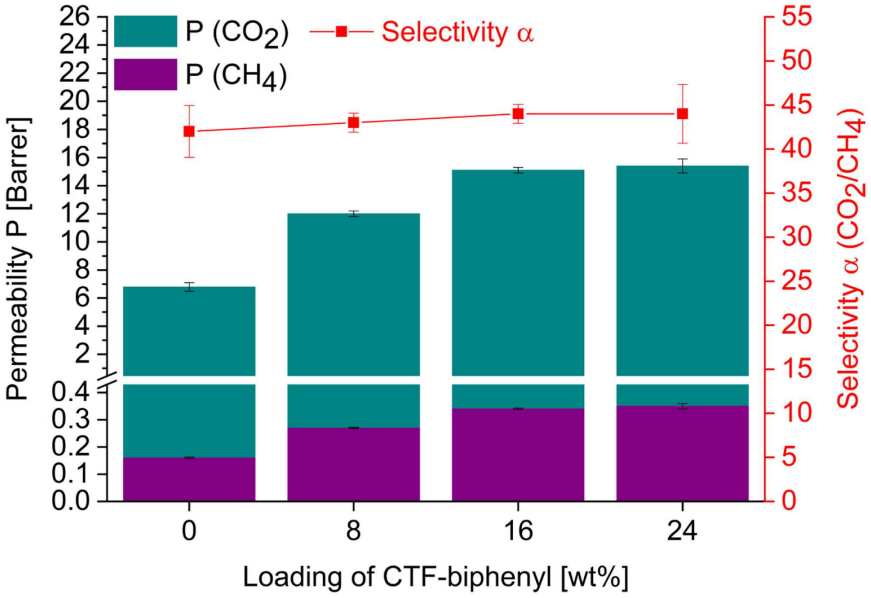

Figure 2. CO_2 and CH_4 permeabilities (*P*) and CO_2/CH_4 selectivities (α) for the pure Matrimid® membranes and CTF/Matrimid® MMMs.

The ratio of the permeability of the MMMs (P_{eff}) and the permeability of the pure continuous phase (P_c) can be predicted for different filler volume fractions (ϕ_d). Different models, such as the Maxwell [42], Bruggeman [43], and Böttcher–Landauer model [44], for porous fillers can

be applied. The simplified form of the Maxwell model for the case $P_d >> P_c$ (P_d: permeability of the dispersed phase) is shown in the following Equation (6):

$$\frac{P_{eff}}{P_c} = \frac{1+2\phi_d}{1-\phi_d} \quad (6)$$

At this point, it should be noted that the validity of the model is given for ϕ_d up to a maximum of 0.2. For the case of $\phi_d > 0.2$, the Bruggeman model (Equation (7)) or the Böttcher–Landauer model (Equation (8)) can be applied:

$$\frac{P_{eff}}{P_c} = \frac{1}{(1-\phi_d)^3} \quad (7)$$

$$\frac{P_{eff}}{P_c} = \frac{1}{(1-3\phi_d)} \quad (8)$$

The experimental results for P_{eff}/P_c versus ϕ_d are given in Figure 3a. The filler contents of 8, 16, and 24 wt% CTF-biphenyl were converted into the volume fractions ϕ_d of 0.12, 0.23, and 0.33, respectively. For this purpose, the determined density of CTF-biphenyl (0.79 g/cm^3) and the density of Matrimid® (1.20 g/cm^3) [45] were used. The errors were calculated from the largest difference in permeability values that can occur in the relative relation of P_{eff}/P_c. Due to the constant CO_2/CH_4 selectivity, P_{eff}/P_c values are higher for the more permeable gas CO_2. Comparing the experimental values with the models, it is noticeable that the permeabilities increase relatively more at lower ϕ_d values. At 8 wt% MMM, the values for P_{eff}/P_c are higher than those predicted by all models. The 16 wt% MMM agrees well with the Bruggeman model. Due to the stagnation of the permeability values with 24 wt% filler, the permeability is much too low compared to the higher filler amount.

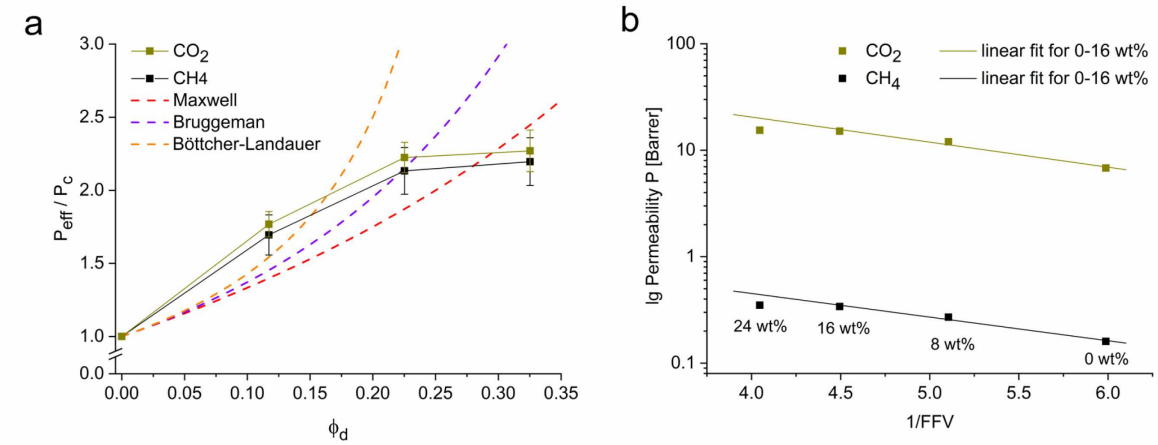

Figure 3. P_{eff}/P_c versus ϕ_d for 0 wt%, 8 wt%, 16 wt%, and 24 wt% CTF-biphenyl/Matrimid® MMMs in comparison to the Maxwell, Bruggeman, and Böttcher–Landauer model for porous fillers (**a**) and logarithm of permeability P versus 1/FFV for 0 wt%, 8 wt%, 16 wt%, and 24 wt% for CTF-biphenyl/Matrimid® (right) MMMs (**b**).

Our explanation is an unexpected poor interfacial compatibility between the CTF and Matrimid® giving a large interface volume and aggregation at higher filler content. At the relatively low filler content of 8 wt%, the filler particles still remain separated, but each particle would be surrounded by its interface volume. When the CTF particles aggregate at 24 wt%, the interface volume is relatively lower as the aggregated particles have a smaller surface-to-volume ratio than the separated particles at 8 wt%. The larger than normal interface volume at 8 wt% will then lead to an increase in permeability, which surmounts the expected increase from the fractional free volume (FFV) of the filler. Hence, the 8 wt% MMM surpasses the predicted P_{eff}/P_c ratio by the Maxwell model. The too low permeability of the 24 wt% MMM must be related to the aggregation effects such that less FFV of the filler is available and at the same time the aggregation also decreases the interface volume.

The influence of the free volume on the permeability can be illustrated by calculating the FFV. This dimensionless quantity can be obtained by multiplying the density and the pore volume of a material. The total FFV of a membrane (Equation (9)) is composed of the values of the polymer and the filler:

$$FFV = FFV_{polymer} * \phi_c + FFV_{filler} * \phi_d \quad (9)$$

For the calculation, the literature value of 0.167 [46] was used for Matrimid®, and all other values were determined from the densities of the materials described above. Plotting the logarithm of permeability *P* against 1/FFV (Figure 3b), it becomes clear that a linear correlation between the permeability and the free filler volume only holds up to the 16 wt% MMM. Considering the logarithmic nature of the correlation, the permeability of the 24 wt% MMM is much too low for its assumed FFV. Instead, the FFV of the 24 wt% MMM corresponds to about the FFV of the 16 wt% MMM. For dense membranes, the permeability (*P*) can be described as the product of the diffusion coefficient (*D*) and solubility (*S*) [47]. In the case of glassy polymers, diffusivity contributes a significantly higher proportion to the overall permeability than solubility [48]. The free volume can therefore have a positive effect on diffusivity and thus on permeability to a certain extent. This relationship becomes evident when comparing the free volume in this membrane system with the permeability. In cases where less free volume was generated, the permeability is also relatively lower compared to the MMMs with a higher contribution of free volume.

Although research on organic fillers in MMMs is increasing, there are few comparable materials embedded in a Matrimid® matrix that are applied for CO_2/CH_4 separation. One of these

materials is the azine-linked covalent organic framework ACOF-1. An equimolar CO_2/CH_4 mixture was used to determine the membrane performance of 8 and 16 wt% ACOF-1/Matrimid® MMMs. With a feed gas pressure of 4 bar at 308 K, the CO_2 permeability of the 8 and 16 wt% MMMs were found to be 9.6 and 15.3 Barrer in comparison to the pure matrix with a value of 6.8 Barrer. The selectivity was found to be constant [19]. The comparison also shows that a relatively high increase in CO_2 permeability can be achieved with 8 wt% CTF-biphenyl while maintaining constant CO_2/CH_4 selectivity. For 16 wt% filler, the comparison with the literature shows an almost identical value. In comparison to other CTFs, such as CTF-fluorene and CTF-1 in Matrimid® or in polysulfone (PSF), the membrane performance of CTF-biphenyl is slightly better or comparable both in permeability and selectivity [21,23]. Exceptions are the fillers SNW-1 and FCTF-1 in the polymer of intrinsic microporosity PIM-1, where already the PIM-1 gives rise to a CO_2 permeability of several thousand Barrer, albeit at low CO_2/CH_4 selectivity (from single-gas measurements). For PIM-1, the filler still increases this permeability but at a similar ratio as seen for other MMMs [20,49]. An overview of organic filler materials in different polymer matrices for CO_2/CH_4 separation is given in Table S9.

In order to gain further insight into this system, investigations on the effect of a ternary component were conducted. Throughout the literature, the incorporation of an IL as a third component is described with highly variable effects on membrane performance (Table S6). Due to the high solubility of CO_2 in ILs [24–26] and noted positive effects of ILs on membrane performance [27–29], we also investigated the incorporation of the IL 1-butyl-3-methylimidazolium bis(trifluoromethanesulfonyl)imide, [BMIm][NTf_2] in the CTF/Matrimid® MMMs (see Sections 3 and 4 in the Supplementary Materials). The introduction of the IL as a ternary component showed no improvement in permeability over the CTF/Matrimid® system. In a few membranes, the selectivity was raised with the IL to about 50–52 compared to about 44 for CTF/Matrimid® (Table S8 vs. Table 1).

4. Conclusions

CTF-biphenyl was synthesized via Friedel–Crafts-alkylation from cyanuric chloride and biphenyl to be applied as porous filler material in Matrimid® matrices. CO_2/CH_4 mixed-gas measurements of the prepared CTF/Matrimid® MMMs resulted in an increase in CO_2 permeability, while maintaining constant selectivity. For the MMMs with 8 wt% CTF, the CO_2 permeabilities could be elevated from 6.8 Barrer for the pure polymer to 12.0 Barrer. Comparison with permeability models showed that these MMMs exhibited a much higher rise in permeability than expected, accompanied by a relatively higher free volume compared to the

MMMs with higher filler contents. With 16 wt% CTF-biphenyl, the CO_2 permeability was increased to 15.1 Barrer, which is in good accordance with the Bruggeman model. A further increase of the filler content to 24 wt% resulted in a stagnation in CO_2 permeability, indicating that the optimum filler content should be used up to a maximum of 16 wt%. Even though CTFs are purely organic fillers, the comparison of the permeability of the CTF/Matrimid® MMMs to theoretical models pointed at unexpected problems of the interface compatibility between the CTF filler and Matrimid® matrix. The CTF filler enhanced the CO_2/CH_4 separation performance but in a way that necessitated a closer look. The success of CTF fillers depends strongly on the interface compatibility. In follow-up studies, we will address this interface problem.

Supplementary Materials: The following are available online at https://www.mdpi.com/article/10.3390/membranes11100795/s1.

Author Contributions: Conceptualization, C.J. and S.B.; Methodology, S.B.; Validation, S.B. and Q.-D.H.; Formal Analysis, S.B., A.S., Y.S. and S.X.; Investigation, S.B. and Q.-D.H., A.S., Y.S. and S.X.; Resources, C.J.; Data Curation, S.B.; Writing—Original Draft Preparation, S.B.; Writing—Review and Editing, C.J.; Visualization, S.B.; Supervision, C.J.; Project Administration, C.J.; Funding Acquisition, C.J. All authors have read and agreed to the published version of the manuscript.

Funding: C.J. is indebted to the DFG for funding within the priority program SPP 1928 "COORNET" (grant Ja466–43/1). S.X. received funding from the Hoffmann Institute of Advanced Materials (HIAM), Shenzhen Polytechnic.

Data Availability Statement: The data presented in this study are available on request from the corresponding author.

Conflicts of Interest: The authors declare that they have no known competing financial interests or personal relationships that could have appeared to influence the work reported in this paper.

References

1. Baker, R.W. Future Directions of Membrane Gas Separation Technology. *Ind. Eng. Chem. Res.* **2002**, *41*, 1393–1411.

2. Baena-Moreno, F.M.; le Saché, E.; Pastor-Pérez, L.; Reina, T.R. Membrane-based technologies for biogas upgrading: A review. *Environ. Chem. Lett.* **2020**, *18*, 1649–1658.

3. Zhang, Y.; Sunarso, J.; Liu, S.; Wang, R. Current status and development of membranes for CO_2/CH_4 separation: A review. *Int. J. Greenh. Gas Control* **2013**, *12*, 84–107.

4. Vinoba, M.; Bhagiyalakshmi, M.; Alqaheem, Y.; Alomair, A.A.; Pérez, A.; Rana, M.S. Recent progress of fillers in mixed matrix membranes for CO_2 separation: A review. *Sep. Purif. Technol.* **2017**, *188*, 431–450.

5. Nik, O.G.; Chen, X.Y.; Kaliaguine, S. Functionalized metal organic framework-polyimide mixed matrix membranes for CO_2/CH_4 separation. *J. Membr. Sci.* **2012**, *413–414*, 48–61.

6. Dechnik, J.; Gascon, J.; Doonan, C.J.; Janiak, C.; Sumby, C.J. Mixed-Matrix Membranes. *Angew. Chem. Int. Ed.* **2017**, *56*, 9292–9310.

7. Lin, R.; Villacorta Hernandez, B.; Ge, L.; Zhu, Z. Metal organic framework based mixed matrix membranes: An overview on filler/polymer interfaces. *J. Mater. Chem. A* **2018**, *6*, 293–312.

8. Ahmad, M.Z.; Peters, T.A.; Konnertz, N.M.; Visser, T.; Téllez, C.; Coronas, J.; Fila, V.; de Vos, W.M.; Benes, N.E. High-pressure CO_2/CH_4 separation of Zr-MOFs based mixed matrix membranes. *Sep. Purif. Technol.* **2020**, *230*, 115858.

9. Deng, J.; Dai, Z.; Hou, J.; Deng, L. Morphologically Tunable MOF Nanosheets in Mixed Matrix Membranes for CO_2 Separation. *Chem. Mater.* **2020**, *32*, 4174–4184.

10. Winarta, J.; Meshram, A.; Zhu, F.; Li, R.; Jafar, H.; Parmar, K.; Liu, J.; Mu, B. Metal–organic framework-based mixed-matrix membranes for gas separation: An overview. *J. Polym. Sci.* **2020**, *58*, 2518–2546.

11. Fan, Y.; Yu, H.; Xu, S.; Shen, Q.; Ye, H.; Li, N. Zn(II)-modified imidazole containing polyimide/ZIF-8 mixed matrix membranes for gas separations. *J. Membr. Sci.* **2020**, *597*, 117775.

12. Wang, Z.; Yuan, J.; Li, R.; Zhu, H.; Duan, J.; Guo, Y.; Liu, G.; Jin, W. ZIF-301 MOF/6FDA-DAM polyimide mixed-matrix membranes for CO_2/CH_4 separation. *Sep. Purif. Technol.* **2021**, *264*, 118431.

13. Guan, W.; Dai, Y.; Dong, C.; Yang, X.; Xi, Y. Zeolite imidazolate framework (ZIF)-based mixed matrix membranes for CO_2 separation: A review. *J. Appl. Polym. Sci.* **2020**, *137*, 48968.

14. Ahmad, M.Z.; Martin-Gil, V.; Supinkova, T.; Lambert, P.; Castro-Muñoz, R.; Hrabanek, P.; Kocirik, M.; Fila, V. Novel MMM using CO_2 selective SSZ-16 and high-performance 6FDA-polyimide for CO_2/CH_4 separation. *Sep. Purif. Technol.* **2021**, *254*, 117582.

15. Zhao, J.; Xie, K.; Liu, L.; Liu, M.; Qiu, W.; Webley, P.A. Enhancing plasticization-resistance of mixed-matrix membranes with exceptionally high CO_2/CH_4 selectivity through incorporating ZSM-25 zeolite. *J. Membr. Sci.* **2019**, *583*, 23–30.

16. Li, J.; Zhou, X.; Wang, J.; Li, X. Two-Dimensional Covalent Organic Frameworks (COFs) for Membrane Separation: A Mini Review. *Ind. Eng. Chem. Res.* **2019**, *58*, 15394–15406.

17. Fang, M.; Montoro, C.; Semsarilar, M. Metal and Covalent Organic Frameworks for Membrane Applications. *Membranes* **2020**, *10*, 107.

18. Li, S.; Prasetya, N.; Ladewig, B.P. Investigation of Azo-COP-2 as a Photoresponsive Low-Energy CO_2 Adsorbent and Porous Filler in Mixed Matrix Membranes for CO_2/N_2 Separation. *Ind. Eng. Chem. Res.* **2019**, *58*, 9959–9969.

19. Shan, M.; Seoane, B.; Rozhko, E.; Dikhtiarenko, A.; Clet, G.; Kapteijn, F.; Gascon, J. Azine-Linked Covalent Organic Framework (COF)-Based Mixed-Matrix Membranes for CO_2/CH_4 Separation. *Chem. Eur. J.* **2016**, *22*, 14467–14470.

20. Jiang, H.; Zhang, J.; Huang, T.; Xue, J.; Ren, Y.; Guo, Z.; Wang, H.; Yang, L.; Yin, Y.; Jiang, Z.; et al. Mixed-Matrix Membranes with Covalent Triazine Framework Fillers in Polymers of Intrinsic Microporosity for CO_2 Separations. *Ind. Eng. Chem. Res.* **2020**, *59*, 5296–5306.

21. Dey, S.; Bügel, S.; Sorribas, S.; Nuhnen, A.; Bhunia, A.; Coronas, J.; Janiak, C. Synthesis and Characterization of Covalent Triazine Framework CTF-1@Polysulfone Mixed Matrix Membranes and Their Gas Separation Studies. *Front. Chem.* **2019**, *7*, 693.

22. Castro-Muñoz, R.; Martin-Gil, V.; Ahmad, M.Z.; Fíla, V. Matrimid® 5218 in preparation of membranes for gas separation: Current state-of-the-art. *Chem. Eng. Commun.* **2018**, *205*, 161–196.

23. Bügel, S.; Spieß, A.; Janiak, C. Covalent triazine framework CTF-fluorene as porous filler material in mixed matrix membranes for CO_2/CH_4 separation. *Micropor. Mesopor. Mat.* **2021**, *316*, 110941.

24. Yokozeki, A.; Shiflett, M.B.; Junk, C.P.; Grieco, L.M.; Foo, T. Physical and Chemical Absorptions of Carbon Dioxide in Room-Temperature Ionic Liquids. *J. Phys. Chem. B* **2008**, *112*, 16654–16663.

25. Zhang, X.; Zhang, X.; Dong, H.; Zhao, Z.; Zhang, S.; Huang, Y. Carbon capture with ionic liquids: Overview and progress. *Energy Environ. Sci.* **2012**, *5*, 6668–6681.

26. Ramdin, M.; de Loos, T.W.; Vlugt, T.J.H. State-of-the-Art of CO_2 Capture with Ionic Liquids. *Ind. Eng. Chem. Res.* **2012**, *51*, 8149–8177.

27. Abdollahi, S.; Mortaheb, H.R.; Ghadimi, A.; Esmaeili, M. Improvement in separation performance of Matrimid®5218 with encapsulated [Emim][Tf_2N] in a heterogeneous structure: CO_2/CH_4 separation. *J. Membr. Sci.* **2018**, *557*, 38–48.

28. Zhao, R.; Wu, H.; Yang, L.; Ren, Y.; Liu, Y.; Qu, Z.; Wu, Y.; Cao, L.; Chen, Z.; Jiang, Z. Modification of covalent organic frameworks with dual functions ionic liquids for membrane-based biogas upgrading. *J. Membr. Sci.* **2020**, *600*, 117841.

29. Solangi, N.H.; Anjum, A.; Tanjung, F.A.; Mazari, S.A.; Mubarak, N.M. A review of recent trends and emerging perspectives of ionic liquid membranes for CO_2 separation. *J. Environ. Chem. Eng.* **2021**, *9*, 105860.

30. Karunakaran, M.; Villalobos, L.F.; Kumar, M.; Shevate, R.; Akhtar, F.H.; Peinemann, K.V., Graphene oxide doped ionic liquid ultrathin composite membranes for efficient CO_2 capture. *J. Mater. Chem. A* **2017**, *5*, 649–656.

31. Kuecken, S.; Schmidt, J.; Zhi, L.; Thomas, A. Conversion of amorphous polymer networks to covalent organic frameworks under ionothermal conditions: A facile synthesis route for covalent triazine frameworks. *J. Mater. Chem. A* **2015**, *3*, 24422–24427.

32. Dey, S.; Bhunia, A.; Esquivel, D.; Janiak, C. Covalent triazine-based frameworks (CTFs) from triptycene and fluorene motifs for CO_2 adsorption. *J. Mater. Chem. A* **2016**, *4*, 6259–6263.

33. Nuhnen, A.; Dietrich, D.; Millan, S.; Janiak, C. Role of Filler Porosity and Filler/Polymer Interface Volume in Metal–Organic Framework/Polymer Mixed-Matrix Membranes for Gas Separation. *ACS Appl. Mater. Interfaces* **2018**, *10*, 33589–33600.

34. Almansour, F.; Alberto, M.; Bhavsar, R.S.; Fan, X.; Budd, P.M.; Gorgojo, P. Recovery of free volume in PIM-1 membranes through alcohol vapor treatment. *Front. Chem. Sci. Eng.* **2021**, *15*, 872–881.

35. Stern, S.A. The "barrer" permeability unit. *J. Polym. Sci. A-2* **1968**, *6*, 1933–1934.

36. Kuhn, P.; Antonietti, M.; Thomas, A. Porous, Covalent Triazine-Based Frameworks Prepared by Ionothermal Synthesis. *Angew. Chem. Int. Ed.* **2008**, *47*, 3450–3453.

37. Bi, J.; Fang, W.; Li, L.; Wang, J.; Liang, S.; He, Y.; Liu, M.; Wu, L. Covalent Triazine-Based Frameworks as Visible Light Photocatalysts for the Splitting of Water. *Macromol. Rapid Commun.* **2015**, *36*, 1799–1805.

38. Dey, S.; Bhunia, A.; Boldog, I.; Janiak, C. A mixed-linker approach towards improving covalent triazine-based frameworks for CO_2 capture and separation. *Micropor. Mesopor. Mat.* **2017**, *241*, 303–315.

39. Thommes, M.; Kaneko, K.; Neimark, A.V.; Olivier, J.P.; Rodriguez-Reinoso, F.; Rouquerol, J.; Sing, K.S.W. Physisorption of gases, with special reference to the evaluation of surface area and pore size distribution (IUPAC Technical Report). *Pure Appl. Chem.* **2015**, *87*, 1051–1069.

40. Lim, H.; Cha, M.C.; Chang, J.Y. Preparation of Microporous Polymers Based on 1,3,5-Triazine Units Showing High CO_2 Adsorption Capacity. *Macromol. Chem. Phys.* **2012**, *213*, 1385–1390.

41. Landers, J.; Gor, G.Y.; Neimark, A.V. Density functional theory methods for characterization of porous materials. *Colloids Surf. A* **2013**, *437*, 3–32.

42. Bouma, R.H.B.; Checchetti, A.; Chidichimo, G.; Drioli, E. Permeation through a heterogeneous membrane: The effect of the dispersed phase. *J. Membr. Sci.* **1997**, *128*, 141–149.

43. Bruggeman, D.A.G. Berechnung verschiedener physikalischer Konstanten von heterogenen Substanzen. I. Dielektrizitätskonstanten und Leitfähigkeiten der Mischkörper aus isotropen Substanzen. *Ann. Phys.* **1935**, *416*, 636–664.

44. Hashin, Z.; Shtrikman, S.A Variational Approach to the Theory of the Effective Magnetic Permeability of Multiphase Materials. *J. Appl. Phys.* **1962**, *33*, 3125–3131.

45. Huang, Y.; Wang, X.; Paul, D.R. Physical aging of thin glassy polymer films: Free volume interpretation. *J. Membr. Sci.* **2006**, *277*, 219–229.

46. Kanehashi, S.; Chen, G.Q.; Scholes, C.A.; Ozcelik, B.; Hua, C.; Ciddor, L.; Southon, P.D.; D'Alessandro, D.M.; Kentish, S.E. Enhancing gas permeability in mixed matrix membranes through tuning the nanoparticle properties. *J. Membr. Sci.* **2015**, *482*, 49–55.

47. Pandey, P.; Chauhan, R.S. Membranes for gas separation. *Prog. Polym. Sci.* **2001**, *26*, 853–893.

48. Ismail, A.F.; Khulbe, K.C.; Matsuura, T. *Gas Separation Membranes: Polymeric and Inorganic*; Springer International Publishing: Cham, Switzerland, 2015, p. 39.

49. Wu, X.; Tian, Z.; Wang, S.; Peng, D.; Yang, L.; Wu, Y.; Xin, Q.; Wu, H.; Jiang, Z. Mixed matrix membranes comprising polymers of intrinsic microporosity and covalent organic framework for gas separation. *J. Membr. Sci.* **2017**, *528*, 273–283.

Supplementary Materials

Biphenyl-based covalent triazine framework/Matrimid® mixed-matrix membranes for CO_2/CH_4 separation

Stefanie Bügel,[1] Quang-Dien Hoang,[1] Alex Spieß,[1] Yangyang Sun,[1] Shanghua Xing,[1,2] Christoph Janiak*[1,2]

[1] Institut für Anorganische Chemie und Strukturchemie, Heinrich-Heine-Universität Düsseldorf, D-40204 Düsseldorf, Germany

[2] Hoffmann Institute of Advanced Materials, Shenzhen Polytechnic, 7098 Liuxian Blvd, Nanshan District, Shenzhen 518055, China

*Corresponding author: Christoph Janiak
Email: stefanie.buegel@uni-duesseldorf.de; quang-dien.hoang@uni-duesseldorf.de; alex.spiess@hhu.de; yasun100@hhu.de; shanghua.xing@hhu.de; janiak@hhu.de

Content

1. Characterization of CTF-biphenyl

1.1. Infrared spectroscopy (IR)

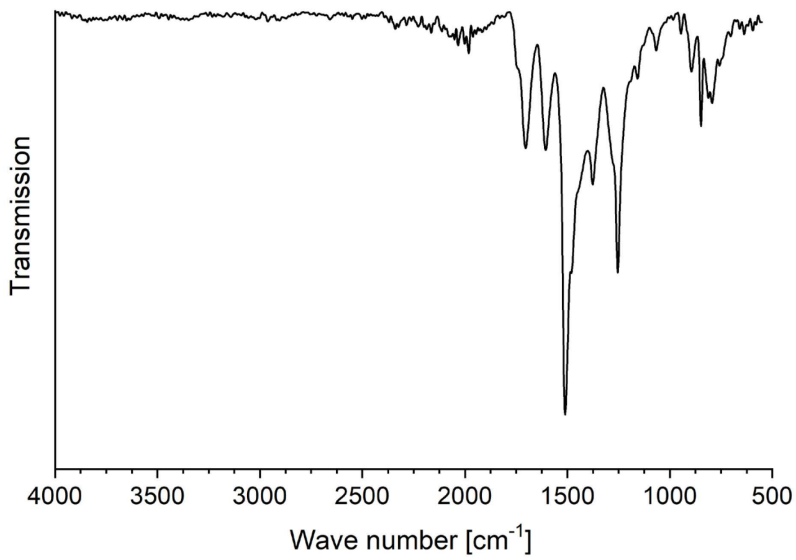

Figure S1. IR spectrum of CTF-biphenyl.

1.2. Elemental analysis

The final composition of CTFs strongly depends on the synthesis conditions. In the case of biphenyl-based CTFs, an optimal C/N ratio cannot be obtained using Friedel-Crafts synthesis, ionothermal synthesis or Suzuki coupling (Table S1). Only the synthesis under Brønsted acidic conditions shows good agreement with the theoretically calculated values. However, since the application of the materials for gas separation is the focus of this work, an appropriate porosity is of crucial importance. Since the BET-surface areas of the CTFs produced under Brønsted acidic conditions are generally lower [1,2], a different method must be employed. The ionothermal method generally produces CTFs with higher BET surface areas. The synthesis temperature plays a crucial role at this point. An increase in temperature leads to the generation of more defects, which increase the porosity but lead to a lower nitrogen content [3]. Another problem is the production of CTFs on a larger scale, which so far can best be solved with Friedel-Crafts alkylation. In a previous work, different synthesis conditions were investigated concerning Friedel-Crafts synthesis [4]. The use of cyanuric chloride in excess resulted in higher nitrogen content, but lower BET surface area. The optimal conditions for a CTF with the linker fluorene were transferred to the synthesis of CTF-biphenyl. A too low nitrogen content can be attributed to the formation of polymer chains through C-C bond formation of biphenyl

units via the Scholl reaction [5,6], which would result in a relative reduced incorporation of triazine units. The remaining mass fraction can be explained by residues of aluminum species from the catalyst $AlCl_3$, as well as by an undetectable oxygen content. The C/H ratio is somewhat lower than theory, that is the hydrogen wt% is higher than expected. This can be due to the presence of adsorbed water/moisture during sample handling and storage before CHN analysis, as discussed in [7,8,9]. Subsequently, the adsorbed water content will also add to the lower than expected nitrogen wt%.

Table S1. Elemental analysis of CTF-biphenyl and other biphenyl-based CTFs prepared by different synthesis methods.

Compound	Synthesis	C [wt%]	H [wt%]	N [wt%]	C/N ratio	C/H ratio	BET [m^2/g]	Ref.
Theoretical[a]		82.33	3.95	13.72	6.00	20.84	-	-
CTF-biphenyl	Friedel-Crafts	71.29	3.80	6.92	10.30	18.76	940	This work
CTF-DCBP	Ionothermal	84.20	2.18	5.41	15.56	38.62	2475	[10]
CTF-2	Suzuki	69.26	4.84	9.00	7.70	14.31	200-400	[11]
CTF-2	Brønsted acidic	75.88	3.81	12.21	6.21	19.92	560	

[a]For idealized structure, see Scheme 1.

1.3. Thermogravimetric analysis (TGA)

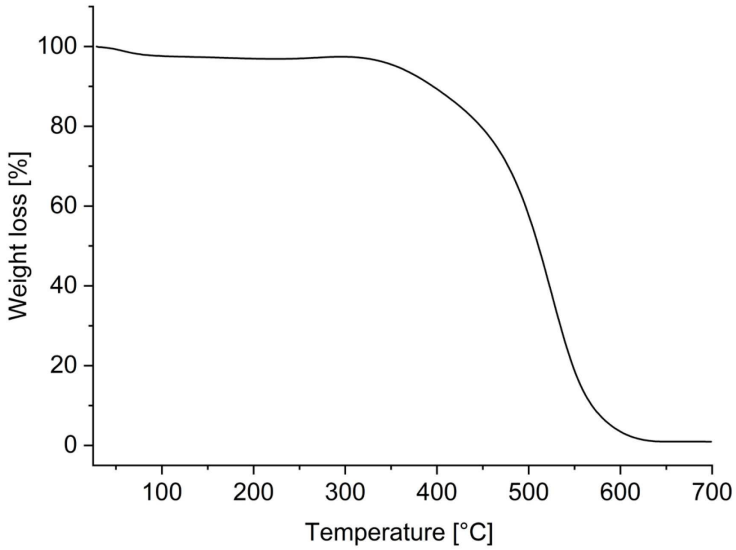

Figure S2: TGA curve of CTF-biphenyl measured under synthetic air.

1.4. Scanning electron microscopy (SEM)

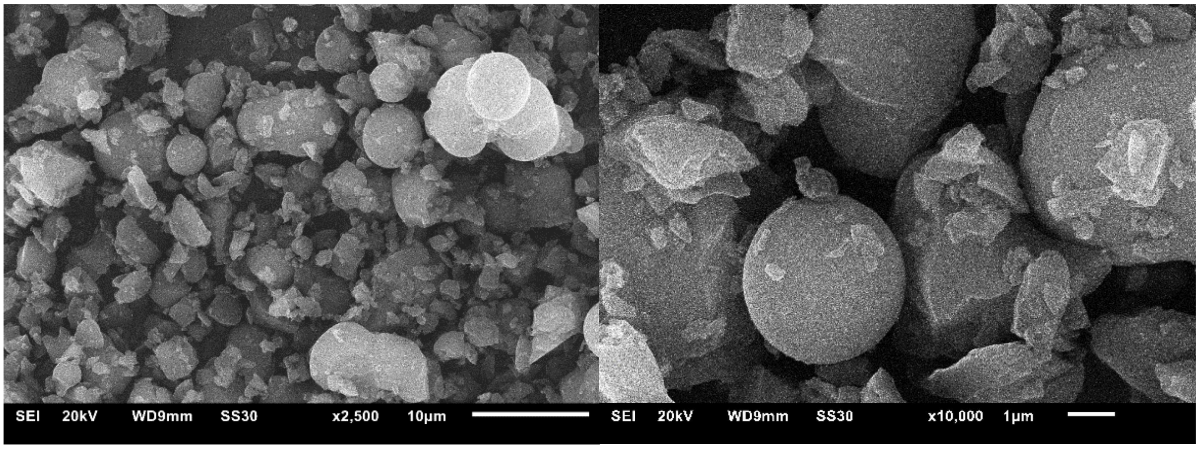

Figure S3. SEM images of CTF-biphenyl.

1.5. N_2-sorption

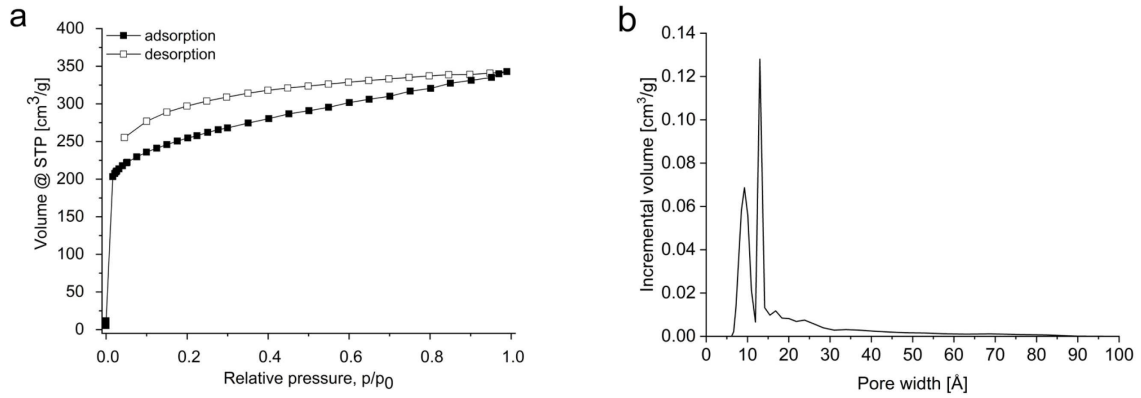

Figure S4. N_2-sorption isotherm (a) and pore size distribution (b, by QSDFT) of CTF-biphenyl.

1.6. CO_2 and CH_4 sorption

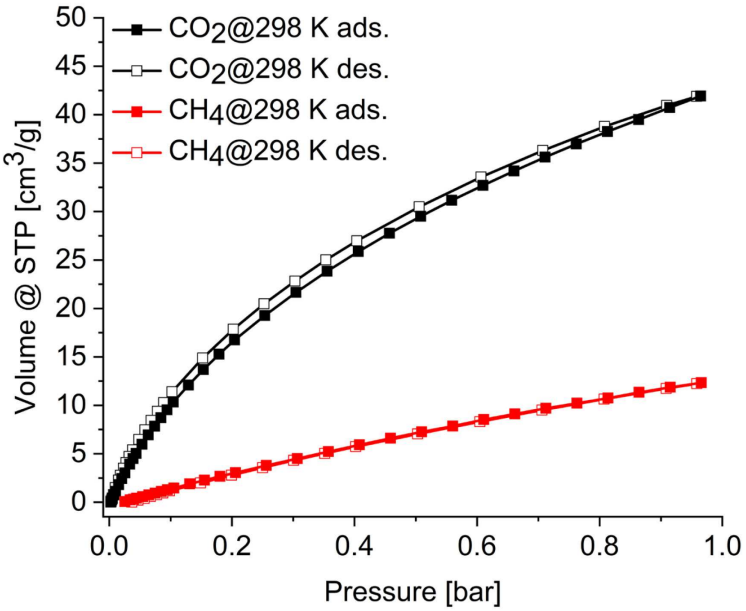

Figure S5. CO_2 and CH_4 sorption isotherms of CTF-biphenyl at 298 K.

Table S2. Comparison of CO_2 uptake capacities and BET-surface areas of different biphenyl-based CTFs (1 bar, 298 K).

CTF material	Synthesis	CO_2 uptake (1 bar, 298 K)	BET surface area, N_2 at 77K [m^2/g]	Reference
CTF-biphenyl	Friedel-Crafts	1.87 mmol/g[a]	940	This work
CTF-2	Brønsted acidic	1.25 mmol/g	560	[11]
CTF-2 Suzuki	Suzuki	0.19 mmol/g	209	
Material 3	Friedel-Crafts	41 cm^3/g	646	[12]

[a] at 0.96 bar

1.7. Ideal adsorbed solution theory (IAST)

The CO_2 and CH_4 isotherms (298 K) of CTF-biphenyl were fitted with the Toth model.

Table S3. Parameters for Toth fitting.

Gas	Temperature [K]	Model	R^2	Affinity constant K [1/bar]	Maximal loading q_{max} [mmol/g]	Heterogeneity exponent t
CO_2	298	Toth	0.9999	1.126	6.246	0.553
CH_4	298	Toth	0.9990	0.771	0.841	2.749

The selectivity of CTF-biphenyl for a binary (50:50; v:v) mixture of the gases CO_2/CH_4 was calculated by applying the ideal adsorbed solution theory, IAST. Figure S6 depicts the CO_2/CH_4 selectivity as a function of the pressure.

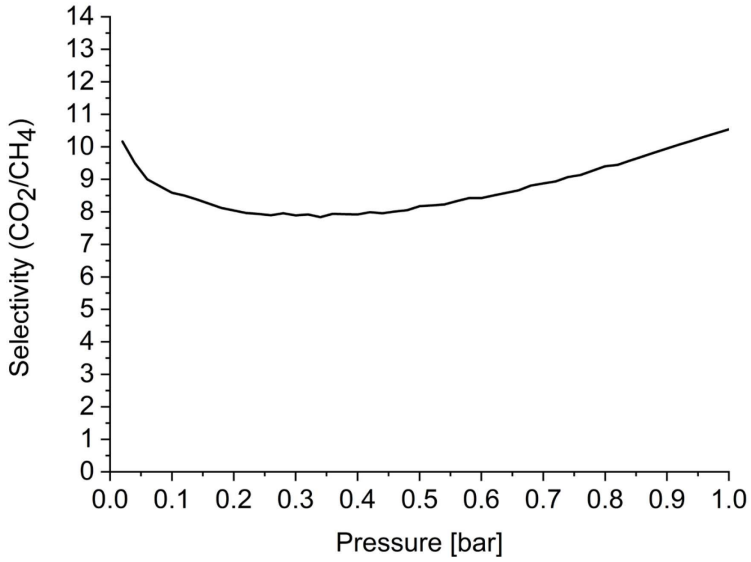

Figure S6. IAST selectivity of CTF-biphenyl for a binary (50:50; v:v) mixture of the gases CO_2/CH_4 at 298 K.

2. Synthesis and characterization of [BMIm][NTf_2]

2.1. Synthesis

[BMIm]Cl was synthesized with 1-methylimidazole (24.63 g, 0.3 mol) and 1-chlorobutane in equimolar proportions (27.77 g, 0.3 mol) via a microwave reaction [13]. The educts were stirred and treated for 1 h at 150 °C and 500 W in a microwave reactor (CEM, Mars 6). The resulting [BMIm]Cl was added dropwise to ice-cold ethyl acetate. After decanting, the solid [BMIm]Cl was dried under vacuum (yield: 47.8 g; 91 %). 1-Butyl-3-methylimidazolium bis(trifluoromethanesulfonyl)imide, [BMIm][NTf_2] was obtained by anion exchange. For the metathesis reaction, [BMIm]Cl (43.67 g, 0.25 mol) and lithium bis(trifluoromethane-sulfonyl)imide (71.77 g, 0.25 mol) were stirred in water for 24 h. The aqueous phase was extracted three times with DCM (200°mL) and subsequently washed with water until the washing solution had a neutral pH and was chloride free (tested with 0.1 mol/L silver nitrate solution). After adding a tip of a spatula of activated carbon, the suspension was stirred overnight and then filtered through acidic aluminum oxide (67 g in a column of 3.2 cm diameter). The product was dried under vacuum (yield: 91.7 g; 88 %). The formation of [BMIm][NTf_2] was confirmed by ^{1}H-NMR and ^{13}C-NMR (Figure S7 and Figure S8). The water content determined by Karl-Fischer titration (KFT) was less than 10 ppm.

2.2. ^{1}H-NMR

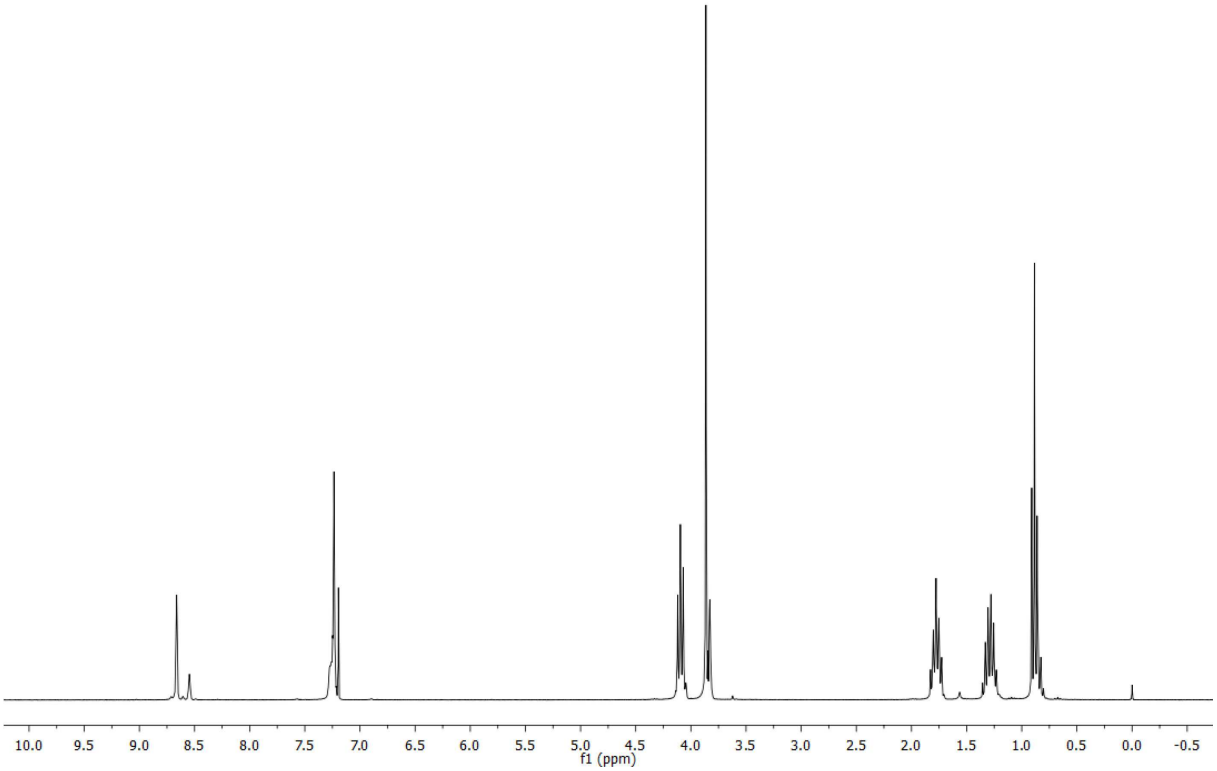

Figure S7. ^{1}H-NMR spectrum of [BMIm][NTf_2] in $CDCl_3$.

^{1}H-NMR (300 MHz, $CDCl_3$): δ = 8.66 (s, -CH_3, 1H), 7.24 (p, J = 2.0 Hz, 2 x -CH, 2H), 4.10 (t, J = 7.5 Hz, -CH_2, 2H), 3.86 (s, -CH_3, 3H), 1.78 (p, J = 7.5 Hz, -CH_2, 2H), 1.29 (h, J = 7.4 Hz, -CH_2, 2H), 0.89 (t, J = 7.4 Hz, -CH_3, 3H).

2.3. ^{13}C-NMR

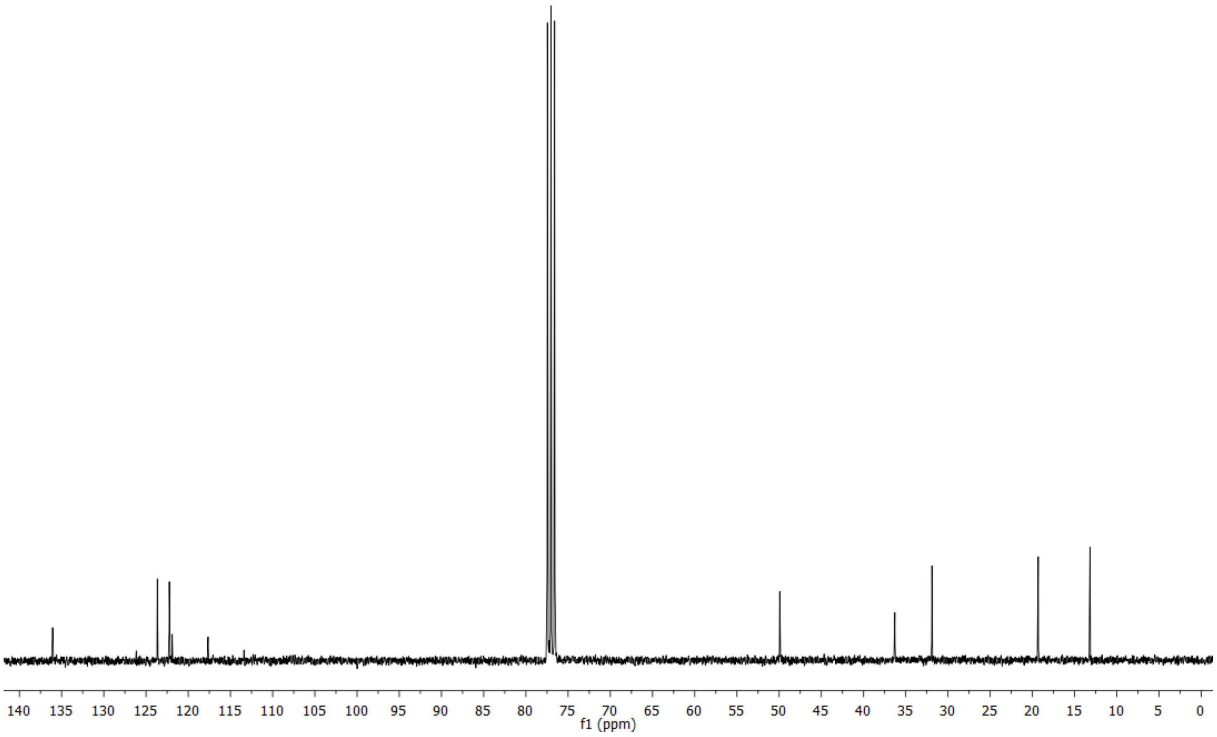

Figure S8. ^{13}C-NMR spectrum of [BMIm][NTf_2] in $CDCl_3$.

^{13}C NMR (75 MHz, $CDCl_3$): δ = 136.06 (s, N-CH-N), 123.66 (s, CH=C), 122.24 (s, CH=C), 117.65 (s, CF_3), 49.93 (s, N-CH_2-C), 36.30 (s, N-CH_3), 31.90 (s, CCH_2-C), 19.31 (s, CCH_2-C), 13.18 (s, C-CH_3).

3. Preparation and characterization of [BMIm][NTf_2]@CTF-biphenyl and IL-containing membranes

3.1. Preparation of [BMIm][NTf_2]@CTF-biphenyl

The IL 1-butyl-3-methylimidazolium bis(trifluoromethanesulfonyl)imide, [BMIm][NTf_2] was incorporated in the pores of CTF-biphenyl by post-impregnation in analogy to the preparation of [BMIm][NTf_2] in the pores of COF-300 [14]. [BMIm][NTf_2] (1.50 g) were dissolved in 95 mL of methanol and stirred for 4 h. CTF-biphenyl (500 mg) was slowly added while stirring. After sonification for 1 h, the dispersion was centrifuged (4 x 5 min, 8000 rpm) and washed with methanol (15 mL). The product was dried at 120 °C for 24 h (yield: 510 mg).

3.2. Elemental analysis

The presence of the IL in the pores of the CTF was confirmed by elemental analysis (Table S4). From the sulfur content of 0.86 wt% of the elemental analysis the IL content of IL@CTF was calculated as 5.62 wt% ([BMIm][NTf_2], $C_{10}H_{15}F_6N_3O_4S_2$, M = 419.36 g/mol) by applying equation 1:

$$IL\ wt\% = \frac{S\ wt\% \times M(IL)}{2 \times M(S)} \qquad (1)$$

Table S4. Elemental analysis of [BMIm][NTf_2]@CTF-biphenyl.

Compound	C [wt%]	H [wt%]	N [wt%]	S [wt%]
[BMIm][NTf_2]@CTF-biphenyl	67.71	3.39	6.34	0.86

3.3. TGA

TGA measurements were carried out under synthetic air to ensure that both the CTF and the IL@CTF composite had a thermal stability of at least 150°C and could therefore be applied as a filler material for membrane preparation. The measurement showed a thermal stability of IL@CTF up to 220 °C and confirmed the expected lower thermal stability of the composite in comparison to the pure CTF [15].

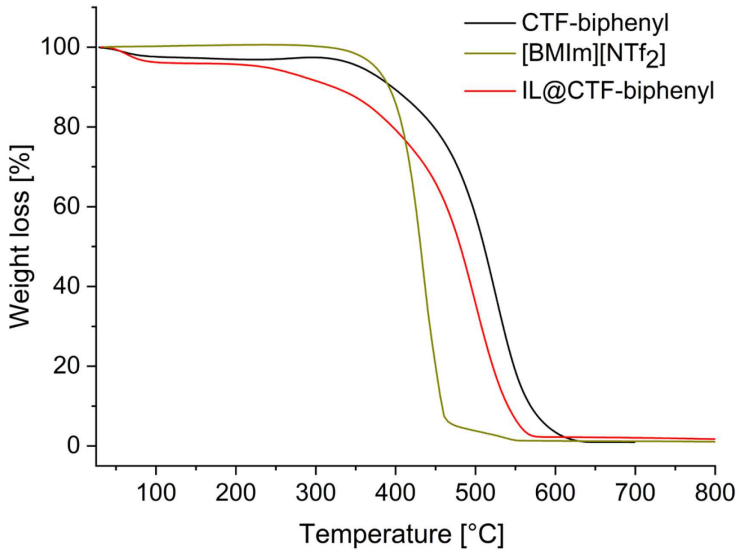

Figure S9. TGA curve of [BMIm][NTf_2]@CTF-biphenyl in comparison to curves of CTF and IL. Measured under synthetic air.

3.4. N_2-sorption

N_2-sorption isotherms (Figure S10a) of IL@CTF supported the incorporation of [BMIm][NTf_2] into the pores of CTF-biphenyl through the reduction of the BET surface area from 940 m^2/g to 502 m^2/g accompanied with a lowering of the total pore volume from 0.53 cm^3/g to 0.26 cm^3/g. A comparison of the pore size distributions in Figure S10b indicated that only the smaller CTF micropores with a pore diameter around 9 Å remained unfilled while the pores above a diameter of 11 Å had essentially vanished. The filling of only the larger pores is in agreement with the dimensions (referred to van der Waals radii) of the IL cation with a length of about 11.4 x 5.5 x 2.8 Å and the IL anion with a length of about 10.9 x 5.1 x 4.7 Å [16].

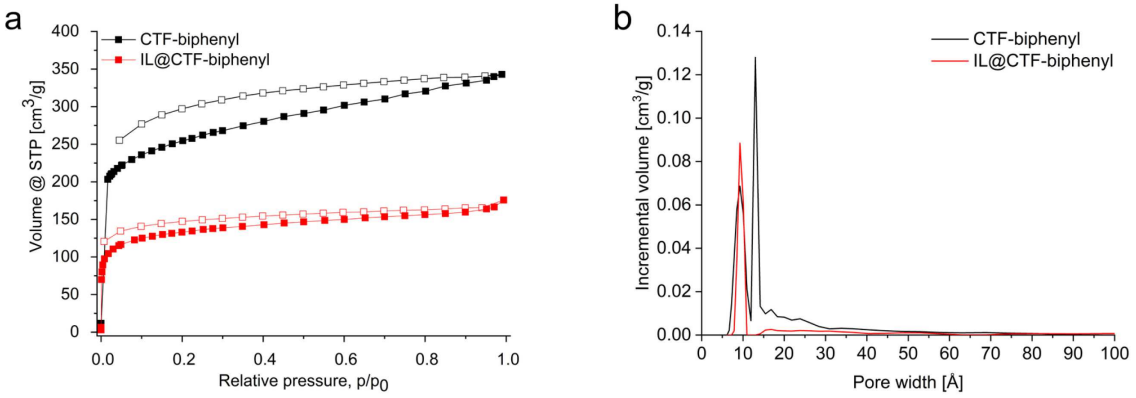

Figure S10. N_2-sorption isotherm (a) and pore size distribution (b, by QSDFT) of [BMIm][NTf_2]@CTF-biphenyl in comparison to the pure CTF.

3.5. Preparation of IL-containing membranes

The IL/Matrimid® membranes were prepared by direct physical mixing in DCM in analogy to the pure Matrimid® membranes. The IL@CTF/Matrimid® MMMs were prepared according to the same procedure by using IL@CTF (35 mg for 8 wt%, 76 mg for 16 wt% and 126.5 mg for 24 wt%) instead of CTF-biphenyl. As noted in the main text, the filler loadings of CTF-biphenyl and IL refer to the combined mass of the polymer and filler according to equation 1. For CTF/IL/Matrimid® MMMs 5 wt% IL (21 mg, based on 400 mg polymer) was added to the Matrimid® DCM solution before the first 24 h of stirring. The further procedure with the addition of the CTF (35 mg for 8 wt%, 76 mg for 16 wt% and 126.5 mg for 24 wt%) was as described above. For all membranes the solution casting and drying was carried out under the same conditions: The mixtures were cast into metal rings placed on a flat glass surface. In order to achieve a controlled evaporation of DCM, an inverted funnel, covered with a paper tissue,

was placed above the metal ring. When the DCM was evaporated, the membrane was cut out with a scalpel and dried in a vacuum oven (150 °C, 20 mbar) overnight.

4. Characterization of membranes

4.1. Membrane thickness

Table S5. Average thickness of CTF-biphenyl/Matrimid®, [BMIm][NTf_2]/CTF-biphenyl/Matrimid® and [BMIm][NTf_2]@CTF-biphenyl/Matrimid® MMMs.

CTF-biphenyl content [wt%]	CTF-biphenyl/ Matrimid®	[BMIm][NTf_2]/ CTF-biphenyl/ Matrimid®	[BMIm][NTf_2] @CTF-biphenyl/ Matrimid®
	Average thickness [µm]		
8	49.5	44	44.5
16	72.5	55	67.5
24	75.5	68.5	72

4.2. Effect of [BMIm][NTf_2] as ternary component.

In addition to the binary membrane system CTF-biphenyl/Matrimid® another binary IL/Matrimid® and two ternary membrane systems were prepared. The resulting [BMIm][NTf_2]/Matrimid®, CTF-biphenyl/[BMIm][NTf_2]/Matrimid® and [BMIm][NTf_2]@CTF-biphenyl/Matrimid® MMMs will be denoted as IL/Matrimid®, CTF/IL/Matrimid® and IL@CTF/Matrimid® MMMs. In order to choose an adequate amount of the IL [BMIm][NTf_2] for the ternary MMMs with CTF-biphenyl and Matrimid®, first only IL and Matrimid® were used to produce binary MMMs. The incorporation of 5 wt% IL into the Matrimid® matrix decreased the permeability but led to an increase in selectivity from 42 for the pure Matrimid® membrane to 49 for the composite. As the IL loading was enhanced to 10 and 15 wt%, both selectivity and permeability decreased (Table S7). Based on this result, the ternary CTF/IL/Matrimid® MMMs were prepared with 5 wt% IL. In the MMM CTF/IL/Matrimid®, the IL was used as a filler material alongside the CTF with the expectation that the IL could serve as a surfactant [15]. In IL@CTF/Matrimid® the IL was encapsulated in the pores of the CTF to enhance the molecular sieving effect by reducing the pore size (Figure S10b). With the incorporation of 5 wt% IL ([BMIm][NTf_2]) as the third component, the IL/CTF/Matrimid® MMMs with 8 and 16 wt% CTF-biphenyl showed essentially no increase in permeability compared to the pristine polymer with 6.8 Barrer (Figure S11a). For 24 wt% CTF-biphenyl the CO_2 permeability was elevated to 11.1 Barrer. However, for the

IL/CTF/Matrimid® system, the permeabilities were lower than those of the binary CTF/Matrimid® MMMs, but an increase in selectivity to 50 for the 24 wt% MMM was observed. Based on these results, it can be assumed that no additional free volume was generated, but that the IL may have had a positive influence due to its good CO_2 affinity resulting in an increased CO_2/CH_4 selectivity. When the IL was incorporated into the pores of CTF-biphenyl and then IL@CTF was added as the filler material in the IL@CTF/Matrimid® MMMs an improvement in CO_2 permeability compared to the pristine polymer was observed. The CO_2/CH_4 selectivity was raised to 52 and 46 for the 16 and 24 wt% MMMs, respectively (Figure S11b) albeit at somewhat lower permeabilities than the binary CTF/Matrimid® MMMs.

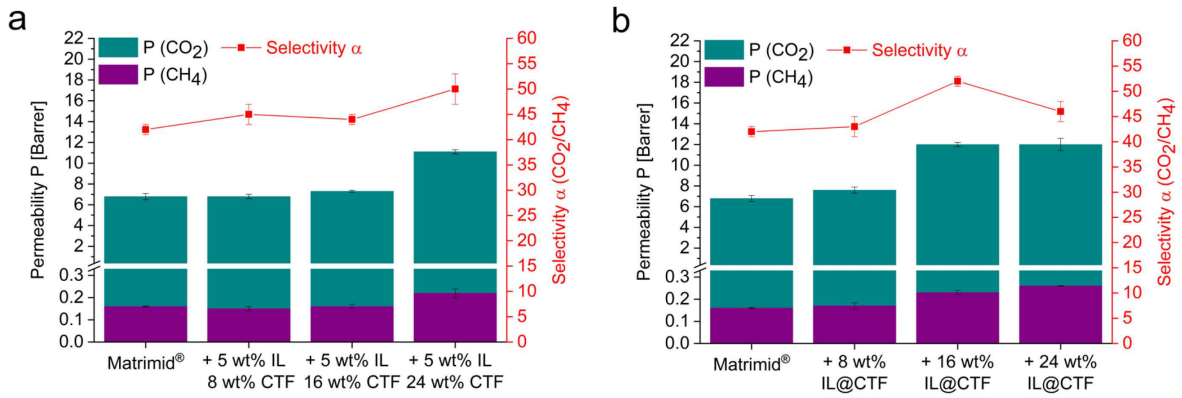

Figure S11. CO and CH_4 permeabilities (*P*) and CO_2/CH_4 selectivities (α) for the pure Matrimid® membranes and IL/CTF-biphenyl/Matrimid® (a) and IL@CTF/Matrimid® (b) MMMs.

Literature reports suggest that incorporated ILs can have different effects on membrane performance. COF-300, synthesized by a condensation reaction of tetrakis(4-aminophenyl)methane and terephthalaldehyde, and the IL [BMIm][NTf_2] were incorporated into a Pebax® 1657 matrix by Zhao et al. [BMIm][NTf_2] in the pores of COF-300 could improve the CO_2 permeability from 81.7 Barrer to 242.1 Barrer with an elevation in CO_2/CH_4 selectivity from 18.8 to 39.5 [14]. Using the same polymer and IL, Li et al. prepared MMMs with the zinc-2-methylimidazolate framework ZIF-8 and investigated the performance with respect to CO_2/CH_4 separation. The highest CO_2 permeability value was achieved with 15 wt% of ZIF-8 in a binary MMM. The ternary system with additional [BMIm][NTf_2] in the pores of the filler material led to a decrease in CO_2 permeability, but an increase to 34.8 in CO_2/CH_4 selectivity [15]. The application of [BMIm][NTf_2] and ZSM-5 in a 6FDA-TeMPD matrix led to a decrease in CO_2 permeability from 1156 to 441 Barrer whilst the selectivity was only slightly increased from 18.6 to 21.1 [17].

Table S6. Comparison of CO_2 and CH_4 permeability and CO_2/CH_4 selectivity for ternary MMMs with the IL [BMIm][NTf_2].

Continuous phase	Filler	IL	P CO_2 [Barrer]	S CO_2/CH_4	Reference
Pebax® 1657[a]	-	-	81.7	18.8	[14]
Pebax® 1657[a]	COF-300 7 wt%	-	109.4	24.4	
Pebax® 1657[a]	COF-300 7 wt%	[BMIm][NTf_2] 3.8 wt%@COF	242.1	28	
Pebax® 1657[b]	-	-	72.5	18.1	[15]
Pebax® 1657[b]	ZIF-8[1] 15 wt%	-	(129)*	(19.5)*	
Pebax® 1657[b]	ZIF-8[1] 15 wt%	[BMIm][NTf_2] 16.5 wt%@ZIF	104.9	34.8	
6FDA-TeMPD[d,2]	-	-	1156 ± 96	18.6 ± 0.3	[18]
6FDA-TeMPD[d,2]	-	[BMIm][NTf_2] 10 ± 1 wt%	412 ± 67	23.9 ± 1.5	
6FDA-TeMPD[e,2]	ZSM-5[3] 15 wt%	[BMIm][NTf_2] 9 wt%	441 ± 17	21.1 ± 0.2	[17]

*information obtained from graph [a]mixed-gas CO_2/CH_4 (30/70 vol%); 1 bar feed pressure; 30 °C [b]single gas; 1 bar feed pressure; 25 °C [c]equimolar mixed-gas CO_2/CH_4; 6 bar feed pressure; 30°C [d]single gas; upstream pressure 75–77 cmHg; 35 °C [e]single gas; upstream pressure 10 atm; 35 °C; [1]zeolitic imidazolate framework; [2]polyimide derived from 4,4-hexa-fluoroisopropylidenediphtalicanhydride (6FDA)/2,3,5,6-tetramethyl-1,4-phenylenediamine(TeMPD); [3]zeolite socony mobil

In our CTF/Matrimid® membrane systems with IL as the ternary component, an improvement in both permeability and selectivity over the neat polymer could be achieved, but the binary CTF/Matrimid® MMMs still exhibited the best overall performance, when economic and environmental aspects are considered in addition to CO_2/CH_4 gas separation performance (IL is usually more expensive and not environmentally friendly due to the high fluorine content).The incorporation of ILs in MMMs is still largely empirical and further in-depth understanding on its polymer compatibility and its role is needed for a more knowledge-based approach.

In summary, two ternary CTF MMMs with the IL [BMIm][NTf_2] were prepared for the first time. The comparison to the binary CTF/Matrimid® MMMs, indicated that the incorporation of an IL as ternary component may not be beneficial for every MMM system.

We decided not to present the three MMM systems with IL in the manuscript because there is no clear improvement in membrane performance. The often-expected effect of ILs to increase membrane performance did not occur. We are critical of the incorporation in this case and can say that IL is not necessarily beneficial. Our first consideration was not to describe the IL MMMs, but we feel that the mention of not so successful experiments is an added value to shed light on certain topics from a different angle.

4.3. Cross-section SEM images of ternary MMMs

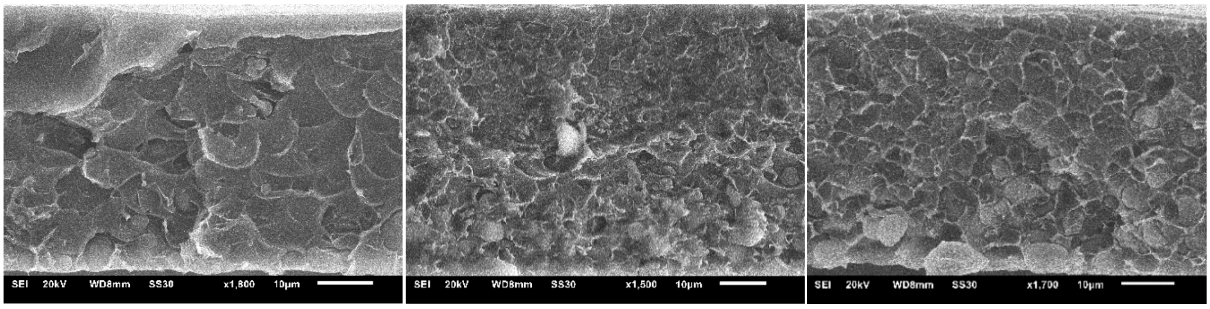

Figure S12. Cross-section SEM images of 8 wt%, 16 wt% and 24 wt% CTF in CTF/IL/Matrimid® MMM (with 5 wt% IL).

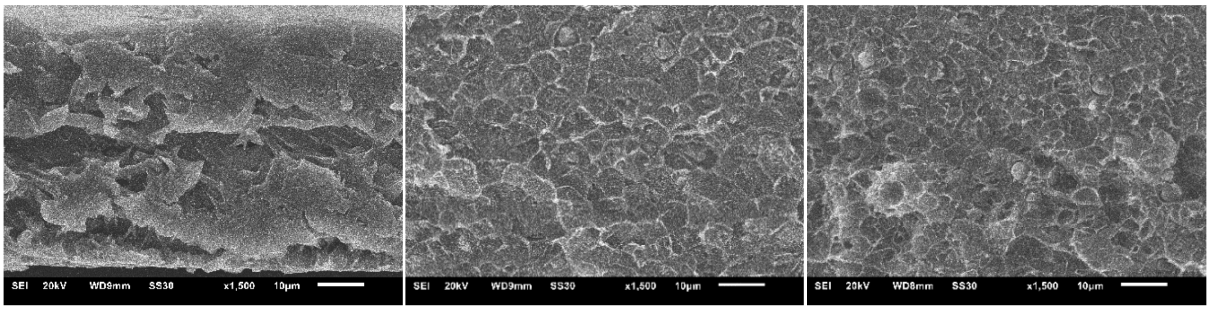

Figure S13. Cross-section SEM images of 8 wt%, 16 wt% and 24 wt% IL@CTF in IL@CTF/Matrimid® MMMs.

4.4. Gas permeabilities (*P*) and mixed-gas selectivity factors (α)

Table S7. Gas permeabilities (*P*) and mixed-gas selectivity factors (α) of [BMIm][NTf_2]/Matrimid® MMMs.[a]

IL [BMIm][NTf_2] [wt%]	P CO_2 [Barrer]	P CH_4 [Barrer]	α CO_2/CH_4
5	5.5 ± 0.1	0.11 ± 0.01	49 ± 1
10	4.3 ± 0.2	0.11 ± 0.01	37 ± 1
15	3.7 ± 0.1	0.11 ± 0.01	34 ± 1

[a]The errors for the permeability (*P*) and for the selectivity (α) were taken from the range of two measurements.

Table S8. Gas permeabilities (*P*) and mixed-gas selectivity factors (α) of the ternary IL/CTF/Matrimid® and IL@CTF/Matrimid® MMMs.[a]

CTF-biphenyl [wt%]	IL [wt%]	combined filler [wt%]	P CO_2 [Barrer]	P CH_4 [Barrer]	α CO_2/CH_4
		IL/CTF/Matrimid®			
8	5	12	6.8 ± 0.2	0.15 ± 0.01	45 ± 2
16	5	20	7.3 ± 0.1	0.16 ± 0.01	44 ± 1
24	5	27	11.1 ± 0.2	0.22 ± 0.02	50 ± 3
		IL@CTF/Matrimid®			
7.6	0.48	8	7.6 ± 0.3	0.17 ± 0.01	43 ± 2
15.2	1.05	16	12.0 ± 0.2	0.23 ± 0.01	52 ± 1
23.0	1.74	24	12.0 ± 0.6	0.26 ± 0.01	46 ± 2

[a]The errors for the permeability (*P*) and for the selectivity (α) were taken from the range of two measurements.

4.5. Comparison of binary MMMs with literature

Table S9. Comparison of CO_2 permeability and CO_2/CH_4 selectivity for COFs/CTFs as porous filler materials in different polymer MMMs.

Filler	Filler content [wt%]	Matrix	*P* CO_2 [Barrer]	α CO_2/CH_4	Ref.
-	-	Matrimid®	6.8 ± 0.1[a]	30.5± 0.6[a]	[19]
ACOF-1[1]	8	Matrimid®	9.6 ± 1.0[a]	31.9 ± 0.8[a]	
	16		15.3 ± 0.7[a]	32.4 ± 1.8[a]	
-	-	PIM-1[3]	3672[b]	10.6[b]	[20]
SNW-1[2]	10	PIM-1[3]	7553[b]	13.5[b]	
-	-	Pebax® 1657	53[c]	17[c]	[21]
CTPP[4]	0.025	Pebax® 1657	73[c]	25[c]	
-	-	PIM-1[3]	5800[d]	11.5[d]	[22]
FCTF-1	2	PIM-1[3]	7300[d]	16.6[d]	
	5		9400[d]	14.8[d]	
-	-	Matrimid®	6.8 ± 0.3[e]	42 ± 1[e]	This work
CTF-biphenyl	8	Matrimid®	12.0 ± 0.2[e]	43 ± 1[e]	
	16		15.1 ± 0.2[e]	44 ± 1[e]	
	24		15.4 ± 0.5[e]	44 ± 1[e]	
-	-	PSF[5]	5.4 ± 0.0[e]	28 ± 2[e]	[4]
CTF-fluorene	8	PSF[5]	6.6 ± 0.3[e]	32 ± 2[e]	
	16		8.8 ± 0.3[e]	29 ± 0[e]	
	24		12.8 ± 0.1[e]	30 ± 3[e]	
-	-	Matrimid®	6.8 ± 0.3[e]	42 ± 1[e]	
CTF-fluorene	8	Matrimid®	9.2 ± 0.4[e]	43 ± 1[e]	
	16		12.6 ± 0.1[e]	45 ± 1[e]	
	24		17.8 ± 0.3[e]	44 ± 2[e]	
-	-	PSF[5]	7.3 ± 0.2[f]	21 ± 3[f]	[23]
CTF-1	8	PSF[5]	9.2 ± 0.6[f]	21 ± 3[f]	
	16		10.7 ± 0.6[f]	21 ± 3[f]	
	24		12.7 ± 0.8[f]	22 ± 3[f]	

[a]Mixed gas; 308 K; feed pressure 4 bar; [b]Single gas; 303 K; feed pressure 2 bar; [c]Single gas; 293 K; feed pressure 4 bar; [d]Single gas; 303 K; feed pressure 1 atm; [e]Mixed gas; 298 K; feed pressure 4 bar; [f]Single gas; 298 K; feed pressure 3 bar; [1]azine-linked covalent organic framework; [2]Schiff base network; [3]polymer of intrinsic microporosity; [4]porous covalent triazine piperazine polymer; [5]polysulfone

References

1. Bi, J.; Fang, W.; Li, L.; Wang, J.; Liang, S.; He, Y.; Liu, M.; Wu, L. Covalent Triazine-Based Frameworks as Visible Light Photocatalysts for the Splitting of Water. *Macromol. Rapid Commun.* **2015**, *36*, 1799-1805.

2. Bhunia, A.; Boldog, I.; Möller, A.; Janiak, C. Highly stable nanoporous covalent triazine-based frameworks with an adamantane core for carbon dioxide sorption and separation. *J. Mater. Chem. A* **2013**, *1*, 14990.

3. Osadchii, D. Y.; Olivos-Suarez, A. I.; Bavykina, A. V.; Gascon, J. Revisiting Nitrogen Species in Covalent Triazine Frameworks. *Langmuir* **2017**, *33*, 14278-14285.

4. Bügel, S.; Spieß, A.; Janiak, C. Covalent triazine framework CTF-fluorene as porous filler material in mixed matrix membranes for CO_2/CH_4 separation. *Micropor. Mesopor. Mat.* **2021**, *316*, 110941

5. Scholl, R.; Mansfeld, J. meso-Benzdianthron (Helianthron), meso-Naphthodianthron, und ein neuer Weg zum Flavanthren. *Ber. Dtsch. Chem. Ges.* **1910**, *43*, 1734-1746.

6. Kovacic, P.; Jones, M.B. Dehydro Coupling of Aromatic Nuclei by Catalyst-Oxidant Systems: Poly(p-phenylene). *Chem. Rev.* **1987**, *87*, 357-379 357.

7. Dey, S.; Bhunia, A.; Esquivel, D.; Janiak, C. Covalent triazine-based frameworks (CTFs) from triptycene and fluorene motifs for CO_2 adsorption. *J. Mater. Chem. A* **2016**, *4*, 6259-6263.

8. Dey, S.; Bhunia, A.; Boldog, I.; Janiak, C. A mixed-linker approach towards improving covalent triazine-based frameworks for CO_2 capture and separation. *Micropor. Mesopor. Mat.* **2017**, *241*, 303-315.

9. Dey, S.; Bhunia, A.; Breitzke, H.; Groszewicz, P.B.; Buntkowsky, G.; Janiak, C. Two linkers are better than one: enhancing CO_2 capture and separation with porous covalent triazine-based frameworks from mixed nitrile linkers. *J. Mater. Chem. A* **2017**, *5*, 3609-3620.

10. Kuhn, P.; Antonietti, M.; Thomas, A. Porous, Covalent Triazine-Based Frameworks Prepared by Ionothermal Synthesis. *Angew. Chem. Int. Ed.* **2008**, *47*, 3450-3453.

11. Meier, C. B.; Sprick, R. S.; Monti, A.; Guiglion, P.; Lee, J.-S. M.; Zwijnenburg, M. A.; Cooper, A. I. Structure-property relationships for covalent triazine-based frameworks: The effect of spacer length on photocatalytic hydrogen evolution from water. *Polymer* **2017**, *126*, 283-290.

12. Lim, H.; Cha, M. C.; Chang, J. Y. Preparation of Microporous Polymers Based on 1,3,5-Triazine Units Showing High CO_2 Adsorption Capacity. *Macromol. Chem. Phys.* **2012**, *213*, 1385-1390.

13. Aupoix, A.; Pégot, B.; Vo-Thanh, G. Synthesis of imidazolium and pyridinium-based ionic liquids and application of 1-alkyl-3-methylimidazolium salts as pre-catalysts for the benzoin condensation using solvent-free and microwave activation. *Tetrahedron* **2010**, *66*, 1352-1356.

14. Zhao, R.; Wu, H.; Yang, L.; Ren, Y.; Liu, Y.; Qu, Z.; Wu, Y.; Cao, L.; Chen, Z.; Jiang, Z. Modification of covalent organic frameworks with dual functions ionic liquids for membrane-based biogas upgrading. *J. Membr. Sci.* **2020**, *600*, 117841.

15. Li, H.; Tuo, L.; Yang, K.; Jeong, H.-K.; Dai, Y.; He, G.; Zhao, W. Simultaneous enhancement of mechanical properties and CO_2 selectivity of ZIF-8 mixed matrix membranes: Interfacial toughening effect of ionic liquid. *J. Membr. Sci.* **2016**, *511*, 130-142.

16. Perkin, S.; Crowhurst, L.; Niedermeyer, H.; Welton, T.; Smith, A. M.; Gosvami, N. N. Self-assembly in the electrical double layer of ionic liquids. *Chem. Commun.* **2011**, *47*, 6572-6574.

17. Shindo, R.; Kishida, M.; Sawa, H.; Kidesaki, T.; Sato, S.; Kanehashi, S.; Nagai, K. Characterization and gas permeation properties of polyimide/ZSM-5 zeolite composite membranes containing ionic liquid. *J. Membr. Sci.* **2014**, *454*, 330-338.

18. Kanehashi, S.; Kishida, M.; Kidesaki, T.; Shindo, R.; Sato, S.; Miyakoshi, T.; Nagai, K. CO_2 separation properties of a glassy aromatic polyimide composite membranes containing high-content 1-butyl-3-methylimidazolium bis(trifluoromethylsulfonyl)imide ionic liquid. *J. Membr. Sci.* **2013**, *430*, 211-222.

19. Shan, M.; Seoane, B.; Rozhko, E.; Dikhtiarenko, A.; Clet, G.; Kapteijn, F.; Gascon, J. Azine-Linked Covalent Organic Framework (COF)-Based Mixed-Matrix Membranes for CO_2/CH_4 Separation. *Chem. Eur. J.* **2016**, *22*, 14467-14470.

20. Wu, X.; Tian, Z.; Wang, S.; Peng, D.; Yang, L.; Wu, Y.; Xin, Q.; Wu, H.; Jiang, Z. Mixed matrix membranes comprising polymers of intrinsic microporosity and covalent organic framework for gas separation. *J. Membr. Sci.* **2017,** *528*, 273-283.
21. Thankamony, R.L.; Li, X.; Das, S.K.; Ostwal, M.M.; Lai, Z. Porous covalent triazine piperazine polymer (CTPP)/PEBAX mixed matrix membranes for CO_2/N_2 and CO_2/CH_4 separations. *J. Membr. Sci.* **2019**, *591*, 117348.
22. Jiang, H.; Zhang, J.; Huang, T.; Xue, J.; Ren, Y.; Guo, Z.; Wang, H.; Yang, L.; Yin, Y.; Jiang, Z.; Guiver, M.D. Mixed-Matrix Membranes with Covalent Triazine Framework Fillers in Polymers of Intrinsic Microporosity for CO_2 Separations. *Ind. Eng. Chem. Res.* **2019**, *59*, 5296-5306.
23. Dey, S.; Bügel, S.; Sorribas, S.; Nuhnen, A.; Bhunia, A.; Coronas, J.; Janiak, C. Synthesis and Characterization of Covalent Triazine Framework CTF-1@Polysulfone Mixed Matrix Membranes and Their Gas Separation Studies. *Front. Chem.* **2019**, *7*, 693.

3.3. Synthesis and characterization of a crystalline imine-based covalent organic framework with triazine node and biphenyl linker and its fluorinated derivate for CO_2/CH_4 separation

Stefanie Bügel, Malte Hähnel, Tom Kunde, Nader de Sousa Amadeu, Yangyang Sun, Alex Spieß, Thi Hai Yen Beglau, Bernd M. Schmidt, Christoph Janiak

Materials **2022**, *15*, 2807.

DOI: 10.3390/ma15082807; [117]

Imine COFs are formed by a condensation reaction based on Schiff base chemistry. The dynamic formation process yields crystalline and permanently porous materials with high chemical and thermal stability. Two new COFs were obtained by a catalyst-free Schiff base reaction. The condensation reaction of 1,3,5-tris-(4-aminophenyl)triazine with 4,4'-biphenyldicarboxaldehyde or 2,2',3,3',5,5',6,6'-octafluoro-4,4'-biphenyldicarboxaldehyde yielded HHU-COF-1 and the fluorinated analog HHU-COF-2. The successful formation of the COFs was confirmed by ^{13}C and ^{19}F CP MAS NMR, IR, XPS and elemental analysis. The resulting crystalline materials were characterized by high BET surface areas of 2352 m^2/g for HHU-COF-1 and 1356 m^2/g for HHU-COF-2. Both syntheses were expanded to larger scales, and the resulting products were applied as filler materials in Matrimid-based MMMs. Mixed-gas CO_2/CH_4 separation experiments revealed the best membrane performance for HHU-COF-2 as a dispersed phase. With 24 wt% of the fluorinated filler, the CO_2 permeability was increased from 6.8 to 13.0 Barrer.

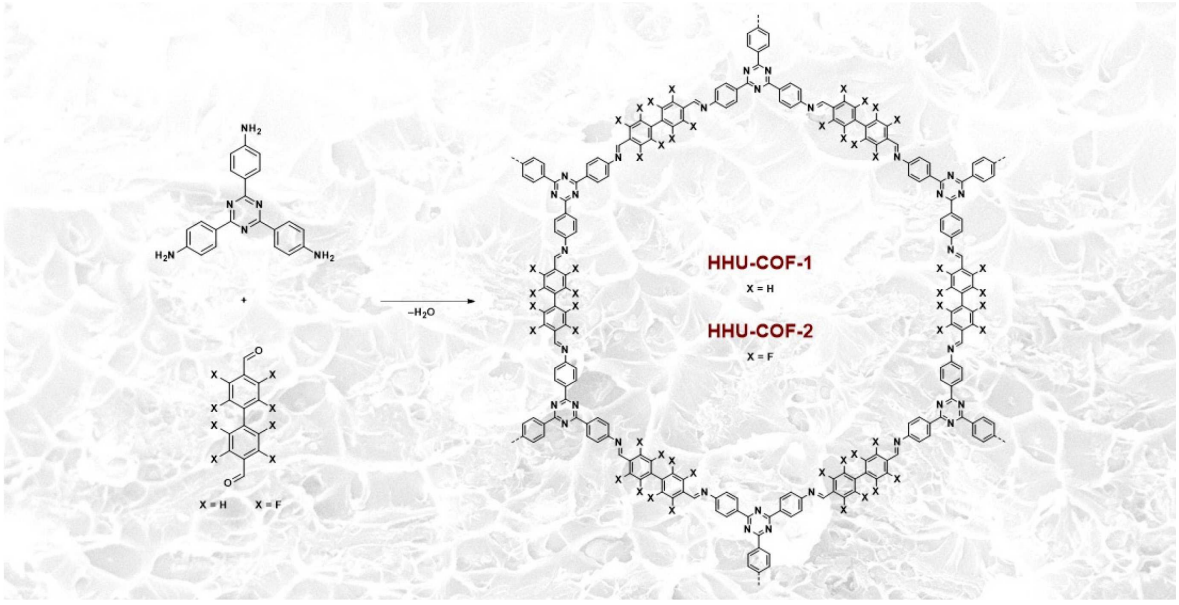

Author's contribution to the work:

- COF syntheses with M. Hähnel
- MMM preparation and CO_2/CH_4 measurements
- Application of permeability models and calculation of the FFV
- Data interpretation
- Manuscript writing with corrections by C. Janiak
- T. Kunde: synthesis of 2,2',3,3',5,5',6,6'-octafluoro-4,4'-biphenyldicarboxaldehyde
- N. de Sousa Amadeu: ^{13}C and ^{19}F CP MAS NMR measurements
- Y. Sun: CO_2 and CH_4 sorption experiments, TGA measurements
- A. Spieß: SEM measurements;
- T.H.Y. Beglau: XPS measurements
- B.M. Schmidt: basic idea

The work presented in this chapter has been published as:

Synthesis and characterization of a crystalline imine-based covalent organic framework with triazine node and biphenyl linker and its fluorinated derivate for CO_2/CH_4 separation

Stefanie Bügel[1], Malte Hähnel[1], Tom Kunde[2], Nader de Sousa Amadeu[3], Yangyang Sun[1], Alex Spieß[1],Thi Hai Yen Beglau[1], Bernd M. Schmidt[2,*] and Christoph Janiak[1,*]

[1]Institut für Anorganische Chemie und Strukturchemie, Heinrich-Heine-Universität Düsseldorf, 40204 Düsseldorf, Germany; stefanie.buegel@hhu.de (S.B.); mahae107@hhu.de (M.H.); yasun100@hhu.de (Y.S.); alex.spiess@hhu.de (A.S.); beglau@hhu.de (T.H.Y.B.)

[2]Institut für Organische Chemie und Makromolekulare Chemie, Heinrich-Heine-Universität Düsseldorf, 40204 Düsseldorf, Germany; kunde@hhu.de

[3]Bundesanstalt für Materialforschung und -Prüfung, Fachbereich 6.3 (Strukturanalytik), 12489 Berlin, Germany; nader.amadeu@bam.de

[*]Correspondence: bernd.schmidt@hhu.de (B.M.S.); janiak@hhu.de (C.J.)

Abstract: A catalyst-free Schiff base reaction was applied to synthesize two imine-linked covalent organic frameworks (COFs). The condensation reaction of 1,3,5-tris-(4-aminophenyl)triazine (TAPT) with 4,4'-biphenyldicarboxaldehyde led to the structure of HHU-COF-1 (HHU = Heinrich-Heine University). The fluorinated analog HHU-COF-2 was obtained with 2,2',3,3',5,5',6,6'-octafluoro-4,4'-biphenyldicarboxaldehyde. Solid-state NMR, infrared spectroscopy, X-ray photoelectron spectroscopy, and elemental analysis confirmed the successful formation of the two network structures. The crystalline materials are characterized by high Brunauer–Emmett–Teller surface areas of 2352 m^2/g for HHU-COF-1 and 1356 m^2/g for HHU-COF-2. The products of a larger-scale synthesis were applied to prepare mixed-matrix membranes (MMMs) with the polymer Matrimid. CO_2/CH_4 permeation tests revealed a moderate increase in CO_2 permeability at constant selectivity for HHU-COF-1 as a dispersed phase, whereas application of the fluorinated COF led to a CO_2/CH_4 selectivity increase from 42 for the pure Matrimid membrane to 51 for 8 wt% of HHU-COF-2 and a permeability increase from 6.8 to 13.0 Barrer for the 24 wt% MMM.

Keywords: *covalent organic framework (COF); imine-COF; fluorinated COF; mixed-matrix membrane (MMM); CO_2/CH_4 separation*

1. Introduction

Covalent organic frameworks (COFs) are porous crystalline materials built entirely by covalent bonds between light elements. Since the first COFs, namely COF-1 and COF-5, were synthesized in 2005 [1], research on COFs has been rapidly developing. The opportunity to change, for example, the linkers or the linkage leads to a broad variety of two-dimensional (2D) or three-dimensional (3D) structures [2]. The associated tunable material characteristics open up the possibility of applications in various areas such as gas storage [3], molecular separation [4–6], catalysis [7], sensing [8], energy storage [9], and optoelectronics [10].

COFs synthesized via a condensation reaction of an aldehyde and an amine represent the class of imine-COFs. The dynamic formation process based on Schiff base chemistry results in crystalline and porous materials with high chemical and thermal stability [11]. In 2009, the first imine-COF (COF-300) was synthesized from tetra-(4-anilyl)methane and terephthalaldehyde (TA), resulting in a crystalline 3D COF with diamond topology. COF-300 exhibited permanent porosity with a Brunauer–Emmett–Teller (BET) surface area of 1360 m^2/g and thermal stability up to 490 °C [12]. Two years later, the first 2D imine-COF was reported by Ding et al. The condensation of 1,3,5-triformylbenzene and 1,4-phenylenediamine yielded the layered COF-LZU1, with hexagonal channels and narrow pores with a distribution around 1.2 nm [13]. Based on this hexagonal 2D structure, more nitrogen-rich COFs were synthesized by using 1,3,5-tris-(4-aminophenyl)triazine (TAPT) and TA in a Schiff base reaction. Gomes et al. applied these educts to synthesize the porous polymer TRITER-1 (Scheme S1) with a BET surface area of 716 m^2/g [14]. In a solvothermal catalyst-free (SCF) synthesis, Liao et al. successfully produced a fluorinated analog by substituting the educt TAPT with 2,3,5,6-tetrafluoroterephthalaldehyde (TFTA). The resulting SCF-FCOF-1 (Scheme S1) showed a suitable crystallinity and a large BET surface area of 2056 m^2/g [15].

Nitrogen-containing covalent triazine frameworks (CTFs) [16–19] and fluorine containing porous materials (metal-organic frameworks; MOFs [20,21] and COFs, including CTFs [22–24]) are sought for their potentially high CO_2 sorption and separation properties. The incorporation of these porous materials as fillers into polymer matrices as a continuous phase leads to the formation of mixed-matrix membranes (MMMs), and the composites are promising for CO_2/CH_4 separation as an application [25–28]. While examples of MOF and COF-based MMMs are frequent, there are fewer cases of CTF-based MMMs [29,30]. With the microporous azine-linked COF material ACOF-1 as a filler in Matrimid, the gas separation performance of the resulting MMM was tested with an equimolar mixture of CO_2/CH_4 at 308 K. With 16 wt%

filler, the CO_2 permeability was increased from 6.8 Barrer for the pure Matrimid membrane to 15.3 Barrer, with no loss of CO_2/CH_4 selectivity [31]. A total of 5 wt% of the fluorinated CTF, FCTF-1, embedded in a PIM-1 matrix led to an improvement in CO_2 permeability from 5800 to 9400 Barrer. In this case, it was also possible to improve the CO_2/CH_4 selectivity from 11.5 to 14.8 [32]. These examples show that higher membrane efficiency can be achieved by incorporating fillers into membranes. Important prerequisites are suitable compatibility between filler and polymer and uniform distribution of the filler without sedimentation.

In this work, we present two large-pore imine-COFs with a triazine node, akin to CTFs, which were synthesized via the catalyst-free Schiff base reaction at 120 °C to avoid any nitrogen and fluorine loss. The standard ionothermal CTF synthesis not only leads to a large loss of nitrogen but also to defluorination during the reaction at >400 °C with high equivalents of $ZnCl_2$ [23,24]. Here, the triazine-based node TAPT and the linkers 4,4'-biphenyldicarboxaldehyde (BPDCA) and 2,2',3,3',5,5',6,6'-octafluoro- 4,4'-biphenyldicarboxaldehyde (OF-BPDCA) were reacted to give the crystalline COFs HHU-COF-1 and HHU-COF-2 (Scheme 1). OF-BPDCA features an inverse electron density distribution due to its fluorine substituents compared to BPDCA and exhibits a larger dihedral angle of 36° between the two aromatic rings (BPDCA 18°). OF-BPDCA has been used in the assembly of helical channels in supramolecular organic frameworks but not as a linker in COFs [33]. In addition, the combination of BPDCA with TAPT to form a COF is novel to the best of our knowledge [11]. Further, the nitrogen-rich structures, which are favorable for CO_2 adsorption due to quadrupole-dipole interactions [34], were applied as filler materials to form MMMs for CO_2/CH_4 mixed-gas separation. The MMM matrix was Matrimid, a glassy polymer with intrinsically high CO_2/CH_4 selectivity [35,36].

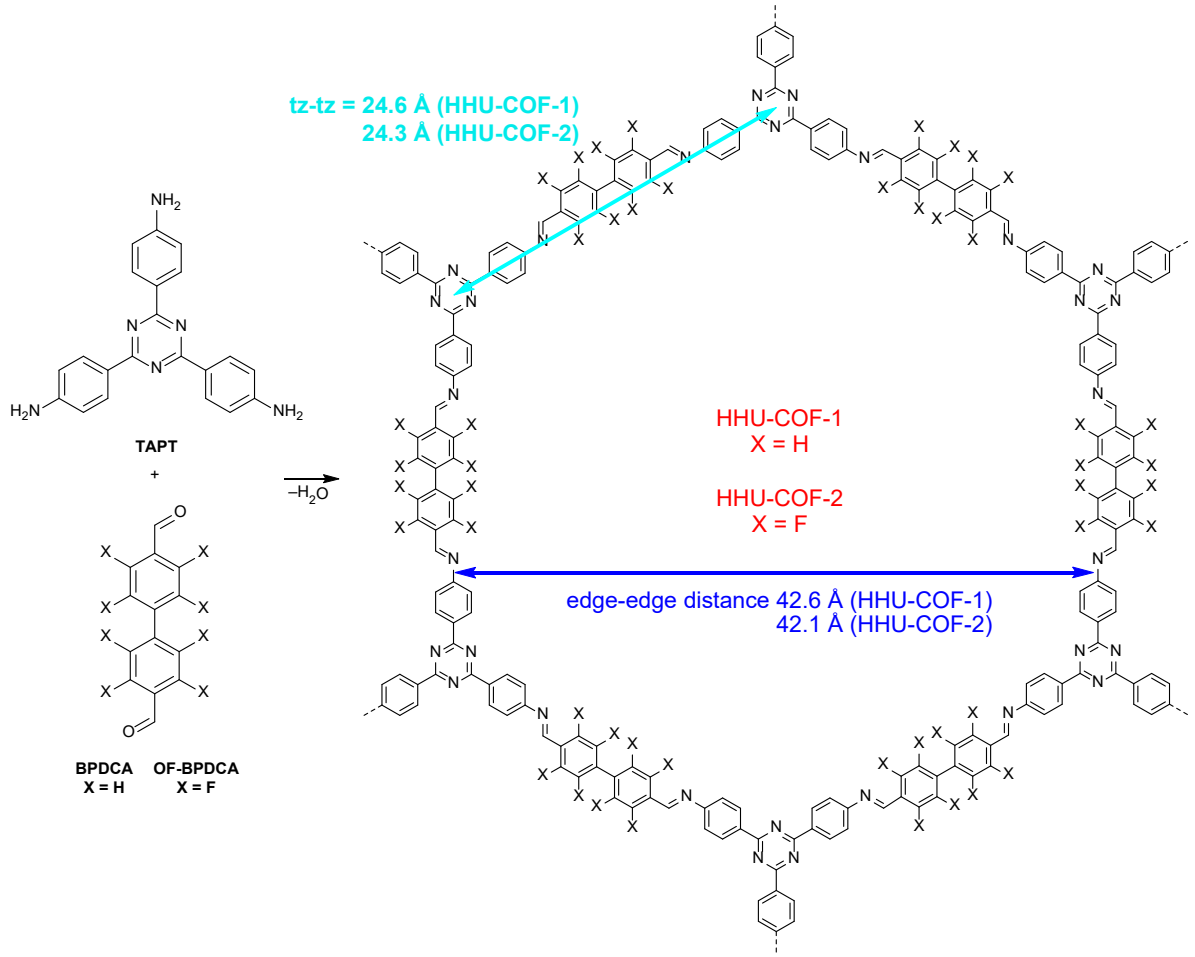

Scheme 1. Schematic formation of HHU-COF-1 and HHU-COF-2 from TAPT and BPDCA or OF-BPDCA, respectively, indicating the idealized hexagonal ring and network in the HHU-COF products (HHU = Heinrich-Heine University). The given triazine-centroid triazine-centroid (tz-tz) distance along the edges and the edge-edge distances were determined from the most intense (100) reflexes in the powder X-ray diffractograms, assuming a hexagonal unit cell for the honeycomb layer (cf. Figure S16). The given tz-tz distance along the edge is half the tz-tz distance across the ring.

2. Materials and Methods

2.1. Materials

For COFs: 4,4'-Biphenyldicarboxaldehyde (BPDCA; 97%) was obtained from ACROS Organics and 1,3,5-tris-(4-aminophenyl)triazine (TAPT; >98%) from TCI. 2,2',3,3',5,5',6,6'-octafluoro-4,4'-biphenyldicarboxaldehyde (OF-BPDCA) was synthesized as described in Section S1 of the Supplementary Materials. The COF syntheses were carried out in analogy to the synthesis of SCF-FCOF-1 [15]. All solvents were purchased from commercial suppliers with a minimum purity of 99.8%.

For membranes: Matrimid® 5218 (BTDA/DAPI) was provided by Huntsman Advanced Materials, and dichloromethane DCM; 99.99%) obtained from Fisher Scientific (Hampton, NH, USA).

Gases: CO_2 (grade 4.5), CH_4 (grade 4.5), and He (grade 5.0) were received from Air Liquide.

2.2. Synthesis of HHU-COF-1

A total of 84.1 mg (0.400 mmol) of BPDCA, 94.5 mg (0.267 mmol) of TAPT, and 1 mL of the solvent mixture of 1,4-dioxane and mesitylene (1:1, *v/v*) were placed in a glass ampoule, followed by an ultra-sonification treatment for 15 min in order to ensure sufficient mixing of the educts. The mixture was degassed by applying three freeze-pump-thaw cycles, and the ampoule was flame sealed under vacuum. After heating at 120 °C for three days, the crude product was washed with THF, followed by Soxhlet extraction for 24 h each in THF and in ethanol to remove unreacted monomers. Drying was performed with supercritical CO_2 (yield: 147 mg; 89.5%).

2.3. Synthesis of HHU-COF-1 (Larger Scale)

A total of 252.3 mg (1.200 mmol) of BPDCA, 283.5 mg (0.800 mmol) of TAPT, and 4 mL of the solvent mixture of 1,4-dioxane and mesitylene (1:1, *v/v*) were placed in a glass ampoule, followed by an ultra-sonification treatment for 30 min and the procedures described in 2.2 (yield: 433 mg; 87.9%).

2.4. Synthesis of HHU-COF-2

A total of 70.8 mg (0.200 mmol) of OF-BPDCA, 47.2 mg (0.133 mmol) of TAPT, and 3 mL of the solvent mixture of 1,4-dioxane and mesitylene (1:1, *v/v*) were placed in a glass ampoule, followed by an ultra-sonification treatment for 30 min and the procedures described in 2.2 (yield: 93 mg; 84.3%).

2.5. Synthesis of HHU-COF-2 (Larger Scale)

A total of 354.3 mg (1.000 mmol) OF-BPDCA, 236.4 mg (0.667 mmol) TAPT, and 6 mL of the solvent mixture of 1,4-dioxane and mesitylene (1:1, *v/v*) were placed in a glass ampoule, followed by an ultra-sonification treatment for 50 min and the procedures described in 2.2 (yield: 485 mg; 87.4%).

2.6. Preparation of HHU-COF-1/Matrimid and HHU-COF-2/Matrimid MMMs

To ensure that all MMMs are prepared from the same batch, the COF materials obtained from the larger-scale syntheses were applied as filler materials in the MMMs. Characterization of these COFs can be found in Section S3, Supplementary Materials. The HHU-COF-1/Matrimid and HHU-COF-2/Matrimid MMMs were prepared by solution casting with filler loadings of 8, 16, and 24 wt% (Figures S23 and S24). The filler loading was calculated according to Equation (1):

$$Filler\ loading\ [wt\%] = \frac{m_{filler}}{m_{polymer} + m_{filler}} \times 100\ \% \quad (1)$$

The 8 wt% membranes were prepared as follows: 250 mg of Matrimid (stored at 80 °C) were dissolved in 3 mL of DCM. A total of 22 mg (48 mg for 16 wt% and 79 mg for 24 wt%) of COF were dispersed in 4 mL of DCM. Both polymer and COF were stirred for 24 h. The COF dispersion was ultrasonicated using a Microtip 630-0419 (VCX 750 Sonics) three times for 15 min (amplitude of 20%) with 30 min stirring between the ultra-sonification steps. Afterward, 0.29 mL (0.62 mL for 16 wt% and 1.01 mL for 24 wt%) of the Matrimid solution was added to the COF dispersion, followed by stirring for another 24 h. The same ultra-sonification procedure was repeated, and the remaining Matrimid solution was added to the COF dispersion. After stirring for two hours, the final dispersion was casted into a metal ring placed on a flat and even glass surface. To ensure slow evaporation of DCM, an inverted funnel covered with a paper tissue was placed above the MMM until the DCM was evaporated. The membrane was cut out of the metal ring with a scalpel. The membranes were dried at 150 °C in a vacuum oven (20 mbar) overnight.

2.7. Instrumentation and Characterization Methods

Supercritical CO_2 drying was conducted with an EMCPD300 (Leica,Wetzlar, Germany). Ethanol was exchanged for CO_2 with 50 cycles for each product. Solid-state NMR experiments were performed with an AVANCE 600 spectrometer (Bruker, Billerica, MA, USA) under a static field of 14 T. The samples were packed into 2.5 mm zirconia rotors with Vespel top and bottom plugs and spun at 35 kHz under the magic angle (MAS) in a double resonant wide-bore probe at room temperature. Typical acquisition parameters for the ^{13}C MAS NMR spectra were a repetition period (d1) equal to or higher than 12 s; 9 ms contact time (cross-polarization), and 1–2 µs for the 90° pulses. During a typical acquisition time of about 10 ms, ^{1}H was decoupled using the spinal64 sequence. Very long experiments with accumulations between 16 and 64 k scans were performed in order to overcome the low sensitivity observed for those samples. For ^{19}F solid-state NMR experiments, the sample was spun in a 2.5 mm zirconia rotor with Vespel top and bottom plugs at 35 kHz (MAS). The EASY pulse program [37] was applied, in which two 90° pulses were irradiated with a little delay in between. By subtracting the FID after each of those pulses, the background signal was canceled. Subsequent processing involved Fourier transformation, phase adjustment, and baseline correction (Bernstein polynomials, fourth-order or higher). Attenuated total reflection infrared spectroscopy (ATR-IR, platinum ATR-QL, diamond) spectra were obtained on a Tensor 37 (Bruker). X-ray photoelectron spectroscopy (XPS) measurements were performed on a VersaProbe II (Ulvac-Phi) with a monochromatic

Al X-ray source (1486.6 eV). The C1s signal at 284.8 eV was taken as the reference for the binding energy scale. Analysis of the spectra was carried out with the program CasaXPS. C, H, N-analysis was carried out on a Vario MICRO cube from Elementar Analysentechnik. Scanning electron microscopy (SEM) images were recorded with a JSM-6510LV (Jeol) with a LaB_6 cathode (20 keV). The membrane cross-sections were obtained by freeze-fracturing with liquid nitrogen and coated with gold by a JFC 1200 (Jeol) sputter coater for imaging. Energy-dispersive X-ray spectroscopy (EDX) was carried out using an Xflash silicon drift detector (Bruker). Thermogravimetric analysis (TGA) was performed under a nitrogen atmosphere with a TG 209 F3 Tarsus (Netzsch, Selb, Germany) in a range from 25 to 1000 °C with a heating rate of 5 K/min.

An Autosorb-6 (Quantachrome, Boynton Beach, FL, USA) was used to perform the nitrogen sorption measurements. Prior to the measurements, all samples were activated by degassing under vacuum at 120 °C for 8 h. The Brunauer–Emmett–Teller (BET) surface area was calculated from the range of 0.05 to 0.3 p/p_0 of the nitrogen adsorption isotherms. CO_2 and CH_4 sorption isotherms were obtained with an Autosorb iQ MP (Quantachrome). The samples were activated in vacuo (5×10^{-3} mbar) at 120 °C for 8 h. In order to calculate the ideal adsorbed solution theory (IAST) selectivity for the gas pair CO_2/CH_4, the sorption isotherms of HHU-COF-1 were fitted with the Langmuir isotherm (LAI) model by applying Equation (2):

$$q_{eq} = q_{max} \times \frac{K \times p}{1 + K \times p} \tag{2}$$

The isotherms of HHU-COF-2 were fitted with the Toth isotherm model (Equation (3)),

$$q_{eq} = q_{max} \times \frac{K \times p}{(1 + K \times p)^{t})^{1/t}} \tag{3}$$

where q and K refer to the loading in mmol/g and the affinity constant, respectively. The heterogeneity exponent is expressed as t with the unit 1/bar. After isotherm fitting, the final IAST selectivity was calculated by Equation (4), where x_i is the absorbed gas amount in mmol/g and y_i is the mole fraction.

$$S = \frac{x_1/y_1}{x_2/y_2} \tag{4}$$

Powder X-ray diffraction (PXRD) patterns were obtained from a Miniflex 600 (Rigaku,Tokyo, Japan) using Cu Kα1 radiation with λ = 1.5406 Å (40 kV, 15 mA, 600 W) and a flat silicon low background sample holder in the range of $2° < 2\theta < 50°$. For determination of the (skeletal) density, a He-pycnometer AccuPyc 1330 (Micromeritics) was used. The density applied for

calculations was obtained by including the total pore volume from N_2-sorption as shown in Equation (5):

$$\rho_{COF} = \frac{m_{COF}}{V_{He} + V_{pores}} \quad (5)$$

The tensile strength of the pure Matrimid membrane and MMMs was measured using a TAXT.plus texture analyzer (Stable Micro Systems). The force (N) was divided by the product of the thickness and width of the membrane to obtain the tensile strength to break the membrane in MPa.

CO_2/CH_4 mixed-gas separation measurements were carried out with an OSMO inspector (Convergence Industry B.V.) connected to an Agilent 490 Micro GC (Agilent Technologies, Santa Clara, CA, USA) with a fused silica column PoraPLOT Q and a thermal conductivity detector. A diagram of the experimental setup is shown in Figure S25. The membranes were placed in the permeation module and fixed with a Viton O-ring with an inner diameter of 3.6 cm (area: 11.3 cm^2) inside the permeation module. A CO_2/CH_4 feed gas volume ratio of 1:1 was applied, and helium was used as the sweep gas. The transmembrane pressure and the temperature were set to 3 bar and 25 °C, respectively. All measurements were carried out every 30 min until the equilibrium state was reached. The permeability P is expressed in the unit Barrer (1 Barrer = 10^{-10} cm^3(STP) cm cm^{-2} s^{-1} $cmHg^{-1}$) and was calculated according to Equation (6):

$$P = \frac{x_A \times Q_{He} \times d}{x_{He} \times A \times (p_2 \times x_A^f - p_1 \times x_A)} \quad (6)$$

x_A describes the molar fraction of the gas A, Q_{He} is the volumetric flow rate of the sweep gas helium, d is the thickness of the membrane (measured at 10 different points) and x_{He} is the molar fraction of the sweep gas. A stands for the area of the membrane (cm^2), p_2 for the feed pressure (cmHg), x_A^f for the molar fraction of the gas A in the feed, and p_1 for the permeate pressure (cmHg). The molar fractions (x) on the permeate and the feed side were used to calculate the selectivity of the two gases (A, B), according to Equation (7):

$$\alpha_{A,B} = \frac{(x_A/x_B)_{permeate\ side}}{(x_A/x_B)_{feed\ side}} \quad (7)$$

3. Results and Discussion

3.1. Characterization of HHU-COF-1 and HHU-COF-2

The Schiff base reaction of 1,3,5-tris-(4-aminophenyl)triazine (TAPT) with either 4,4'-biphenyldicarboxaldehyde (BPDCA) or the corresponding octafluoro derivative OFBPDCA

yielded the two COFs HHU-COF-1 and HHU-COF-2 as yellow and orange powder (Scheme 1, Figure S17). A three-day synthesis was carried out in ampoules to allow for a slow, reversible reaction leading to crystalline products. Both COFs were reproducibly synthesized on the scale of 0.13 to 0.8 mmol of TAPT in a 1:1.5 ratio with (OF-)BPDCA under the same reaction conditions (cf. Supplementary Materials). Yields ranging from 84% to 90% could be reached. ^{13}C CP MAS NMR spectra confirmed the formation of the imine bond at 158 ppm for HHU-COF-1 and 153 ppm for HHU-COF-2 (Figure 1). These values agree well with the related TRITER-1 (158 ppm) [14] and SCF-FCOF-1 (152 ppm) [15] for their carbon atoms of the imine bond. Both COFs exhibited a peak at 171 ppm, referring to the carbon atoms of the triazine ring again identical to TRITER-1 [14]. The signals in the range from 120 to 150 ppm can be assigned to the carbon atoms in the benzene rings. For HHU-COF-1, the small peak at 191 ppm can be attributed to some unreacted aldehyde [38]. Because of the extensive purification with Soxhlet extraction, we assume that the aldehyde signal did not originate from unreacted monomers and is instead caused by partially incomplete network formation, that is, defect sites. In the ^{19}F CP MAS NMR spectrum of HHU-COF-2 (Figure 2), the two peaks expected from solution NMR of OF-BPDCA at –136 and –144 ppm (Figure S3) can only be seen as one peak at –141 ppm due to the line broadening in solid-state NMR.

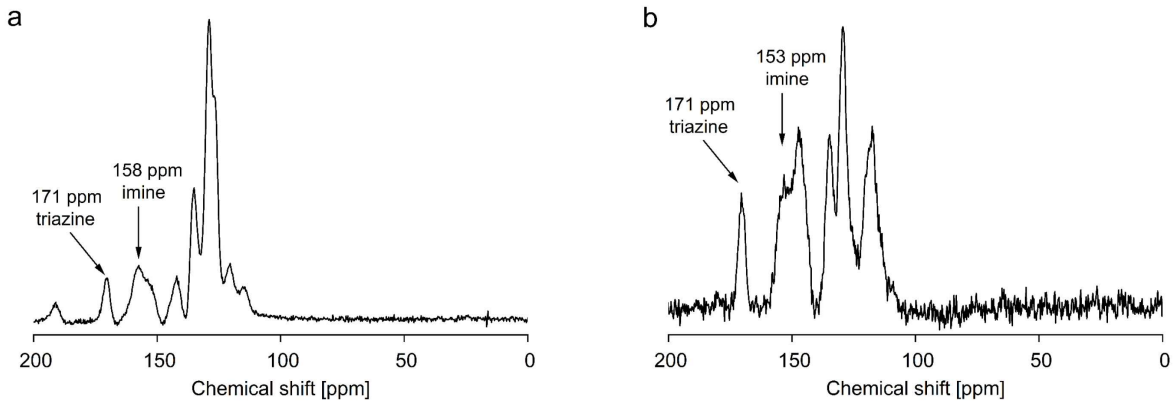

Figure 1. ^{13}C CP MAS NMR spectra of (**a**) HHU-COF-1 and (**b**) HHU-COF-2. Spectra were obtained at 150 MHz, cross-polarization with decoupling spinal and 35 kHz spinning.

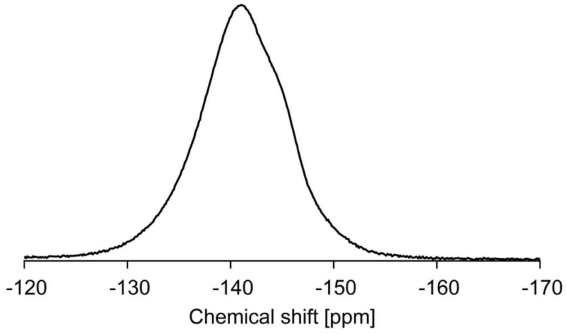

Figure 2. ^{19}F CP MAS NMR spectra of HHU-COF-2.

FT-IR spectra (Figure 3) showed weak bands at 1626 and 1193 cm^{-1} for HHU-COF-1 and at 1624 and 1211 cm^{-1} for HHU-COF-2, which could be assigned to the imine bond [12]. N-H stretching bands from the amino groups in TAPT, which typically appear between 3500 and 3300 cm^{-1}, were no longer visible in the spectra of the two COFs, proving the conversion of the amine groups and, therefore, the consumption of the linker molecule TAPT. The C=O stretching band of BPDCA at 1686 cm^{-1} can still be detected as a small band in the spectrum of HHU-COF-1 (at 1700 cm^{-1}), indicating residual aldehyde, as was already seen in the ^{13}C NMR spectrum (Figure 1a). The absence of the C=O stretching band of OF-BPDCA at 1708 cm^{-1} in the respective COF indicates a complete conversion of the aldehyde groups of the educt in HHU-COF-2.

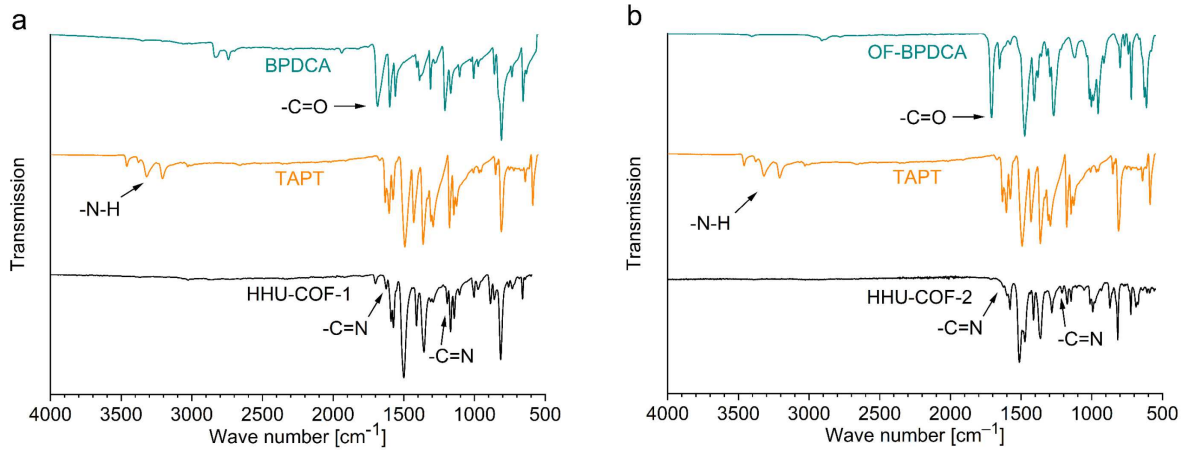

Figure 3. IR-spectra of (**a**) HHU-COF-1 and (**b**) HHU-COF-2 in comparison with the spectra of the educts.

The XPS survey spectra in the range of binding energies from 0 to 1100 eV can be seen in Figure S7. In this overview, C1s peaks and N1s peaks are visible for both COFs, as well as additional peaks in the F1s and F2s region. In the high-resolution C1s XPS spectra of HHU-COF-1 (Figure S8), the peaks at 284.8 and 286.2 eV were assigned to the carbon-

carbon/carbon-hydrogen bonds and the carbon-nitrogen bonds (C=N-C), respectively [39]. Fitting of the N1s region revealed a peak at 398.8 eV corresponding to the imine bond formed by the Schiff base reaction as well as the carbon-nitrogen bonds in the triazine unit [22,40]. For HHU-COF-2, the corresponding peaks in the C1s region (Figure S9) were located at 284.6 and 286.1 eV. The additional peak at 287.8 eV refers to the C-F bonds. The nitrogen-carbon bonds are evident in the N1s region, with a peak at again 398.8 eV [39]. The F1s peak was detected at 687.7 eV (Figure S10), and by integrating the peak area, a fluorine content of 19.5 at%, which corresponds to 27.3 wt% within C, N, and F, was determined for HHU-COF-2 (Table S1), which matches well with the calculation of 27.4 wt% from the ideal formula. Hydrogen cannot be detected by XPS, so the H wt% has to remain unaccounted for. Its missing share increases the wt% of C, N, and F.

The CHN elemental analysis of HHU-COF-1 and HHU-COF-2 in Table 1 was in suitable accordance with the calculated theoretical values for both COFs. In agreement with the XPS data (F wt% = 27.3 wt%), the residual content of 26.78 wt% in the CHN elemental analysis for HHU-COF-2 can be mainly attributed to the fluorine content.

Table 1. Elemental analysis of HHU-COF-1 and HHU-COF-2.

COF	C [wt%]	H [wt%]	N [wt%]
HHU-COF-1 Calculated	81.93	4.42	13.65
HHU-COF-1	81.09	4.27	13.17
HHU-COF-2 Calculated[a]	60.66	1.82	10.11
HHU-COF-2[b]	60.94	1.93	10.35

[a]This leaves calculated 27.41 wt% for fluorine. [b]26.78 wt% difference to 100 wt%.

A uniform distribution of fluorine in HHU-COF-2 was shown with element mapping by SEM-EDX (Figure 4). SEM images exhibited agglomerated spherical particles with an average size between 2 and 5 µm in diameter for both COFs (Figures 4, S11 and S12).

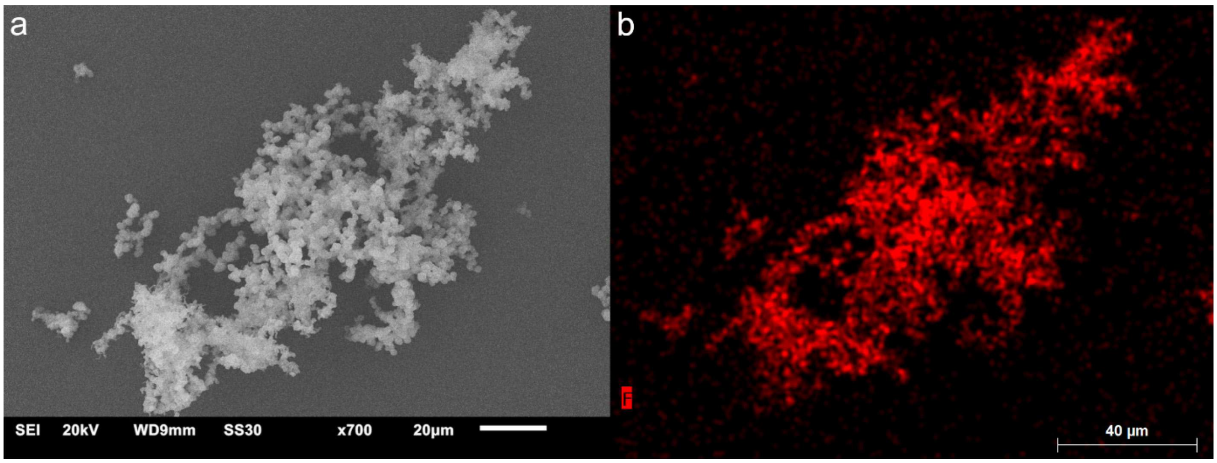

Figure 4. (**a**) SEM image of HHU-COF-2 and (**b**) associated fluorine elemental mapping.

The thermal stabilities of the two COFs were investigated by TGA measurements under a nitrogen atmosphere (Figure 5a). The decomposition of HHU-COF-1 started at 450 °C with a maximum weight loss of about 40% up to 800 °C and ~55% at 1000 °C. For HHU-COF-2, gradual decomposition started at the lower temperature of ~180 °C and rather steadily continued up to 1000 °C, amounting to a weight loss of 70%. In the related TRITER-1 and SCF-FCOF-1, decomposition started at 480 and 430 °C, respectively (Figure S32).

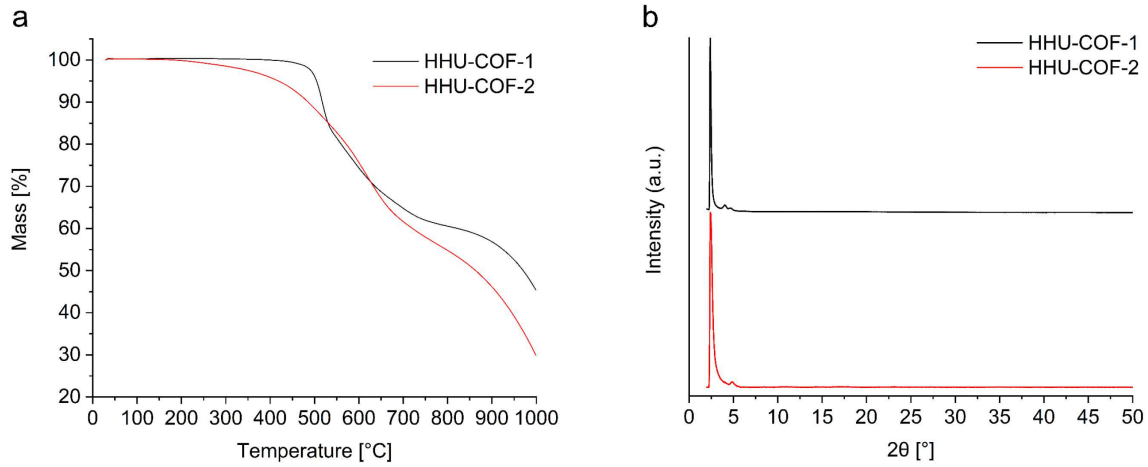

Figure 5. (**a**) TGA curves acquired under nitrogen atmosphere with a heating rate of 5 K/min and (**b**) PXRD pattern of HHU-COF-1 and HHU-COF-2. The first derivative of the TGA curves is given in Figure S15.

PXRD patterns (Figure 5b) confirmed the crystalline nature of the materials. For HHUCOF-1 and HHU-COF-2, an intense diffraction peak was observed at 2.39° 2θ (d = 36.9 Å) and 2.42° 2θ (d = 36.5 Å), respectively, which corresponds to the peak at 2.93° 2θ (d = 30.2 Å) for SCF-FCOF-1 and 3.11° 2θ (d = 28.4 Å) for the (100) plane [15]. Two additional peaks for HHU-COF-1 were found at 4.03° (d = 21.9 Å) and 4.68° 2θ (d = 18.9 Å) for the (110) and (200) planes. HHU-COF-2 exhibited a smaller peak at 4.06° (d = 21.8 Å), barely detectable under the

broadening of the most intense peak, and another peak at 4.85° 2θ (d = 18.2 Å). Compared to the values for SCF-FCOF-1 at 4.98° and 5.85° 2θ for the (110) and (200) planes, respectively [15], the peaks for the HHU-COFs were shifted to lower 2θ values due to the larger linker molecule. If one assumes a honeycomb (hcb) lattice with almost eclipsed stacked layers, the three measured peaks and corresponding (100), (110), and (200) planes can be matched to the edge-edge distance of the hexagonal rings (Scheme 1, Figure S16). Notably, a diffraction peak at about 25°–26° 2θ for the (001) plane from the interlayer π-π stacking is not seen.

N_2-sorption (Figure 6a) showed type IV(a) isotherms for both COFs, which turn into a type II or III isotherm at higher relative pressure. The type IV isotherm with a narrow H1 hysteresis loop reflects the micro-mesoporous nature of the COFs. The type II or III isotherm with an H4 hysteresis reflects the condensation of N_2 in the macroporous interparticle voids from the aggregation of the COF particles [41]. HHU-COF-1 and HHU-COF-2 exhibited high BET surface areas of 2352 m^2/g (p/p_0 = 0.18–0.28) and 1356 m^2/g (p/p_0 = 0.15–0.25), respectively. The total pore volumes (at p/p_0 = 0.97) of HHU-COF-1 and its fluorinated analog were determined as 0.78 and 0.73 cm^3/g, respectively. We note that the trend in surface area was reversed for the TA analogs SCF-HCOF-1 (S_{BET} = 318 m^2/g, no V_{pore} given) and SCF-FCOF-1 (S_{BET} = 1602–2056 m^2/g, 5 h to 3 d synthesis time, V_{pore} = 1.69 cm^3/g) [15]. However, the data for SCF-HCOF-1 cannot be taken as representative since the product was obtained in only 45% yield (96% for SCF-FCOF-1) and was noted to be of poor crystallinity, possibly due to the low activity of the TA under the solvothermal catalyst-free (SCF) synthesis conditions [15]. Under a 12 h reflux synthesis in DMF, the SCF-HCOF-1-identical TRITER-1 (cf. Scheme S1) showed a BET surface area of 716 m^2/g [14]. In this respect, it is remarkable that BPDCA and its octafluoro-congener exhibit no differences in reactivity and yield. Concerning the high porosity of the SCF-FCOF-1 products with the triazine ring node, it is peculiar that the SCF-FCOF-2 analog with the benzene node (cf. Scheme S1) has only a BET surface area of 1245 m^2/g and a pore volume of 0.64 cm^3/g. We also synthesized the SCF-HCOF-1 (TRITER-1) and SCF-FCOF-1 with the smaller linkers TA and TFTA (Scheme S1, Figure S34). The synthesis and analytical results can be found in Section S5, Supplementary Materials. From our synthesis it was possible to obtain BET surface areas for SCF-HCOF-1 of 977 m^2/g (V_{pore} = 0.64 cm^3/g) and for SCF-FCOF-1 of 2276 m^2/g (V_{pore} = 1.46 cm^3/g). Although it was possible to generate SCF-HCOF-1 with a larger surface area, the reversed trend in surface area is still evident for the HHU-COFs with the larger linkers. This was also observed with the larger-scale products (Section S3, Supplementary Materials), where HHU-COF-1 (larger scale) exhibited the larger BET surface area of 2351 m^2/g (V_{pore} = 0.69 cm^3/g) compared to HHU-COF-2 (larger scale)

with 1346 m^2/g (V_{pore} = 0.68 cm^3/g). A similar trend to the HHU-COFs was observed for CTFs, which were ionothermally trimerized from 4,4'-biphenyldicarbonitrile and its octafluoro derivative. The BET surface area of the fluorinated CTF was about 35% lower compared to the non-fluorinated compound [23].

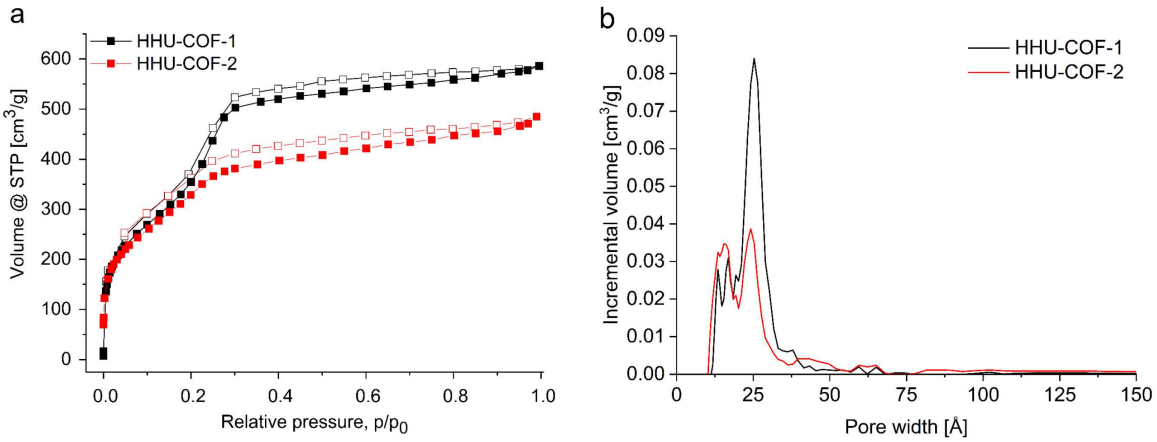

Figure 6. (**a**) Nitrogen sorption isotherms at 77 K and (**b**) pore size distributions of HHU-COF-1 and HHU-COF-2.

Pore size distributions for HHU-COF-1 and HHU-COF-2 were calculated by applying the carbon slit-pore, non-local density functional theory (NLDFT) equilibrium model and revealed maxima at 13, 17, and 25 Å for HHU-COF-1 (Figure 6b). The maxima for HHU-COF-2 were located at 13, 16, and 24 Å. In the region of the larger ~25 Å pores, a lower incremental volume was found for HHU-COF-2, which is consistent with the presence of fluorine atoms. The diameters of the hexagonal rings in the idealized hcb lattice are estimated from Scheme 1 to 37–39 Å by taking into account the aryl ring radii, C-H and C-F bond lengths, and the vdW radii of the surface H and F atoms (1.2 and 1.35 Å, respectively).

In addition, CO_2 and CH_4 sorption studies were performed at a temperature of 273 K (Figure S13). HHU-COF-2 exhibited a higher CO_2 uptake than the non-fluorinated HHU-COF-1, as would be expected for fluorinated materials, which are generally associated with a CO_2-philic character [42]. HHU-COF-1 and HHU-COF-2 showed maximum CO_2 uptakes of 1.08 and 1.74 mmol/g, respectively, which can be considered moderate compared with other imine-COFs (Table S3). The CH_4 adsorption capacities were found to be 0.52 and 0.66 mmol/g for HHU-COF-1 and HHU-COF-2, respectively. The adsorption isotherms at 273 K were further applied to calculate the IAST selectivity for the gas pair CO_2/CH_4. Therefore, the isotherms of HHU-COF-1 were fitted with the Langmuir (LAI) isotherm model and the isotherms of HHU-COF-2 with the Toth model (Table S4). The CO_2/CH_4 selectivity (Figure S14) for a

binary (50:50; *v:v*) mixture of the gases at 1 bar pressure was 2.1 for HHU-COF-1 and 2.6 for HHU-COF-2, respectively.

3.2. Characterization of MMMs

In order to investigate the distribution of the dispersed phase in the Matrimid matrices, cross-section SEM images (Figure 7) were acquired. No major defects that could lead to a reduction in selectivity were observed in any of the MMMs. However, with the increasing filler content of HHU-COF-1, more minor defects became visible. This was especially the case for the 24 wt% MMM, where slight sedimentation was observed as well. For all MMMs with HHU-COF-2 as filler, a uniform distribution of the filler particles and a defect-free appearance could be confirmed. These observations suggest a better dispersion of the fluorinated COF with the Matrimid matrix, which agrees with the gas separation performance.

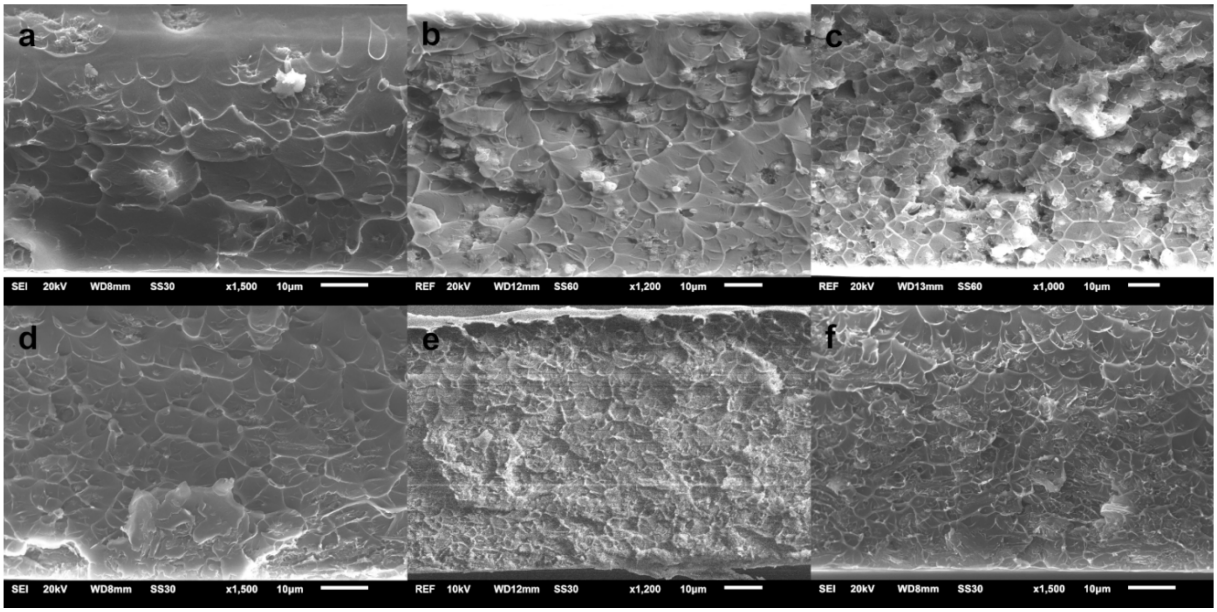

Figure 7. Cross-section SEM images of HHU-COF-1/Matrimid with (**a**) 8 wt%, (**b**) 16 wt%, and (**c**) 24 wt% filler and HHU-COF-2/Matrimid MMMs with (**d**) 8 wt%, (**e**) 16 wt%, and (**f**) 24 wt% filler.

In addition, SEM images were taken of the top surface of the MMMs (Figure S26). As expected, more particles are visible on the surface at higher loadings, so that complete sedimentation of the COF particles can be excluded. The distribution of the filler HHU-COF-2 in the MMMs was investigated by fluorine element mapping using SEM-EDX (Figure S27). Due to the inaccuracy of EDX measurements for elements lighter than fluorine, these results should be considered critically. However, it can be seen that the COF particles are present throughout the whole membrane cross-sections.

The mechanical stability of the MMMs was investigated by determining the tensile strength. The maximum applied force until fracture of the respective MMM is summarized in Table S7. As expected, the pure Matrimid membrane exhibits the highest tensile strength of 91 MPa. For the MMMs with 8 and 16 wt% filler, values between 74 and 79 MPa were obtained. High loading of 24 wt% COF resulted in a reduction in the mechanical stability to below 60 MPa.

3.3. Gas Permeability and Selectivity

The membrane performance of the two systems, HHU-COF-1/Matrimid and HHU-COF-2/Matrimid (Table 2; Figure 8), was investigated with respect to CO_2/CH_4 separation. The pure membranes and the membranes with 8, 16, and 24 wt% filler content were prepared in duplicate. Final permeability P was calculated with the thickness of the membranes given in Table S6. The CO_2 permeability of the 8 and 16 wt% HHU-COF-1/Matrimid MMMs increased to 9.1 Barrer compared to the neat polymer membrane with 6.8 Barrer. This was accompanied by a moderate CO_2/CH_4 selectivity increase from 42 to 46. However, this increase from 6.8 to 9.1 Barrer is not very significant when compared with other porous organic framework MMMs (vide infra). With an increase in the filler content to 24 wt%, the permeability and selectivity decreased again to the approximate value of the neat Matrimid membrane, in line with the sedimentation noted from SEM. The HHU-COF-2-based MMMs showed a continuous enhancement in CO_2 permeability upon increasing the filler content from 8 to 24 wt%. The CO_2/CH_4 selectivity was raised from 42 for neat Matrimid to 51 for the 8 wt% MMM. For the 16 and 24 wt% MMMs, the selectivity was back at the level of the pure polymer. The lower membrane efficiency of the HHU-COF-1-based membranes in comparison to HHU-COF-2 as filler material could be related to the blocking of the pores by (inter)penetrating polymer chains as well as the aggregation of the filler particles. A lower filler content of HHU-COF-1 seems to be recommended to achieve the optimum membrane performance for this system. For HHU-COF-2 as a dispersed phase, the known trade-off relationship between (high/low) permeability and (low/high) selectivity is seen as in the Robeson plots [43,44]. It was possible to consistently increase permeability with increasing filler content, which at the same time led to a decrease in selectivity. Overall, the fluorinated material showed better compatibility with the Matrimid matrix and led to a better separation performance for the gas pair CO_2/CH_4.

Table 2. Gas permeabilities (P) and mixed-gas selectivity factors (α) of the pristine Matrimid membrane and COF/Matrimid MMMs.[1]

Filler material	Filler content [wt%]	P CO_2 [Barrer]	P CH_4 [Barrer]	α CO_2/CH_4
-	0	6.8 ± 0.3	0.16 ± 0.01	42 ± 1
HHU-COF-1	8	9.1 ± 0.2	0.19 ± 0.01	46 ± 2
	16	9.1 ± 1.0	0.20 ± 0.02	46 ± 1
	24	5.8 ± 0.7	0.14 ± 0.02	41 ± 1
HHU-COF-2	8	7.1 ± 0.3	0.14 ± 0.01	51 ± 1
	16	10.2 ± 0.3	0.23 ± 0.02	44 ± 2
	24	13.0 ± 1.0	0.32 ± 0.02	40 ± 1

[1]The errors for the permeability (P) and for the selectivity (α) were taken from the range of two to three measurements and include the upper and lower value.

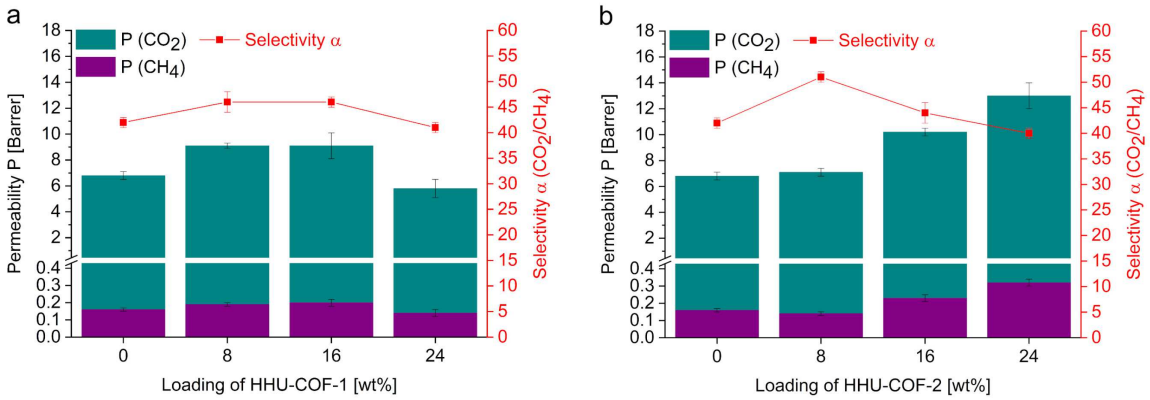

Figure 8. CO_2 and CH_4 permeabilities (P) and CO_2/CH_4 selectivities (α) for (**a**) HHU-COF-1/Matrimid and (**b**) HHU-COF-2/Matrimid MMMs.

For a better understanding and classification of the permeation results, the fractional free volume (FFV) was calculated, and a comparison with permeability models was drawn. For the density (1.20 g/cm^3) [45] and the FFV (0.167) [46] of Matrimid, the values reported in the literature were applied. The FFV of HHU-COF-1 and HHU-COF-2 was obtained by multiplying pore volume and density (from Equation (5)) and was calculated to be 0.558 and 0.560, respectively. The FFV of a MMM is the sum of the FFV of the polymer multiplied by

the volume fraction of the continuous phase ϕ_c and the FFV of the filler material multiplied by the volume fraction of the dispersed phase ϕ_d, as given in Equation (8):

$$FFV = FFV_{polymer} * \phi_c + FFV_{filler} * \phi_d \quad (8)$$

The FFV does not contain the interface (void) volume. The logarithm of the CO_2 and CH_4 permeability versus 1/FFV for 0 to 24 wt% HHU-COF-1 and HHU-COF-2 as dispersed phases in Matrimid MMMs is plotted in Figure 9. Relating the free volume to the CO_2 and CH_4 permeability, HHU-COF-1 shows only a small increase up to a content of 16 wt%. For HHU-COF-1/Matrimid, the permeability of the 24 wt% MMM corresponds to the neat polymer (within experimental error) (Table 2). In turn, the actually available FFV of the 24 wt% MMM would only be that of the neat polymer. Thus, the theoretically calculated free volume from the filler is not available for permeation due to its aggregation and blocking or filling of the filler pores by polymer chains, as becomes clear when the FFV is put in relation to the permeability. For HHU-COF-2, lg*P* increases as 1/FFV decreases (i.e., when the amount of filler is increased) as expected. This is relatively more pronounced at high filler contents since the FFV of the filler material (0.560) is higher than that of the polymer (0.167).

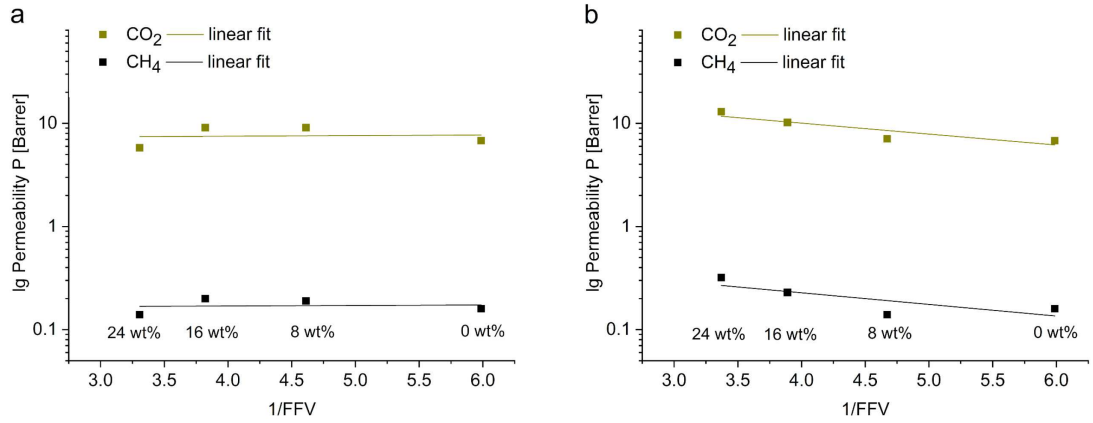

Figure 9. Lg permeability versus 1/FFV for 0 to 24 wt% (**a**) HHU-COF-1 and (**b**) HHU-COF-2 as dispersed phases in Matrimid MMMs.

To better assess the filler volume-dependent CO_2 permeability increase, a comparison with the Maxwell model was carried out [47]. At first, it should be noted that this model describes an ideal particle distribution of the filler in the polymer. It also assumes spherical particles with a volume fraction of the dispersed filler phase ϕ_d up to 0.2. The simplified Maxwell model for the case that the permeability of the dispersed phase, P_d, is much higher than the permeability of the pure continuous (polymer) phase, P_c, is shown in Equation (9), where P_{eff} stands for the permeability of the MMMs:

$$\frac{P_{eff}}{P_c} = \frac{1+2\phi_d}{1-\phi_d} \quad (9)$$

In addition, three further modified models were used, which assume $P_d = 8P_c$, $P_d = 4P_c$, and $P_d = 2P_c$. Models that are applicable to higher ϕ_d [48,49] also show much higher values for P_{eff}/P_c as a function of ϕ_d and are not applicable for a comparison in this case. Figure 10 plots the ratio P_{eff}/P_c of the gas CO_2 versus ϕ_d for the filler materials HHU-COF-1 and HHU-COF-2 in the polymer Matrimid in comparison to the Maxwell model and the modified models. The higher volume fractions of HHU-COF-1 over HHU-COF-2 are due to the lower density of the HHU-COF-1 for equivalent mass percentages. For the HHU-COF-1 MMMs, a low filler efficiency is confirmed with respect to CO_2 permeability. Only the 8 wt% MMM shows an increase in permeability, which agrees with the Maxwell model for $P_d = 8P_c$. The 16 wt% HHU-COF-1 MMM already exceeds the filler volume fraction of 0.2, for which the Maxwell model is applicable. As the filler content of HHU-COF-2 increases, the P_{eff}/P_c ratio increases significantly higher. The 8 wt% MMM agrees with the model prediction for $P_d = 2P_c$ and the 16 wt% MMM with $P_d = 8P_c$. The 24 wt% MMM represents the most efficient membrane in terms of CO_2 permeability. With a P_{eff}/P_c ratio of 1.9, it exceeds the Maxwell model for $P_d = 8P_c$.

A comparison with literature values of Matrimid-based MMMs for CO_2/CH_4 separation shows that the performance of the 8 wt% HHU-COF-1 MMM with a CO_2 permeability of 9.1 Barrer agrees with comparable systems, such as ACOF-1 [31] or CTF-fluorene [50] in Matrimid. The system with 8 wt% of the azine-linked structure ACOF-1 in Matrimid achieved a CO_2 permeability value of 9.6 Barrer, and the corresponding weight percentage of CTF-fluorene in Matrimid increased the CO_2 permeability to 9.2 Barrer. The application of 8 wt% of a biphenyl-based CTF with a larger pore volume resulted in a value of 12.0 Barrer [36]. At this point, it is once again confirmed that increasing the pore size is only beneficial up to a certain level. A comparison with different filler materials in matrices such as 6FDA-DAM [51], Pebax [52], and PIM-1 [32,53] can be found in Table S9. In contrast, the higher filler amounts of HHU-COF-2 showed a much larger increase in CO_2 permeability. Compared to the pure Matrimid membrane, the CO_2 permeability for the 24 wt% MMM was increased by 91% to 13.0 Barrer.

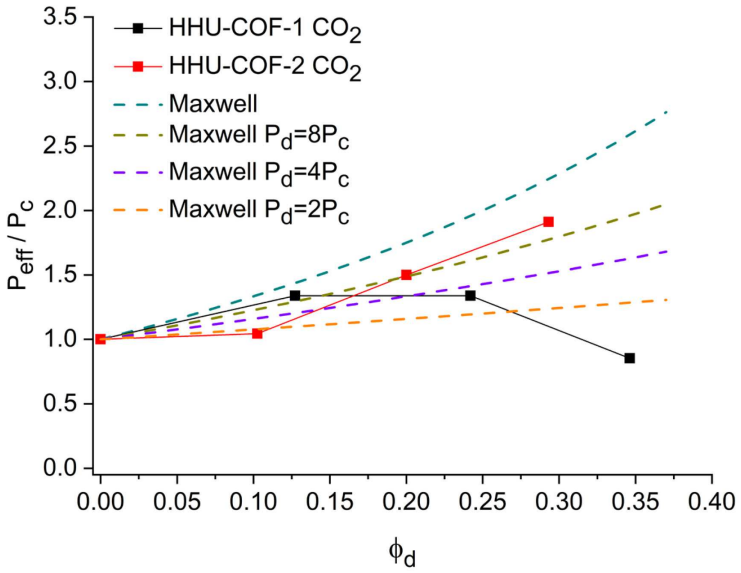

Figure 10. P_{eff}/P_c of the gas CO_2 versus ϕ_d for 0 to 24 wt% HHU-COF-1 and HHU-COF-2 as dispersed phases in Matrimid matrices.

To test the long-term stability of the MMMs, we performed permeability measurements again after one year (Table S8). All 12 MMMs were covered but stored without further protection at an average temperature of 20 °C in ambient air. The 8 and 16 wt% HHU-COF-1/MMMs showed reduced CO_2 permeability with values of 8.6 and 8.0 Barrer, respectively. The 24 wt% MMM proved to be stable in terms of CO_2 permeability, but the CO_2/CH_4 selectivity was reduced to 28, so the MMM can be considered defective. The HHU-COF-2 MMMs not only showed the best results in terms of initial membrane performance but also exhibited consistent CO_2 permeability after one year of storage. CO_2 permeability of 7.1 (8 wt%), 10.5 (16 wt%), and 12.9 Barrer (24 wt%) was measured with CO_2/CH_4 selectivity between 44 and 45 after this one year.

In summary, from the permeability and FFV values, it is evident that the high theoretical filler FFV does not contribute to a significant increase in permeability. Evidently, the pore openings in HHU-COF-1 and HHU-COF-2 are too large (cf. Scheme 1) so that they allow for (inter)penetration of polymer chains that then drastically decrease this fractional free volume contribution from the filler. The higher increase in permeability for HHU-COF-2 over HHU-COF-1 for the 16 and 24 wt% MMMs indicates that HHU-COF-2 with the fluorinated linker has a higher filler contribution. This is explained by a hindrance of the (inter)penetration of the non-fluorinated polymer chains into the fluorous HHU-COF-2 inner pores, akin to fluorous chemistry with the lower affinity or even separation of perfluorinated compounds from non-fluorinated phases.

4. Conclusions

Two imine-linked COFs were synthesized via a Schiff base reaction applying 1,3,5-tris-(4-aminophenyl)triazine as an amine compound. 4,4'-biphenyldicarboxaldehyde and the corresponding octafluoro derivative were chosen as linkers to form HHU-COF-1 and HHU-COF-2. The successful formation of the materials was confirmed by ^{13}C and ^{19}F CP MAS NMR, IR, XPS, and elemental analysis. Both materials are crystalline, and the synthesis with the biphenyl-based linkers led to high BET surface areas of 2352 m^2/g for HHU-COF-1 and 1356 m^2/g for HHU-COF-2. Moreover, both syntheses were successfully carried out on a larger scale in order to apply the products as filler materials in Matrimid-based MMMs for CO_2/CH_4 separation, where the fluorinated COF led to the better membrane performance with a CO_2 permeability increase from 6.8 to 13.0 Barrer for the 24 wt% MMM.

Supplementary Materials: The following supporting information can be downloaded at: https://www.mdpi.com/article/10.3390/ma15082807/s1, Scheme S1. Schematic formation of TRITER-1 (=SCF-HCOF-1) and SCF-FCOF-1 from TAPT and TA or TFTA, respectively. (TAPB = 1,3,5-tris(4-aminophenyl) benzene, TAPT = 2,4,6-tris(4-aminophenyl)-1,3,5-triazine, TA = terephthalaldehyde, TFTA = 2,3,5,6-tetrafluoroterephthaldehyde). The edge-edge distance was taken from the literature of SCF-FCOF-1 and -2; Figure S1. ^{19}F NMR spectrum of perfluorinated nitrile 1; Figure S2. ^{1}H NMR spectrum of perfluorinated aldehyde 2; Figure S3. ^{19}F NMR spectrum of perfluorinated aldehyde 2; Figure S4. $^{13}C\{^{1}H\}$ NMR spectrum of perfluorinated aldehyde 2; Figure S5. EI-MS (at 80 °C) spectrum of perfluorinated aldehyde 2; Figure S6. AT-IR spectrum of perfluorinated aldehyde 2; Figure S7. XPS survey spectra of HHU-COF-1 and HHU-COF-2; Figure S8. High-resolution XPS spectra of the C1s region and N1s region of HHU-COF-1; Figure S9. High-resolution XPS spectra of the C1s region and N1s region of HHU-COF-2; Figure S10. High-resolution XPS spectra of the F1s region of HHU-COF-2; Figure S11. SEM images of HHU-COF-1; Figure S12. SEM image of HHU-COF-2; Figure S13. CO_2 and CH_4 sorption isotherms at 273 K of HHU-COF-1 and HHU-COF-2, respectively; Figure S14. IAST selectivities of HHU-COF-1 and HHU-COF-2 for a binary (50:50; v:v) mixture of the gases CO_2/CH_4 at 273 K; Figure S15. First derivative of TGA curves of HHU-COF-1 and HHU-COF-2. Measurement under nitrogen atmosphere with a heating rate of 5 K/min; Figure S16. Correlation of the 2theta (2θ) values from the powder X-ray diffractograms in Figure 5 in the main text with the reflection planes and the d spacing according to the Bragg equation $n \lambda = 2d \sin \theta$ or $d = n \lambda /(2 \sin\theta)$ with $\lambda = 1.5406$ Å and $n = 1$. Note that the edge-edge distances a and the triazine-centroid triazine-centroid (tz-tz) distances along the edge derived therefrom as (a/2)/cos30° were determined from the most

intense and, thus, most accurately measurable (100) reflexes in the powder-X-ray diffractograms of HHU-COF-1 and -2; Figure S17. Images of HHU-COF-1 and HHU-COF-2; Figure S18. IR spectra of HHU-COF-1 (larger scale) and HHU-COF-2 (larger scale); Figure S19. Nitrogen sorption isotherm and pore size distribution calculated with slit pore, NLDFT equilibrium model of HHU-COF-1 (larger scale); Figure S20. Nitrogen sorption isotherm and pore size distribution calculated with slit pore, NLDFT equilibrium model of HHU-COF-2 (larger scale); Figure S21. TGA curves of HHU-COF-1 (larger scale) and HHU-COF-2 (larger scale). Acquired under nitrogen atmosphere with a heating rate of 5 K/min; Figure S22. PXRD pattern of HHU-COF-1 (larger scale) and HHU-COF-2 (larger scale); Figure S23. Schematic preparation of the pure Matrimid membrane and MMMs, using the 16 wt% HHU-COF-2 MMM as an example; Figure S24. Preparation of membranes by solution casting: casting the solution, drying, cutting with a scalpel, and removing the membrane; Figure S25. Setup for CO_2/CH_4 mixed-gas separation measurements; Figure S26. Top-surface SEM images of HHU-COF-1/Matrimid with 8, 16, and 24 wt% filler and HHU-COF-2/Matrimid MMMs with 8, 16, and 24 wt% filler; Figure S27. SEM images of HHU-COF-2/Matrimid MMMs with 8, 16, and 24 wt% filler and associated fluorine elemental mapping; Figure S28. IR spectra of TRITER-1 and SCF-FCOF-1; Figure S29. SEM image of SCF-FCOF-1 and associated fluorine elemental mapping; Figure S30. Nitrogen sorption isotherm and pore size distribution calculated with slit pore, NLDFT equilibrium model of TRITER-1; Figure S31. Nitrogen sorption isotherm and pore size distribution calculated with slit pore, NLDFT equilibrium model of SCF-FCOF-1; Figure S32. TGA curves of TRITER-1 and SCF-FCOF-1. Acquired under nitrogen atmosphere with a heating rate of 5 K/min; Figure S33. PXRD pattern of TRITER-1 and SCF-FCOF-1; Figure S34. Images of TRITER-1 and SCF-FCOF-1; Table S1. at% and wt% of the elements in HHU-COF-1 and HHU-COF-2 obtained from XPS survey spectra; Table S2. EDX analysis of HHU-COF-2; Table S3. Comparison of CO_2 uptake and BET surface area of imine-linked/azine COFs; Table S4. Parameters for LAI and Toth fitting; Table S5. Elemental analysis of HHU-COF-1 (larger scale) and HHU-COF-2 (larger scale); Table S6. Average thickness of MMMs; Table S7. Tensile strength of pure Matrimid and MMMs. Table S8. Gas permeabilities (P) and mixed-gas selectivity factors (α) for COF/Matrimid MMMs when stored for one year under ambient conditions; Table S9. Comparison of CO_2 permeability and CO_2/CH_4 selectivity for COFs/CTFs as porous filler materials in different polymer MMMs; Table S10. Elemental analysis of TRITER-1 and SCF-FCOF-1; Table S11. EDX analysis of SCF-FCOF-1. References [54–59] cited in Supplementary Materials.

Author Contributions: Conceptualization, S.B., B.M.S. and C.J.; methodology, S.B., M.H. and T.K.; validation, S.B. and M.H.; formal analysis, S.B. and N.d.S.A.; investigation, S.B., M.H., T.K., N.d.S.A., Y.S., A.S. and T.H.Y.B.; resources, C.J.; data curation, S.B. and M.H.; writing—original draft preparation, S.B.; writing—review and editing, S.B. and C.J.; visualization, S.B. and M.H. supervision, C.J.; project administration, C.J.; funding acquisition, C.J. All authors have read and agreed to the published version of the manuscript.

Funding: C.J. is indebted to the DFG for funding within the priority program SPP 1928 "COORNET" (grant Ja466–43/1).

Institutional review board statement: Not applicable.

Informed consent statement: Not applicable.

Data availability statement: The data presented in this study are available on request from the corresponding author.

Acknowledgments: We thank Dennis Woschko for TGA measurements and Anja Göbel (Institut für Pharmazeutische Technologie und Biopharmazie) for her assistance in measuring mechanical stability.

Conflicts of interest: The authors declare no conflict of interest.

References

1. Côté, A.P.; Benin, A.I.; Ockwig, N.W.; O'Keeffe, M.; Matzger, A.J.; Yaghi, O.M. Porous, Crystalline, Covalent Organic Frameworks. *Science* **2005**, *310*, 1166–1170.

2. Chen, X.; Geng, K.; Liu, R.; Tan, K.T.; Gong, Y.; Li, Z.; Tao, S.; Jiang, Q.; Jiang, D. Covalent Organic Frameworks: Chemical Approaches to Designer Structures and Built-In Functions. *Angew. Chem. Int. Ed.* **2020**, *59*, 5050–5091.

3. Furukawa, H.; Yaghi, O.M. Storage of Hydrogen, Methane, and Carbon Dioxide in Highly Porous Covalent Organic Frameworks for Clean Energy Applications. *J. Am. Chem. Soc.* **2009**, *131*, 8875–8883.

4. Guan, X.; Li, H.; Ma, Y.; Xue, M.; Fang, Q.; Yan, Y.; Valtchev, V.; Qiu, S. Chemically stable polyarylether-based covalent organic frameworks. *Nat. Chem.* **2019**, *11*, 587–594.

5. Morris, R.E.;Wheatley, P.S. Gas Storage in Nanoporous Materials. *Angew. Chem. Int. Ed.* **2008**, *47*, 4966–4981.

6. Wang, Z.; Zhang, S.; Chen, Y.; Zhang, Z.; Ma, S. Covalent organic frameworks for separation applications. *Chem. Soc. Rev.* **2020**, *49*, 708–735.

7. Rogge, S.M.J.; Bavykina, A.; Hajek, J.; Garcia, H.; Olivos-Suarez, A.I.; Sepúlveda-Escribano, A.; Vimont, A.; Clet, G.; Bazin, P.; Kapteijn, F.; et al. Metal–organic and covalent organic frameworks as single-site catalysts. *Chem. Soc. Rev.* **2017**, *46*, 3134–3184.

8. Liu, X.; Huang, D.; Lai, C.; Zeng, G.; Qin, L.; Wang, H.; Yi, H.; Li, B.; Liu, S.; Zhang, M.; et al. Recent advances in covalent organic frameworks (COFs) as a smart sensing material. *Chem. Soc. Rev.* **2019**, *48*, 5266–5302.

9. Hu, Y.; Dunlap, N.; Wan, S.; Lu, S.; Huang, S.; Sellinger, I.; Ortiz, M.; Jin, Y.; Lee, S.-H.; Zhang, W. Crystalline Lithium Imidazolate Covalent Organic Frameworks with High Li-Ion Conductivity. *J. Am. Chem. Soc.* **2019**, *141*, 7518–7525.

10. Keller, N.; Bein, T. Optoelectronic processes in covalent organic frameworks. *Chem. Soc. Rev.* **2021**, *50*, 1813–1845.

11. Segura, J.L.; Mancheño, M.J.; Zamora, F. Covalent organic frameworks based on Schiff-base chemistry: Synthesis, properties and potential applications. *Chem. Soc. Rev.* **2016**, *45*, 5635–5671.

12. Uribe-Romo, F.J.; Hunt, J.R.; Furukawa, H.; Klöck, C.; O'Keeffe, M.; Yaghi, O.M. A Crystalline Imine-Linked 3-D Porous Covalent Organic Framework. *J. Am. Chem. Soc.* **2009**, *131*, 4570–4571.

13. Ding, S.-Y.; Gao, J.; Wang, Q.; Zhang, Y.; Song, W.-G.; Su, C.-Y.; Wang, W. Construction of Covalent Organic Framework for Catalysis: Pd/COF-LZU1 in Suzuki–Miyaura Coupling Reaction. *J. Am. Chem. Soc.* **2011**, *133*, 19816–19822.

14. Gomes, R.; Bhanja, P.; Bhaumik, A. A triazine-based covalent organic polymer for efficient CO_2 adsorption. *Chem. Commun.* **2015**, *51*, 10050–10053.

15. Liao, Q.; Ke, C.; Huang, X.; Zhang, G.; Zhang, Q.; Zhang, Z.; Zhang, Y.; Liu, Y.; Ning, F.; Xi, K. Catalyst-free and efficient fabrication of highly crystalline fluorinated covalent organic frameworks for selective guest adsorption. *J. Mater. Chem. A* **2019**, *7*, 18959–18970.

16. Wessely, I.D.; Schade, A.M.; Dey, S.; Bhunia, A.; Nuhnen, A.; Janiak, C.; Bräse, S. Covalent Triazine Frameworks Based on the First Pseudo-Octahedral Hexanitrile

Monomer via Nitrile Trimerization: Synthesis, Porosity, and CO_2 Gas Sorption Properties. *Materials* **2021**, *14*, 3214.

17. Wang, G.; Leus, K.; Zhao, S.; Van Der Voort, P. Newly Designed Covalent Triazine Framework Based on Novel N-Heteroaromatic Building Blocks for Efficient CO_2 and H_2 Capture and Storage. *ACS Appl. Mater. Interfaces* **2018**, *10*, 1244–1249.

18. Bhunia, A.; Boldog, I.; Möller, A.; Janiak, C. Highly stable nanoporous covalent triazine-based frameworks with an adamantane core for carbon dioxide sorption and separation. *J. Mater. Chem. A* **2013**, *1*, 14990–14999.

19. Wang, H.; Jiang, D.; Huang, D.; Zeng, G.; Xu, P.; Lai, C.; Chen, M.; Cheng, M.; Zhang, C.; Wang, Z. Covalent triazine frameworks for carbon dioxide capture. *J. Mater. Chem. A* **2019**, *7*, 22848–22870.

20. Bhatt, P.M.; Belmabkhout, Y.; Cadiau, A.; Adil, K.; Shekhah, O.; Shkurenko, A.; Barbour, L.J.; Eddaoudi, M. A Fine-Tuned Fluorinated MOF Addresses the Needs for Trace CO_2 Removal and Air Capture Using Physisorption. *J. Am. Chem. Soc.* **2016**, *138*, 9301–9307.

21. Zhang, D.-S.; Chang, Z.; Li, Y.-F.; Jiang, Z.-Y.; Xuan, Z.-H.; Zhang, Y.-H.; Li, J.-R.; Chen, Q.; Hu, T.-L.; Bu, X.-H. Fluorous Metal-Organic Frameworks with Enhanced Stability and High H_2/CO_2 Storage Capacities. *Sci. Rep.* **2013**, *3*, 3312.

22. Zhao, Y.F.; Yao, K.X.; Teng, B.Y.; Zhang, T.; Han, Y. A perfluorinated covalent triazine-based framework for highly selective and water–tolerant CO_2 capture. *Energy Environ. Sci.* **2013**, *6*, 3684–3692.

23. Wang, G.; Leus, K.; Jena, H.S.; Krishnaraj, C.; Zhao, S.; Depauw, H.; Tahir, N.; Liu, Y.-Y.; Van Der Voort, P. A fluorine-containing hydrophobic covalent triazine framework with excellent selective CO_2 capture performance. *J. Mater. Chem. A* **2018**, *6*, 6370–6375.

24. Dey, S.; Bhunia, A.; Breitzke, H.; Groszewicz, P.B.; Buntkowsky, G.; Janiak, C. Two linkers are better than one: Enhancing CO_2 capture and separation with porous covalent triazine-based frameworks from mixed nitrile linkers. *J. Mater. Chem. A* **2017**, *5*, 3609–3620.

25. Dechnik, J.; Gascon, J.; Doonan, C.J.; Janiak, C.; Sumby, C.J. Mixed-Matrix Membranes. *Angew. Chem. Int. Ed.* **2017**, *56*, 9292–9310.

26. Dechnik, J.; Sumby, C.J.; Janiak, C. Enhancing Mixed-Matrix Membrane Performance with Metal-Organic Framework Additives. *Cryst. Growth Des.* **2017**, *17*, 4467–4488.

27. Vinoba, M.; Bhagiyalakshmi, M.; Alqaheem, Y.; Alomair, A.A.; Pérez, A.; Rana, M.S. Recent progress of fillers in mixed matrix membranes for CO_2 separation: A review. *Sep. Purif. Technol.* **2017**, *188*, 431–450.

28. Li, J.; Zhou, X.; Wang, J.; Li, X. Two-Dimensional Covalent Organic Frameworks (COFs) for Membrane Separation: A Mini Review. *Ind. Eng. Chem. Res.* **2019**, *58*, 15394–15406.

29. Cheng, Y.; Wang, Z.; Zhao, D. Mixed Matrix Membranes for Natural Gas Upgrading: Current Status and Opportunities. *Ind. Eng. Chem. Res.* **2018**, *57*, 4139–4169.

30. Dey, S.; Bügel, S.; Sorribas, S.; Nuhnen, A.; Bhunia, A.; Coronas, J.; Janiak, C. Synthesis and Characterization of Covalent Triazine Framework CTF-1@Polysulfone Mixed Matrix Membranes and Their Gas Separation Studies. *Front. Chem.* **2019**, *7*, 693.

31. Shan, M.; Seoane, B.; Rozhko, E.; Dikhtiarenko, A.; Clet, G.; Kapteijn, F.; Gascon, J. Azine-Linked Covalent Organic Framework (COF)-Based Mixed-Matrix Membranes for CO_2/CH_4 Separation. *Chem. Eur. J.* **2016**, *22*, 14467–14470.

32. Jiang, H.; Zhang, J.; Huang, T.; Xue, J.; Ren, Y.; Guo, Z.; Wang, H.; Yang, L.; Yin, Y.; Jiang, Z.; et al. Mixed-Matrix Membranes with Covalent Triazine Framework Fillers in Polymers of Intrinsic Microporosity for CO_2 Separations. *Ind. Eng. Chem. Res.* **2019**, *59*, 5296–5306.

33. Kunde, T.; Pausch, T.; Reiss, G.J.; Schmidt, B.M. Highly Fluorinated Trianglimine Macrocycles: A Supramolecular Organic Framework. *Synlett* **2022**, *33*, 161–165.

34. Li, Z.; Feng, X.; Zou, Y.; Zhang, Y.; Xia, H.; Liu, X.; Mu, Y. A 2D azine-linked covalent organic framework for gas storage applications. *Chem. Commun.* **2014**, *50*, 13825–13828.

35. Loloei, M.; Moghadassi, A.; Omidkhah, M.; Amooghin, A.E. Improved CO_2 separation performance of Matrimid®5218 membrane by addition of low molecular weight polyethylene glycol. *Greenh. Gas. Sci. Technol.* **2015**, *5*, 530–544.

36. Bügel, S.; Hoang, Q.-D.; Spieß, A.; Sun, Y.; Xing, S.; Janiak, C. Biphenyl-Based Covalent Triazine Framework/Matrimid® Mixed-Matrix Membranes for CO_2/CH_4 Separation. *Membranes* **2021**, *11*, 795.

37. Jaeger, C.; Hemmann, F. EASY: A simple tool for simultaneously removing background, deadtime and acoustic ringing in quantitative NMR spectroscopy—Part I: Basic principle and applications. *Solid State Nucl. Magn. Reson.* **2014**, *57–58*, 22–28.

38. Mullangi, D.; Shalini, S.; Nandi, S.; Choksi, B.; Vaidhyanathan, R. Super-hydrophobic covalent organic frameworks for chemical resistant coatings and hydrophobic paper and textile composites. *J. Mater. Chem. A* **2017**, *5*, 8376–8384.

39. Chen, T.; Li, W.-Q.; Hu, W.-B.; Hu, W.-J.; Liu, Y.A.; Yang, H.; Wen, K. Direct synthesis of covalent triazine-based frameworks (CTFs) through aromatic nucleophilic substitution reactions. *RSC Adv.* **2019**, *9*, 18008–18012.

40. Hu, Y.; Goodeal, N.; Chen, Y.; Ganose, A.M.; Palgrave, R.G.; Bronstein, H.; Blunt, M.O. Probing the chemical structure of monolayer covalent-organic frameworks grown via Schiff-base condensation reactions. *Chem. Commun.* **2016**, *52*, 9941–9944.

41. Thommes, M.; Kaneko, K.; Neimark, A.V.; Olivier, J.P.; Rodriguez-Reinoso, F.; Rouquerol, J.; Sing, K.S.W. Physisorption of gases, with special reference to the evaluation of surface area and pore size distribution (IUPAC Technical Report). *Pure Appl. Chem.* **2015**, *87*, 1051–1069.

42. Chen, H.; Yang, Z.; Do-Thanh, C.-L.; Dai, S. What Fluorine Can Do in CO_2 Chemistry: Applications from Homogeneous to Heterogeneous Systems. *ChemSusChem* **2020**, *13*, 6182–6200.

43. Robeson, L.M. Correlation of separation factor versus permeability for polymeric membranes. *J. Membr. Sci.* **1991**, *62*, 165–185.

44. Robeson, L.M. The upper bound revisited. *J. Membr. Sci.* **2008**, *320*, 390–400.

45. Huang, Y.; Wang, X.; Paul, D.R. Physical aging of thin glassy polymer films: Free volume interpretation. *J. Membr. Sci.* **2006**, *277*, 219–229.

46. Kanehashi, S.; Chen, G.Q.; Scholes, C.A.; Ozcelik, B.; Hua, C.; Ciddor, L.; Southon, P.D.; D'Alessandro, D.M.; Kentish, S.E. Enhancing gas permeability in mixed matrix membranes through tuning the nanoparticle properties. *J. Membr. Sci.* **2015**, *482*, 49–55.

47. Bouma, R.H.B.; Checchetti, A.; Chidichimo, G.; Drioli, E. Permeation through a heterogeneous membrane: The effect of the dispersed phase. *J. Membr. Sci.* **1997**, *128*, 141–149.

48. Bruggeman, D.A.G. Berechnung verschiedener physikalischer Konstanten von heterogenen Substanzen. I. Dielektrizitätskonstanten und Leitfähigkeiten der Mischkörper aus isotropen Substanzen. *Ann. Phys.* **1935**, *416*, 636–664.

49. Hashin, Z.; Shtrikman, S.A. Variational Approach to the Theory of the Effective Magnetic Permeability of Multiphase Materials. *J. Appl. Phys.* **1962**, *33*, 3125–3131.

50. Bügel, S.; Spieß, A.; Janiak, C. Covalent triazine framework CTF-fluorene as porous filler material in mixed matrix membranes for CO_2/CH_4 separation. *Micropor. Mesopor. Mater.* **2021**, *316*, 110941.

51. Cheng, Y.; Zhai, L.; Ying, Y.; Wang, Y.; Liu, G.; Dong, J.; Ng, D.Z.L.; Khan, S.A.; Zhao, D. Highly efficient CO_2 capture by mixed matrix membranes containing three-dimensional covalent organic framework fillers. *J. Mater. Chem. A* **2019**, *7*, 4549–4560.

52. Thankamony, R.L.; Li, X.; Das, S.K.; Ostwal, M.M.; Lai, Z. Porous covalent triazine piperazine polymer (CTPP)/PEBAX mixed matrix membranes for CO_2/N_2 and CO_2/CH_4 separations. *J. Membr. Sci.* **2019**, *591*, 117348.

53. Wu, X.; Tian, Z.; Wang, S.; Peng, D.; Yang, L.; Wu, Y.; Xin, Q.; Wu, H.; Jiang, Z. Mixed matrix membranes comprising polymers of intrinsic microporosity and covalent organic framework for gas separation. *J. Membr. Sci.* **2017**, *528*, 273–283.

54. Chen, T.-H.; Popov, I.; Zenasni, O.; Daugulis, O.; Miljanić, O.Š. Superhydrophobic perfluorinated metal–organic frameworks. *Chem. Commun.* **2013**, *49*, 6846–6848.

55. de la Peña Ruigómez, A.; Rodríguez-San-Miguel, D.; Stylianou, K.C.; Cavallini, M.; Gentili, D.; Liscio, F.; Milita, S.; Roscioni, O.M.; Ruiz-González, M.L.; Carbonell, C.; et al. Direct On-Surface Patterning of a Crystalline Laminar Covalent Organic Framework Synthesized at Room Temperature. *Chem. Eur. J.* **2015**, *21*, 10666–10670.

56. Huang, N.; Chen, X.; Krishna, R.; Jiang, D. Two-Dimensional Covalent Organic Frameworks for Carbon Dioxide Capture through Channel-Wall Functionalization. *Angew. Chem. Int. Ed.* **2015**, *54*, 2986–2990.

57. Kandambeth, S.; Shinde, D.B.; Panda, M.K.; Lukose, B.; Heine, T.; Banerjee, R. Enhancement of Chemical Stability and Crystallinity in Porphyrin-Containing Covalent Organic Frameworks by Intramolecular Hydrogen Bonds. *Angew. Chem. Int. Ed.* **2013**, *52*, 13052–13056.

58. Kaleeswaran, D.; Vishnoi, P.; Murugavel, R. [3+3] Imine and β-ketoenamine tethered fluorescent covalent-organic frameworks for CO_2 uptake and nitroaromatic sensing. *J. Mater. Chem. C* **2015**, *3*, 7159–7171.

59. Kandambeth, S.; Mallick, A.; Lukose, B.; Mane, M.V.; Heine, T.; Banerjee, R. Construction of Crystalline 2D Covalent Organic Frameworks with Remarkable Chemical (Acid/Base) Stability via a Combined Reversible and Irreversible Route. *J. Am. Chem. Soc.* **2012**, *134*, 19524–19527.

Supplementary Materials

Synthesis and characterization of a crystalline imine-based covalent organic framework with triazine node and biphenyl linker and its fluorinated derivate for CO_2/CH_4 separation

Stefanie Bügel[1], Malte Hähnel[1], Tom Kunde[2], Nader de Sousa Amadeu[3], Yangyang Sun[1], Alex Spieß[1], Thi Hai Yen Beglau[1], Bernd M. Schmidt[2,*] and Christoph Janiak[1,*]

[1]Institut für Anorganische Chemie und Strukturchemie, Heinrich-Heine-Universität Düsseldorf, 40204 Düsseldorf, Germany; stefanie.buegel@hhu.de (S.B.); mahae107@hhu.de (M.H.); yasun100@hhu.de (Y.S.); alex.spiess@hhu.de (A.S.); beglau@hhu.de (T.H.Y.B.)

[2]Institut für Organische Chemie und Makromolekulare Chemie, Heinrich-Heine-Universität Düsseldorf, 40204 Düsseldorf, Germany; kunde@hhu.de

[3]Bundesanstalt für Materialforschung und -Prüfung, Fachbereich 6.3 (Strukturanalytik), 12489 Berlin, Germany; nader.amadeu@bam.de

* Correspondence: bernd.schmidt@hhu.de (B.M.S.); janiak@hhu.de (C.J.)

Table of Contents

1. Synthetic procedure for 2,2',3,3',5,5',6,6'-octafluoro-4,4'-biphenyldicarboxaldehyde

1.1. Synthesis of 1,1'-(dicyano)-2,2',3,3',5,5',6,6'-octafluoro-4,4'-biphenyl (1)

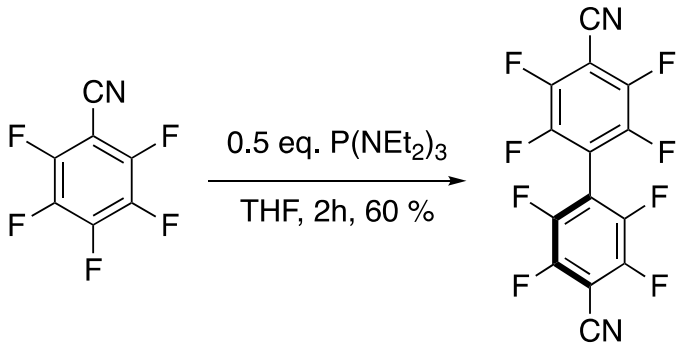

Pentafluorobenzonitrile (8.10 mL, 12.30 g, 64 mmol) was dissolved in 200 mL of dry THF and Tris(diethylamino)phosphine (8.16 g, 0.52 eq.) were added dropwise under nitrogen and stirring. The mixture was allowed to stir for 2 hours at room temperature. After the TLC indicated the complete consumption of the starting material, the reaction was quenched *via* the addition of 40 mL 2N hydrochloric acid. The mixture was extracted with diethyl ether (3 x 50 mL) and was dried over anhydrous magnesium sulphate. After evaporation of the solvent the oily residue was left to crystallize to yield faint yellow crystalline blocks. yield: 6.68 g; 19 mmol; 60%

The analytical data was in accordance with the literature [1].

^{19}F NMR(282 MHz, $CDCl_3$): δ -129.65 (d, Ar-$\mathbf{F_A}$), -133.47 (d, Ar-$\mathbf{F_B}$)

1.2. Synthesis of 2,2',3,3',5,5',6,6'-octafluoro-4,4'-biphenyldicarboxaldehyde (2)

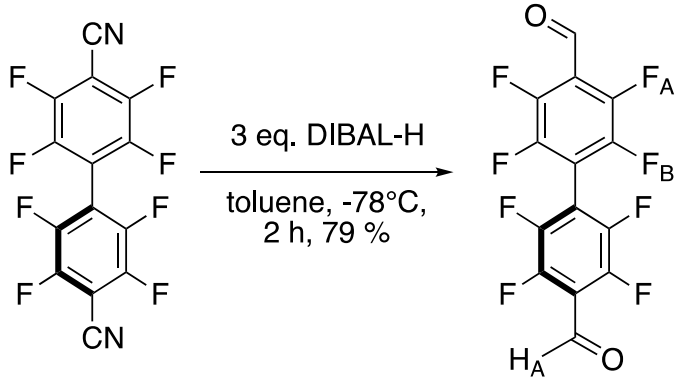

1,1'-(Dicyano)-2,2',3,3',5,5',6,6'-octafluoro-4,4'-biphenyl (2.00 g, 5.74 mmol) was dissolved in toluene (50 mL) and the resulting solution was thoroughly degassed *via* purging with argon for 15 minutes. A solution of diisobutylaluminium hydride (DIBAL-H) in toluene (1.5 M, 11.5 mL, 17.22 mmol) was added dropwise over a period of 30 minutes at -78 °C. After

complete addition, the resulting mixture was stirred for additional 2 hours. The reaction was quenched by addition of 10 mL of ethyl acetate and 30 mL of 2N hydrochloric acid. The organic phase was separated and the aqueous phase was extracted with dichloromethane (2 x 100 mL). The combined organic phases were dried over magnesium sulphate and the solvent was evaporated under reduced pressure to yield **2** as a colorless powder. yield: 1.6 g; 4.51 mmol; 79%

^{1}H NMR(300 MHz, $CDCl_3$): δ 10.39 (s, -C**H$_A$**O); **^{19}F NMR**(282 MHz, $CDCl_3$): δ -136.15 (m, Ar-**F$_A$**), -143.70 (m, Ar-**F$_B$**); **^{13}C{1H} NMR** (75 MHz, $CDCl_3$) δ 181.90 (s, Ar-**C**H$_A$O), 147.24 (d, J = 210.5 Hz, **C$_{Ar}$**-F$_A$), 143.76 (d, J = 207.0 Hz, **C$_{Ar}$**-F$_B$), 117.05 (t, J = 9.8 Hz, **C$_{Ar}$**-CH$_A$O), 111.89 (m, **C$_4$**/**C$_{4'}$**); **FT-IR (ATR):** $\tilde{\nu}$(cm^{-1}) = 2910.6 (w), 2358.9 (w), 2339.7 (w), 1712.8 (s), 1651.1 (m), 1575.8 (w), 1473.6 (s), 1408.0 (m), 1381.0 (m), 1357.9 (w), 1317.4 (w), 1298.1 (m), 1276.9 (s), 1114.9 (w), 1018.4 (s), 1003.0 (s), 989.5 (s), 956.7 (s), 914.3 (m), 800.5 (m), 721.4 (s); **EI-MS (80 °C):** calc. for $[C_{14}H_2F_8O_2–H]^+$ = 352.9843 m/z; found: 353.0 m/z (100%, $[M-H]^+$), 324.9 (27%, $[M-CHO]^+$), 297.0 m/z (26%, $[M-2(CHO)+H]^+$), 278.0 m/z (48%, $[M(297\ m/z)-F]^+$); **M$_p$:** 144.8-145.1 °C.

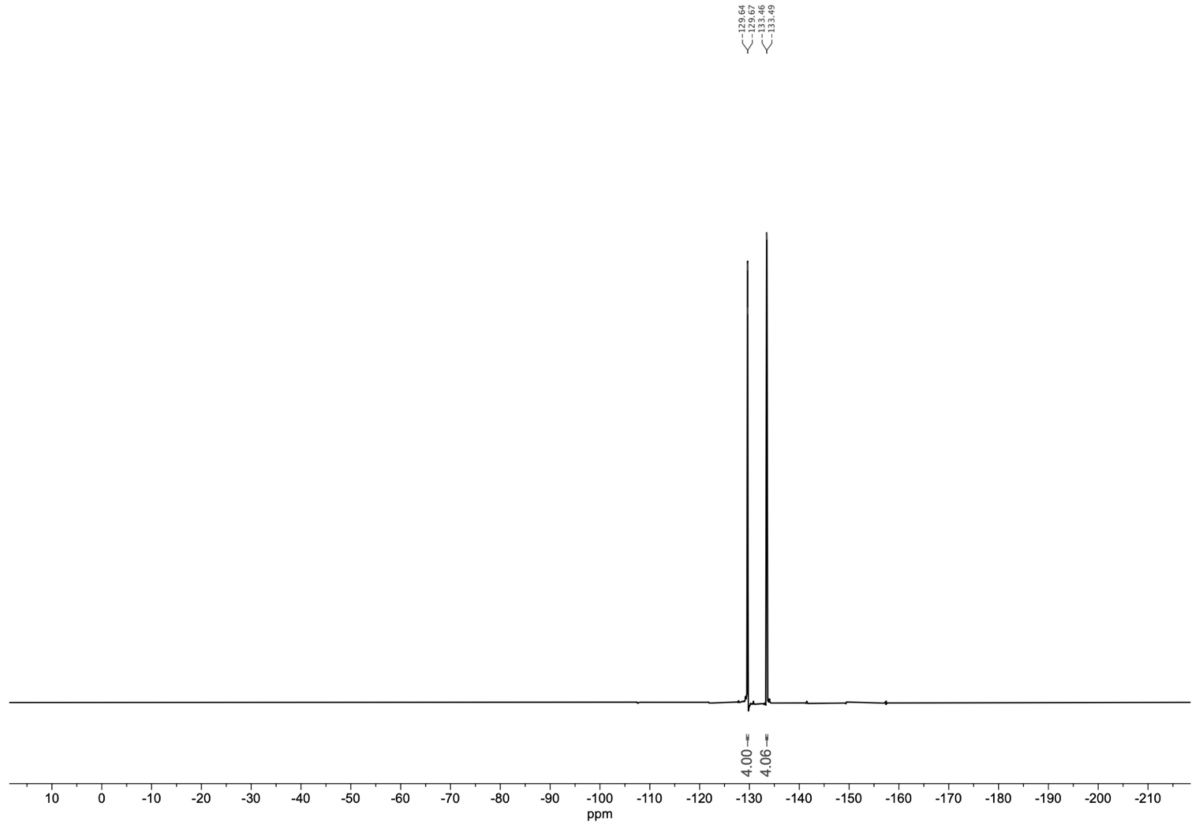

Figure S1. ^{19}F NMR spectrum of perfluorinated nitrile **1**.

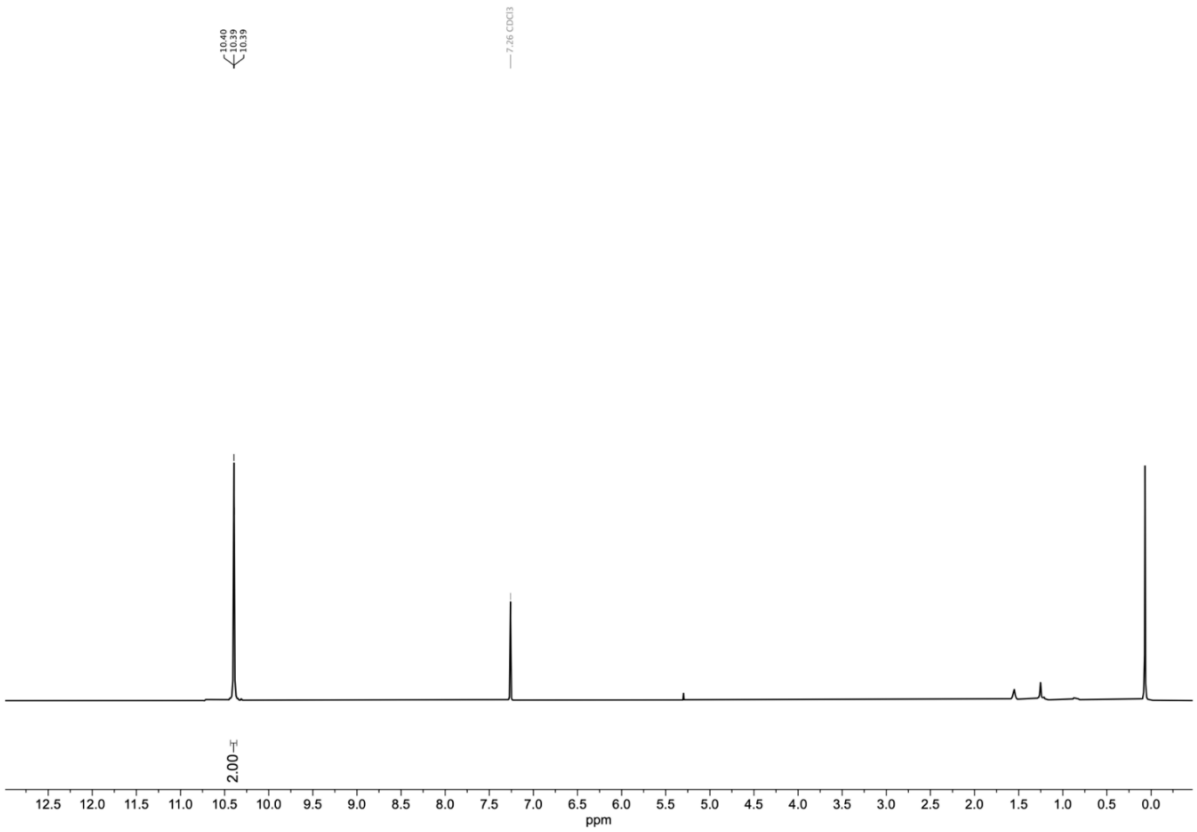

Figure S2. ^{1}H NMR spectrum of perfluorinated aldehyde **2**.

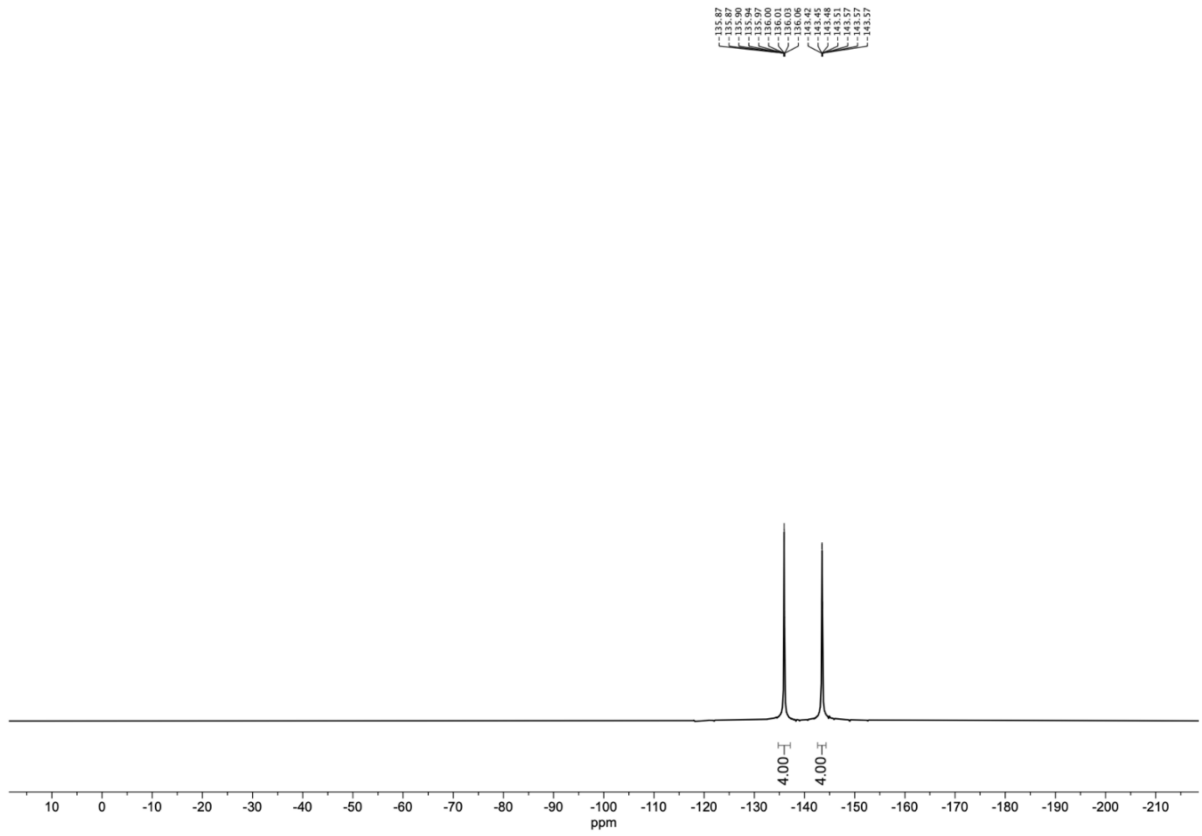

Figure S3. ^{19}F NMR spectrum of perfluorinated aldehyde **2**.

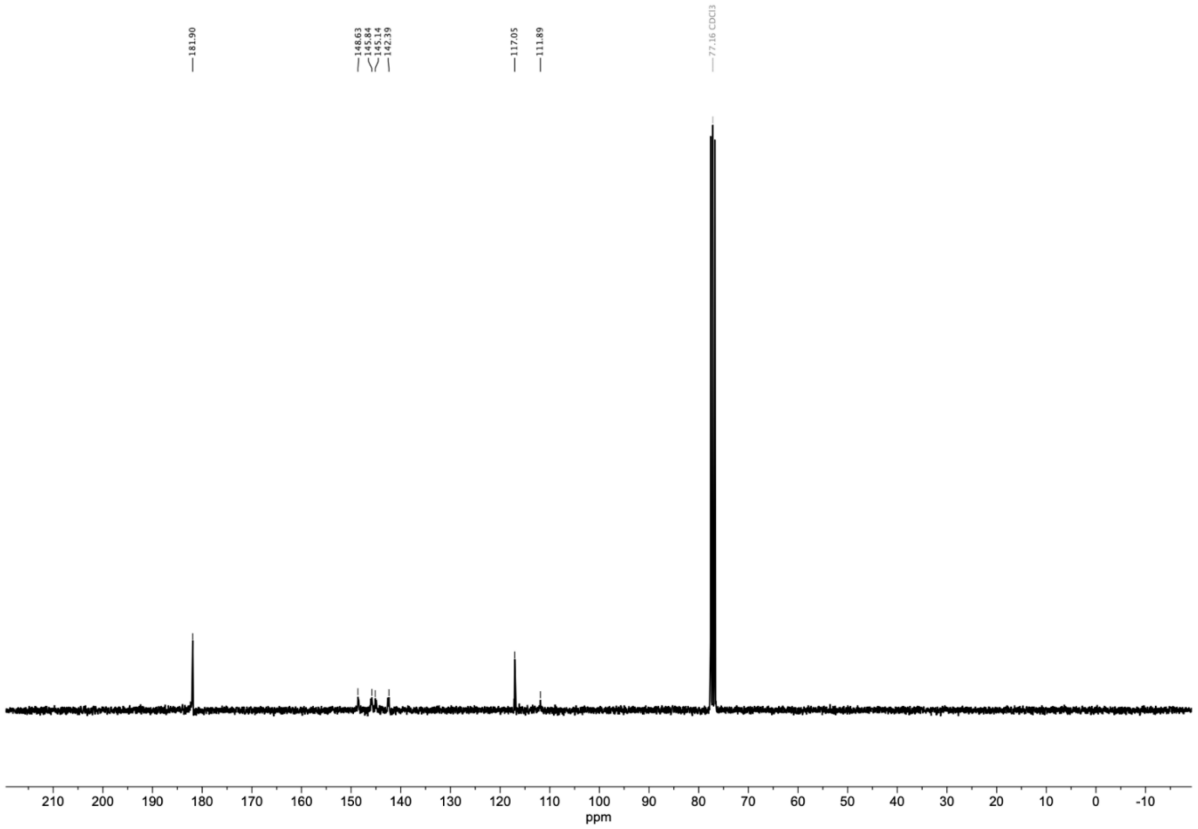

Figure S4. $^{13}C\{^{1}H\}$ NMR spectrum of perfluorinated aldehyde **2**.

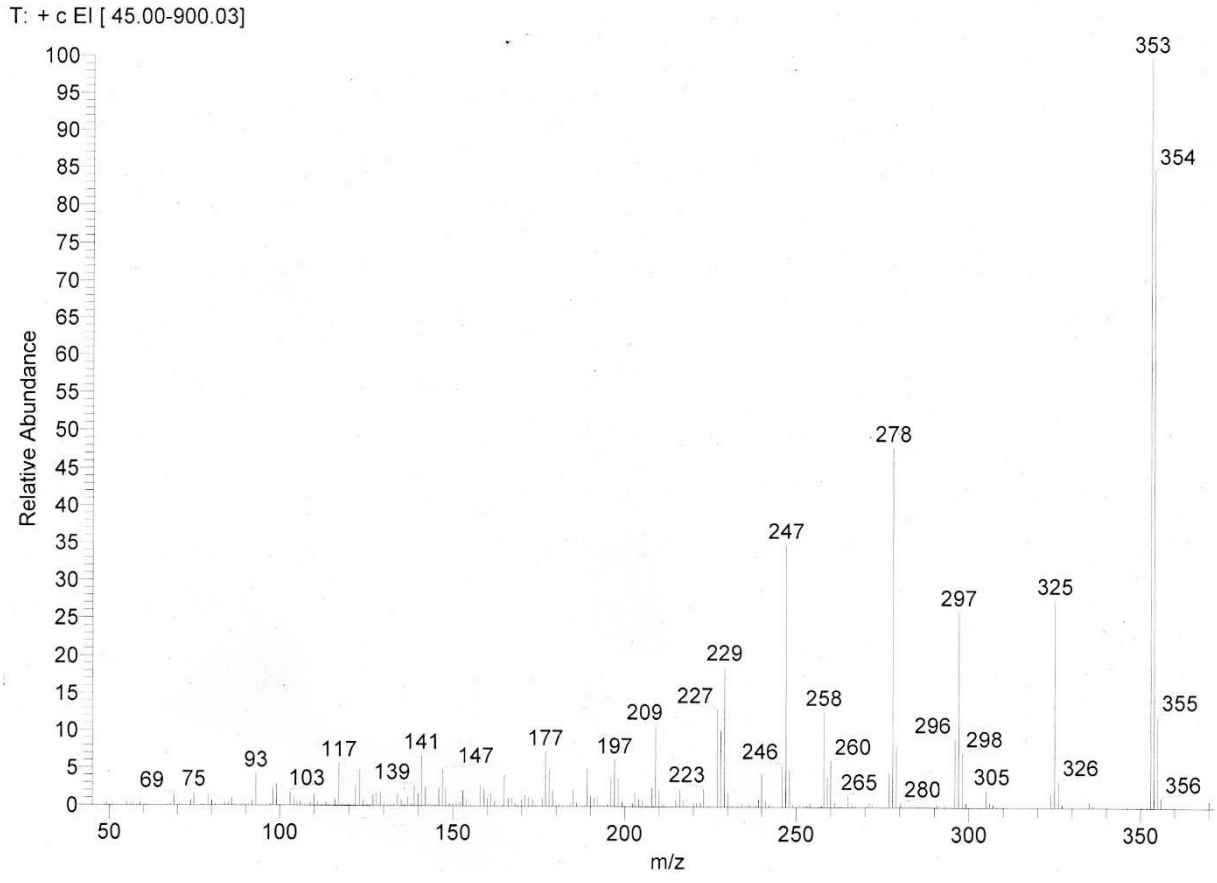

Figure S5. EI-MS (at 80 °C) spectrum of perfluorinated aldehyde **2**.

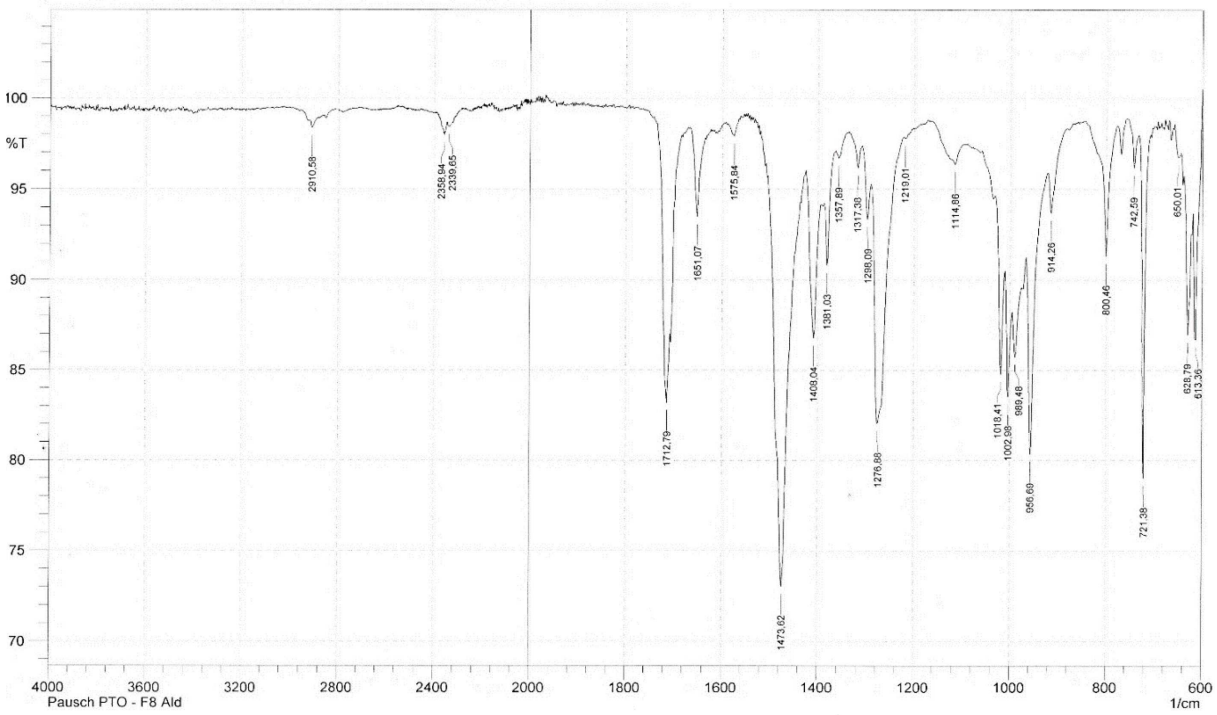

Figure S6. AT-IR spectrum of perfluorinated aldehyde **2**.

2. Characterization of HHU-COF-1 and HHU-COF-2

2.1. X-ray photoelectron spectroscopy (XPS)

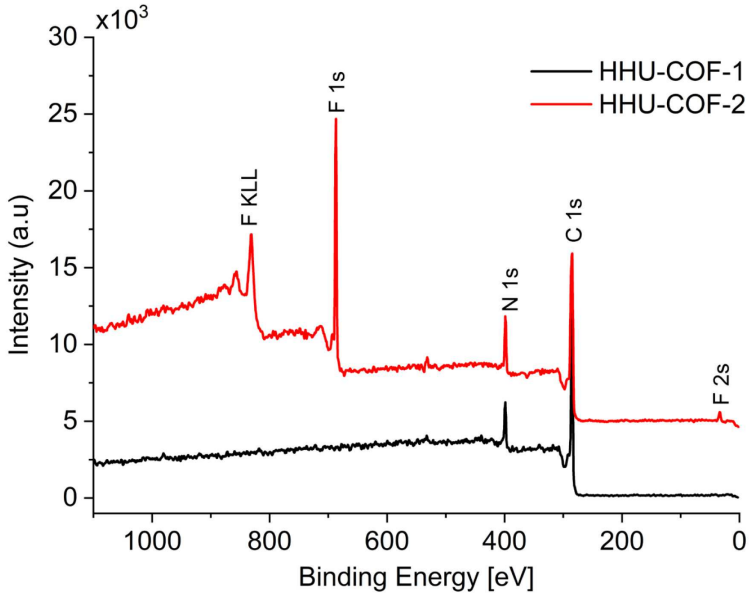

Figure S7. XPS survey spectra of HHU-COF-1 and HHU-COF-2.

Table S1. at% and wt% of the elements in HHU-COF-1 and HHU-COF-2 obtained from XPS survey spectra.

COF	C1s		N 1s		F1s	
	[at%]	[wt%]	[at%]	[wt%]	[at%]	[wt%]
HHU-COF-1	89.2	87.6	10.9	12.4	-	-
HHU-COF-2	70.8	62.7	9.8	10.1	19.5	27.3

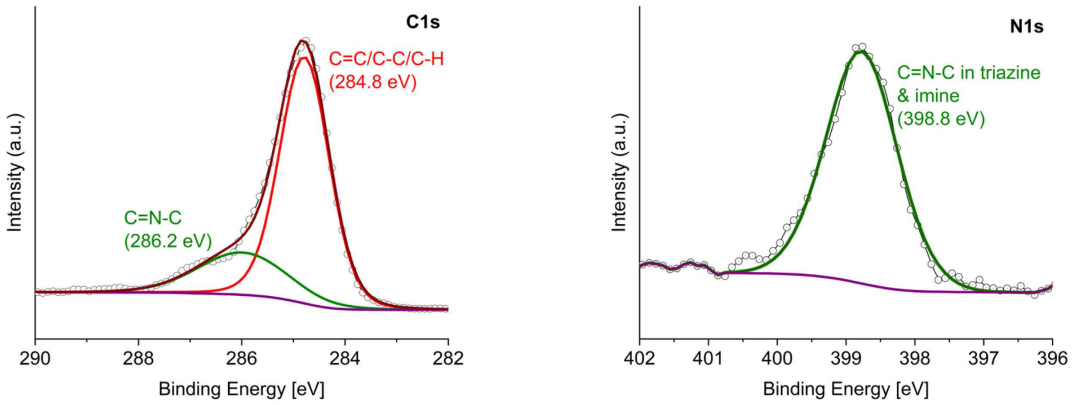

Figure S8. High-resolution XPS spectra of the C1s region (left) and N1s region (right) of HHU-COF-1.

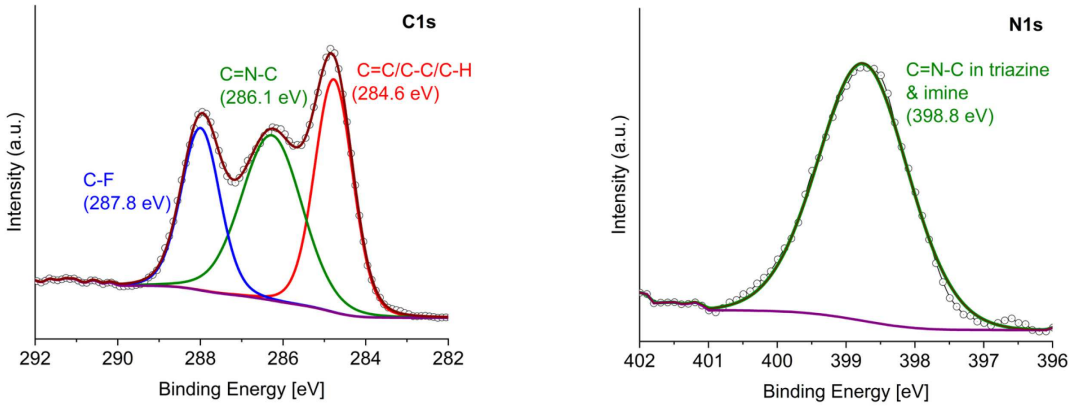

Figure S9. High-resolution XPS spectra of the C1s region (left) and N1s region (right) of HHU-COF-2.

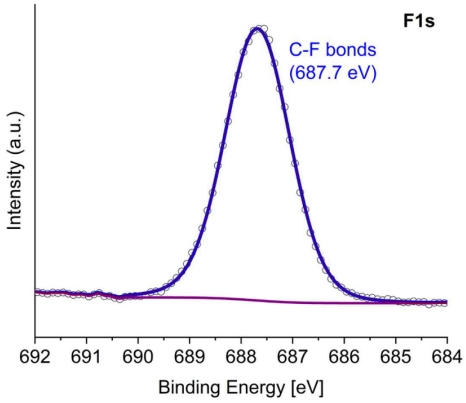

Figure S10. High-resolution XPS spectra of the F1s region of HHU-COF-2.

2.2. Scanning electron microscopy (SEM)

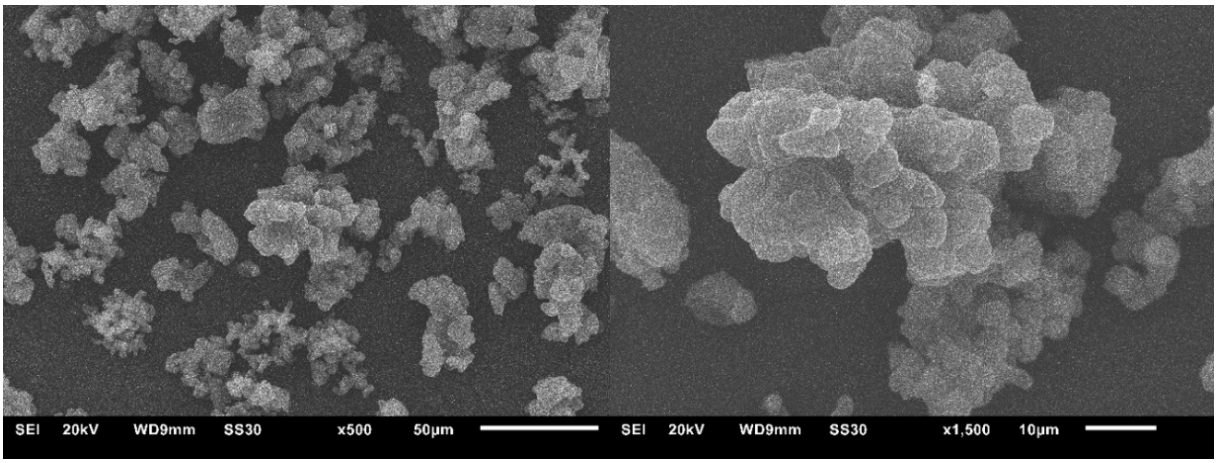

Figure S11. SEM images of HHU-COF-1.

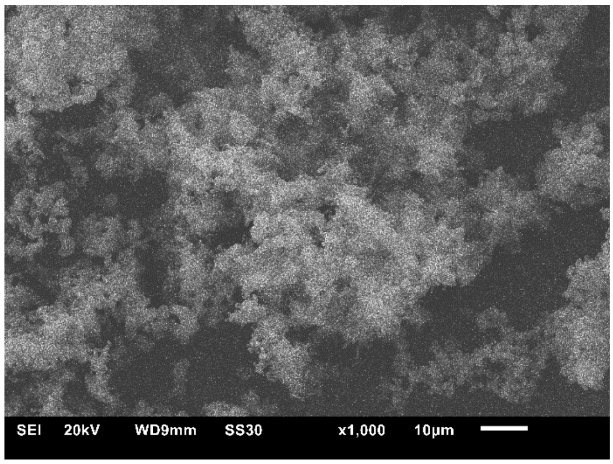

Figure S12. SEM image of HHU-COF-2.

2.3. Energy dispersive X-ray spectroscopy (SEM-EDX)

Table S2. EDX analysis of HHU-COF-2.

	C	H	F	N	O	Au	Cu	Zn	Sum
Ideal [wt%]	60.66	1.82	27.41	10.11	-	-	-	-	100.0
EDX [wt%][a]	63.1	-	16.3	7.3	3.5	7.7	1.2	0.9	100.0
EDX [wt%] with C,F,N	63.1	-	16.3	7.3	-	-	-	-	86.7
EDX [wt%][a] with C,F,N	72.8	-	18.8	8.4	-	-	-	-	100.0

[a] normalized

2.4. CO_2- and CH_4-sorption

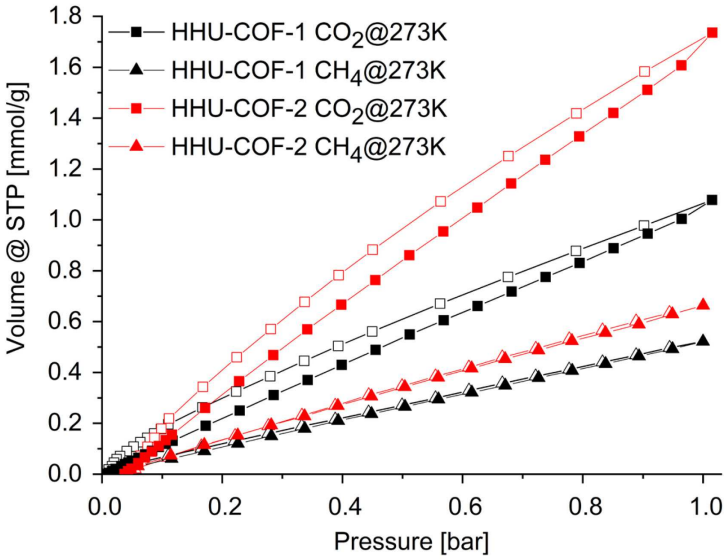

Figure S13. CO_2 and CH_4 sorption isotherms at 273 K of HHU-COF-1 and HHU-COF-2, respectively.

Table S3. Comparison of CO_2 uptake and BET surface area of imine-linked/azine COFs.

Material	CO_2 uptake, 1 bar, 273 K	BET surface area, N_2 at 77 K [m^2/g]	Reference
HHU-COF-1	1.08 mmol/g	2352	This work
HHU-COF-2	1.74 mmol/g	1356	
RT-COF-1[a]	44 cm^3/g (1.96 mmol/g)*	329	[2]
$[HO]_{25\%}$-H_2P-COF[b]	54 mg/g (1.23 mmol/g)	1054	[3]
$[HO]_{100\%}$-H_2P-COF[b]	63 mg/g (1.43 mmol/g)	1284	
$[HO_2C]_{50\%}$-H_2P-COF[c]	96 mg/g (2.18 mmol/g)	786	
$[HO_2C]_{100\%}$-H_2P-COF[c]	174 mg/g (3.95 mmol/g)	364	
DhaTph[d]	65 cm^3/g (2.90 mmol/g)	1305	[4]
DmaTph[e]	37 cm^3/g (1.65 mmol/g)	431	
TAPB-TFPB[f]	40.1 mg/g (0.91 mmol/g)	229	[5]
iPrTAPB-TFPB[g]	31.2 mg/g (0.71 mmol/g)	391	
TAPB-TFP[h]	180 mg/g (4.09 mmol/g)	567	
*i*PrTAPB-TFP[i]	105.2 mg/g (2.39 mmol/g)	756	
TpPa-1[j]	78 cm^3/g (3.48 mmol/g)	535	[6]
TpPa-2 [k]	64 cm^3/g (2.86 mmol/g)	339	

* data obtained from graph; [a] synthesized from 1,3,5-tris(4-aminophenyl)benzene (TAPB) and 1,3,5-benzenetricarbaldehyde (BTCA); [b] imine-linked 2D COF with porphyrin scaffold and phenol units on the pore walls; [c] based on $[HO]_{100\%}$-H_2P-COF with additional open carboxylic acid groups; [d] COF synthesized by reaction of 2,5-dihydroxyterephthalaldehyde (Dha) with 5,10,15,20-tetrakis(4-aminophenyl)-21*H*,23*H*-porphine (Tph); [e] COF synthesized by reaction of 2,5-dimethoxyterephthalaldehyde (Dma) with 5,10,15,20-tetrakis(4-aminophenyl)-21*H*,23*H*-porphine (Tph); [f] COF synthesized by reaction of 1,3,5-tris(4′-aminophenyl)benzene (TAPB) with 1,3,5-tris(4′-formylphenyl)benzene (TFPB); [g] COF synthesized by reaction of 1,3,5-tris(4′-amino-3′,5′-isopropylphenyl)benzene (*i*PrTAPB) with 1,3,5-tris(4′-formylphenyl)benzene (TFPB); [h] COF synthesized by reaction of 1,3,5-tris(4′-aminophenyl)benzene (TAPB) with 1,3,5-triformylphluroglucinol (TFP); [i] COF synthesized by reaction of 1,3,5-tris(4′-amino-3′,5′-isopropylphenyl)benzene (*i*PrTAPB) with 1,3,5-triformylphluroglucinol (TFP); [j] COF synthesized by reaction of 1,3,5-triformylphloroglucinol (Tp) with *p*-phenylenediamine (Pa-1); [k] COF synthesized by reaction of 1,3,5-triformylphloroglucinol (Tp) 2,5-dimethyl-*p*-phenylenediamine (Pa-2)

2.5. Ideal adsorbed solution theory (IAST) selectivities

The CO_2 and CH_4 isotherms of HHU-COF-1 were fitted with the Langmuir (LAI) isotherm model and the isotherms of HHU-COF-2 were fitted with the Toth model.

Table S4. Parameters for LAI and Toth fitting.

Gas	Temperature [K]	Model	R^2	Affinity constant K [1/bar]	Maximal loading q_{max} [mmol/g]	Heterogenity exponent t
HHU-COF-1						
CO_2	273	LAI	0.9999	0.070	15.870	-
CH_4	273	LAI	0.9999	0.393	16.221	-
HHU-COF-2						
CO_2	273	Toth	0.9962	0.501	3.343	7.762
CH_4	273	Toth	0.9996	0.440	1.551	2.273

The CO_2/CH_4 selectivities for a binary (50:50; v:v) mixture of the gases were calculated by applying the ideal adsorbed solution theory (IAST). Figure S14 shows the IAST selectivities as a function of the pressure.

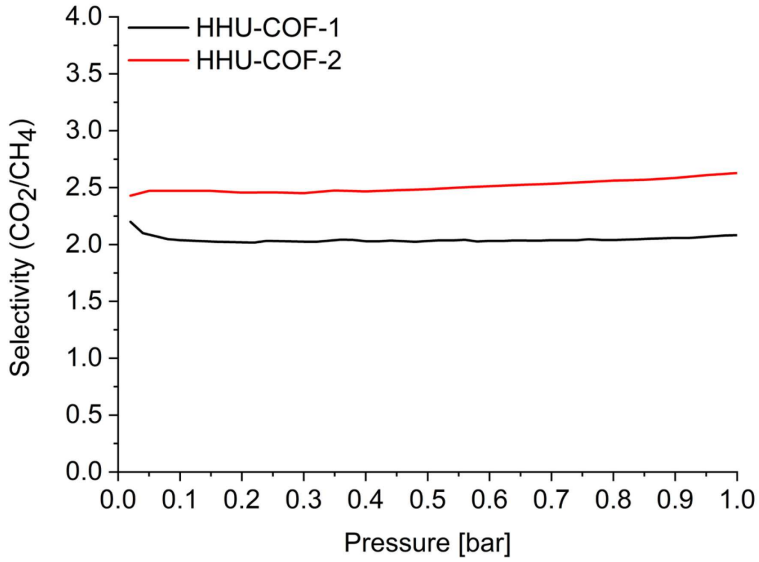

Figure S14. IAST selectivities of HHU-COF-1 and HHU-COF-2 for a binary (50:50; v:v) mixture of the gases CO_2/CH_4 at 273 K.

2.6. Thermogravimetric analysis (TGA)

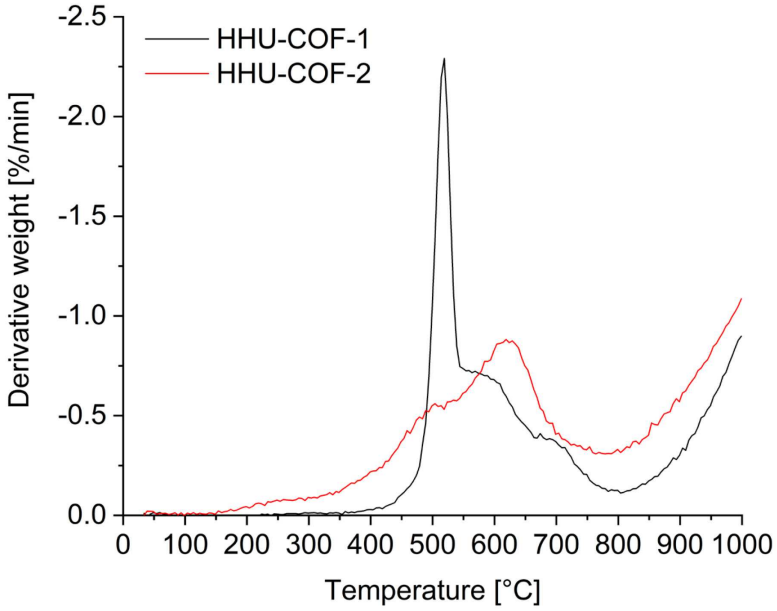

Figure S15. First derivative of TGA curves of HHU-COF-1 and HHU-COF-2. Measurement under nitrogen atmosphere with a heating rate of 5 K/min.

2.7. Correlation of 2theta values

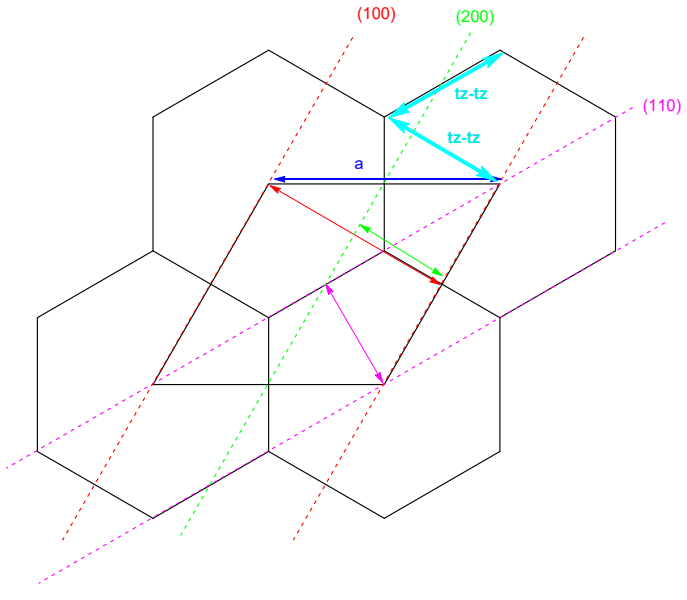

HHU-COF-1

2theta (°)	plane	d (Å)
2.39	(100)	36.9
4.03	(110)	21.9
4.68	(200)	18.9

a = d(100)/cos30° = **42.6 Å**
= ring-centroid-centroid distance
= edge-edge distance across ring

(a = 2 x d(110) = 43.8 Å)

tz-tz = (a/2)/cos30° = **24.6 Å**
centroid-centroid distance between triazine rings along edges, half the vertex-vertex distance across ring, 2(tz-tz) = **49.2 Å**

HHU-COF-2

2theta (°)	plane	d (Å)
2.42	(100)	36.5
4.06	(110)	21.8
4.85	(200)	18.2

a = d(100)/cos30° = **42.1 Å**
= ring-centroid-centroid distance
= edge-edge distance across ring

(a = 2 x d(110) = 43.6 Å)

tz-tz = (a/2)/cos30° = **24.3 Å**
centroid-centroid distance between triazine rings along edges, half the vertex-vertex distance across ring, 2(tz-tz) = **48.6 Å**

Figure S16. Correlation of the 2theta (2θ) values from the powder X-ray diffractograms in Figure 5 in the main text with the reflection planes and the d spacing according to the Bragg equation n λ= 2d sinθ or d = n λ /(2 sinθ) with λ = 1.5406 Å and n = 1. Note that the edge-edge distances a and the triazine-centroid triazine-centroid (tz-tz) distances along the edge derived therefrom as (a/2)/cos30° were determined from the most intense and, thus, most accurately measurable (100) reflexes in the powder-X-ray diffractograms of HHU-COF-1 and -2.

2.8. Images of HHU-COF-1 and HHU-COF-2

Figure S17. Images of HHU-COF-1 (left) and HHU-COF-2 (right).

3. Characterization of HHU-COF-1 (larger scale) and HHU-COF-2 (larger scale)

3.1. Infrared (IR) spectroscopy

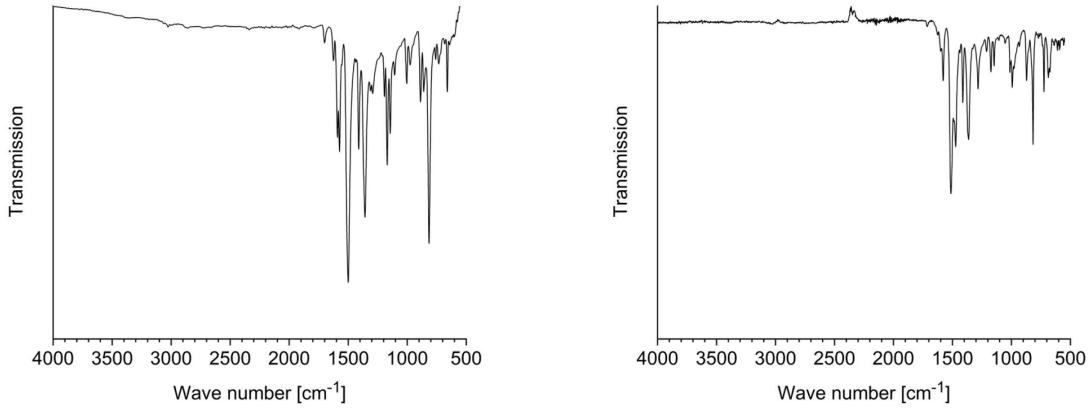

Figure S18. IR-spectra of HHU-COF-1 (larger scale; left) and HHU-COF-2 (larger scale; right).

3.2. Elemental analysis

Table S5. Elemental analysis of HHU-COF-1 (larger scale) and HHU-COF-2 (larger scale).

	C [wt%]	H [wt%]	N [wt%]	Rest [wt%]
HHU-COF-1 Calculated	81.93	4.42	13.65	-
HHU-COF-1 (larger scale)	80.86	4.27	13.03	1.84
HHU-COF-2 Calculated	60.66	1.82	10.11	27.41
HHU-COF-2 (larger scale)	60.23	1.75	10.01	28.01

3.3. N_2-sorption

The nitrogen sorption isotherm of HHU-COF-1 (larger scale) is shown in Figure S. The BET surface area was determined as 2351 m^2/g and the total pore volume as 0.69 cm^3/g. The pore size distribution (Figure S19) showed a maximum at a pore diameter between 25 Å and 27 Å. Three further maxima were at pore diameters of 14 Å and 18 Å

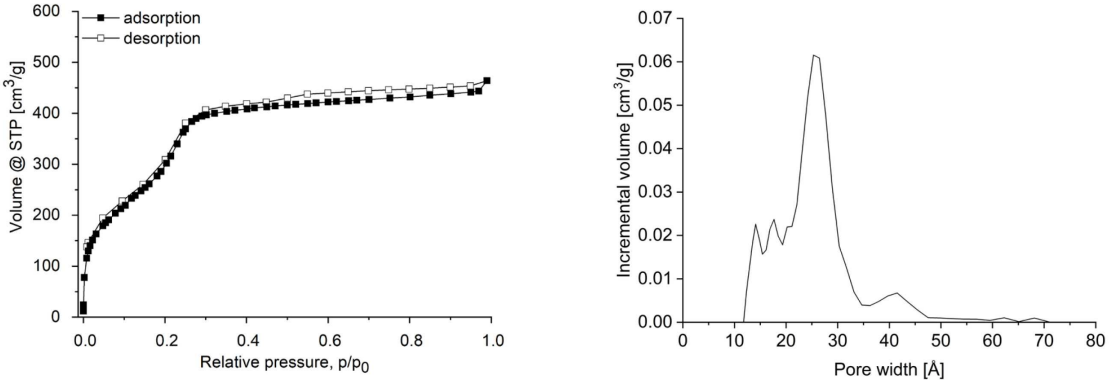

Figure S19. Nitrogen sorption isotherm (left) and pore size distribution calculated with slit pore, NLDFT equilibrium model (right) of HHU-COF-1 (larger scale).

The nitrogen sorption isotherm of HHU-COF-2 (larger scale) is shown in Figure S. The BET surface area was determined as 1346 m^2/g and the total pore volume as 0.68 cm^3/g. The pore size distribution (Figure S20) mainly revealed pore diameters between 10 to 30 Å. In addition, a minor contribution of pores up to 200 Å in diameter was observed.

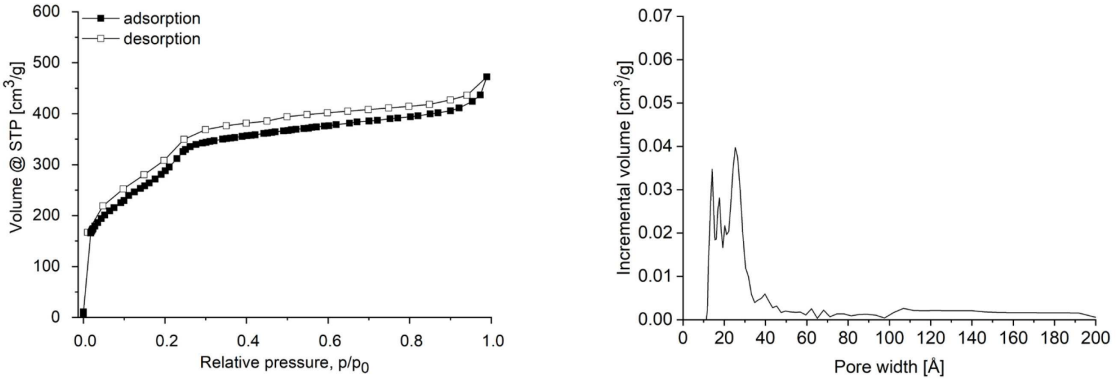

Figure S20. Nitrogen sorption isotherm (left) and pore size distribution calculated with slit pore, NLDFT equilibrium model (right) of HHU-COF-2 (larger scale).

3.4. TGA

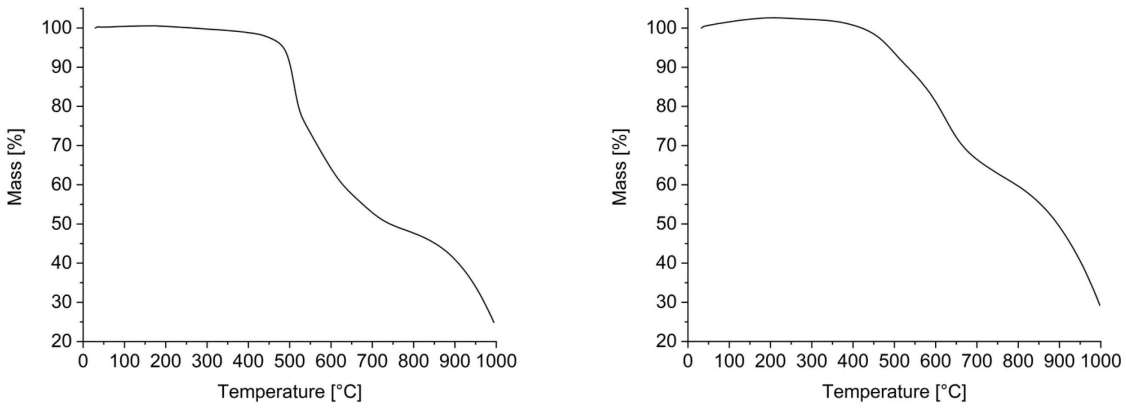

Figure S21. TGA curves of HHU-COF-1 (larger scale; left) and HHU-COF-2 (larger scale; right). Acquired under nitrogen atmosphere with a heating rate of 5 K/min.

3.5. Powder X-Ray diffraction (PXRD)

The PXRD of HHU-COF-1 (larger scale) (Figure S22; left) showed, in addition to the characteristic reflex between 2° and 3° 2θ, two reflexes with lower intensity at 4° and about 5° 2θ. The PXRD of HHU-COF-2 (larger scale) (Figure S22; right) exhibited a reflex between 2° and 3° 2θ. Another reflex could be observed at 5° 2θ. Both COFs showed no evidence of an amorphous character.

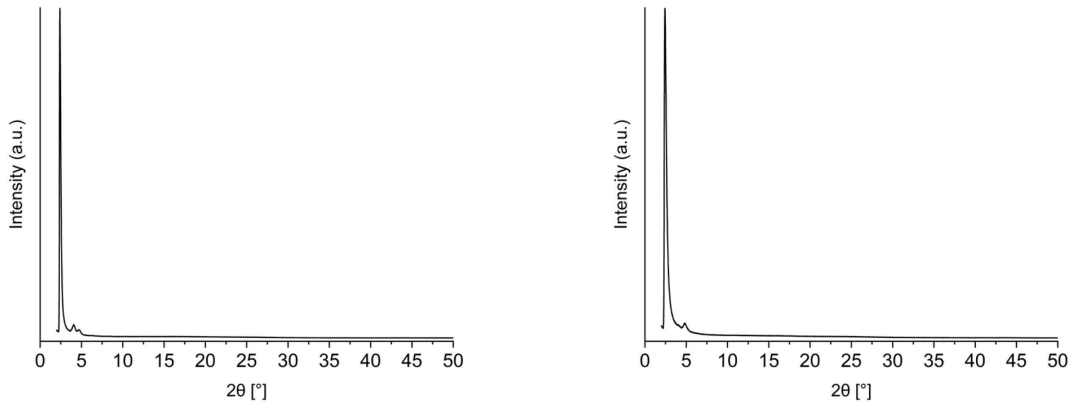

Figure S22. PXRD pattern of HHU-COF-1 (larger scale; left) and HHU-COF-2 (larger scale; right).

4. Preparation and characterization of MMMs

4.1. Schematic preparation of the pure polymer membrane and MMMs

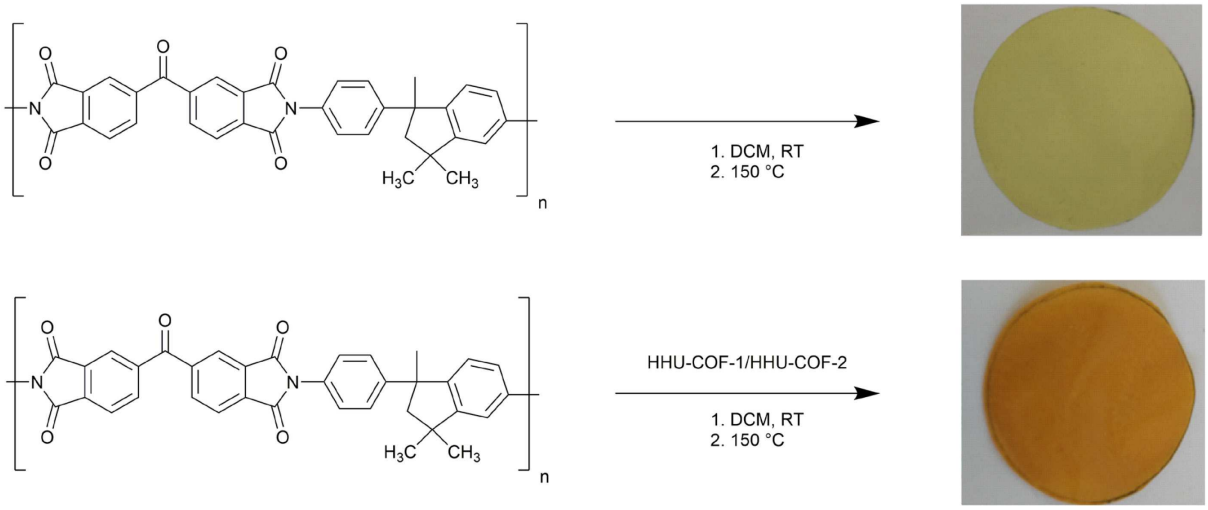

Figure S23. Schematic preparation of the pure Matrimid membrane (top) and MMMs, using the 16 wt% HHU-COF-2 MMM as an example (bottom).

4.2. Casting procedure

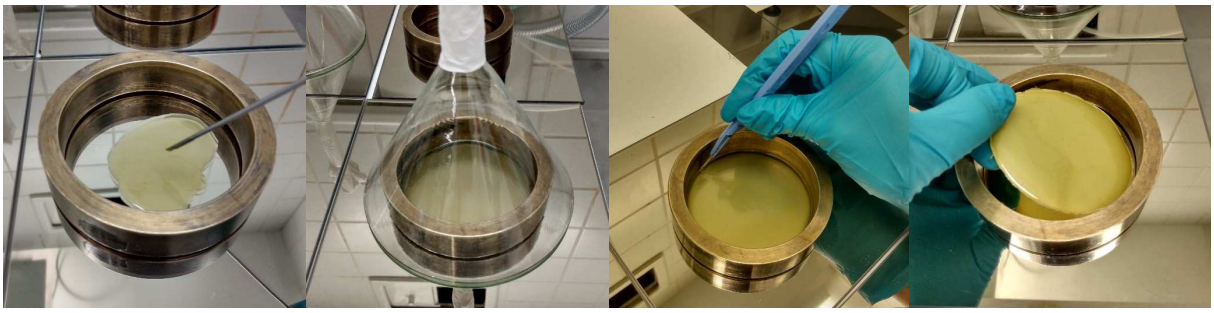

Figure S24. Preparation of membranes by solution casting (from left to right): casting the solution, drying, cutting with a scalpel and removing the membrane.

4.3. Set-up for CO_2/CH_4 mixed gas separation measurements

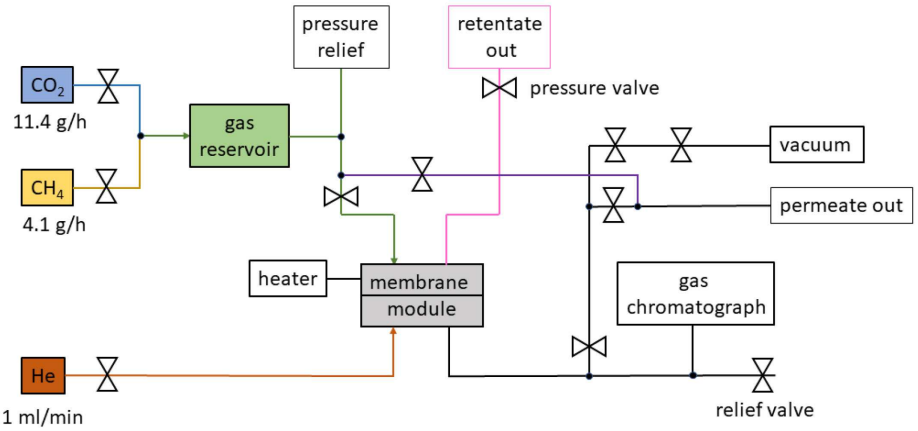

Figure S25. Set-up for CO_2/CH_4 mixed gas separation measurements [7].

4.4. Membrane thickness

Table S6. Average thickness of MMMs.

COF content [wt%]	HHU-COF-1/ Matrimid	HHU-COF-2/ Matrimid
	Average thickness [µm]	
8	74.9	74.6
16	72.4	68.6
24	73.0	73.0

4.5. SEM images of membrane surfaces

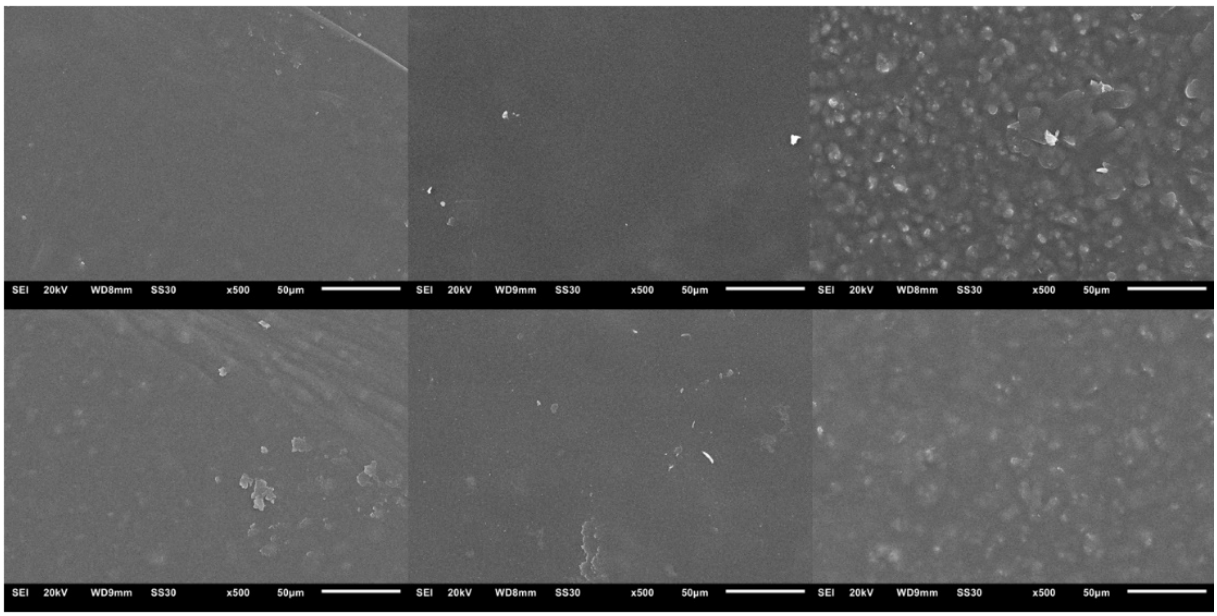

Figure S26. Top-surface SEM images of HHU-COF-1/Matrimid (top) with 8 wt% (left), 16 wt% (middle) and 24 wt% filler (right) and HHU-COF-2/Matrimid MMMs (bottom) with 8 wt% (left), 16 wt% (middle) and 24 wt% filler (right).

4.6. SEM-EDX of HHU-COF-2/Matrimid MMMs

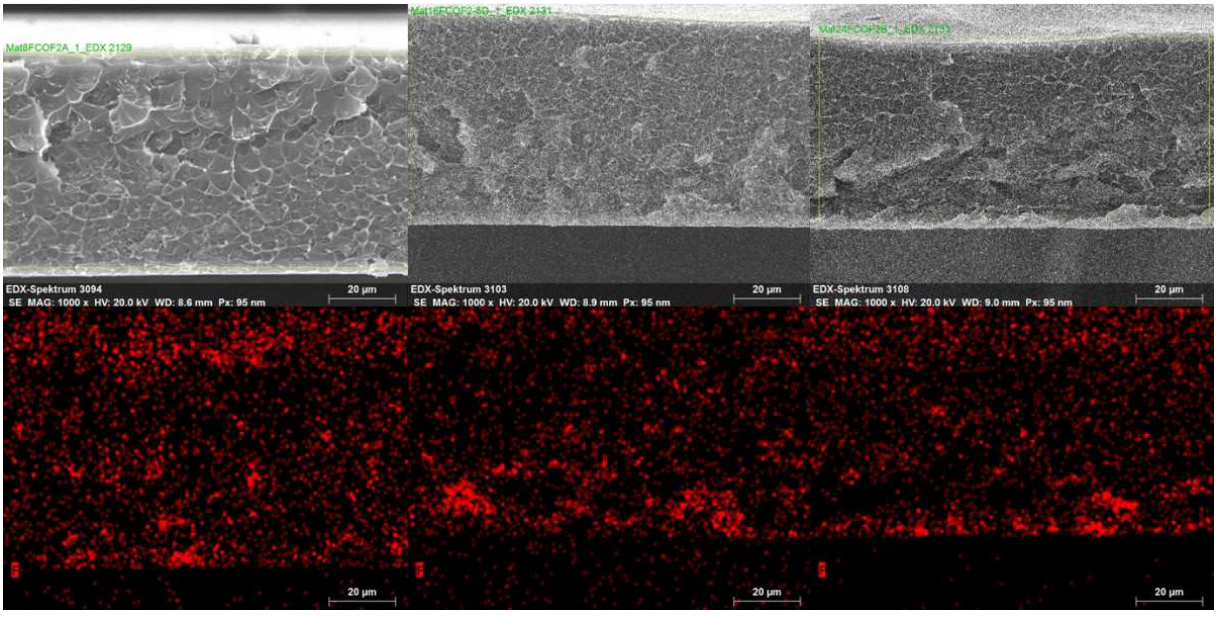

Figure S27. SEM images of HHU-COF-2/Matrimid MMMs (top) with 8 wt% (left), 16 wt% (middle) and 24 wt% filler (right) and associated fluorine elemental mapping (bottom).

4.7. Tensile strength

Table S7. Tensile strength of pure Matrimid and MMMs.

Filler material	-	HHU-COF-1			HHU-COF-2		
Filler content [wt%]	-	8	16	24	8	16	24
Tensile strength [MPa]	91	74	79	51	76	75	59

4.8. Long-term stability of MMMs

Table S8. Gas permeabilities (*P*) and mixed-gas selectivity factors (α) for COF/Matrimid MMMs when stored for one year under ambient conditions.

Filler material	Filler content [wt%]	P CO_2 [Barrer]	P CH_4 [Barrer]	α CO_2/CH_4
HHU-COF-1	8	8.6 ± 1.1	0.19 ± 0.03	44 ± 2
	16	8.0 ± 0.4	0.17 ± 0.01	46 ± 2
	24	5.8*	0.20*	28*
HHU-COF-2	8	7.1 ± 0.1	0.16 ± 0.01	45 ± 1
	16	10.5 ± 0.2	0.24 ± 0.01	44 ± 1
	24	12.9 ± 0.7	0.29 ± 0.02	45 ± 1

*Only one measurement due to breaking of the second MMM

4.9. Comparison of membrane performance

Table S9. Comparison of CO_2 permeability and CO_2/CH_4 selectivity for COFs/CTFs as porous filler materials in different polymer MMMs.

Filler	Filler content [wt%]	Matrix	*P* CO_2 [Barrer]	*P* CO_2 elevation [%]	*S/α* CO_2/CH_4	Ref.
-	-	Matrimid	6.8 ± 0.3	-	42 ± 1	This work
HHU-COF-1	8	Matrimid	9.1 ± 0.2	34	46 ± 2	
	16		9.1 ± 1.0	34	46 ± 1	
	24		5.8 ± 0.7	-	41 ± 1	
HHU-COF-2	8	Matrimid	7.1 ± 0.3	4	51 ± 1	
	16		10.2 ± 0.3	50	44 ± 2	
	24		13.0 ± 1.0	91	40 ± 1	
-	-	Matrimid	6.8 ± 0.1[a]	-	30.5± 0.6[a]	[8]
ACOF-1[1]	8	Matrimid	9.6 ± 1.0[a]	41	31.9 ± 0.8[a]	
	16		15.3 ± 0.7[a]	125	32.4 ± 1.8[a]	
	-	6FDA-DAM	767 ± 24[b]	-	22.3 ± 2.1[b]	[9]
COF-300	7	6FDA-DAM	1185 ± 41[b]	55	30.3 ± 1.5[b]	
	10		2842 ± 76[b]	271	24.6 ± 1.7[b]	
-	-	Pebax	73 ± 4[b]	-	18.7 ± 1.2[b]	
COF-300	10	Pebax	107 ± 6[b]	47	25.5 ± 1.3[b]	
-	-	Pebax	53[c]	-	17[c]	[10]
CTPP[2]	0.025	Pebax	73[c]	38	25[c]	
-	-	PIM-1[4]	3672[d]	-	10.6[d]	[11]
SNW-1[3]	10	PIM-1[4]	7553[d]	106	13.5[d]	
-	-	PIM-1[4]	5800[e]	-	11.5[e]	[12]
FCTF-1	2	PIM-1[4]	7300[e]	26	16.6[e]	
	5		9400[e]	62	14.8[e]	
-	-	Matrimid	6.8 ± 0.3[f]	-	42 ± 1[f]	[13]
CTF-biphenyl	8	Matrimid	12.0 ± 0.2[f]	76	43 ± 1[f]	
	16		15.1 ± 0.2[f]	122	44 ± 1[f]	
	24		15.4 ± 0.5[f]	126	44 ± 1[f]	
-	-	Matrimid	6.8 ± 0.3[f]	-	42 ± 1[f]	[7]
CTF-fluorene	8	Matrimid	9.2 ± 0.4[f]	35	43 ± 1[f]	
	16		12.6 ± 0.1[f]	85	45 ± 1[f]	
	24		17.8 ± 0.3[f]	162	44 ± 2[f]	

[a]Mixed gas; 308 K; feed pressure 4 bar; [b]Mixed gas; 298 K; transmembrane pressure 1 bar; [c]Single gas; 293 K; feed pressure 4 bar; [d]Single gas; 303 K; feed pressure 2 bar; [e]Single gas; 303 K; feed pressure 1 atm; [f]Mixed gas; 298 K; feed pressure 4 bar; [1]azine-linked covalent organic framework; [2]porous covalent triazine piperazine polymer; [3]Schiff base network; [4]polymer of intrinsic microporosity

5. Synthesis and characterization of TRITER-1 (= SCF-HCOF-1) and SCF-FCOF-1

5.1. Materials and Synthesis

Terephthalaldehyde (TA; 99%) was obtained from Sigma-Aldrich, 2,3,5,6-tetrafluoroterephthalaldehyde (TFTA; 98%) from BLDpharm and 1,3,5-tris-(4-aminophenyl)triazine (TAPT; > 98%) from TCI.

Synthesis of TRITER-1 (= SCF-HCOF-1)

TRITER-1 was synthesized in analogy to the literature [14]: 53.6 mg terephthalaldehyde (TA; 0.400 mmol), 94.4 mg TAPT (0.267 mmol) and 1 mL of the solvent mixture of 1,4-dioxane and mesitylene (1:1, v/v) were placed in a glass ampoule, followed by an ultra-sonification treatment for 15 min in order to ensure sufficient mixing of the educts. The mixture was degassed by applying three freeze-pump-thaw cycles and the ampoule was flame sealed under vacuum. After heating at 120 °C for three days, the crude product was washed with THF followed by Soxhlet extraction for 24 h each in THF and in ethanol to remove unreacted monomers. Drying was performed with supercritical CO_2. (yield: 113.0 mg; 84.4%).

Synthesis of SCF-FCOF-1

SCF-FCOF-1 was synthesized in analogy to the literature [14]: 82.4 mg 2,3,5,6-tetrafluoroterephthalaldehyde (TFTA; 0.400 mmol), 94.4 mg TAPT (0.267 mmol) and 1 mL of the solvent mixture of 1,4-dioxane and mesitylene (1:1, v/v) were placed in a glass ampoule, followed by an ultra-sonification treatment for 30 min in order to ensure sufficient mixing of the educts. The mixture was degassed by applying three freeze-pump-thaw cycles and the ampoule was flame sealed under vacuum. After heating at 120 °C for three days, the crude product was washed with THF followed by Soxhlet extraction for 24 h each in THF and in ethanol to remove unreacted monomers. Drying was performed with supercritical CO_2. (yield: 121.7 mg; 74.8%)

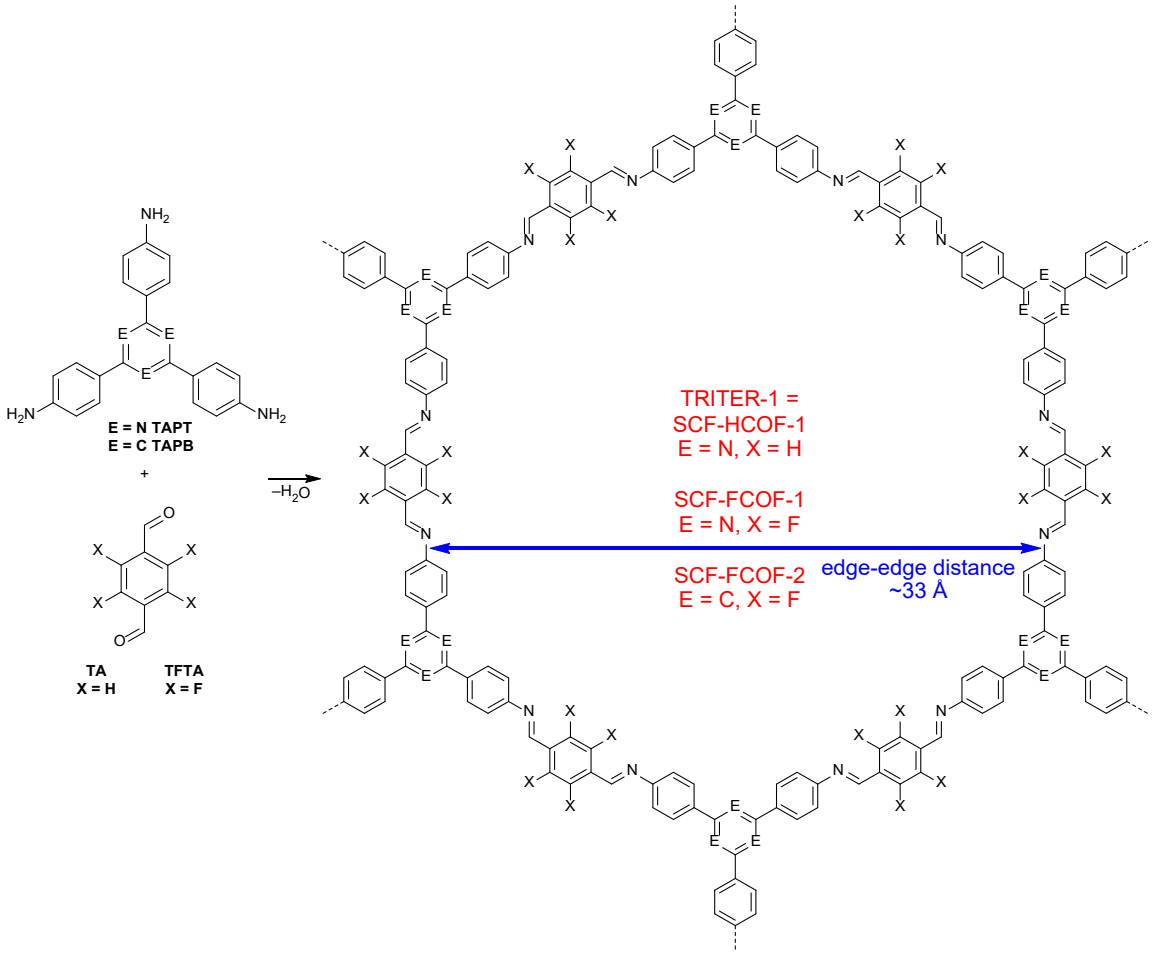

Scheme S1. Schematic formation of TRITER-1 (= SCF-HCOF-1) and SCF-FCOF-1 from TAPT and TA or TFTA, respectively [14,15]. (TAPB = 1,3,5-tris(4-aminophenyl) benzene, TAPT = 2,4,6-tris(4-aminophenyl)-1,3,5-triazine, TA = terephthalaldehyde, TFTA = 2,3,5,6-tetrafluoroterephthaldehyde). The edge-edge distance was taken from the literature of SCF-FCOF-1 and -2 [14].

5.2. IR spectroscopy

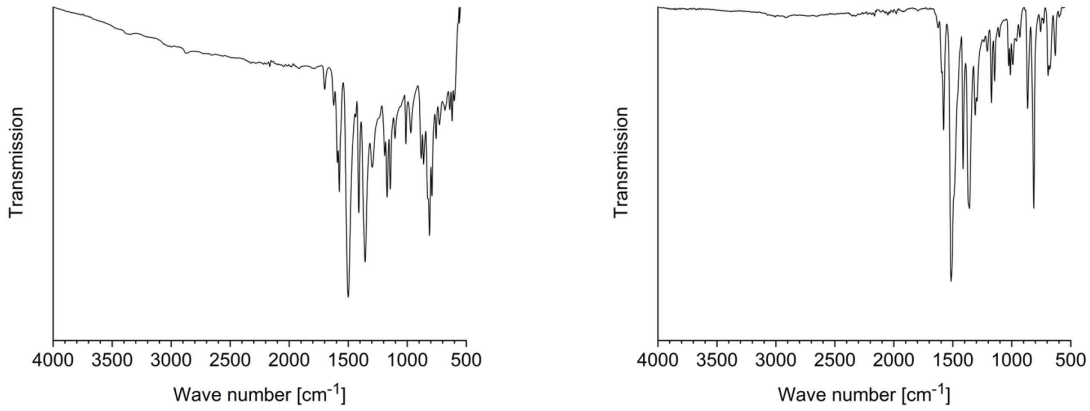

Figure S28. IR-spectra of TRITER-1 (left) and SCF-FCOF-1 (right).

5.3. Elemental analysis

Table S10. Elemental analysis of TRITER-1 and SCF-FCOF-1.

	C [wt%]	H [wt%]	N [wt%]	Rest [wt%]
TRITER-1 Calculated	79.04	4.19	16.77	-
TRITER-1	77.52	4.02	16.29	2.17
SCF-FCOF-1 Calculated	65.03	2.48	13.79	18.70
SCF-FCOF-1	65.19	2.67	13.64	18.50

5.4. SEM-EDX

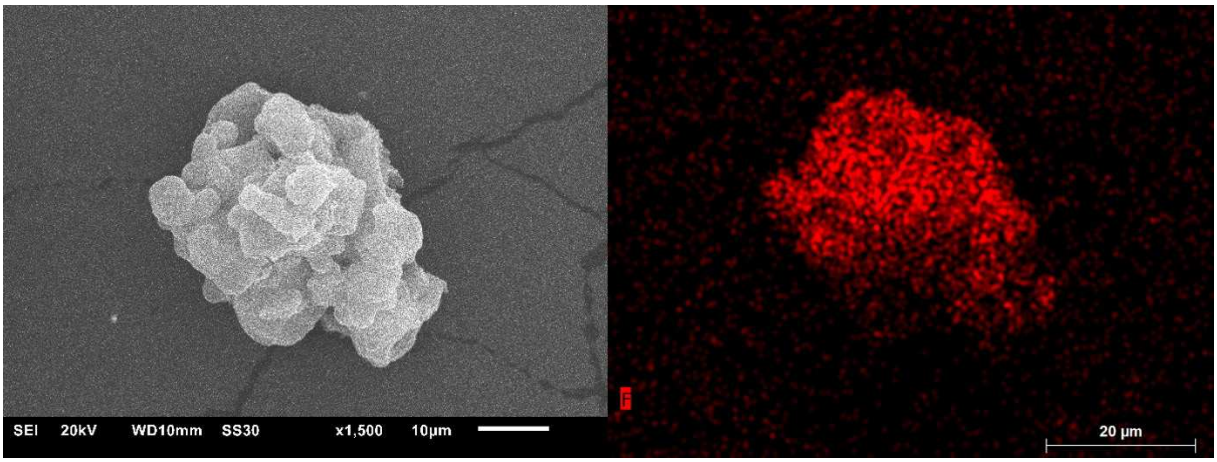

Figure S29. SEM image (left) of SCF-FCOF-1 and associated fluorine elemental mapping (right).

Table S11. EDX analysis of SCF-FCOF-1.

	C	H	F	N	O	Au	Si	Al	Sum
Ideal [wt%]	65.03	2.48	18.70	13.79	-	-	-	-	100
EDX [wt%]	47.9	-	9.5	6.7	0.9	8.6	0.2	0.1	73.9
EDX [wt%] without Au	47.9	-	9.5	6.7	0.9	-	0.2	0.1	65.3
EDX [wt%][a] without Au	73.4	-	14.5	10.3	1.4	-	0.3	0.2	100

[a] normalized

5.5. N_2-sorption

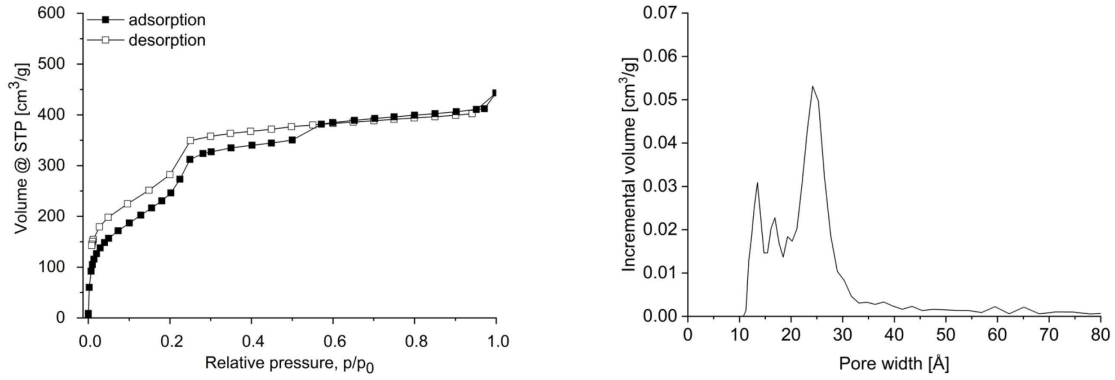

Figure S30. Nitrogen sorption isotherm (left) and pore size distribution calculated with slit pore, NLDFT equilibrium model (right) of TRITER-1.

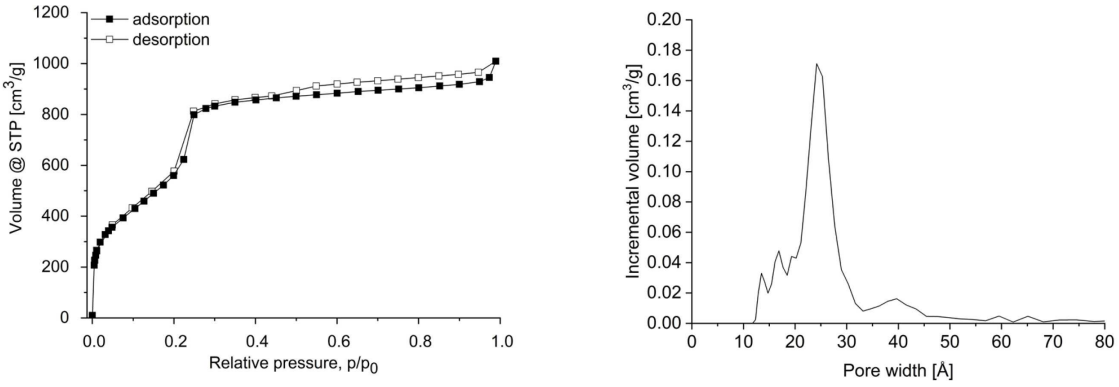

Figure S31. Nitrogen sorption isotherm (left) and pore size distribution calculated with slit pore, NLDFT equilibrium model (right) of SCF-FCOF-1.

5.6. TGA

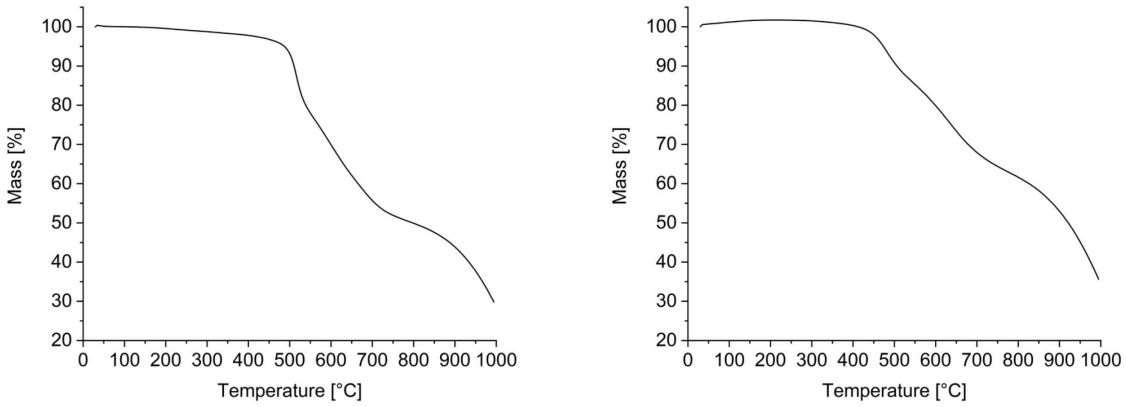

Figure S32. TGA curves of TRITER-1 (left) and SCF-FCOF-1 (right). Acquired under nitrogen atmosphere with a heating rate of 5 K/min.

5.7. PXRD

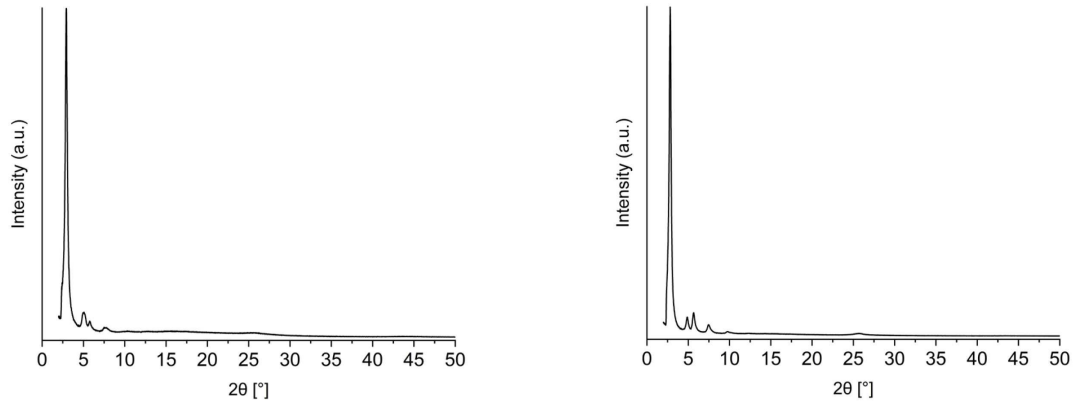

Figure S33. PXRD pattern of TRITER-1 (left) and SCF-FCOF-1 (right) prepared in this work.

5.8. Images of TRITER-1 and SCF-FCOF-1

Figure S34. Images of TRITER-1 (left) and SCF-FCOF-1 (right).

6. References

1. Chen, T.-H.; Popov, I.; Zenasni, O.; Daugulis, O.; Miljanić, O.Š. Superhydrophobic perfluorinated metal–organic frameworks. *Chem. Commun.* **2013**, *49*, 6846–6848. DOI: 10.1039/C3CC41564C

2. de la Peña Ruigómez, A.; Rodríguez-San-Miguel, D.; Stylianou, K.C.; Cavallini, M.; Gentili, D.; Liscio, F.; Milita, S.; Roscioni , O.M.; Ruiz-González, M.L.; Carbonell, C.; Maspoch, D.; Mas-Ballesté, R.; Segura, J.L.; Zamora, F. Direct On-Surface Patterning of a Crystalline Laminar Covalent Organic Framework Synthesized at Room Temperature. *Chem. Eur. J.* **2015**, *21*, 10666–10670. DOI: 10.1002/chem.201501692

3. Huang, N.; Chen, X.; Krishna, R.; Jiang, D. Two-Dimensional Covalent Organic Frameworks for Carbon Dioxide Capture through Channel-Wall Functionalization. *Angew. Chem. Int. Ed.* **2015**, *54*, 2986–2990. DOI: 10.1002/anie.201411262

4. Kandambeth, S.; Shinde, D.B.; Panda, M.K.; Lukose, B.; Heine, T.; Banerjee, R. Enhancement of Chemical Stability and Crystallinity in Porphyrin-Containing Covalent Organic Frameworks by Intramolecular Hydrogen Bonds. *Angew. Chem. Int. Ed.* **2013**, *52*, 13052–13056. DOI: 10.1002/anie.201306775

5. Kaleeswaran, D.; Vishnoi, P.; Murugavel, R. [3+3] Imine and β-ketoenamine tethered fluorescent covalentorganic frameworks for CO_2 uptake and nitroaromatic sensing. *J. Mater. Chem. C* **2015**, *3*, 7159–7171. DOI: 10.1039/C5TC00670H

6. Kandambeth, S.; Mallick, A.; Lukose, B.; Mane, M.V.; Heine, T.; Banerjee, R. Construction of Crystalline 2D Covalent Organic Frameworks with Remarkable Chemical (Acid/Base) Stability via a Combined Reversible and Irreversible Route. *J. Am. Chem. Soc.* **2012**, *134*, 19524–19527. DOI: 10.1021/ja308278w

7. Bügel, S.; Spieß, A.; Janiak, C. Covalent triazine framework CTF-fluorene as porous filler material in mixed matrix membranes for CO_2/CH_4 separation. *Micropor. Mesopor. Mat.* **2021**, *316*, 110941. DOI: 10.1016/j.micromeso.2021.110941

8. Shan, M.; Seoane, B.; Rozhko, E.; Dikhtiarenko, A.; Clet, G.; Kapteijn, F.; Gascon, J. Azine-Linked Covalent Organic Framework (COF)-Based Mixed-Matrix Membranes for CO_2/CH_4 Separation. *Chem. Eur. J.* **2016**, *22*, 14467–14470. DOI: 10.1002/chem.201602999

9. Cheng, Y.; Zhai, L.; Ying, Y.; Wang, Y.; Liu, G.; Dong, J.; Ng, D.Z.L.; Khan, S.A.; Zhao, D. Highly efficient CO_2 capture by mixed matrix membranes containing three-dimensional covalent organic framework fillers. *J. Mater. Chem. A* **2019**, *7*, 4549–4560. DOI: 10.1039/C8TA10333J

10. Thankamony, R.L.; Li, X.; Das, S.K.; Ostwal, M.M.; Lai, Z. Porous covalent triazine *piperazine* polymer (CTPP)/PEBAX mixed matrix membranes for CO_2/N_2 and CO_2/CH_4 separations. *J. Membr. Sci.* **2019**, *591*, 117348. DOI: 10.1016/j.memsci.2019.117348

11. Wu, X.; Tian, Z.; Wang, S.; Peng, D.; Yang, L.; Wu, Y.; Xin, Q.; Wu, H.; Jiang, Z. Mixed *matrix* membranes comprising polymers of intrinsic microporosity and covalent organic framework for gas separation. *J. Membr. Sci.* **2017**, *528*, 273–283. DOI: 10.1016/j.memsci.2017.01.042

12. Jiang, H.; Zhang, J.; Huang, T.; Xue, J.; Ren, Y.; Guo, Z.; Wang, H.; Yang, L.; Yin, Y.; Jiang, Z.; Guiver, M.D. Mixed-Matrix Membranes with Covalent Triazine Framework Fillers in Polymers of Intrinsic Microporosity for CO_2 Separations. *Ind. Eng. Chem. Res.* **2019**, *59*, 5296–5306. DOI: 10.1021/acs.iecr.9b04632

13. Bügel, S.; Hoang, Q.-D.; Spieß, A.; Sun, Y.; Xing, S.; Janiak, C. Biphenyl-Based Covalent Triazine Framework/Matrimid® Mixed-Matrix Membranes for CO_2/CH_4 Separation. *Membranes* **2021**, *11*, 795. DOI: 10.3390/membranes11100795

14. Liao, Q.; Ke, C.; Huang, X.; Zhang, G.; Zhang, Q.; Zhang, Z.; Zhang, Y.; Liu, Y.; Ning, F.; Xi, K. Catalystfree and efficient fabrication of highly crystalline fluorinated covalent organic frameworks for selective guest adsorption. *J. Mater. Chem. A* **2019**, *7*, 18959–18970. DOI: 10.1039/C9TA06214A

15. Gomes, R.; Bhanja, P.; Bhaumik, A. A triazine-based covalent organic polymer for efficient CO_2 adsorption. *Chem. Commun.* **2015**, *51*, 10050–10053. DOI: 10.1039/C5CC02147B

3.4. Synthesis and characterization of covalent triazine framework CTF-1@polysulfone mixed matrix membranes and their gas separation studies

Subarna Dey, Stefanie Bügel, Sara Sorribas, Alexander Nuhnen, Asamanjoy Bhunia, Joaquín Coronas, Christoph Janiak

Front. Chem. **2019**, *7*, 693.

DOI: 10.3389/fchem.2019.00693; [118]

MMMs have attracted major attention in the field of gas separation due to their low cost and high permeability. In this work, MMMs consisting of the covalent triazine framework CTF-1 as the dispersed phase and PSF as the matrix are presented for the first time. Permeability and selectivity studies were performed for the pure membrane and for MMMs containing 8, 16 and 24 wt% CTF-1. Permeability was enhanced for O_2, N_2, CO_2 and CH_4 and no loss of selectivity was observed for the gas pairs O_2/N_2, CO_2/CH_4 and CO_2/N_2. With 24 wt% CTF-1, CO_2 permeability was increased from 7.3 Barrer for the pure PSF membrane to 12.7 Barrer. Further, comparisons were made with theoretical permeability models, and a modified Maxwell model was successfully applied. The calculation of the FFV confirmed that the porosity of the filler contributes substantially to the gas transport through the membrane.

Author's contribution to the work:

- Application of permeability models
- Density measurements and calculation of the FFV
- Data evaluation and
- Manuscript writing with corrections by C. Janiak
- S. Dey: membrane preparation and draft writing
- S. Sorribas: mixed-gas measurements
- A. Nuhnen: participated in calculations for Maxwell model and FFV
- A. Bhunia: provided CTF-1 and analytical information

The work presented in this chapter has been published as:

Synthesis and characterization of covalent triazine framework CTF-1@polysulfone mixed matrix membranes and their gas separation studies

Subarna Dey[1†], Stefanie Bügel[1†], Sara Sorribas[2], Alexander Nuhnen[1], Asamanjoy Bhunia[1], Joaquín Coronas[2] and Christoph Janiak[1*]

[1] Institut für Anorganische Chemie und Strukturchemie, Heinrich-Heine-Universität Düsseldorf, Düsseldorf, Germany

[2] Chemical and Environmental Engineering Department and Instituto de Nanociencia de Aragon, Instituto de Ciencia de Materiales de Aragón (ICMA), Universidad de Zaragoza-CSIC, Zaragoza, Spain

[†]These authors have contributed equally to this work

*Correspondence: Christoph Janiak; janiak@uni-duesseldorf.de

Abstract

Covalent triazine framework CTF-1 and polysulfone (PSF) are used to form mixed-matrix membranes (MMMs) with 8, 16, and 24 wt% of the porous filler material CTF-1. Studies on permeability and selectivity are carried out concerning the gases O_2, N_2, CO_2 and CH_4. CO_2 permeability of the synthesized MMMs increases by 5.4 Barrer in comparison to the pure PSF membrane. The selectivity remains unchanged for O_2/N_2 and CO_2/CH_4 but was found to be increased for CO_2/N_2. Further, comparisons to theoretical models for permeability prediction yield a permeability for CTF-1 which is about six times higher than the permeability of PSF. The inverse of the sum of the free fractional volumes (FFV) of the polymer and the filler correlate linearly to the logarithm of the permeabilities of the gases which conversely indicates that the porosity of the filler contributes to the gas transport through the membrane.

Keywords: *covalent triazine framework (CTF), polysulfone (PSF), mixed-matrix membrane (MMM), gas selectivity, free fractional volume*

Introduction

During the last decades membrane-based separation technology has experienced a major expansion in the gas separation industry due to advantages like low operating costs, ease of operation, minimum energy requirement, and environmental friendliness. Currently membrane-

based technology is used in the chemical and petrochemical industry, for natural gas purification, hydrogen separation, nitrogen recovery, and olefin/paraffin separation (Koros and Fleming, 1993; Strathmann, 2001; Baker, 2002; Zhang et al., 2008). Polymeric membranes have been studied widely for their low costs, high processability, and good intrinsic transport properties. However, pure polymer membranes face a reciprocal trade-off relationship between permeability and selectivity (Shimekit et al., 2011). Inorganic membranes, in spite of having outstanding separation properties, good thermal, mechanical and chemical stability, suffer from high production costs, lack of processability, difficulties in large-scale production, and brittleness (Dong et al., 2013). As an alternative to polymer and inorganic membranes, mixed matrix membranes (MMMs) have attracted major attention due to their low costs, high permeabilities, and possibly selectivities above the Robeson upper-bound limit (Dong et al., 2013). A typical MMM contains a bulk continuous polymer phase and a dispersed inorganic particle phase. Polymers that are generally used to fabricate MMMs include polysulfone, polyarylates, polycarbonates, poly(arylethers), poly(arylketones), and polyimides (Tanh Jeazet et al., 2012). Porous materials that are generally incorporated to fabricate MMMs are carbon molecular sieves, zeolites, mesoporous materials, activated carbons, carbon nanotubes, and metal organic frameworks (MOFs) (Buonomenna et al., 2012; Tanh Jeazet et al., 2012; Bastani et al., 2013; Dong et al., 2013). In recent years porous organic polymers (POPs) or covalent organic frameworks (COFs) have also been explored to fabricate such membranes (Dechnik et al., 2017). A subcategory of POPs/COFs are nitrogen-rich covalent triazine frameworks (CTFs). CTFs were first developed by Kuhn et al. by a polymerization reaction of aromatic di- or trinitrile building blocks under ionothermal conditions at 400–700°C using an excess of ZnCl2. The latter acts as a Lewis acid catalyst and solvent (porogen) for the polymerization reaction (Kuhn et al., 2008). Up to now, only few examples of CTF membranes were reported. Tang et al. reported an in situ fabricated neat CTF-membrane made from 4,4′-biphenyldicarbonitrile, which exhibits a high water permeability of 75600 Barrer and a water/ethanol selectivity of 101 for the dehydration of an 85 wt% ethanol aqueous solution at 45°C (Tang et al., 2015). Ying et al. developed a strategy for a graphene-oxide assisted restacking method to fabricate an ultrathin CTF-1 membrane, which showed a H_2/CO_2 selectivity of 22.3 (Ying et al., 2016). High surface area, low density, excellent thermal and chemical stability with a large number of nitrogen functionalities make CTFs potential candidates for gas storage and separation (Bhunia et al., 2013; Dey et al., 2017). These facts suggested us to fabricate MMMs by using CTF-1 as a filler. The glassy polymer PSF was chosen as a matrix due to its good mechanical properties including a good film-formation

behavior (Dechnik et al., 2016). The prepared MMMs (8, 16, and 24 wt% of CTF-1) were tested for O_2/N_2, CO_2/N_2, and CO_2/CH_4 separation.

Materials and Methods

Materials

All chemicals were purchased from commercial suppliers (Sigma-Aldrich, Acros Organics, and Alfa Aesar chemical company). Polysulfone (PSF) Ultrason S 6010 Natural was provided by BASF AG, Ludwigshafen, Germany. The gases O_2, N_2, CO_2, and CH_4 were supplied by Air Liquide (Germany) and used as received (purity 99.99%).

Methods

Elemental analysis (CHN) was carried out on a PerkinElmer 2400 series 2 elemental analyzer. Thermal gravimetric analysis (TGA) was performed on a Netzsch TG 209 F3 Tarsus thermal gravimetric analyzer with a ramp rate of 5°C/min. A Bruker FT-IR Tensor 37 Spectrometer was used to obtain infrared (IR) spectra in the 4,000–550 cm^{-1} region with a 2 cm^{-1} resolution. Measurements were carried out on KBr disks. Powder X-ray diffraction (PXRD) was performed on a Bruker D2 Phaser diffractometer using Cu $K_{\alpha1/\alpha2}$ radiation with $\lambda = 1.5418$ Å at 30 kV. 2θ angles in the range of 5–80° over a time of 2 h (0.01°/sec) were covered. Scanning electron microscopy (SEM) images were created by using a secondary electron (SE) detector equipped ESEM Quanta 400 FEG SEM. Sorption isotherms were obtained from a Micromeritics ASAP 2020 automatic gas sorption analyzer equipped with an oil-free vacuum pump (ultimate vacuum $<10^{-8}$ mbar). Selectivity factors based on ideal adsorbed solution theory (IAST) were calculated using the software 3Psim version 1.1.0.7. Skeletal density was determined with a Helium pycnometer, Micromeritics AccuPyc 1330. For determination of the permeability of the membranes, firstly the thickness of the membranes was measured on 10 different points using a micrometer screw. The gas permeation experiments were performed as described by Tanh Jeazet et al. (2016). The membrane with an area of 11.3 cm^2 was placed into a permeation cell. First the permeate side was evacuated followed by evacuation of the feed side. The valve on the feed side was kept closed while pressurizing to approximately 3 bar for 2 h with a single gas. The line between vacuum pump and permeate side was closed followed by the adjustment of the feed pressure. The pressure on the permeate side was increased as the gas permeated from the feed side through the membrane to the permeate side. The linear rise of the pressure, recorded with an x-y printer, was used to calculate the permeability P in Barrer units. Permeability is defined as the gas flow rate multiplied by the thickness of the material, divided by the area and by the pressure difference across the material:

$$Permeability\ (P) = \frac{flow\ rate \times thickness}{area \times pressure\ difference} \quad (1)$$

$$P(1Barrer) = 10^{-10}\ \frac{cm^3(STP) \times cm}{cm^2 \times s \times cmHg} \quad (2)$$

In CGS system permeability unit is expressed as follows:

$$P = \frac{g \times cm}{sec \times cm^2 \times (dyne \times cm^{-2})} \quad (3)$$

The relationship of permeability in Barrer unit and CGS unit is

$$1\left[\frac{g \times cm}{sec \times cm^2 \times (dyne \times cm^{-2})}\right] = \frac{(2.9882 \times 10^{18})}{M}\left[10^{-10}\ \frac{cm^3(STP) \times cm}{sec \times cm^3 \times cm\ Hg}\right] \quad (4)$$

The ideal gas selectivity was calculated from the single gas permeabilities by using the following equation:

$$\alpha_{ideal\left(\frac{O_2}{N_2}\right)} = \frac{P_{O_2}}{P_{N_2}} \quad (5)$$

Synthesis of CTF-1

CTF-1 has been synthesized according to the following procedure (Kuhn et al., 2008): a mixture of terephthalonitrile (1.28 g, 10 mmol) and anhydrous $ZnCl_2$ (6.8 g, 50 mmol) were placed into a Pyrex ampoule under inert conditions. The ampoule was evacuated, sealed, and heated for 48 h at 400°C followed by cooling to room temperature. The black product was stirred with water for 72 h. Afterwards the product was isolated by filtration and again stirred with 200 mL of 2 mol/L aqueous HCl for 24 h. The resulting black powder was further washed with water, tetrahydrofuran (THF), acetone and dried under vacuum (yield 90 %).

Preparation of MMMs

The MMMs were prepared with 0, 8, 16, and 24 wt% of CTF-1. The filler loadings were calculated according to the following equation (6) where the filler mass must be divided by the total mass of the composite:

$$Filler\ loading\ (wt\%) = \frac{m_{filler}}{m_{polymer} + m_{filler}} \times 100\ \% \quad (6)$$

The PSF polymer (300mg) was dissolved in chloroform ($CHCl_3$) and CTF-1 was added to the polymer solution. The obtained dispersion was stirred for 1 week. Afterwards, the casting solution was treated for 30 min in an ultrasonic bath and was stirred for 30min again. This cycle was repeated three times. Before casting, the dispersion was kept under stirring for 30 more minutes. The dispersion was cast into metal rings placed on a flat glass surface. A paper tissue

covered funnel which was placed over the membrane after casting to prevent the contamination from dust particles as well as to control the evaporation rate. After solvent evaporation, the membrane was removed from the metal ring and was dried in a vacuum oven at 120°C overnight. The evaporation of $CHCl_3$ from the membrane dispersion forms smooth defect/crack free films upon evaporation. The preparation of MMMs with weight percentages higher than 24 was not possible due to instability and brittleness of the resulting membranes.

Results and discussion

Characterization of MMMs

The synthesized membranes were characterized by scanning electron microscopy (SEM) with the images depicted in **Figures 1**–**3**. **Figure 1** shows the top side and cross-section of a pure PSF flat membrane cast from $CHCl_3$.

The CTF-1 composite MMMs had black appearance and were more brittle than the pure PSF membrane. **Figures 2**, **3** depict top surface (air side) and cross section images of 8, 16, and 24 wt% of CTF-1 composite MMMs, respectively. **Figure 2** shows some, but rather few, of the CTF-1 particles at the top surfaces of the membranes. In case of sedimentation the specifically less dense CTF-1 particles should collect at the upper surface of the CH_2Cl_2 dispersion, which is obviously not the case. The SEM images of the membrane cross-sections (**Figure 3**) also indicate uniform dispersion of the CTF-1 material in the polymer matrix and no sedimentation of the CTF-1 particles was visible. The difference of the CTF-1 loading resulted in variation in the thickness of the composite membranes (**Table S4**). The surface images showed the incorporation of the CTF-1 particles into the polymer matrix which indicate the strong interfacial contact between PSF and CTF-1 material. The visible CTF-1 content is increased with its loading.

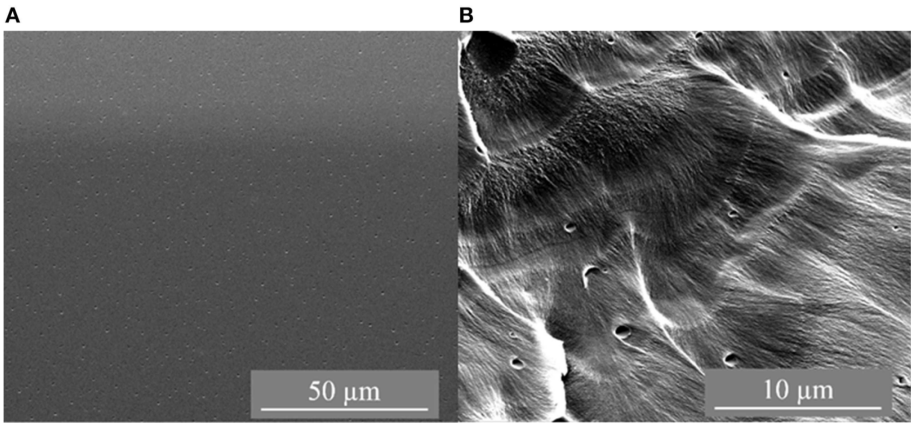

Figure 1: SEM images of pure PSF membrane [**(A)**: top side view; **(B)**: cross section view].

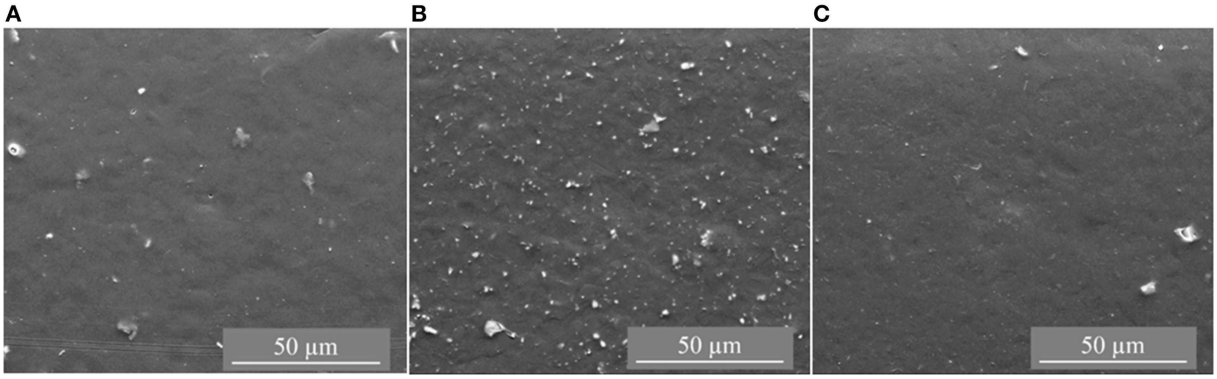

Figure 2: Top surface SEM images of 8 wt% **(A)**, 16 wt% **(B)** and 24 wt% **(C)** of CTF-1@PSF composite MMMs.

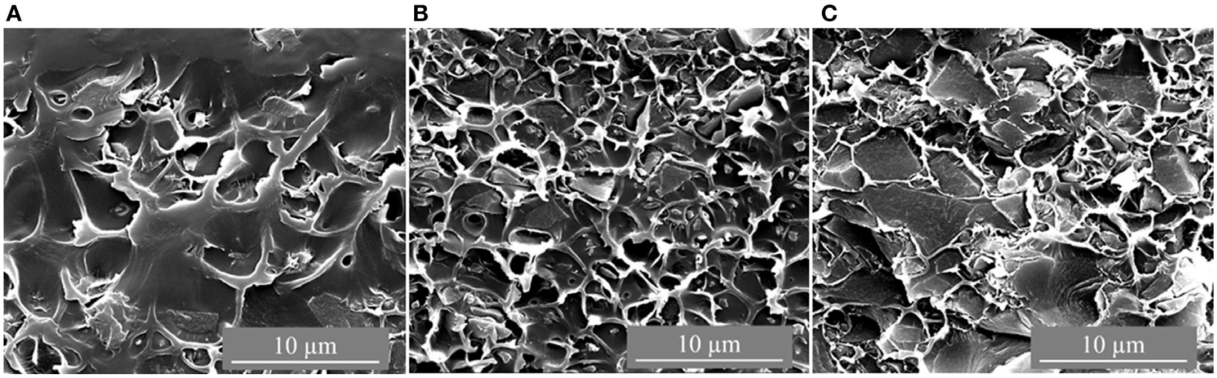

Figure 3: Cross-section SEM images of 8 wt% **(A)**, 16 wt% **(B)** and 24 wt% **(C)** of CTF-1@PSF MMM.

Gas Permeability and Selectivity

In order to examine the gas separation performance of the pure PSF membrane and CTF-1@PSF MMMs, single-gas (O_2, N_2, CO_2, and CH_4) permeation was carried out at 25°C and 3 bar. The gas permeabilities (O_2, N_2, CO_2, CH_4) and ideal selectivity factors (O_2/N_2, CO_2/CH_4, CO_2/N_2) for the pure PSF and CTF-1@PSF composite membranes are provided in **Table 1**.

Table 1: Gas permeabilities (O_2, N_2, CO_2, CH_4) and ideal selectivity factors (O_2/N_2, CO_2/CH_4, CO_2/N_2) for the pure PSF and CTF-1@PSF composite membranes.

CTF-1 load (wt%)	P O_2 (Barrer)	P N_2 (Barrer)	P CO_2 (Barrer)	P CH_4 (Barrer)	S O_2/N_2	S CO_2/N_2	S CO_2/CH_4
0	1.6 ± 0.0	0.3 ± 0.0	7.3 ± 0.2	0.3 ± 0.0	5 ± 1	23 ± 3	21 ± 3
8	2.1 ± 0.1	0.4 ± 0.0	9.2 ± 0.6	0.4 ± 0.0	5 ± 1	23 ± 3	21 ± 3
16	2.2 ± 0.1	0.4 ± 0.0	10.7 ± 0.6	0.5 ± 0.0	5 ± 1	24 ± 3	21 ± 3
24	2.6 ± 0.2	0.5 ± 0.0	12.7 ± 0.8	0.6 ± 0.0	5 ± 1	26 ± 3	22 ± 3

From exemplary case studies where we had the same membrane prepared several times and measured each of these membranes also several times we can generally deduce an error of 6% for permeability and 12% for selectivity through error propagation (6% + 6% for each gas permeability).

For dense polymer membranes, gas separation is usually explained by a solution–diffusion mechanism (Pandey and Chauhan, 2001; Tanh Jeazet et al., 2012), which states the permeability of gas molecules through membrane as a product of diffusivity (*D*) and solubility (*S*) (Chung et al., 2007):

$$P = D \times S \tag{7}$$

Diffusivity is the mobility of individual gas molecules passing through the voids between the polymeric chains of a membrane whereas gas solubility is controlled by the affinity of gas molecules toward the polymer. Addition of fillers to the polymeric membrane may affect both diffusivity and solubility which is related to physical properties of the fillers like particle size and particle agglomerations, and the polymer/particle interface morphologies, although the trend may not always be the same (Shan et al., 2016).

The permeability for the gases increases in proportion to the amount of CTF-1 present in the MMMs (**Figure 4**). The highest permeability for all the gases was found for the 24 wt% CTF-1@PSF membrane. The O_2 permeability is increased by 63 % (from 1.6 to 2.6 Barrer), N_2 permeability by 67 % (from 0.3 to 0.5 Barrer), CO_2 permeability by 74 % (from 7.3 to 12.7 Barrer), and CH_4 permeability is increased by 100 % (from 0.3 to 0.6 Barrer).

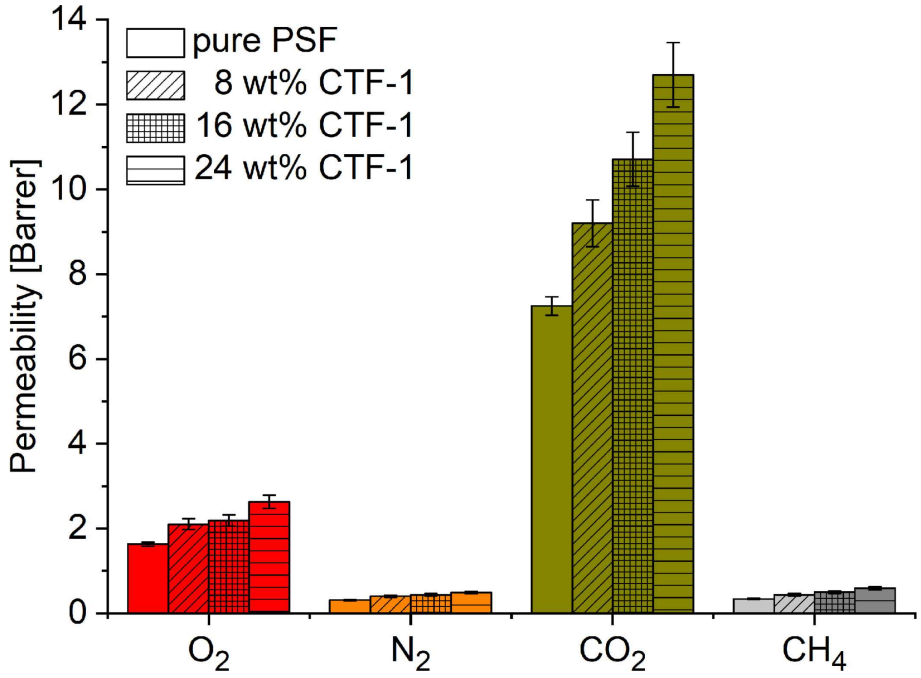

Figure 4: Gas permeability of 0, 8, 16, and 24 wt% of CTF-1@PSF composite MMMs for O_2, N_2, CO_2, and CH_4.

Figure 5 shows the graphical representation of the ideal selectivity values. There is no significant improvement observed for O_2/N_2 and CO_2/CH_4 selectivity. On the other hand, CO_2/N_2 selectivity was found to be increased from 23 to 26.

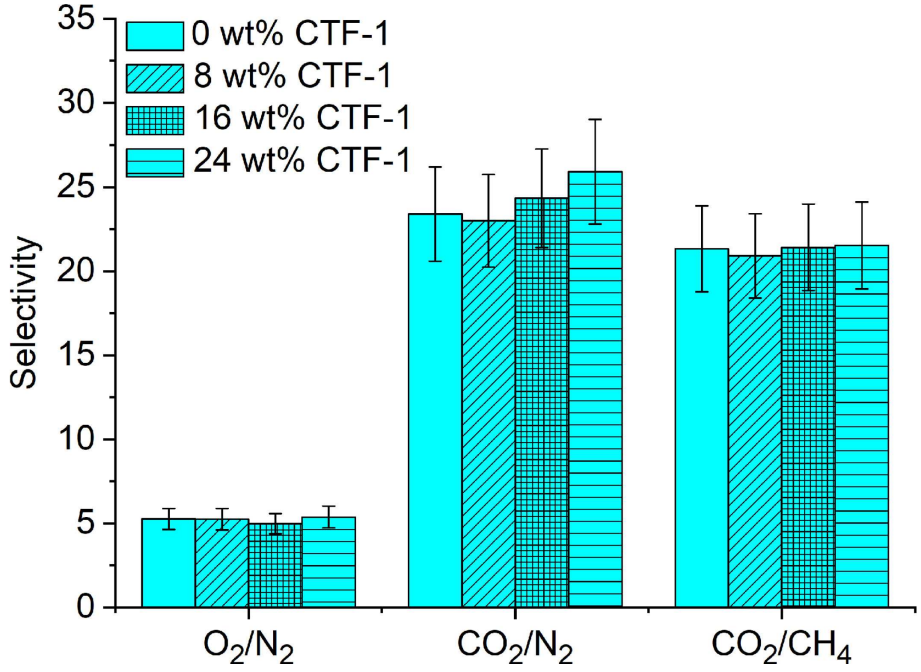

Figure 5: Gas selectivity of 0, 8, 16, and 24 wt% of CTF-1@PSF composite MMMs for O_2, N_2, CO_2, and CH_4.

Selective CO_2 over N_2 adsorption of pure CTF-1 (**Figure S7**; Section Ideal Adsorbed Solution Theory (IAST) Calculation in the **Supplementary Material**) was confirmed by application of

IAST (Myers and Prausnitz, 1965). The ideal selectivity factor for a binary CO_2/N_2 gas mixture at 1 bar pressure at 293 K is 46 and therefore explains the increase of selectivity with higher filler content in the MMMs. The higher CO_2 permeability as well as CO_2/N_2 separation factors measured for the MMMs can be rationalized by the selective adsorption of CO_2 in the nitrogen rich CTF-1 through dipole–quadrupole interactions (Li et al., 2014). When porous fillers (i.e., CTF-1) are added, the solubility may increase which is due to the higher affinity of CO_2 toward CTF-1, as well as selective diffusivity may increase as the free volume of MMMs increases. The presence of the microporous CTF with pore diameters mainly distributed at 5, 6, and 12 Å could also exert some preferential sieving of CO_2 (kinetic diameter of 0.33 nm) over N_2 (0.364 nm) or CH_4 (0.38 nm) (Li et al., 2004; Cecopieri-Gómez et al., 2007).

Generally, POPs or COFs (albeit not CTFs) were already used as filler materials in different MMMs for example with the polymers polybenzimidazole (PBI),Matrimid, or polyvinylamine (PVAm). Kang et al. incorporated two 2D COFs NUS-2 and NUS-3 as a filler in a polymer matrix (Ultem and PBI) and the membrane with 20 wt% of NUS-2 loading in PBI exhibited a H_2/CO_2 selectivity of 31.4 on single gas tests at high pressure which surpassed the 2008 Robeson upper bound limit (Kang et al., 2016). Shan et al. reported a MMM, using Matrimid and an azine linked COF i.e., ACOF-1, where the MMM with 16 wt% of ACOF-1 showed a CO_2 permeability two times higher than the pure Matrimid membrane (Shan et al., 2016). A more than 3-fold elevation in CO_2 permeability compared to the pure PVAm membrane was reported with an imine-linked COF (COF-LZU1) as filler (Cao et al., 2016). Fu et al. synthesized a COF/MOF (COF-300/ZIF-8) composite membrane which gives a H_2/CO_2 selectivity of 13.5 in comparison to the respective COF-300 (6.0) and ZIF-8 (9.1) membranes (Fu et al., 2016). Biswal et al. introduced two hybrid membranes such as TpPa-1@PBI-BuI and TpBD@PBI-BuI (BuI = 5-t-butylisophthalic acid). Almost seven times higher permeabilities for the gases H_2, N_2, CO_2, and CH_4 could be achieved compared to the pure polymer membranes (Biswal et al., 2016). These aforementioned types of POPs have, however, low chemical and thermal stability, which limits the use for MMM based gas separation. Porous CTFs on the other hand, feature high thermal and chemical stability and often show a high CO_2 uptake capacity and good selectivity toward CO_2/N_2 (Zhao et al., 2013; Hug et al., 2015).

So far, no CTF-based mixed-matrix membranes have been studied for gas permeation, to the best of our knowledge. A direct comparison can be made to a pure CTF membrane, named TFM-1 derived from 4,4′-biphenyldicarbonitrile (DCBP). The single gas CO_2/N_2 selectivity value of 26 for the 24 wt% CTF-1 membrane is comparable to CO_2/N_2 selectivity of this pure

TFM-1 membrane (29 ± 2) (Zhu et al., 2012). Further, we can compare our CTF-1@PSF MMMs only to related porous organic polymer MMMs. From an N-rich Schiff based porous organic framework (SNW-1) which was constructed from melamine and di-aldehydes the derived best PSF-MMMs yielded higher CO_2 and N_2 gas permeabilities than CTF-1@PSF but a similar CO_2/N_2 selectivity of 29 in single gas measurements (Gao et al., 2014). The CO_2 permeability of 12.7 Barrer and the selectivity of 26 in the 24 wt% CTF-1@PSF MMM is similar or even slightly better to the performance of the azobenzene-based nanoporous polymer, called Azo-COP-2, in a PSF matrix with 14.8 Barrer and a CO_2/N_2 selectivity of 23 (Li et al., 2019).

We have also performed mixed gas separation measurements for 400mg PSF membranes (**Table S5**) for 8 and 16 wt% CTF-1@PSF MMMs. The selectivities of 8 wt% and 16 wt% of CTF-1 loading MMMs for an equimolar (50/50) gas mixture of CO_2 and CH_4 were found to be 40 and 42 which is higher than the single gas selectivity. Compared to single gas permeation tests, mixed gas permeation tests give higher selectivity due to the competitive adsorption and diffusion of the binary gas components in the membrane. Due to the smaller molecular size and high affinity of the CO_2 molecule to the basic triazine unit of CTF-1, CO_2 favorably adsorbed to the CTF-1 loaded MMMs, which reduces the diffusion of CH_4 in the membranes due to pore blocking by adsorbed CO_2 (Kang et al., 2016).

Maxwell Model

A way to predict the permeability of MMMs is the application of the Maxell model. In its original form it can be used for low filler contents (ϕ_d up to 0.2), to exclude interactions among the filler particles (Bouma et al., 1997; Kanehashi et al., 2015). The Maxwell equation can be expressed by Equation (8):

$$P_{eff} = P_c \times \frac{P_d + 2P_c - 2\phi_d \times (P_c - P_d)}{P_d + 2P_c + \phi_d \times (P_c - P_d)} \quad (8)$$

P_d is given as the filler permeability and P_c is the permeability of the pure polymer membrane. ϕ_d is the volume fraction of the filler phase according to Equation (9).

$$\phi_d = \frac{w_d / \rho_d}{\frac{w_c}{\rho_c} + \frac{w_d}{\rho_d}} \quad (9)$$

A "reduced permeation polarizability" β can be defined as given in Equation (10) (Basu et al., 2010),

$$\beta = \frac{P_d - P_c}{P_d + 2P_c} \tag{10}$$

and consequently Equation (8) can be simplified to Equation (11):

$$P_{eff} = P_c \times \frac{1 + 2\beta \times \phi_d}{1 - \beta \times \phi_d} \tag{11}$$

The value of β describes the difference in permeability between the continuous or polymer phase (with P_c) and the dispersed or filler phase (with P_d). There are three limiting cases which can be considered: The filler is much more permeable than the polymer, that is $P_d >> P_c$ and $\beta \approx 1$; both filler and polymer are equally permeable, that is $P_d = P_c$ and $\beta = 0$ and the filler is nonpermeable or $P_d << P_c$ and $\beta \approx -0.5$ (Basu et al., 2010). In case of CTF-1 being regarded as a highly-permeable filler material ($P_d >> P_c$), the following equation (12) is used:

$$\frac{P_{eff}}{P_c} = \frac{1 + 2\phi_d}{1 - \phi_d} \tag{12}$$

The plot P_{eff}/P_c vs. ϕ_d is presented in **Figure 6**. The comparison with the theoretical Maxwell plot shows an agreement only in the range of very low filler contents. With a higher volume fraction of the filler, the theoretical Maxwell model predicts a higher increase in permeability. The Maxwell model describes an ideal case, which is also based on the assumption of an ideal distribution of the filler particles and the spherical shape of the filler particles (Bouma et al., 1997). The deviation from the model could be explained by the non-spherical shape of the CTF-1 particles. Another reason could be the penetration of PSF polymer chains into the pores of CTF-1 and thus a loss off free volume of the filler (Li et al., 2005).

If the pores in CTF-1 would be fully blocked and the filler thereby becomes nearly non-permeable we have the limiting case of $P_d << P_c$ and $\beta \approx -0.5$ with equation (13), with the plot of P_{eff}/P_c vs. ϕ_d also included in **Figure 6**:

$$\frac{P_{eff}}{P_c} = \frac{1 - \phi_d}{1 + 0.5\phi_d} \tag{13}$$

From **Figure 6** it is evident that the measured permeability lies between the limiting case with $P_d >> P_c$ and the case where both filler and polymer are equally permeable, that is $P_d = P_c$ with $P_{eff}/P_c = 1$. In order to therefore approximate the experimental permeability, we can assume $P_d = 6P_c$ with $\beta = 0.625$ to give Equation (14):

$$\frac{P_{eff}}{P_c} = \frac{1 + 1.25\phi_d}{1 - 0.625\phi_d} \tag{14}$$

The plot of Equation (14) is depicted in **Figure 6** and the experimental values show good agreement with the model.

An overview of other models for the case $P_d >> P_c$, including Bruggeman (1935), Higuchi (Higuchi and Higuchi, 1960; Shen and Lua, 2013), and Böttcher-Landauer (Hashin and Shtrikman, 1962) for P_{eff}/P_c vs. filler fraction is given in **Figure S9** (Section Other Permeability Models for 300mg Membranes in the **Supplementary Material**). It is evident that the other models overestimate the permeability even more strongly than the Maxwell model for $P_d >> P_c$.

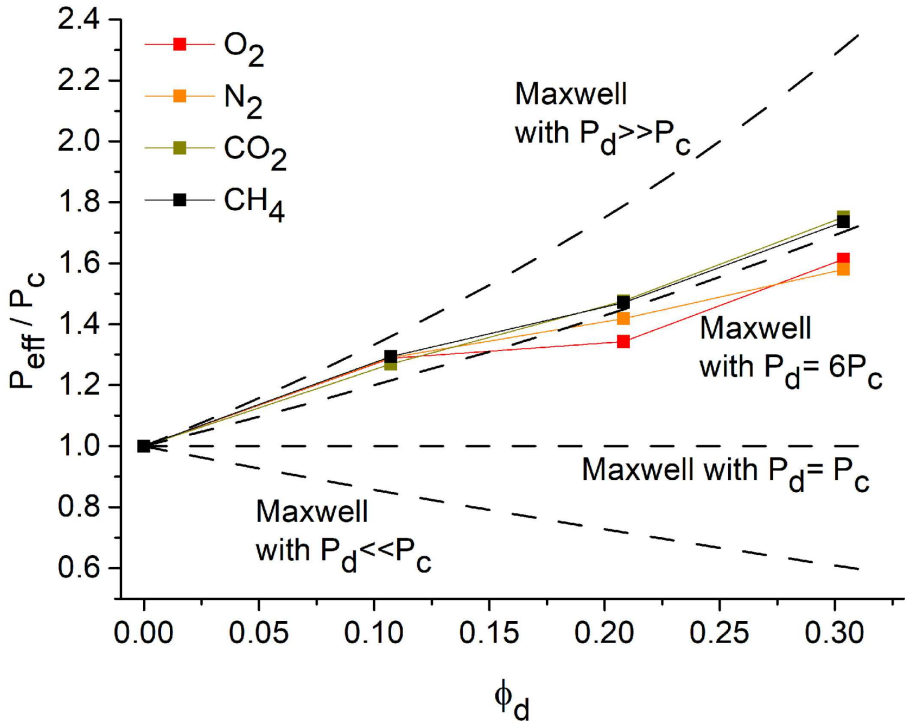

Figure 6: P_{eff}/P_c vs. ϕ_d. Measured permeabilities for the pure polymer and the polymer with 8, 16, and 24 wt% of the filler in comparison to the Maxwell model with different relations between P_{eff} and P_c (dashed lines).

Fractional Free Volume (FFV)

The FFV of the filler was calculated by multiplication of the density (ρ_d in g/cm^3) and the pore volume (cm^3/g) (Thran et al., 1999). He-pycnometry combined with BET-sorption measurement was used to determine the density (ρ_d) of CTF-1 (ρ_d = 0.89 g/cm^3, dispersed phase) and the pore volume of 0.42 cm^3/g was given by BET-sorption analysis. The density of PSF (ρ_d = 1.23 g/cm^3, continuous phase) as well as the $FFV_{polymer}$ (0.156) is used according to the literature (Thran et al., 1999; Anaya et al., 2014). In order to calculate the (total) FFV of the MMM both the FFV of the polymer and of the filler are multiplied by their respective volume fractions, ϕ_c and ϕ_d, and summed up according to Equation (15). The volume fraction of the polymer ϕ_c was determined in analogy to Equation (9).

$$(total)FFV = FFV_{polymer} \times \phi_c + FFV_{filler} \times \phi_d \quad (15)$$

Figure 7 presents the logarithm of the measured gas permeabilities (lg *P*) for O_2, N_2, CO_2, and CH_4 as a function of the inverse FFV for pure PSF, 8, 16, and 24 wt% of CTF-1. The FFV for 8 wt% of the filler is 0.18, loadings of 16 and 24 wt% show values of 0.20 and 0.22. Independent from gas all plots show a linear correlation.

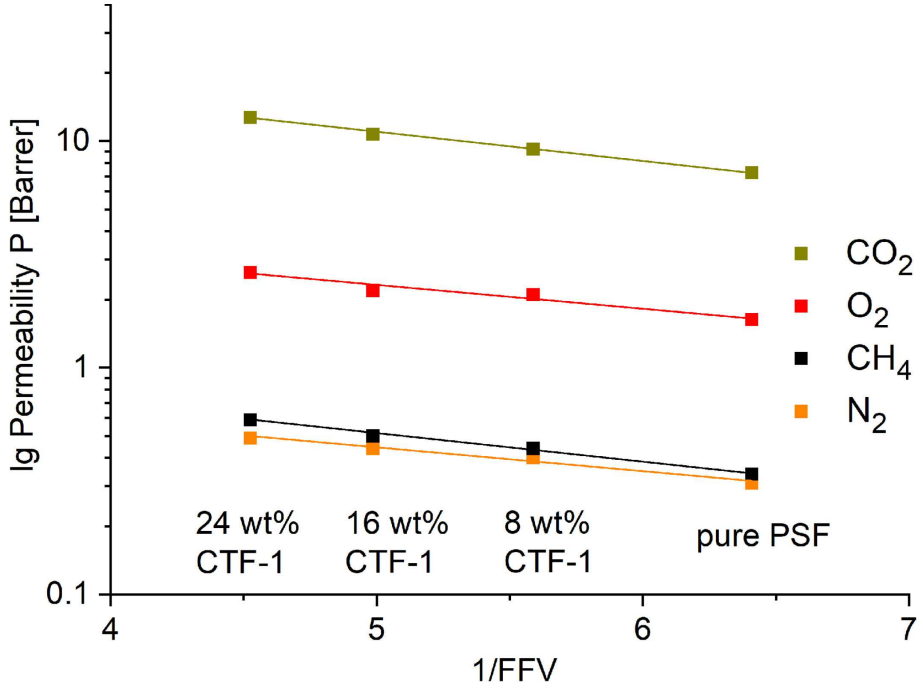

Figure 7: Logarithmic plot of the experimental O_2, N_2, CO_2, and CH_4 permeabilities vs. the inverse (total) FFV of the pure polymer and the polymer with 8, 16, and 24 wt% of the filler.

Conclusion

In summary, we have successfully synthesized for the first time mixed matrix membranes containing thermally and chemically stable CTF-1 and PSF. Overall six MMMs have been casted in this study by using PSF with 8, 16, and 24 wt% CTF-1. The SEM images of the membrane cross-sections show uniform dispersion of the CTF-1 material in the polymer matrix, whereas the surface images of the MMMs indicate the strong interfacial contact between PSF and CTF-1 material. The fabricated membranes exhibit higher CO_2 permeabilities (12.7 Barrer for 24 wt% of CTF-1 loading) than the pure PSF membrane (7.3 Barrer). For other gases there are no significant improvements in the permeability. The MMMs show higher CO_2/N_2 selectivity (26 for 24 wt% of CTF-1 loading) compared to pure PSF membrane (23), the selectivity increases with increasing of CTF loading. The results for higher filler contents differ from the Maxwell model for porous fillers, but a constant increase of permeability can be observed for the gases CO_2 and CH_4 and a modified Maxwell model was successfully applied. The increased gas permeability follows linearly the inverse of the total free fractional volume,

which indicates that both free fractional volume of the polymer and the filler contribute to the permeability.

Data availability statement

All datasets generated for this study are included in the article/**SupplementaryMaterial.**

Author contributions

SD synthesized membranes and wrote half of the manuscript. SB wrote half of manuscript and applied permeability models, FFV, and drew the graphics. SS carried out mixed gas measurements. AN participated in calculations for Maxwell model and FFV. AB provided CTF-1 and related analytical information. JC was involved in mixed gas measurements and interpretation. CJ proofread and refined the manuscript.

Funding

Open access publication fees were covered by Heinrich-Heine-University.

Acknowledgments

Financial support from the Spanish MINECO and FEDER (MAT2016-77290-R), the Aragón Government (T43-17R), and the ESF was gratefully acknowledged by JC. The work of CJ was supported by the Federal German Ministry of Education and Research (BMBF) under grant Optimat 03SF0492C.

Supplementary materials

The Supplementary Material for this article can be found online at: https://www.frontiersin.org/articles/10.3389/fchem.2019.00693/full#supplementary-material

Conflict of Interest: The authors declare that the research was conducted in the absence of any commercial or financial relationships that could be construed as a potential conflict of interest.

References

Anaya, S., Serrano, B., Herrero, B., Cervera, A., and Baselga, J. (2014). g-alumina modification with long chain carboxylic acid surface nanocrystals for biocompatible polysulfone nanocomposites. *ACS Appl. Mater. Interfaces* 6, 14460–14468. doi: 10.1021/am503744z

Baker, R. W. (2002). Future directions of membrane gas separation technology. *Ind. Eng. Chem. Res.* 41, 1393–1411. doi: 10.1021/ie0108088

Bastani, D., Esmaeili, N., and Asadollahi, M. (2013). Polymeric mixed matrix membranes containing zeolites as a filler for gas separation applications: a review. *J. Ind. Eng. Chem.* 19, 375–393. doi: 10.1016/j.jiec.2012.09.019

Basu, S., Cano-Odena, A., and Vankelecom, I. F. J. (2010). Asymmetric Matrimid® /[$Cu_3(BTC)_2$] mixed-matrix membranes for gas separations. *J. Membr. Sci.* 362, 478–487. doi: 10.1016/j.memsci.2010.07.005

Bhunia, A., Vasylyeva, V., and Janiak, C. (2013). From a supramolecular tetranitrile to a porous covalent triazine-based framework with high gas uptake capacities. *Chem. Commun.* 49, 3961–3963. doi: 10.1039/c3cc41382a

Biswal, B. P., Chaudhari, H. D., Banerjee, R., and Kharul, U. K. (2016). Chemically stable covalent organic framework (COF)-polybenzimidazole hybrid membranes: enhanced gas separation through pore modulation. *Chem. Eur. J.* 22, 4695–4699. doi: 10.1002/chem.201504836

Bouma, R. H. B., Checchetti, A., Chidichimo, G., and Drioli, E. (1997). Permeation through a heterogeneous membrane: the effect of the dispersed phase. *J. Membr. Sci.* 128, 141–149. doi: 10.1016/S0376-7388(96)00303-1

Bruggeman,D. A. G. (1935). Berechnung verschiedener physikalischer Konstanten von heterogenen Substanzen. 1. Dielektrizitätskonstanten und Leitfähigkeiten der Mischkörper aus isotropen Substanzen. *Ann. Phys.* 24, 636–679. doi: 10.1002/andp.19354160705

Buonomenna, M. G., Yave, W., and Golemme, G. (2012). Some approaches for high performance polymer based membranes for gas separation: block copolymers, carbon molecular sieves and mixed matrix membranes, *RSC Adv*. 2, 10745–10773. doi: 10.1039/c2ra20748f

Cao, X., Qiao, Z., Wang, Z., Zhao, S., Li, P., Wang, J., et al. (2016). Enhanced performance of mixed matrix membrane by incorporating a highly compatible covalent organic framework into poly(vinylamine) for hydrogen purification. *Int. J. Hydrogen Energy* 41, 9167–9174. doi: 10.1016/j.ijhydene.2016.01.137

Cecopieri-Gómez, M. L., Palacios-Alquisira, J., and Domínguez, J. M. (2007). On the limits of gas separation in CO_2/CH_4, N_2/CH_4 and CO_2/N_2 binary mixtures using polyimide membranes. *J. Membr. Sci.* 293, 53–65. doi: 10.1016/j.memsci.2007.01.034

Chung, T.-S., Jiang, L. Y., Li, Y., and Kulprathipanja, S. (2007). Mixed matrix membranes (MMMs) comprising organic polymers with dispersed inorganic fillers for gas separation. *Prog. Polym. Sci.* 32, 483–507. doi: 10.1016/j.progpolymsci.2007.01.008

Dechnik, J., Gascon, J., Doonan, C. J., Janiak, C., and Sumby, C. J. (2017). Mixed-matrix membranes. *Angew. Chem. Int. Ed.* 56, 9292–9310. doi: 10.1002/anie.201701109

Dechnik, J., Muhlbach, F., Dietrich, D., Wehner, T., Gutmann, M., Luhmann, T., et al. (2016). Luminescent metal–organic framework mixed-matrix membranes from lanthanide metal–organic frameworks in polysulfone and matrimid. *Eur. J. Inorg. Chem.* 4408–4415. doi: 10.1002/ejic.201600235

Dey, S., Bhunia, A., Boldog, I., and Janiak, C. (2017). A mixed-linker approach towards improving covalent triazine-based frameworks for CO_2 capture and separation. *Micropor. Mesopor. Mater.* 241, 303–315. doi: 10.1016/j.micromeso.2016.11.033

Dong, G., Li, H., and Chen, V. (2013). Challenges and opportunities for mixed matrix membranes for gas separation. *J. Mater. Chem. A* 1, 4610–4630. doi: 10.1039/c3ta00927k

Fu, J., Das, S., Xing, G., Ben, T., Valtchev, V., and Qiu, S. (2016). Fabrication of COF-MOF composite membranes and their highly selective separation of H_2/CO_2. *J. Am. Chem. Soc.* 138, 7673–7680. doi: 10.1021/jacs.6b03348

Gao, X., Zou, X., Ma, H., Meng, S., and Zhu, G. (2014). Highly selective and permeable porous organic framework membrane for CO_2 capture. *Adv. Mater.* 26, 3644–3648. doi: 10.1002/adma.201400020

Hashin, Z., and Shtrikman, A. (1962). Variational approach to the theory of the effective magnetic permeability of multiphase materials. *J. Appl. Phys.* 33, 3125–3131. doi: 10.1063/1.1728579

Higuchi, W. I., and Higuchi, T. (1960). Theoretical analysis of diffusional movement through heterogeneous barriers. *J. Am. Pharm. Assoc. Sci.* 49, 598–606. doi: 10.1002/jps.3030490910

Hug, S., Stegbauer, L., Oh, H., Hirscher, M., and Lotsch, B. V. (2015). Nitrogen-rich covalent triazine frameworks as high-performance platforms for selective carbon capture and storage. *Chem. Mater.* 27, 8001–8010. doi: 10.1021/acs.chemmater.5b03330

Kanehashi, S., Chen, G. Q., Scholes, C. A., Ozcelik, B., Hua, C., Ciddor, L., et al. (2015). Enhancing gas permeability in mixed matrix membranes through tuning the nanoparticle properties. *J. Membr. Sci.* 482, 49–55. doi: 10.1016/j.memsci.2015.01.046

Kang, Z., Peng, Y., Qian, Y., Yuan, D., Addicoat, M. A., Heine, T., et al. (2016). Mixed matrix membranes (MMMs) comprising exfoliated 2D covalent organic frameworks (COFs) for efficient CO_2 separation. *Chem. Mater.* 28, 1277–1285. doi: 10.1021/acs.chemmater.5b02902

Koros, W. J., and Fleming, G. K. (1993). Membrane-based gas separation. *J. Membr. Sci.* 83, 1–80. doi: 10.1016/0376-7388(93)80013-N

Kuhn, P., Antonietti, M., and Thomas, A. (2008). Porous, covalent triazine-based frameworks prepared by ionothermal synthesis. *Angew. Chem. Int. Ed.* 47, 3450–3453. doi: 10.1002/anie.200705710

Li, S., Falconer, J. L., and Noble, R. D. (2004). SAPO-34 membranes for CO_2/CH_4 separation, *J. Membr. Sci.* 241, 121–135. doi: 10.1016/j.memsci.2004.04.027

Li, S., Prasetya, N., and Ladewig, B. P. (2019). Investigation of Azo-COP-2 as a photoresponsive low-energy CO_2 adsorbent and porous filler in mixed matrix membranes for CO_2/N_2 separation. *Ind. Eng. Chem. Res.* 58, 9959–9969. doi: 10.1021/acs.iecr.9b00762

Li, Y., Chung, T.-S., Cao, C., and Kulprathipanja, S. (2005). The effects of polymer chain rigidification, zeolite pore size and pore blockage on polyethersulfone (PES)-zeolite A mixed matrix membranes. *J. Membr. Sci.* 260, 45–55. doi: 10.1016/j.memsci.2005.03.019

Li, Z., Feng, X., Zou, Y., Zhang, Y., Xia, H., Liu, X., et al. (2014). A 2D azine-linked covalent organic framework for gas storage applications. *Chem. Commun.* 50, 13825–13828. doi: 10.1039/C4CC05665E

Myers, A. L., and Prausnitz, J. M. (1965). Thermodynamics of mixed-gas adsorption. *AICHE J.* 11, 121–127. doi: 10.1002/aic.690110125

Pandey, P., and Chauhan, R. S. (2001). Membranes for gas separation. *Prog. Polym. Sci.* 26, 853–893. doi: 10.1016/S0079-6700(01)00009-0

Shan, M., Seoane, B., Rozhko, E., Dikhtiarenko, A., Clet, G., Kapteijn, F., et al. (2016). Azine-linked covalent organic framework (COF)-based mixed matrix membranes for CO_2/CH_4 separation. *Chem. Eur. J.* 22, 14467–14470. doi: 10.1002/chem.201602999

Shen, Y., and Lua, A. I. (2013). Theoretical and experimental studies on the gas transport properties of mixed matrix membranes based on polyvinylidene fluoride. *AICHE J.* 59, 4715–4726. doi: 10.1002/aic.14186

Shimekit, B., Mukhtar, H., and Murugesan, T. (2011). Prediction of the relative permeability of gases in mixed matrix membranes. *J. Membr. Sci.* 373, 152–159. doi: 10.1016/j.memsci.2011.02.038

Strathmann, H. (2001). Membrane separation processes: current relevance and future opportunities. *AICHE J.* 47, 1077–1087. doi: 10.1002/aic.690470514

Tang, Y. P., Wang, H., and Chung, T. S. (2015). Towards high water permeability in triazine-framework-based microporous membranes for dehydration of ethanol. *ChemSusChem* 8, 138–147. doi: 10.1002/cssc.201402816

Tanh Jeazet, H. B., Sorribas, S., Román-Marín, J. M., Zornoza, B., Téllez, C., and Coronas, J. (2016). Increased selectivity in CO_2/CH_4 separation with mixed matrix membranes of polysulfone and mixed-MOFs MIL-101(Cr) and ZIF-8. *Eur. J. Inorg. Chem.* 27, 4363–4367. doi: 10.1002/ejic.201600190

Tanh Jeazet, H. B., Staudt, C., and Janiak, C. (2012). Metal–organic frameworks in mixed-matrix membranes for gas separation. *Dalton Trans.* 41, 14003–14027. doi: 10.1039/c2dt31550e

Thran, S., Kroll, G., and Faubel, F. (1999). Correlation between fractional free volume and diffusivity of gas molecules in glassy polymers. *J. Polym. Sci. B* 37, 3344–3358. doi: 10.1002/(SICI)1099-0488(19991201)37:23<3344::AIDPOLB10>3.0.CO;2-A

Ying, Y., Liu, D., Ma, J., Tong, M., Zhang, W., Huang, H., et al. (2016). A GO-assisted method for the preparation of ultrathin covalent organic framework membranes for gas separation. *J. Mater. Chem. A* 4, 13444–13449. doi: 10.1039/C6TA04579K

Zhang, Y., Musselman, I. H., Ferraris, J. P., and Balkus, J.r., K.J. (2008). Gas permeability properties of Matrimid membranes containing the metal-organic framework Cu–BPY–HFS. *J. Membr. Sci.* 313, 170–181. doi: 10.1016/j.memsci.2008.01.005

Zhao, Y. F., Yao, K. X., Teng, B. Y., Zhang, T., and Han, Y. (2013). A perfluorinated covalent triazine-based framework for highly selective and water–tolerant CO_2 capture. *Energy Environ. Sci.* 6, 3684–3692. doi: 10.1039/c3ee42548g

Zhu, X., Tian, C., Mahurin, S. M., Chai, S.-H., Wang, C., Brown, S., et al. (2012). A Superacid-catalyzed synthesis of porous membranes based on triazine frameworks for CO_2 separation. *J. Am. Chem. Soc.* 134, 10478–10484. doi: 10.1021/ja304879c

Supplementary Material

Synthesis and characterization of covalent triazine framework CTF-1@polysulfone mixed matrix membranes and their gas separation studies

Table of contents

S.1. Characterization of CTF-1

CTF-1 was used from the same batch as mentioned in the work of Bhunia et al. (Bhunia et al., 2015). The idealized structure of CTF-1 is shown in Scheme S1.

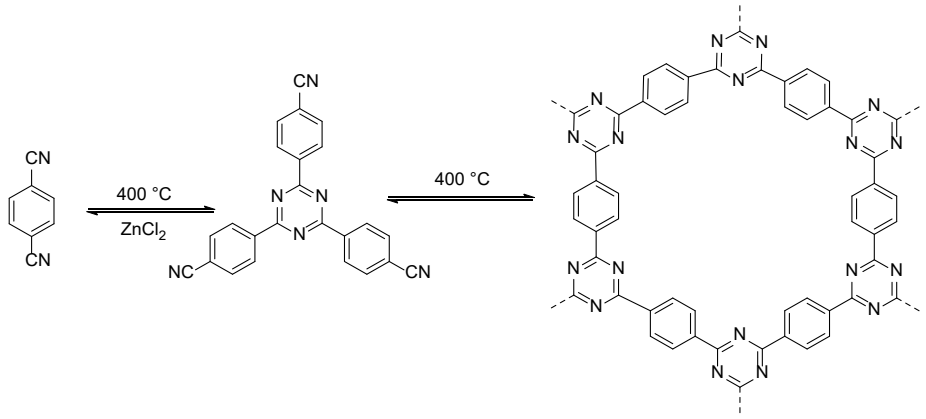

Scheme S1: Idealized structure of CTF-1 from the polymerization of terephthalonitrile.

The IR spectrum (**Fig. S1**) at 2225 cm^{-1} indicated the presence of unreacted nitrile groups in the polymer. The strong IR band around 1514 cm^{-1} is due to the C–N stretching mode of the triazine ring, whereas the band at 1352 cm^{-1} is due to in-plane stretching vibrations of the triazine ring (Hug et al., 2014). From TGA it is observed that the CTF-1 is stable up to 450 °C. The PXRD pattern (**Fig. S2**) displayed the crystalline nature of the CTF with hexagonal packing of pores (Bhunia et al., 2013). The SEM image (**Fig. S3**) showed that the material consisted particles of irregular shapes with an average particle size of about 10 μm. Elemental analysis of CTF-1 (**Table S1**) showed much lower nitrogen content which is due to nitrogen elimination during the high temperature polymerization reaction as observed by us and others (Bhunia et al., 2013). The density of CTF-1 was determined by addition of the volume of CTF-1 measured by He-pycnometry and the pore volume obtained by N_2 sorption. The mass of the sample was divided by the sum of the volumes.

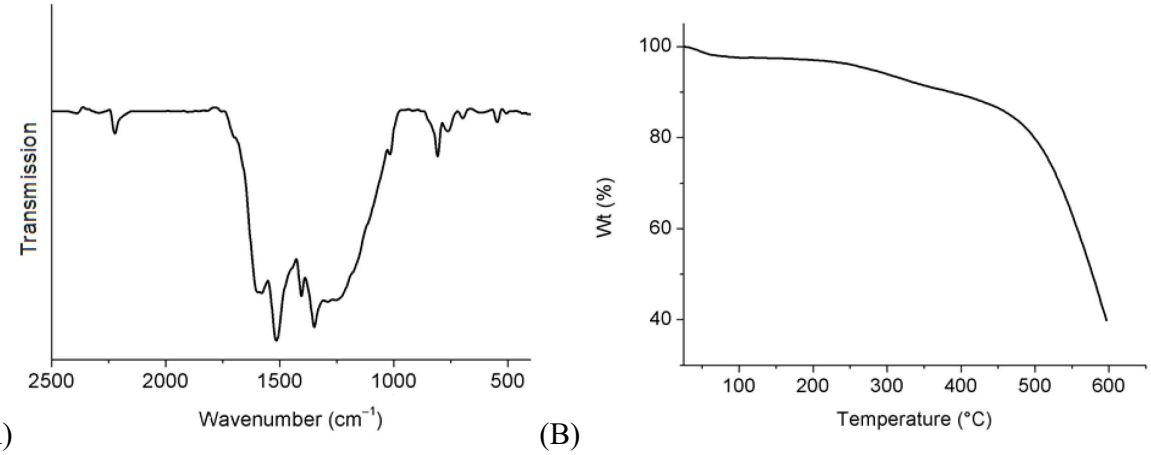

(A) (B)

Fig. S1: FT-IR spectrum (A) and TGA data (B) for CTF-1**.**

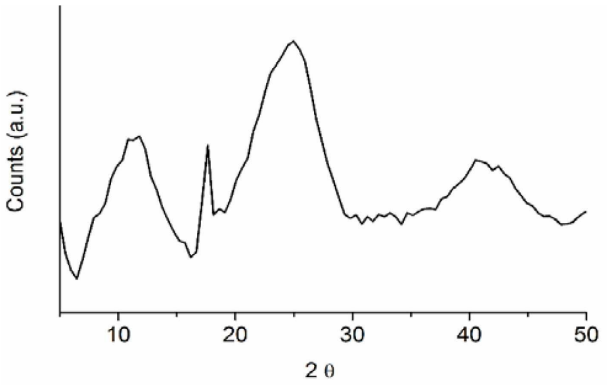

Fig. S2: Powder X-ray diffraction pattern of CTF-1.

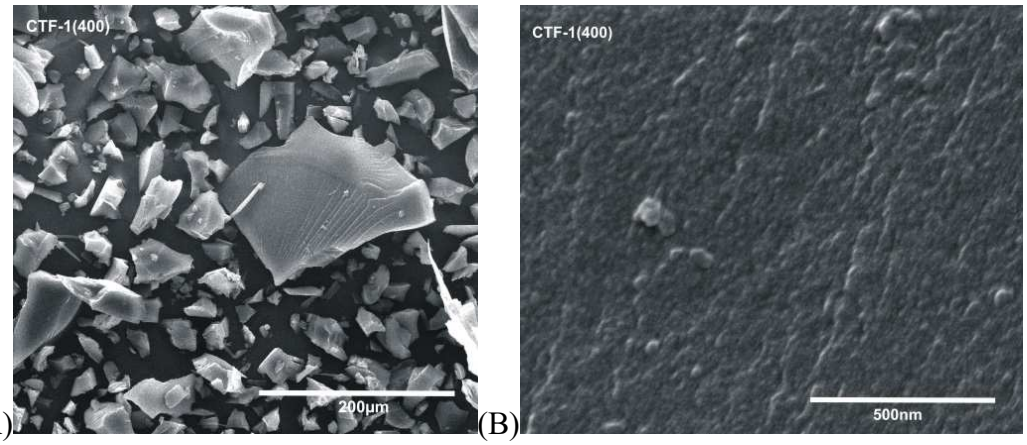

(A) (B)

Fig. S3: SEM images of CTF-1.

Table S1: Elemental analysis of CTF-1.

Compound	Temp. (°C)	Calculated (wt%)					Found (wt%)				
		C	H	N	C/H	C/N	C	H	N	C/H	C/N
CTF-1	400	74.99	3.15	21.86	1.98	4.00	72.03	2.96	13.82	2.03	6.08

S1.1. N_2 sorption and pore size distribution

The porosity of the CTF-1 was characterized by N_2 sorption measurements as the accepted standard for surface area and pore size determination. The materials were activated by degassing at 200 °C for 24 h. The measured BET surface area for CTF-1 is 968 m^2/g. To understand the nature of porosity, non-local density functional theory (NLDFT) pore size distributions using a slit-pore model based on the N_2 adsorption isotherms were calculated. A narrow distribution of micropores centered mainly at 5, 6 and 12 Å were observed for CTF-1.

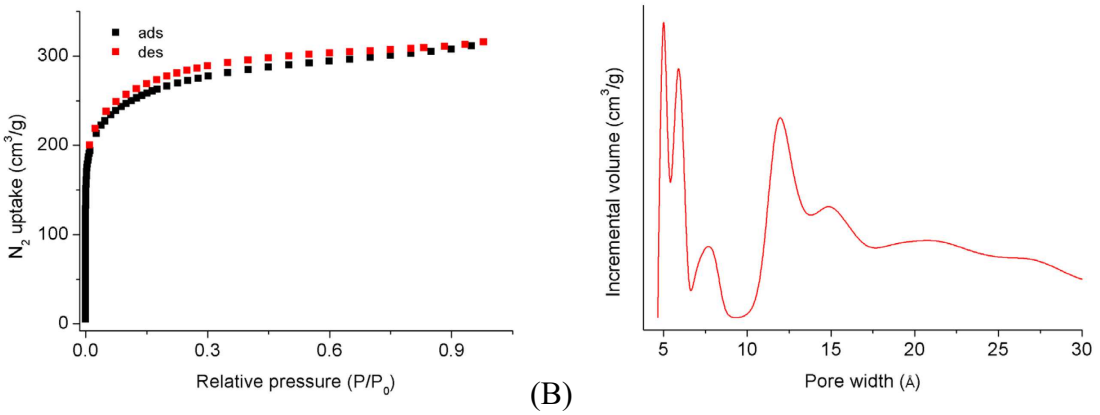

(A) (B)

Fig. S4: Nitrogen adsorption-desorption isotherms for CTF-1 (A). NL-DFT pore size distribution curve of CTF-1 (B).

We also measured N_2 sorption at 293 K for CTF-1 (**Fig. S5**). The maximal N_2 uptake was 4.6 cm^3/g at a pressure of 724 mmHg.

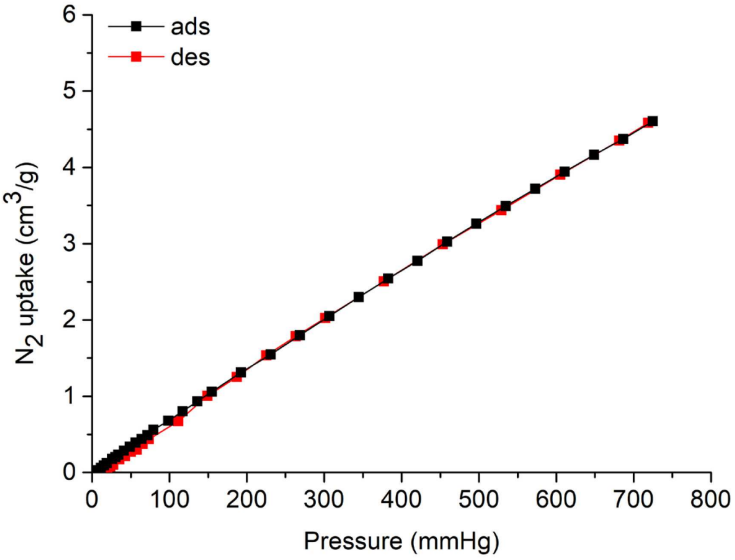

Fig. S5: Nitrogen adsorption-desorption isotherms for CTF-1 at 293 K.

S1.2. H_2 and CO_2 sorption

We investigated the adsorption of other gases, such as H_2 and CO_2 at low pressure (**Table S2**, **Fig. S5**). CTF-1 adsorbed 1.2 wt% (136 cm^3/g) H_2 at 77 K and 1 bar. The CO_2 uptake capacities of CTF-1 were measured at two different temperatures at 1 bar. The volume of CO_2 adsorption on CTF-1 at 273 K and 293 K were 72 and 49 cm^3/g, respectively.

Table S2: Gas uptake of CTF-1.

Compound	S_{BET} $(m^2/g)^a$	S_{Lang} (m^2/g)	H_2 uptake at 77 K $(cm^3/g)^b$	CO_2 uptake at 273 K $(cm^3/g)^b$	CO_2 uptake at 293 K $(cm^3/g)^b$
CTF-1	968	1181	136	72.4	49.2

[a]Calculated BET surface area over the pressure range 0.01–0.05 P/P_0. [b]Gas uptake at 1 bar.

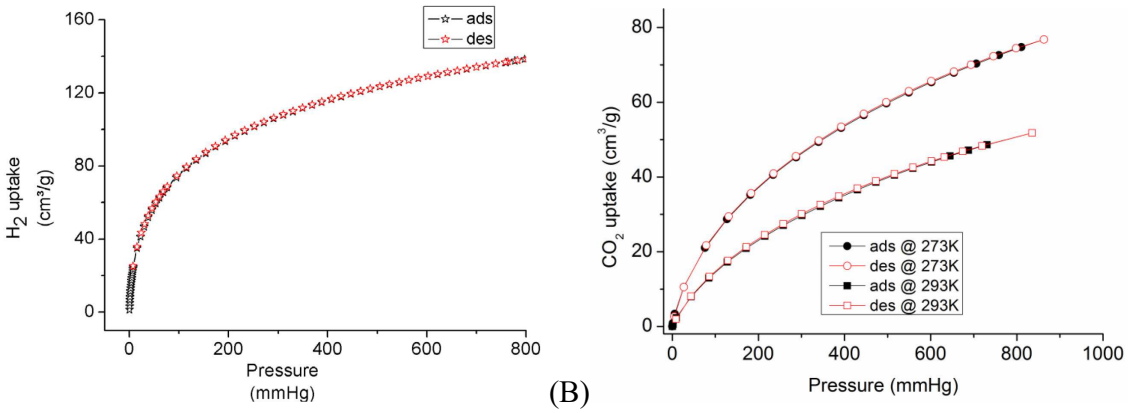

(A) (B)

Fig. S6: H_2 sorption at 77 K (A) and CO_2 sorption at 273 K and 293 K (B) for CTF-1.

S1.3. Ideal adsorbed solution theory (IAST) calculation

CO_2 and N_2 sorption measurements were carried out at 293 K (**Fig. S5** and **Fig. S6B**). The CO_2/N_2 selectivity at 293 K (**Fig. S7**) of CTF-1 was calculated using dual-site Langmuir (DSLAI) fitted isotherm data based on following equation (1):

$$q_{eq} = q_{max1} \times \frac{K_1 \times p}{1 + K_1 \times p} + q_{max2} \times \frac{K_2 \times p}{1 + K_2 \times p} \quad (1)$$

The selectivities were calculated using following equation (2):

$$S = \frac{x_1/y_1}{x_2/y_2} \quad (2)$$

with: xi - absorbed gas amount (mmol/g); yi – mole fraction

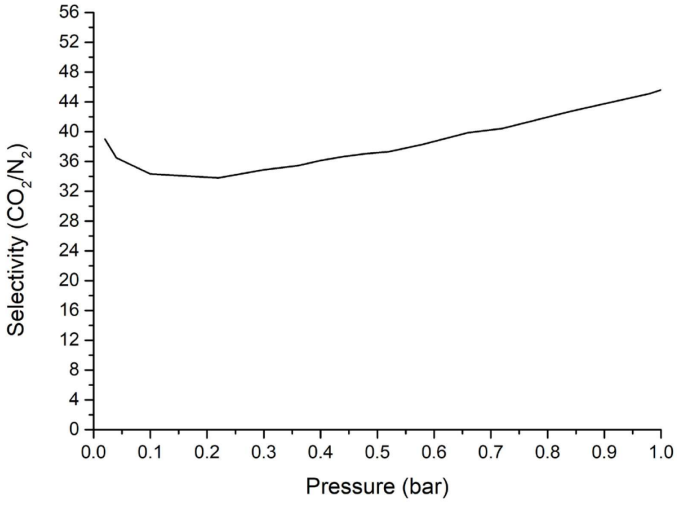

Fig. S7: IAST selectivity of CTF-1 in dependence of the pressure for a binary (50:50; v:v) mixture of the gases CO_2/N_2 at 293 K.

Table S3: Parameters for DSLAI fitting.

Gas	Temp. [K]	Model	R^2	Affinity const. 1 [1/bar]	Max. loading 1 [mmol/g]	Affinity const. 2 [1/bar]	Max. loading 2 [mmol/g]
CO_2	293	DSLAI	0.999	11.290	0.533	0.594	4.108
N_2	293	DSLAI	0.992	2.221	0.011	0.197	1.192

S2. Membrane thickness of CTF-1@ polysulfone mixed matrix membranes

The thickness of the 300 mg PSF membranes (54 µm - 76 µm) and the thickness of the 400 mg membranes (54 µm - 72 µm) is summarized in **Table S4**.

Table S4: Thickness of pure PSF membranes and MMMs.

CTF-1 load (wt%)	Thickness (µm)	
	300 mg PSF	400 mg PSF
0	54	54
8	42	72
16	50	71
24	76	70

S3. CTF-1@ polysulfone (400 mg) mixed matrix membranes

The following membranes were synthesized analogue to the 300 mg membranes.

S3.1. Scanning electron microscopy (SEM)

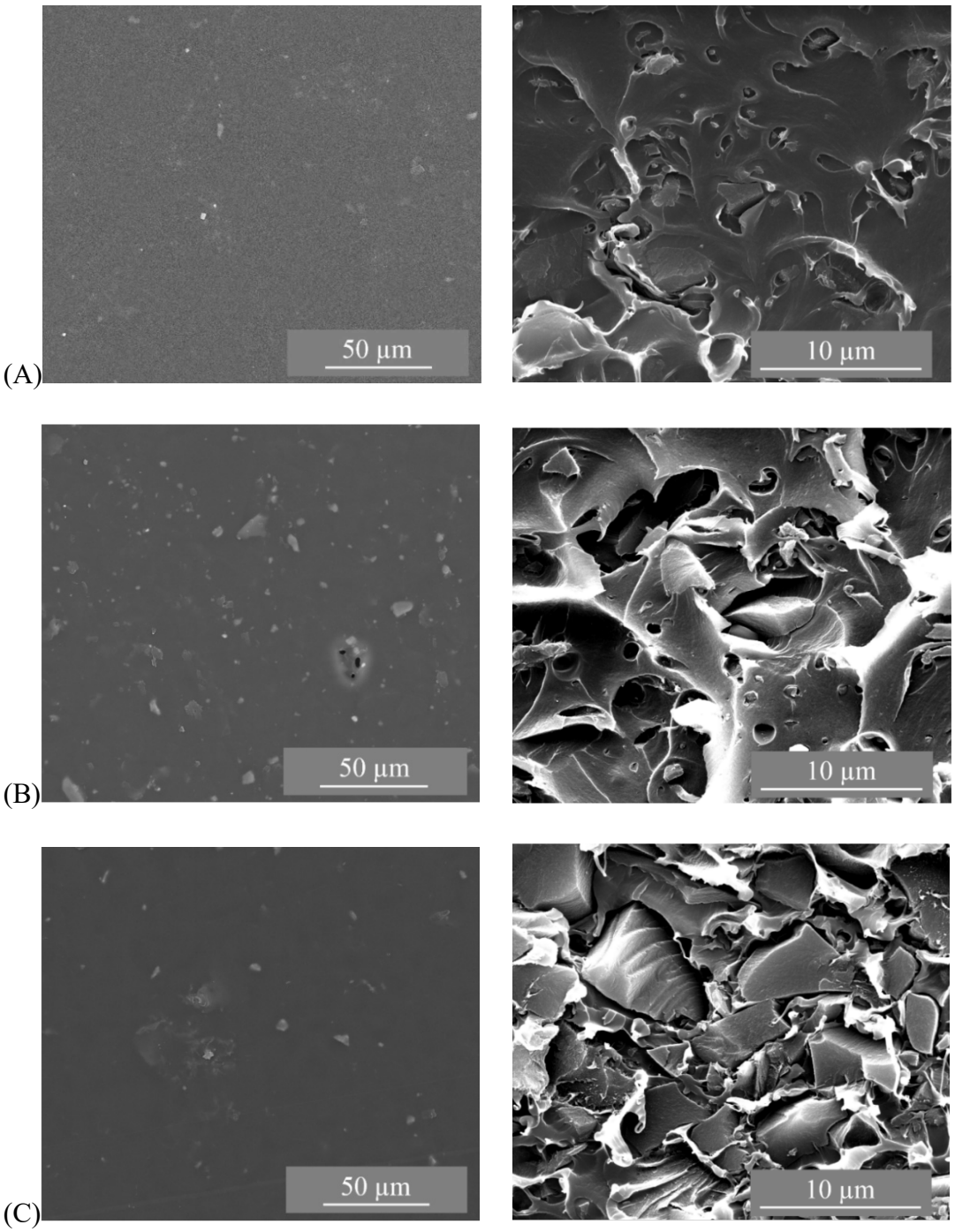

Fig. S8. Top surface SEM images (left side) and cross-section SEM images (right side) of 8 wt% (A), 16 wt% (B) and 24 wt% (C) of CTF-1/PSF (400 mg) composite MMMs.

S3.2. Mixed gas measurements

Mixed gas permeability and selectivity was determined as explained by Jeazet et al. (Jeazet et al., 2016). The membranes were placed inside a permeability module built of two stainless steel rings with a macroporous disk support (20 µm nominal pore size, Mott Corp.) gripped inside with Viton o-rings. Feed and sweep gas were provided to the membrane module by mass-flow meter controllers (Alicat Scientific). The retentate side was fed with a CO_2/CH_4 (25/25 cm^3 (STP)/min) mixture stream at ~200 kPa, while a 1 cm^3 (STP)/min mass-flow controlled stream of Ar at 110–120 kPa (slightly higher than the atmospheric pressure) swept the permeate side. An Agilent 3000A on-line gas micro-chromatograph equipped with a thermal conductivity detector (TCD) was used to analyze the gas concentrations in the outgoing stream. After the exit stream of the membrane was stabilized the permeability was obtained in Barrer (1 Barrer = $10^{-10}$$cm^3$(STP)·cm/($cm^2$·s·cmHg)). The real separation selectivity of the mixtures was calculated as the ratio of permeabilities. Permeation measurements were performed at 35°C controlled by a Memmert UNE 200 oven.

The CO_2 and CH_4 permeabilities as well as the CO_2/CH_4 selectivities for pure PSF and CTF-1 loadings of the MMMs with 8 wt% and 16 wt% were measured (**Table S5**). The values are shown for 400 mg polymer amount. The measurements were done at a temperature of 35 °C.

Table S5: Mixed gas separation of pure PSF and CTF-PSF MMMs.

Polymer Amount (mg)	CTF loading (wt%)	P (CO_2) (Barrer)	P (CH_4) (Barrer)	S (CO_2/CH_4)
400	0	6.1	0.2	31
400	8	7.2	0.2	40
400	16	9.3	0.2	42

S4. Other permeability models for 300 mg membranes

Besides the Maxwell model for following assumptions: $P_d >> P_c$, $P_d = P_c$, $P_d << P_c$ and $P_d = 6P_c$ (**Fig. 6** in the manuscript) the Bruggeman model (Bruggeman, 1935) was applied using following equation (3):

$$\frac{P_{eff}}{P_c} = \frac{1}{(1-\phi_d)^3} \qquad (3)$$

The Higuchi model (Higuchi and Higuchi, 1960; Shen and Lua, 2013) can be calculated as in equation (4):

$$\frac{P_{eff}}{P_c} = \frac{0.22+2.78\phi_d}{0.22-0.22\phi_d} \quad (4)$$

Böttcher-Landauer model (Hashin and Shtrikman, 1962) was simplified to the following equation (5):

$$\frac{\boldsymbol{P_{eff}}}{\boldsymbol{P_c}} = \frac{\mathbf{1}}{(\mathbf{1-3\phi_d})} \quad (5)$$

All applied models are valid for the assumption $P_d >> P_c$. **Fig. S9** shows the graph P_{eff}/P_c versus the filler fraction ϕ_d.

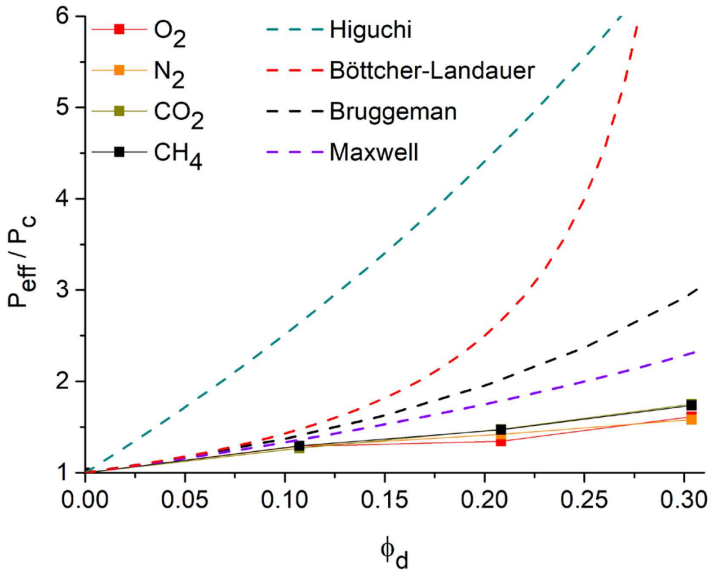

Fig. S9: P_{eff}/P_c versus ϕ_d. Measured permeabilities for the pure polymer and the polymer with 8 wt%, 16 wt% and 24 wt% of the filler CTF-1 in comparison to the Higuchi, Böttcher-Landauer, Bruggeman and Maxwell model for the assumption $P_d >> P_c$.

S5. References

Bhunia, A., Vasylyeva, V. and Janiak, C. (2013). From a supramolecular tetranitrile to a porous covalent triazine-based framework with high gas uptake capacities. *Chem. Commun.* 49, 3961−3963. doi: 10.1039/C3CC41382A

Bhunia, A., Dey, S., Bous, M., Zhang, C., von Rybinski, W. and Janiak, C. (2015). High adsorptive properties of covalent triazine-based frameworks (CTFs) for surfactants from aqueous solution. *Chem. Commun.* 51, 484−486. doi: 10.1039/C4CC06393G

Bruggeman, D.A.G. (1935). Berechnung verschiedener physikalischer Konstanten von heterogenen Substanzen. 1. Dielektrizitätskonstanten und Leitfähigkeiten der Mischkörper aus isotropen Substanzen. *Ann. Phys.* 24, 636–679. doi: 10.1002/andp.19354160705

Hashin, Z. and Shtrikman A. (1962). Variational Approach to the Theory of the Effective Magnetic Permeability of Multiphase Materials. *J. Appl. Phys.* 33, 3125−3131. doi: 10.1063/1.1728579

Higuchi, W.I. and Higuchi T. (1960). Theoretical analysis of diffusional movement through heterogeneous barriers. *J. Am. Pharm. Assoc. Sci.* 49, 598−606. doi: 10.1002/jps.3030490910

Hug, S., Mesch, M.B., Oh, H., Popp, N., Hirscher, M and Senkerd, J. (2014). A fluorene based covalent triazine framework with high CO_2 and H_2 capture and storage capacities. *J. Mater. Chem. A* 2, 5928–5936. doi: 10.1039/C3TA15417C

Tanh Jeazet, H.B., Sorribas, S., Román-Marín, J.M., Zornoza, B., Téllez, C. and Coronas, J. (2016). Increased Selectivity in CO_2/CH_4 Separation with Mixed-Matrix Membranes of Polysulfone and Mixed-MOFs MIL-101(Cr) and ZIF-8. *Eur. J. Inorg. Chem*. 27, 4363−4367. doi: 10.1002/ejic.201600190

Shen, Y. and Lua, A.I. (2013). Theoretical and Experimental Studies on the Gas Transport Properties of Mixed Matrix Membranes Based on Polyvinylidene Fluoride *AIChE J*, 59, 4715–4726. doi: 10.1002/aic.14186

4. Unpublished part

This chapter presents unpublished studies conducted as part of this dissertation.

4.1. CTF-carbazole/Matrimid MMMs

CTFs from mechanochemical syntheses generally have higher nitrogen contents and lower residues in elemental analysis than CTFs prepared via Friedel-Crafts alkylation under reflux. Previous experiments on the mechanochemical synthesis of CTFs at this institute were unsuccessful, as the energy input of the vibrating mill used was too low. CTF-carbazole was provided by Daniel Baier and Tilo Rensch from Lehrstuhl für Anorganische Chemie I, Ruhr-Universität Bochum, D-44801 Bochum, Germany. The analytical work regarding CTF-carbazole, MMM preparation and CO_2/CH_4 mixed-gas measurement was performed at Heinrich-Heine Universität.

CTF-carbazole was analyzed by attenuated total reflection infrared spectroscopy (ATR-IR). ATR-IR (Figure 13) revealed bands at 3330-3400 cm^{-1} (br) from the N-H vibration of carbazole and at 1487 cm^{-1} (vs) and 1350 cm^{-1} (vs), which can be assigned to the C=N vibrations of the triazine ring.[84]

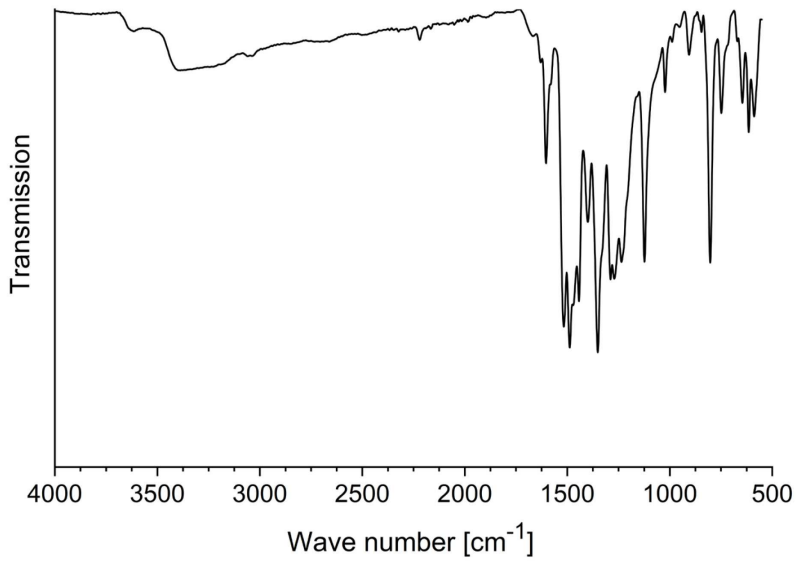

Figure 13: ATR-IR spectrum of CTF-carbazole.

The elemental analysis of CTF-carbazole showed good accordance with the calculated values for the ideal structure. The rest of 5.7 wt% could be attributed to water molecules (Table 3).

Table 3: Elemental analysis of CTF-carbazole.

Compound	C [wt%]	H [wt%]	N [wt%]	Rest [wt%]
Ideal	77.41	3.25	19.34	-
CTF-carbazole_$AlCl_3$[84]	68.61	3.32	17.13	10.94
CTF-carbazole	73.67	3.82	16.84	5.67

From the N_2-sorption isotherm (Figure 14; left) a BET-surface area of 519 m^2/g and a total pore volume of 0.39 cm^3/g was calculated. These values were slightly lower than the ones of the literature-known CTF-CBZ_$AlCl_3$, which exhibits a BET-surface area of 580 m^2/g and a pore volume of 0.41 cm^3/g.[84] The pore size distribution (Figure 14; right) mainly showed pores with a diameter of 9 Å and an additional broad distribution of mesopores.

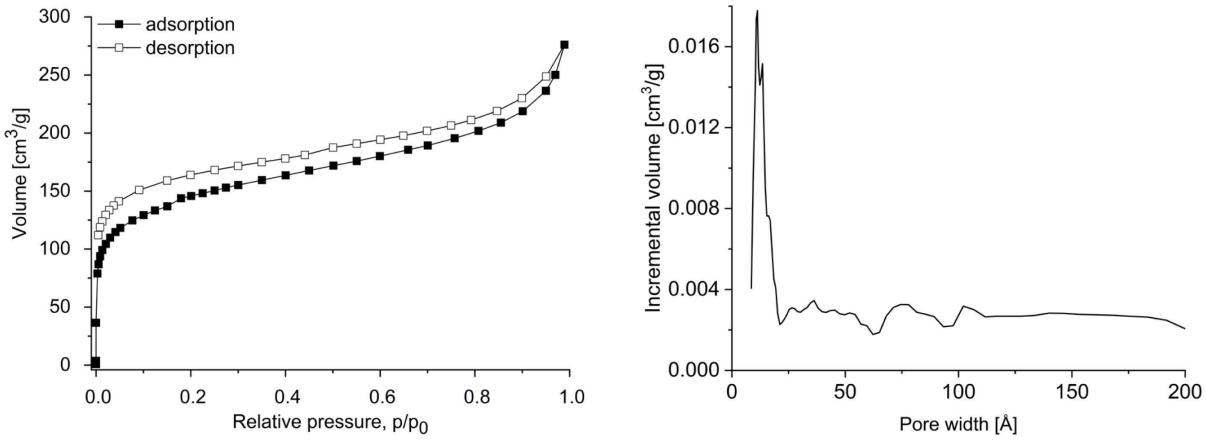

Figure 14: N_2-sorption isotherm (left) and non-local density functional theory (NLDFT)-based pore size distribution (right) of CTF-carbazole

Scanning electron microscope (SEM) images (Figure 15) showed agglomerated, non-spherical particles and thermogravimetric analysis (TGA) under synthetic air (Figure 16) confirmed a thermal stability up to over 450 °C.

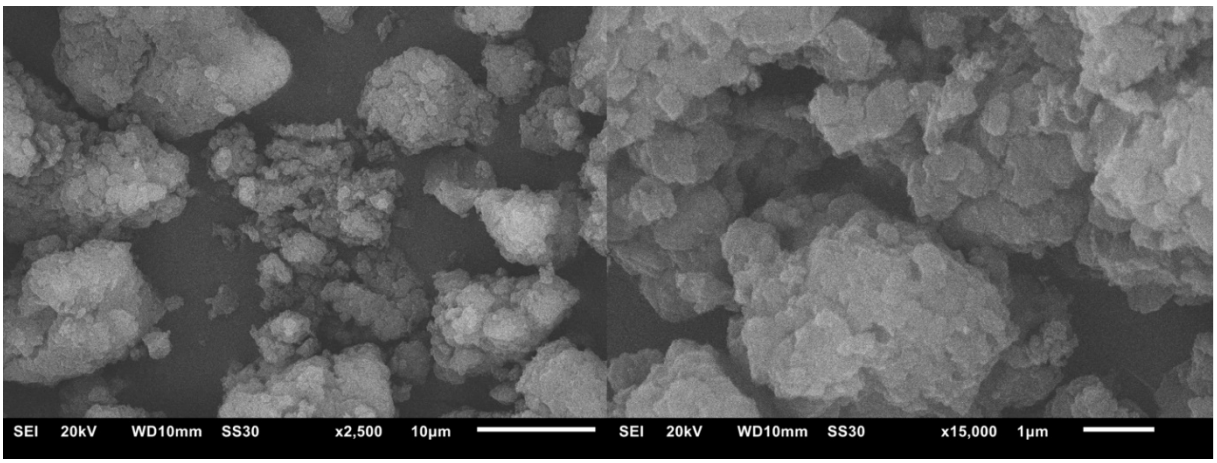

Figure 15: SEM images of CTF-carbazole.

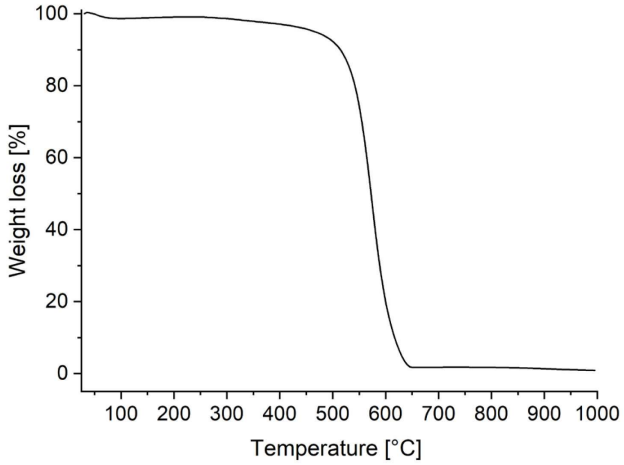

Figure 16: TGA of CTF-carbazole under synthetic air with a heating rate of 5 K/min.

MMMs were prepared with 8, 16 and 24 wt% of CTF-carbazole in a matrix of Matrimid. The SEM images of the CTF-carbazole MMMs (Figure 17) reveal that neither strong sedimentation nor agglomeration of the filler particles occurred.

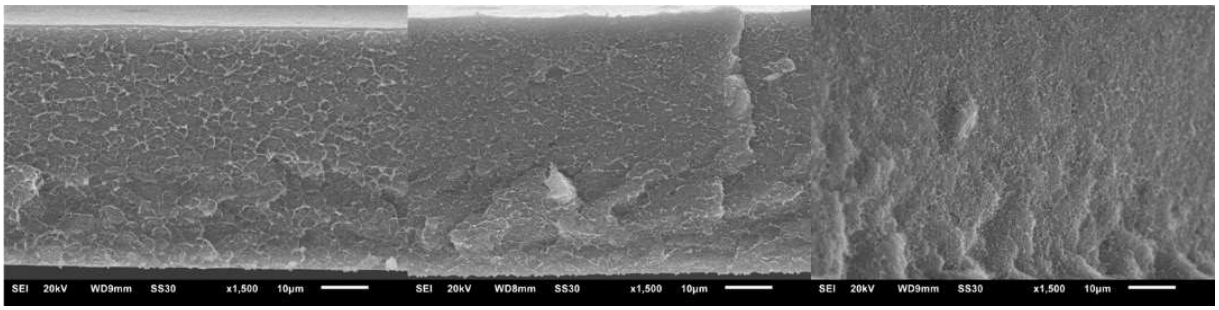

Figure 17: Cross-section SEM images of 8 wt% (left), 16 wt% (middle) and 24 wt% (right) CTF-carbazole/Matrimid MMMs.

The CTF-carbazole/MMMs showed an enhancement in CO_2 and CH_4 permeability when the filler content was increased from 8 to 24 wt%. The CO_2 permeability was continuously enhanced from 8.3 Barrer for the 8 wt% MMM to 12.0 Barrer for the 24 wt% MMM. For the 8 and 16 wt% MMMs a small rise in CO_2/CH_4 selectivity was observed and the selectivity for the 24 wt% MMM was equal to the pristine Matrimid membrane (Table 4; Figure 18).

Table 4: Gas permeability (CO_2, CH_4) and mixed-gas selectivity factors (CO_2/CH_4) of the pure Matrimid membrane and CTF-carbazole/Matrimid MMMs.

Filler content [wt%]	P CO_2 [Barrer]	P CH_4 [Barrer]	α CO_2/CH_4
0	6.8 ± 0.3	0.16 ± 0.01	42 ± 1
CTF-carbazole			
8	8.3 ± 0.1	0.17 ± 0.01	46 ± 1
16	10.7 ± 0.3	0.23 ± 0.01	45 ± 1
24	12.0 ± 0.2	0.28 ± 0.01	42 ± 2

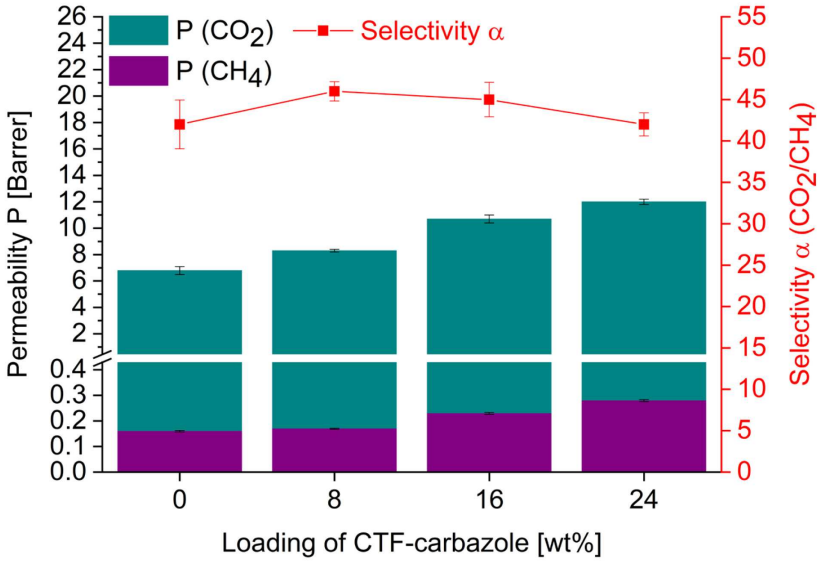

Figure 18: CO_2 and CH_4 permeability and CO_2/CH_4 selectivity for the pure Matrimid membrane and CTF-carbazole/Matrimid MMMs.

4.2. Materials and methods

All chemicals were purchased from commercial sources. For CTF-carbazole synthesis, anhydrous aluminum chloride ($AlCl_3$; 98%) was obtained from Merck, cyanuric chloride (98%) from Alfa Aesar and the linker carbazole (95%) was received from Sigma-Aldrich. The polymer Matrimid® 5218 (BTDA/DAPI) was provided by Huntsman Advanced Materials. The gases CO_2 (grade 4.5), CH_4 (grade 4.5) and He (grade 5.0) were received from Air Liquide.

ATR-IR spectrum was measured using a Tensor 37 (Bruker) in the range from 4000 cm^{-1} to 500 cm^{-1}. Elemental (C, H, N, S) analysis was carried out on a vario MICRO cube (elementar). Nitrogen sorption measurement was performed on an Autosorb-6 (Quantachrome) at 77 K. BET surface area was calculated from the nitrogen adsorption isotherm. For this purpose, a

multipoint analysis in the range of 0.05 to 0.3 p/p_0 with a correlation coefficient of at least r = 0.999994 was chosen. Prior to taking SEM images, the samples were coated with gold using a JFC 1200 (Jeol) coater. SEM images were taken using a JSM-6510LV (Jeol) with a LaB_6 cathode (20 keV). TGA measurement was performed under synthetic air with a heating rate of 5 K/min using a TG 209 F3 Tarsus (Netzsch). CO_2/CH_4 mixed-gas separation experiments were conducted with an OSMO inspector (Convergence Industry B.V.) connected to an Agilent 490 Micro GC (Agilent Technologies) with a fused silica column PoraPLOT Q. The membranes were placed in a permeation module and fixed with a Viton O-ring with an inner diameter of 3.6 cm leading to a membrane area of 11.3 cm^2. The feed gas consisted of CO_2/CH_4 in a volume ratio of 1:1 and helium was applied as sweep gas. All experiments were carried out with a transmembrane pressure of 3 bar at 25 °C. GC measurements were performed every 30 min until an equilibrium state was reached (after about 5–8 h). At minimum the last three GC measurements were used to calculate the characteristic permeability. Each membrane was prepared and measured twice. The permeability P in Barrer ($1\ \text{Barrer} = 10^{-10}\text{cm}^3(STP) \times \text{cm} \times \text{cm}^{-2} \times s^{-1} \times cmHg^{-1}$) was calculated according to Equation (10):

$$P = \frac{x_A \times Q_{He} \times d}{x_{He} \times A \times (p_2 \times x_A^f - p_1 \times x_A)} \tag{10}$$

where x_A, Q_{He}, and d are the molar fraction of the gas A, the volumetric flow rate of the sweep gas helium and the membrane thickness, respectively. x_{He}, A, p_2, x_A^f, and p_1 are the molar fraction of the sweep gas (permeate), the membrane area, the feed pressure, the molar fraction of the gas A (feed) and the permeate pressure, respectively. The mixed-gas selectivity of two gases A and B (Equation 11) was calculated from their molar fractions (x) on the permeate side divided by their molar fractions on the feed side:

$$\alpha_{A,B} = \frac{(x_A/x_B)_{permeate\ side}}{(x_A/x_B)_{feed\ side}} \tag{11}$$

4.3. Synthesis and preparation

CTF-carbazole was synthesized via a mechanochemical Friedel-Crafts alkylation (Figure 19) under inert conditions analogue to previous performed synthesis.[84] Carbazole (2.276 g, 13.61 mmol) and anhydrous $AlCl_3$ (6.050 g, 45.38 mmol) were filled in a 45 mL grinding jar with 22 tungsten carbide (WC) grinding balls (10 mm diameter). After milling in a planetary ball mill (Fritsch Pulverisette 7 premium line) for 2 minutes at 800 rpm, cyanuric chloride (1.674 g, 9.08 mmol) was added and the mixture was milled under the same conditions

for another 60 min. The crude product was poured into water and subsequently purified by Soxhlet extraction with water and THF. The solvent was exchanged for acetone and the product was dried with supercritical CO_2. (yield: 2.929 g; 99.0%)

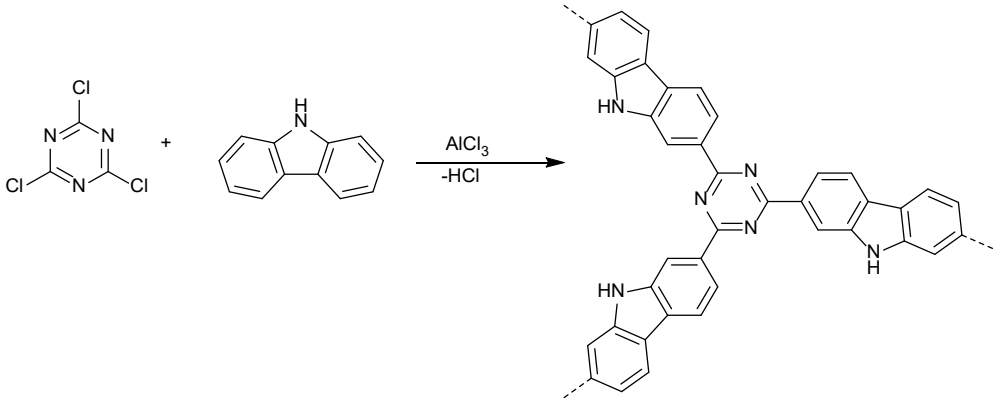

Figure 19: Schematic synthesis of CTF-carbazole (idealized structure).

All membranes were prepared by solution casting. The filler loadings of CTF-carbazole refer to the combined mass of the polymer Matrimid and filler according to Equation (12):

$$Filler\ loading\ [wt\%] = \frac{m_{filler}}{m_{polymer} + m_{filler}} \times 100\% \qquad (12)$$

Matrimid was dried for 7 days at 80 °C. For the pure Matrimid membranes, 400 mg of the polymer were dissolved in 5 mL of dichloromethane (DCM) and stirred for 24 h. For the CTF/Matrimid MMMs 400 mg Matrimid was dissolved in 3.5 mL of DCM and stirred for 24 h. Meanwhile, CTF-carbazole (35 mg for 8 wt%, 76 mg for 16 wt%, and 126.5 mg for 24 wt%) was dispersed in 4.5 mL of DCM and stirred for 24 h. The CTF dispersion was ultrasonicated (VCX 750 Sonics; Microtip 630-0419) with an amplitude of 20% three times for 15 min each. After each 15 min ultrasonication step, the dispersion was stirred for 30 min. Part of the polymer solution (0.33 mL for 8 wt%, 0.72 mL for 16 wt% and 1.20 mL for 24 wt%) was added to the CTF dispersion followed by another 24 h of stirring. After repetition of the same three 15 min ultra-sonification steps the remaining polymer solution was added and stirred for 1 h. Solution casting and drying was carried out as follows: The mixtures were cast into metal rings placed on a flat mirror. An inverted funnel, covered with a paper tissue, was placed above the metal ring to achieve a controlled evaporation of DCM. After evaporation of DCM, the membrane was cut out with a scalpel and subsequently dried in a vacuum oven at 150 °C and 20 mbar overnight.

5. Summary

COFs and CTFs are materials formed by covalent bonds between light elements. Most of these materials are characterized by high thermal and chemical stability as well as permanent porosity. The possibility to combine and further functionalize different building blocks makes them attractive for various applications. In particular, their application in gas storage and separation is currently gaining attention due to that area's environmental and economic importance. The use of membranes offers a possibility to achieve continuous gas separation. A further increase in membrane performance can be achieved by using MMMs, in which a filler serves as a dispersed phase in a polymer matrix. The combination of COFs/CTFs as filler and polymers as the membrane matrix leads to higher separation performance compared to pure polymer membranes. In this work, the focus is on COF/CTF-based MMMs for CO_2/CH_4 separation, which is relevant for natural gas sweetening and biogas upgrading.

The filler material CTF-fluorene was synthesized by Friedel-Crafts alkylation starting from cyanuric chloride, fluorene and anhydrous aluminum chloride. With this synthesis method, it was possible to generate the product on a gram scale and to ensure the preparation of MMMs from one batch. The resulting CTF exhibited a BET surface area of 762 m^2/g and a total pore volume of 0.38 cm^3/g. CO_2 and CH_4 sorption measurements were performed at 298 K, and Langmuir model-fitted CO_2 and CH_4 sorption isotherms were applied to calculate IAST selectivity. CTF-fluorene exhibited a CO_2/CH_4 (50:50; v:v) selectivity of 7.6 at 1 bar pressure. Subsequently, MMMs were prepared with 8, 16 and 24 wt% CTF-fluorene as filler in PSF and Matrimid matrices. Mixed gas separation studies with an equimolar CO_2/CH_4 mixture revealed an improvement in CO_2 permeability from 5.4 Barrer for the pure PSF membrane to 12.8 Barrer for the MMM with 24 wt% CTF-fluorene. Incorporation of 24 wt% CTF-fluorene in a Matrimid matrix resulted in an increase in CO_2 permeability from 6.8 Barrer for the pure polymer membrane to 17.8 Barrer. For all MMMs, the selectivity was preserved considering for error. Comparison with permeability models showed that the current experimental values for the CTF-fluorene/PSF MMMs were between the predicted values of the Maxwell models for $P_d = 8P_c$ and for $P_d >> P_c$. The experimental curve of the CTF-fluorene/Matrimid MMMs, agreed with the Bruggeman model, except for a filler content of 24 wt%, where the permeability showed an even stronger increase than predicted. The effect of free volume on the overall permeability of the membranes was illustrated by calculating the total FFV.

The influence of pore volume of the filler in a MMM was investigated by preparing CTF-biphenyl/Matrimid MMMs. CTF-biphenyl synthesized via Friedel-Crafts alkylation exhibited

a BET surface area of 940 m^2/g and a pore volume of 0.53 cm^3/g. CTF-biphenyl showed maximum CO_2 and CH_4 uptakes of 1.87 mmol/g and 0.55 mmol/g at 298 K, respectively. The IAST selectivity for the gas pair CO_2/CH_4 was calculated to be 10.5 at a pressure of 1 bar for a 50:50 (v:v) mixture. MMMs prepared with 8, 16 and 24 wt% of the filler CTF-biphenyl were investigated by permeability measurements with a binary CO_2/CH_4 gas mixture. The MMM with 8 wt% CTF as dispersed phase exhibited an increase in CO_2 permeability from 6.8 Barrer for the pure Matrimid membrane to 12.0 Barrer, which was a higher increase than could be assumed by comparison with permeability models. With a CTF-biphenyl loading of 16 wt%, a CO_2 permeability of 15.1 Barrer was achieved while maintaining the intrinsically high CO_2/CH_4 selectivity of Matrimid. The permeability enhancement of the16 wt% MMM was in good agreement with the Bruggeman model and showed the best overall performance, considering separation efficiency and filler consumption. FFV calculations showed that in the case of MMMs with low filler contents, relatively more free volume was generated than for MMMs with higher filler content. Overall, the larger pore volume of the filler proved to be beneficial for increasing the CO_2 permeability of MMMs containing up to 16 wt% of the filler material.

In another work, two new fluorinated imine-COFs were synthesized by a condensation reaction of an aldehyde and an amine. The reactions in ampoules led to crystalline and porous materials with high chemical and thermal stability. The Schiff base reaction between 1,3,5-tris-(4-aminophenyl)triazine with 4,4'-biphenyldicarboxaldehyde or 2,2',3,3',5,5',6,6'-octafluoro-4,4'-biphenyldicarboxaldehyde, yielded compounds HHU-COF-1 and HHU-COF-2, respectively. Sorption measurements were performed in addition to confirming the successful formation of the two structures by solid-state NMR, IR, XPS and elemental analysis. Based on CO_2 and CH_4 sorption isotherms measured at 273 K, maximum CO_2 uptakes of 1.08 mmol/g for HHU-COF-1 and 1.74 mmol/g for HHU-COF-2, respectively, were obtained. From N_2-sorption, BET surface areas of 2352 m^2/g for HHU-COF-1 and 1356 m^2/g for HHU-COF-2 and total pore volumes of 0.78 cm^3/g and 0.73 cm^3/g for HHU-COF-1 and its fluorinated analog were determined. In addition to that work, larger scale syntheses were carried out and 8, 16 and 24 wt% of the COFs were applied to prepare MMMs with the polymer Matrimid. CO_2/CH_4 separation studies indicated that a lower filler content of HHU-COF-1 is recommended to achieve optimal membrane performance for this MMM system. The fluorinated material showed better overall compatibility with the Matrimid matrix. With an increase in CO_2 permeability from 6.8 to 13.0 Barrer at constant selectivity, this system showed the best separation performance.

CTF-1, prepared via trimerization reaction starting from dicyanobenzene, was applied as dispersed phase in a matrix of the polymer PSF. MMMs containing 8, 16 and 24 wt% CTF-1 were prepared by solution casting and single gas permeation studies were performed with the gases O_2, N_2, CO_2 and CH_4. The permeability could be increased for all measured gases and no loss of selectivity was observable for any of the gas pairs O_2/N_2, CO_2/CH_4 and CO_2/N_2. With 24 wt% CTF-1 embedded in the PSF matrix, CO_2 permeability increased from 7.3 for the pure PSF membrane to 12.7 Barrer. Comparisons were drawn with known theoretical permeability models, and the Maxwell model was modified and applied, showing the best agreement with the Maxwell model for $P_d = 6P_c$. The calculation of the FFV was carried out and the logarithmic plot of the experimental O_2, N_2, CO_2, and CH_4 permeability versus the inverse (total) FFV of the pure polymer membrane and MMMs with 8, 16 and 24 wt% of the filler CTF-1 showed a linear correlation. This additionally confirmed the contribution of the filler porosity to the gas transport properties of the membranes.

In summary, the pore volume of a filler was a decisive factor with regard to the free volume created in a MMM. Thus, the use of CTFs or COFs with a certain pore volume increased the permeability. In addition, the right proportion of filler in the MMM must also be considered. Incorporation of 24 wt% CTF-fluorene into a Matrimid matrix gave the optimum performance in terms of CO_2/CH_4 separation. When CTF-biphenyl with a higher pore volume was applied as filler, the optimum was already achieved with 16 wt%. However, if the pore volume or pore aperture was too large, as in the case of HHU-COF-1, the permeability decreased due to interpenetration of polymer chains into the pores of the filler. In this case, functionalization of the COF, as in the case of HHU-COF-2, was beneficial. A further study with fillers in which only the linker length is changed could lead to a detailed comparison in the future and advance research in this field.

6. List of figures and tables

7. References

[1] M. Mulder, *Basic Principles of Membrane Technology*, Kluwer Academic Publishers, Dordrecht, **1996**, p. 7.

[2] C. Charcosset, *Desalination* **2009**, *245*, 214−231.

[3] W.-J. Lau, A.F. Ismail, *Desalination* **2009**, *245*, 321−348.

[4] P. Bernardo, E. Drioli, G. Golemme, *Ind. Eng. Chem. Res.* **2009**, *48*, 4638−4663.

[5] R.W. Baker, Future directions of membrane gas-separation technology, *Ind. Eng. Chem. Res.* **2002**, *41*, 1393−1411.

[6] Y. Zhang, J. Sunarso, S. Liu, R. Wang, *Int. J. Greenh. Gas Control* **2013**, *12*, 84−107.

[7] D.M. D'Alessandro, B. Smit, J.R. Long, *Angew. Chem. Int. Ed.* **2010**, *49*, 6058−6082.

[8] W.J. Koros, R. Mahajan, *J. Membr. Sci.* **2000**, *175*, 181−196.

[9] N.F. Himma, A.K. Wardani, N. Prasetya, P.T.P. Aryanti, I.G. Wenten, *Rev. Chem. Eng.* **2019**, *35*, 591−625.

[10] H.B. Tanh Jeazet, C. Staudt, C. Janiak, *Dalton Trans.* **2012**, *41*, 14003−14027.

[11] S.A. Stern, *J. Polym. Sci., Part A-2* **1968**, *6*, 1933−1934.

[12] A.F. Ismail, K. Khulbe, T. Matsuura, *Gas Separation Membranes: Polymeric and Inorganic*, Springer International Publishing, Switzerland, **2015**, pp. 17−19.

[13] P. Pandey, R.S. Chauhan, *Prog. Polym. Sci.* **2001**, *26*, 853−893.

[14] J.G. Wijmans, R.W. Baker, *J. Membr. Sci.* **1995**, *107*, 1−21.

[15] H. Strathmann, *AIChE J.* **2001**, *47*, 1077−1087.

[16] W.J. Koros, C. Zhang, *Nat. Mater.* **2017**, *16*, 289−297.

[17] A.F. Ismail, K. Khulbe, T. Matsuura, *Gas Separation Membranes: Polymeric and Inorganic*, Springer International Publishing, Switzerland, **2015**, p. 89.

[18] K. Dalane, Z. Dai, G. Mogseth, M. Hillestad, L. Deng, *J. Nat. Gas Sci. Eng*. **2017**, *39*, 101−117.

[19] H. Verweij, *Curr. Opin. Chem. Eng.* **2012**, *1*, 156–162.

[20] W. Mazyan, A. Ahmadi, H. Ahmed, M. Hoorfar, *J. Nat. Gas Sci. Eng.* **2016**, *30*, 487−514.

[21] T. Graham, *Philos. Mag.* **1866**, *32*, 401−420.

[22] R.W. Baker, *Membranes for vapor/gas separation*, Membrane Technology and Research, Inc. **2006**, p. 3.

[23] J.O. Hirschfelder, C.F. Curtiss, R.B. Bird, *Molecular Theory of Gases and Liquids*, John Wiley and Sons, Inc., New York, **1954**.

[24] N. Mehio, S. Dai, D.-e. Jiang, *J. Phys. Chem. A* **2014**, *118*, 1150−1154.

[25] R.W. Baker, *Membrane Technology and Applications*, John Wiley and Sons Ltd., Chichester, United Kingdom, **2012**, p. 567.

[26] P.W. Atkins, J. de Paula, *Physikalische Chemie*, 5th ed., WILEY-VCH Verlag GmbH & Co. KGaA, Weinheim, Germany, **2010**, p. 980.

[27] N.W. Ockwig, T.M. Nenoff, *Chem. Rev.* **2007**, *107*, 4078−4110.

[28] L.M. Robeson, Q. Liu, B.D. Freeman, D.R. Paul, *J. Membr. Sci.* **2015**, *476*, 421−431.

[29] A. Bos, I.G.M. Pünt, M. Wessling, H. Strathmann, *J. Membr. Sci.* **1999**, *155*, 67−78.

[30] Arkema, high performance polymers, Colombes, France, product text, Pebax® MH 1657, https://www.extrememateriales-arkema.com/en/product-families/pebax/ pebax-elastomer-material-database/products/datasheet/Pebax%C2%AE%20MH%201657. (Accessed 1 December 2021)

[31] A. Volkov, in *Encyclopedia of Membranes* (Eds.: E. Drioli, L. Giorno), Springer Berlin Heidelberg, Berlin, Heidelberg, **2015**, pp. 1−2.

[32] D.R. Paul, D.R. Kemp, *J. Polym. Phys.* **1973**, *41*, 79−93.

[33] D. Bastani, N. Esmaeili, M. Asadollahi, *J. Ind. Eng. Chem.* **2013**, *19*, 375−393.

[34] M.G. Buonomenna, W. Yave, G. Golemme, *RSC Adv.* **2012**, *2*, 10745−10773.

[35] M.A. Aroon, A.F. Ismail, T. Matsuura, M.M. Montazer-Rahmati, *Sep. Purif. Technol.* **2010**, *75*, 229−242.

[36] B. Zornoza, C. Tellez, J. Coronas, J. Gascon, F. Kapteijn, *Microporous Mesoporous Mater.* **2013**, *166*, 67−78.

[37] J. Dechnik, J. Gascon, C.J. Doonan, C. Janiak, C.J. Sumby, *Angew. Chem. Int. Ed.* **2017**, *56*, 9292−9310.

[38] L.M. Robeson, *J. Membr. Sci.* **1991**, *62*, 165−185.

[39] L.M. Robeson, *J. Membr. Sci.* **2008**, *320*, 390−400.

[40] H. Cong, M. Radosz, B.F. Towler, Y. Shen, *Sep. Purif. Technol.* **2007**, *55*, 281−291.

[41] N.M. Wara, L.F. Francis, B.V. Velamakanni, *J. Membr. Sci.* **1995**, *104*, 43−49.

[42] I. Genné, S. Kuypers, R. Leysen, *J. Membr. Sci.* **1996**, *113*, 343−350.

[43] A. Doucouré, C. Guizard, J. Durand, R. Berjoan, L. Cot, *J. Membr. Sci.* **1996**, *117*, 143−150.

[44] B.-S. Ge, T. Wang, H.-X. Sun, W. Gao, H.-R. Zhao, *Polym. Adv. Technol.* **2018**, *29*, 1334−1343.

[45] M. Iwata, T. Adachi, M. Tomidokoro, M. Ohta, T. Kobayashi, *J. Appl. Polym. Sci.* **2003**, *88*, 1752−1759.

[46] T.-S. Chung, L.Y. Jiang, Y. Li, S. Kulprathipanja, *Prog. Polym. Sci.* **2007**, *32*, 483−507.

[47] I.F.J. Vankelecom, E. Merckx, M. Luts, J.B. Uytterhoeven, *J. Phys. Chem.* **1995**, *99*, 13187−13192.

[48] M. Moaddeb, W.J. Koros, *J. Membr. Sci.* **1997**, *125*, 143−163.

[49] Y. Li, T.-S. Chung, C. Cao, S. Kulprathipanja, *J. Membr. Sci.* **2005**, *260*, 45−55.

[50] T.T. Moore, R. Mahajan, D.Q. Vu, W.J. Koros, *AIChE J.* **2004**, *50*, 311−321.

[51] J.C. Maxwell, *Treatise on Electricity and Magnetism*, Clarendon Press, Oxford, United Kingdom, **1873**.

[52] R.H.B. Bouma, A. Checchetti, G. Chidichimo, E. Drioli, *J. Membr. Sci.* **1997**, *128*, 141−149.

[53] D.A.G. Bruggeman, *Ann. Phys.* **1935**, *416*, 636−664.

[54] S. Li, N. Prasetya, B.P. Ladewig, *Ind. Eng. Chem. Res.* **2019**, *58*, 9959−9969.

[55] M. Thommes, K. Kaneko, A.V. Neimark, J.P. Olivier, F. Rodriguez-Reinoso, J. Rouquerol, K.S.W. Sing, *Pure Appl. Chem.* **2015**, *87*, 1051−1069.

[56] K.S.W. Sing, D.H. Everett, R.A.W. Haul, L. Moscou, R.A. Pierotti, J. Rouquérol, T. Siemieniewska, *Pure Appl. Chem.* **1985**, *57*, 603−619.

[57] T.D. Bennett, F.-X. Coudert, S.L. James, A.I. Cooper, *Nat. Mater.* **2021**, *20*, 1179−1187.

[58] Y. Zhang, S.N. Riduan, *Chem. Soc. Rev.* **2012**, *41*, 2083−2094.

[59] J.-X. Jiang, F. Su, A. Trewin, C.D. Wood, N.L. Campbell, H. Niu, C. Dickinson, A.Y. Ganin, M.J. Rosseinsky, Y.Z. Khimyak, A.I. Cooper, *Angew. Chem. Int. Ed.* **2007**, *46*, 8574−8578.

[60] A.P. Côté, A.I. Benin, N.W. Ockwig, M. O'Keeffe, A.J. Matzger, O.M. Yaghi, *Science* **2005**, *310*, 1166−1170.

[61] P. Kuhn, M. Antonietti, A. Thomas, *Angew. Chem. Int. Ed.* **2008**, *47*, 3450−3453.

[62] M. Rose, W. Böhlmann, M. Saboa, S. Kaskel, *Chem. Commun.* **2008**, 2462−2464.

[63] T. Ben, H. Ren, S. Ma, D. Cao, J. Lan, X. Jing, W. Wang, J. Xu, F. Deng, J.M. Simmons, S. Qiu, G. Zhu, *Angew. Chem.* **2009**, *121*, 9621−9624.

[64] N.B. McKeown, P.M. Budd, K.J. Msayib, B.S. Ghanem, H.J. Kingston, C.E. Tattershall, S. Makhseed, K.J. Reynolds, D. Fritsch, *Chem. Eur. J.* **2005**, *11*, 2610−2620.

[65] W. Lu, D. Yuan, D. Zhao, C.I. Schilling, O. Plietzsch, T. Muller, S. Bräse, J. Guenther, J. Blümel, R. Krishna, Z. Li, H.-C. Zhou, *Chem. Mater.* **2010**, *22*, 5964−5972.

[66] M.G. Schwab, B. Fassbender, H.W. Spiess, A. Thomas, X. Feng, K. Müllen, *J. Am. Chem. Soc.* **2009**, *131*, 7216−7217.

[67] W. Zhang, B. Aguila, S. Ma, *J. Mater. Chem. A* **2017**, *5*, 8795−8824.

[68] L. Zou, Y. Sun, S. Che, X. Yang, X. Wang, M. Bosch, Q. Wang, H. Li, M. Smith, S. Yuan, Z. Perry, H.-C. Zhou, *Adv. Mater.* **2017**, *29*, 1700229.

[69] L. Huang, R. Liu, J. Yang, Q. Shuai, B. Yuliarto, Y.V. Kaneti, Y. Yamauchi, *Chem. Eng. J.* **2021**, *408*, 127991.

[70] S. Lu, Q. Liu, R. Han, M. Guo, J. Shi, C. Song, N. Ji, X. Lu, D. Ma, *J. Environ. Sci*. **2021**, *105*, 184−203.

[71] D. Chen, C. Liu, J. Tang, L. Luo, G. Yu, *Polym. Chem.* **2019**, *10*, 1168−1181.

[72] X. Liu, C.-F. Liu, W.-Y. Lai, W. Huang, *Adv. Mater. Technol.* **2020**, *5*, 2000154.

[73] S. Hug, M.B. Mesch, H. Oh, N. Popp, M. Hirscher, J. Senker, B.V. Lotsch, *J. Mater. Chem. A* **2014**, *2*, 5928−5936.

[74] D.R. Anderson, J.M. Holovka, *J. Polym. Sci. A: Polym. Chem.* **1966**, *4*, 1689−1702.

[75] S. Ren, M.J. Bojdys, R. Dawson, A. Laybourn, Y.Z. Khimyak, D.J. Adams, A.I. Cooper, *Adv. Mater.* **2012**, *24*, 2357−2361.

[76] H. Lim, M.C. Cha, J.Y. Chang, *Macromol. Chem. Phys.* 2012, 213, 1385−1390.

[77] P. Puthiaraj, S.-S. Kim, W.-S. Ahn, *Chem. Eng. J.* **2016**, *283*, 184−192.

[78] S. Dey, A. Bhunia, D. Esquivel, C. Janiak, *J. Mater. Chem. A* **2016**, *4*, 6259−6263.

[79] L. Xiang, Y. Zhu, S. Gu, D. Chen, X. Fu, Y. Zhang, G. Yu, C. Pan, Y. Hu, *Macromol. Rapid Commun.* **2015**, *36*, 1566−1571.

[80] X. Zhu, SM. Mahurin, S.-H. An, C.-L. Do-Thanh, C. Tian, Y. Li, L.W. Gill, E.W. Hagaman, Z. Bian, J.-H. Zhou, J. Hu, H. Liu, S. Dai, *Chem. Commun.* **2014**, *50*, 7933−7936.

[81] S. Gu, J. Guo, Q. Huang, J. He, Y. Fu, G. Kuang, C. Pan, G. Yu, *Macromolecules* **2017**, *50*, 8512−8520.

[82] P. Puthiaraj, S.-M. Cho, Y.-R. Lee, W.-S. Ahn, *J. Mater. Chem. A* **2015**, *3*, 6792−6797.

[83] Y. Luo, J. Liu, Y. Liu, Y. Lyu, *J. Polym. Sci. Part A: Polym. Chem.* **2017**, *55*, 2594−2600.

[84] E. Troschke, S. Grätz, T. Lübken, L. Borchardt, *Angew. Chem.* **2017**, *129*, 6963−6967.

[85] K. Wang, L.-M. Yang, X. Wang, L. Guo, G. Cheng, C. Zhang, S. Jin, B. Tan, A. Cooper, *Angew. Chem. Int. Ed.* **2017**, *56*, 14149−14153.

[86] M. Liu, Q. Huang, S. Wang, Z. Li, B. Li, S. Jin, B. Tan, *Angew. Chem. Int. Ed.* **2018**, *57*, 11968−11972.

[87] N.K. Bhattacharyya, S. Jha, T.Y. Bhutia, G. Adhikary, *Int. J. Chem. Appl.* **2012**, *4*, 295−304.

[88] S.-Y. Yu, J. Mahmood, H.-J. Noh, J.-M. Seo, S.-M. Jung, S.-H. Shin, Y.-K. Im, I.-Y. Jeon, J.-B. Baek, *Angew. Chem. Int. Ed.* **2018**, *57*, 8438−8442.

[89] C. Krishnaraj, H.S. Jena, K. Leus, P. Van Der Voort, *Green Chemistry* **2020**, *22*, 1038−1071.

[90] Z. Li, X. Feng, Y. Zou, Y. Zhang, H. Xia, X. Liu, Y. Mu, *Chem. Commun.* **2014**, *50*, 13825−13828.

[91] S. Mukherjee, M. Das, A. Manna, R. Krishna, S. Das, *Chem. Mater.* **2019**, *31*, 3929−3940.

[92] K. Wang, H. Huang, D. Liu, C. Wang, J. Li, C. Zhong, *Environ. Sci. Technol.* **2016**, *50*, 4869−4876.

[93] X. Zhu, C. Tian, G.M. Veith, C.W. Abney, J. Dehaudt, S. Dai, *J. Am. Chem. Soc.* **2016**, *138*, 11497−11500.

[94] F.J. Uribe-Romo, C.J. Doonan, H. Furukawa, K. Oisaki, O.M. Yaghi, *J. Am. Chem. Soc.* **2011**, *133*, 11478−11481.

[95] S. Dalapati, S. Jin, J. Gao, Y. Xu, A. Nagai, D. Jiang, *J. Am. Chem. Soc.* **2013**, *135*, 17310−17313.

[96] Q. Fang, Z. Zhuang, S. Gu, R.B. Kaspar, J. Zheng, J. Wang, S. Qiu, Y. Yan, *Nat. Commun.* **2014**, *5*, 4503.

[97] F.J. Uribe-Romo, J.R. Hunt, H. Furukawa, C. Klöck, M. O'Keeffe, O.M. Yaghi, *J. Am. Chem. Soc.* **2009**, *131*, 4570−4571.

[98] T. Ma, E.A. Kapustin, S.X. Yin, L. Liang, Z. Zhou, J. Niu, L.-H. Li, Y. Wang, J. Su, J. Li, X. Wang, W.D. Wang, W. Wang, J. Sun, O.M. Yaghi, *Science* **2018**, *361*, 48−52.

[99] S.-Y. Ding, J. Gao, Q. Wang, Y. Zhang, W.-G. Song, C.-Y. Su, W. Wang, *J. Am. Chem. Soc.* **2011**, *133*, 19816−19822.

[100] R. Gomes, P. Bhanja, A. Bhaumik, *Chem. Commun.* **2015**, *51*, 10050−10053.

[101] Q. Liao, C. Ke, X. Huang, G. Zhang, Q. Zhang, Z. Zhang, Y. Zhang, Y. Liu, F. Ning, K. Xi, *J. Mater. Chem. A* **2019**, *7*, 18959−18970.

[102] H. Yang, H. Wu, F. Pan, Z. Li, H. Ding, G. Liu, Z. Jiang, P. Zhang, X. Cao, B. Wang, *J. Membr. Sci.* **2016**, *520*, 583−595.

[103] P.H.H. Duong, V.A. Kuehl, B. Mastorovich, J.O. Hoberg, B.A. Parkinson, K.D. Li-Oakey, *J. Membr. Sci.* **2019**, *574*, 338−348.

[104] X. Yuan, Y. Wang, G. Deng, X. Zong, C. Zhang, S. Xue, *Polym. Adv. Technol.* **2019**, *30*, 417−424.

[105] K. Duan, J. Wang, Y. Zhang, J. Liu, *J. Membr. Sci.* **2019**, *572*, 588−595.

[106] M. Shan, B. Seoane, E. Rozhko, A. Dikhtiarenko, G. Clet, F. Kapteijn, J. Gascon, *Chem. Eur. J.* **2016**, *22*, 14467−14470.

[107] Y. Cheng, L. Zhai, Y. Ying, Y. Wang, G. Liu, J. Dong, D.Z.L. Ng, S.A. Khan, D. Zhao, *J. Mater. Chem. A* **2019**, *7*, 4549−4560.

[108] X. Wu, Z. Tian, S. Wang, D. Peng, L. Yang, Y. Wu, Q. Xin, H. Wu, Z. Jiang, *J. Membr. Sci.* **2017**, *528*, 273−283.

[109] X. Gao, X. Zou, H. Ma, S. Meng, G. Zhu, *Adv. Mater.* **2014**, *26*, 3644−3648.

[110] J. Liu, M. Liu, J. Lu, *High Perform. Polym.* **2019**, *31*, 671−678.

[111] Z. Kang, Y. Peng, Y. Qian, D. Yuan, M.A. Addicoat, T. Heine, Z. Hu, L. Tee, Z. Guo, D. Zhao, *Chem. Mater.* **2016**, *28*, 1277−1285.

[112] B.P. Biswal, H.D. Chaudhari, R. Banerjee, U.K. Kharul, *Chem. Eur. J.* **2016**, *22*, 4695−4699.

[113] R.L. Thankamony, X. Li, S.K. Das, M.M. Ostwal, Z. Lai, *J. Membr. Sci.* **2019**, *591*, 117348.

[114] H. Jiang, J. Zhang, T. Huang, J. Xue, Y. Ren, Z. Guo, H. Wang, L. Yang, Y. Yin, Z. Jiang, M.D. Guiver, *Ind. Eng. Chem. Res.* **2020**, *59*, 5296−5306.

[115] S. Bügel, A. Spieß, C. Janiak, *Microporous Mesoporous Mater.* **2021**, *316*, 110941.

[116] S. Bügel, Q.-D. Hoang, A. Spieß, Y. Sun, S. Xing, C. Janiak, *Membranes* **2021**, *11*, 795.

[117] S. Bügel, M. Hähnel, T. Kunde, N. de Sousa Amadeu, Y. Sun, A. Spieß, T.H.Y. Beglau, B.M. Schmidt, C. Janiak, *Materials* **2022**, *15*, 2807

[118] S. Dey, S. Bügel, S. Sorribas, A. Nuhnen, A. Bhunia, J. Coronas, C. Janiak, *Front. Chem.* **2019**, *7*, 693.